MT-IT JV
18, St. John Street, Fgura FGR 1447 Malta
T: +356 21803374 E: info@ais.com.mt

Studio di Impatto Ambientale
Allegato 3 – Studio modellistico del trasporto dei sedimenti marini

Malta-Italy Gas pipeline interconnection

Report Type

CESI-VDP REF. NO: R_SDM_001/2020
CLIENT REF. NO: CT3109/2018

Publication Date

01 June 2020

Co-financed by the European Union
Connecting Europe Facility

DOCUMENT REVISION HISTORY

Date	Revision	Comments	Authors/Contributors
18/12/2019	1.0	Issue for Comments (IFC)	(CESI- VDP) - MT-IT JV
06/04/2020	2.0	Approved for Design (AFD)	(CESI- VDP) - MT-IT JV

AMENDMENT RECORD

Approval Level	Name	Signature
Internal Check	Caterina De Bellis (CESI), Silvia Martorana (VDP)	
Internal Approval	Cesare Pertot (CESI), Francesco Ventura (VDP)	

DISCLAIMER

Index

Index of figures

Index of Tables

APPENDIX

APPENDIX A – MIKE 3 HD FM

APPENDIX B – MIKE 3 MT FM

APPENDIX C – MIKE 21 SW FM

APPENDIX D – Mediterranean Wind Wave Model (MWM)

1.0 INTRODUCTION

The main policy of the Maltese Government aims at reducing the cost and the environmental impact of electricity generation in Malta by switching from liquid fuels to natural gas. To meet these objectives, the government's policy is promoting independent investment in Malta's energy infrastructure in the form of new facilities, favoring the import of natural gas and new high efficiency generating plant at the site of Delimara Power Station.

The studies performed in the previous phases concluded that the most preferable solution in terms of feasibility under present market conditions, is to connect Malta to the European Gas Network by means of a Gas Pipeline. The option of linking Malta to Gela is preferred due to the existence of the required transmission infrastructure on the shoreline.

National and Local Regulations (SIN, ZPS and prescriptions from Capitaneria di Porto) at the Italian landfall prescribe that the pipeline cannot be placed above the seabed from the shoreline up to the end of the marine archaeological area (approximately 1200m offshore). Additionally, starting from the shoreline and up to a water depth of about 20m (KP 14.5), the seafloor is covered by a sensitive marine habitat (*Cymodocea nodosa*). Therefore, according to the above constraints and prescriptions, the Horizontal Directional Drilling (HDD) method has been selected as the most preferable alternative for the pipeline shore approach, at the Italian side.

However, due to technical constraints of the current HDD technology, the end point of the trenchless section is going to be placed at a depth of approximately 8.4m, beyond the archaeological area and where the marine vegetation is scattered. An open trench is required at the HDD exit point in order to create a smooth transition between the natural seabed and the drilling path inside the HDD; the trench transition shall be excavated prior to jack up mobilization and rig set up.

Within this framework, in order to meet the environmental goals and obtain the required authorizations, MT-IT JV (CESI-VDP) have developed a numerical modelling study of sediment transport and deposition process during dredging operations at the HDD exit point area. The aim of the study is to quantify the maximum suspended sediment concentration (plume) and consequent sediment deposition that may occur during the excavation period (given the design trench geometry, the sediments properties and the met-ocean conditions), in order to identify potential impacts on the surrounding area.

The following sections present the methodological approach, the available datasets, the assumptions and setups of high-resolution numerical models and, finally, the obtained results (maps of suspended sediment concentration and deposition of fine sediments).

2.0 APPROACH AND METHODOLOGY

The transport and fate of fine sediment at nearshore / shallow water sites require to account for both offshore (large scale circulation) and coastal processes, such as wave breaking and wave generated currents. The methodological approach, developed within the present study, allows to simulate the coastal processes (at high spatial resolution) starting from offshore conditions / large scale models (at lower spatial resolution) according to state-of-the-art *downscaling* techniques.

The simulation of a long period hydrodynamics (in the order of months or more) allows to study the dispersion and transport of the sediment according to a fully realistic approach, thus overcoming the limits of synthetic / most probable scenarios approach. Through a "moving time-windows" approach, the dredging operations can be simulated several times under different hydrodynamic conditions, in full compliance with the indications provided by ISPRA in its guidelines [1].

In the present study, two periods of 1 month each have been simulated: one is representative for the summer/spring season (higher thermal stratification, lower current speed) and the other one for the winter/autumn period (weaker thermal stratification, higher current speed). The "moving window" approach essentially implies that the dredging operations (which are very fast, i.e. about 2 days) might take place in a number of sub-periods within the representative period of 1 month. A number of 10 simulations of sediment transport and fate (i.e. moving time windows) have been carried out for each of the two representative months.

This methodology has manifold benefits: first of all, it allows to account the high spatial and temporal variability of hydrodynamic conditions on the evolution and fate of the sediment plume. Moreover, it provides the basis for a meaningful analysis of the results from a statistical point of view, if compared to a classical scenario-based approach, thus allowing a probabilistic interpretation of the spatial distribution of the sediment plume, including persistence analysis of prescribed thresholds of suspended sediment concentration / deposition in the sensitive areas.

The large-scale hydrodynamics data are provided through the core model of HYCOM (described in section 3.6), a global nowcast / forecast system produced by the HYCOM Consortium for data-assimilative ocean modelling. The deep knowledge of the general circulation of the Sicily Channel and the Gulf of Gela and a thorough analysis of the hydrodynamic conditions performed on the HYCOM dataset allowed to identify the optimal position and extension of the high-resolution 3D model in order to include the most relevant features of the general circulation, and to avoid possible issues related to undesirable numerical boundary effects.

In order to select the two representative months to simulate, a specific multi-yearly analysis of the HYCOM dataset has been carried out to identify periods without specific anomalies from a meteomarine and hydrodynamic point of view within the Gulf of Gela. For the two selected months (January and June 2017) a local, high resolution 3D circulation model has been implemented, through the application of MIKE 3 HD [2], as described in chapter 6.0. The hydrodynamic model has been then coupled with the sediment transport module MIKE 3 MT

[3], which allowed to simulate the transport and fate of the sediment plume and deposition resulting from dredging operations (chapter 7.0).

The effect of incoming waves at the seabed has also been accounted, while the wave generated currents (*longshore currents*) is assumed to be negligible.

Longshore currents are generated by the shore component of the stresses associated to wave breaking, shoaling and refraction processes, the so-called "radiation stresses". This current is the dominant component in the nearshore area, with the highest values laying within the wave breaking zone ("surf zone"). Longshore currents are generally parallel to the coastline and their magnitude vary according to the wave height and direction at breaking. As the position of wave breaking constantly shifts due to the irregularity of natural wave fields, the distribution of the longshore current in the coastal profile will vary accordingly. The width of the wave breaking zone is limited by the so-called "closure depth", i.e. the depth of a beach profile where the wave generated sediment transport becomes negligible. In a previous study developed in this area to meet the environmental prescriptions of the Ministry for Environment, Land and Sea Protection [4], the closure depths in the Gulf of Gela have been estimated around 3.5m. Considering that the trench is planned at a depth of about 8-9m (chapter 5.0), it is possible to assume that wave generated currents are not relevant for the dispersion and fate of the sediment released during dredging operations.

The main contribution of waves here is therefore associated to the orbital velocities at the seabed, that in case of storms can be strong enough to resuspend sediments after deposition. Given the very limited period of dredging operations (about 2 days), it can be assumed that storm conditions will be avoided with proper short-term planning. At the same time, after operations, for a period in the order of weeks / months a storm might easily put in suspension the fine sediment released during operations. The effect of a real storm (7 March 2017) has been therefore modelled, in order to compare the natural turbidity generated by high waves resuspending the whole sediment at the seabed and the contribution of the sediment "freshly" deposited after operations.

3.0 SITE CHARACTERIZATION

The area where the submarine pipeline is planned is the Malta Channel, from Gela, in Sicily, to Delimara in Malta (Figure 3-1).

The Malta Channel separates the island of Malta from the southern coast of Sicily and it is located in the eastern part of the Sicily Channel. The Sicily Channel is the strait between Sicily and Tunisia and divides the Western Mediterranean from the Eastern Mediterranean Sea. It is characterised by a complex bathymetry with wide continental shelves, deep and shallow channels as well as wide abyssal plains. The area of the Sicily Channel extends from 35° to 38°N and between 10° and 15°E.

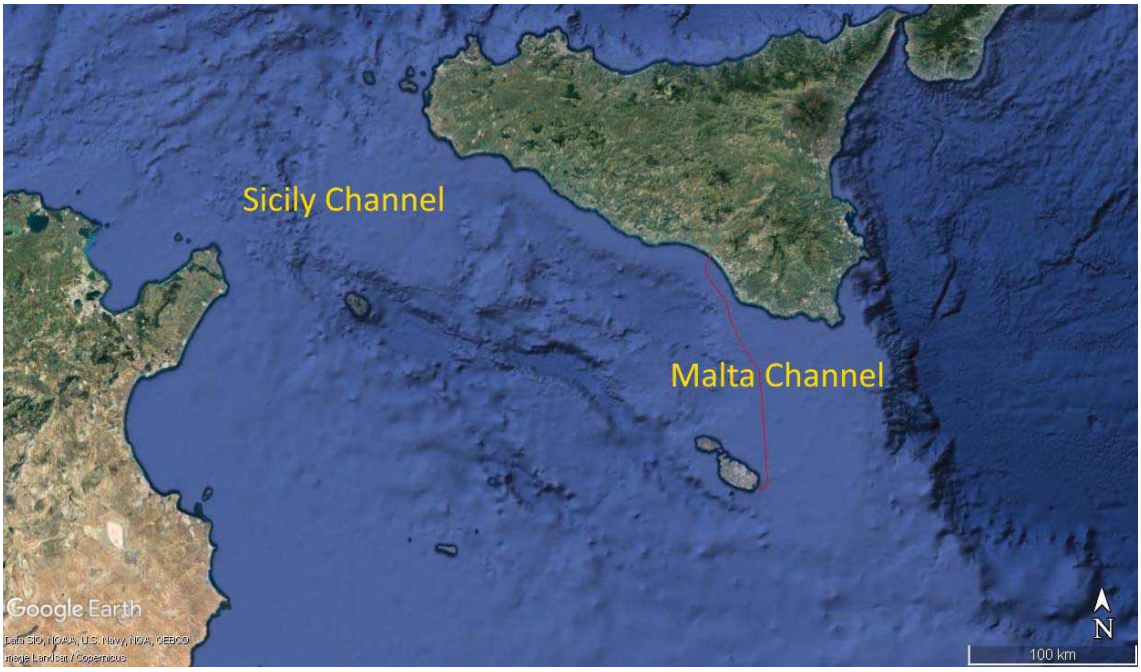

Figure 3-1 Localisation of the Sicily Channel, the Malta Channel and the planned route (in red) of the submarine pipeline from Gela (Sicily) to Delimara (Malta)

The following sections provide a general overview of the data used for the site characterization (presence of protected areas, bathymetry, sediment grain size, wind and wave conditions, currents, temperature and salinity).

3.1 Protected areas

In the Italian nearshore area crossed by the pipeline route there are several areas subject to environmental and archaeological interest, as reported in the list below and shown in Figure 3-2:

- SIC (Sito di Interesse Comunitario): area from the coastline to KP 6.862. This area is related to Natura 2000 project, whose aim is to preserve the flora and fauna;
- ZPS (Zona di Protezione Speciale – yellow area in Figure 3-2): area Natura 2000 extending up to KP 9.5 offshore;

- SIN (Sito Contaminato di Interesse Nazionale – white area in Figure 3-2): area extending up to KP 10.6. This area has been defined by the Italian law 426/98 as polluted site, subject to risk for health and ecologic issues;
- Restricted marine archaeological area from the coastline to KP 8.3. This area, whose limits have been confirmed by Ordinanza n° 27/2019 of the "Capitaneria di Porto di Gela", is restricted from anchorage, fishing activities, diving and any other activity which could jeopardize the remains of the second world war found in the vicinity of the Sicilian coast;
- Level 3 Woodland area of landscape protection from the temporary yard fence to the coastline. In this area it is not allowed to build infrastructures.

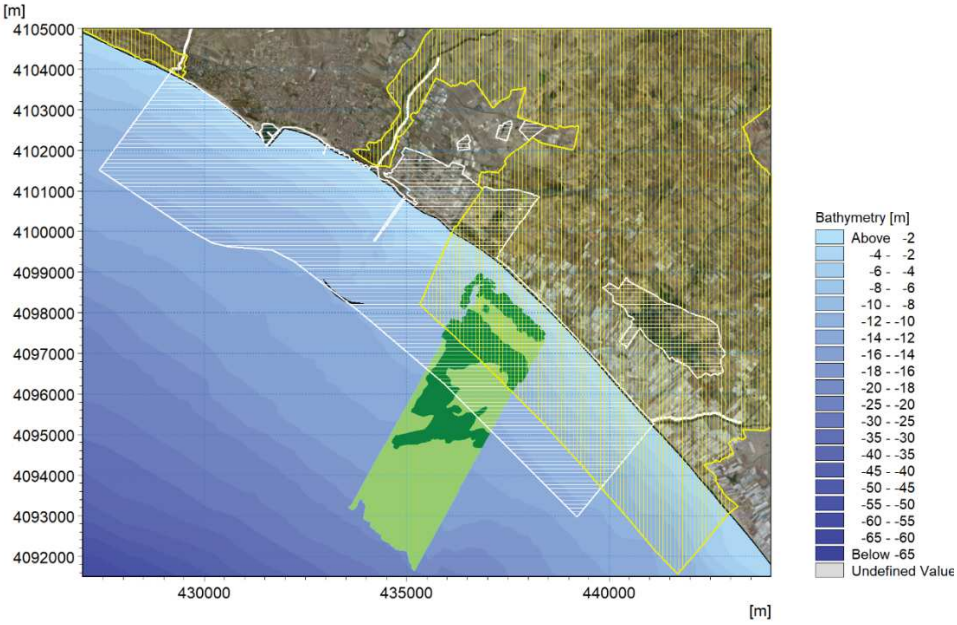

Figure 3-2 Protected areas in the Italian nearshore zone crossed by the pipeline route. In white the SIN area, in yellow the ZPS area, in light green Cymodocea Nodosa scattered meadows, in dark green Cymodocea Nodosa dense meadows

As fully described in the study carried out by Lighthouse in 2019 [5], the seabed nearshore Gela coastline is covered by patches of variable size of *Cymodocea Nodosa* meadows, from scattered (light green area in Figure 3 3) to dense (dark green area in Figure 3 3), which become progressively sparse passing to the deeper areas, up to approximately -20m WD (approx. KP14.5).

3.2 Bathymetry data

Two different bathymetric datasets have been considered, in order to define the bathymetry for the study:

- C-MAP dataset, based on the extensive and continuously updated CM-93 [6] nautical charts database, managed and maintained by Jeppesen [7]. These data can be directly imported within MIKE by DHI software environment, allowing the automatic digitization of the bathymetry;

- detailed data derived from the geophysical survey conducted by Lighthouse in June 2019 [8]. The survey has been carried out in a nominal 1.5km corridor centred on the pipeline route. Bathymetric data is reported as isolines every 1m depth.

C-MAP dataset is presented in Figure 3-3, while Figure 3-4 shows the data of the aforementioned detailed survey. The white dot located at a depth of about 8.3m represents the excavation area.

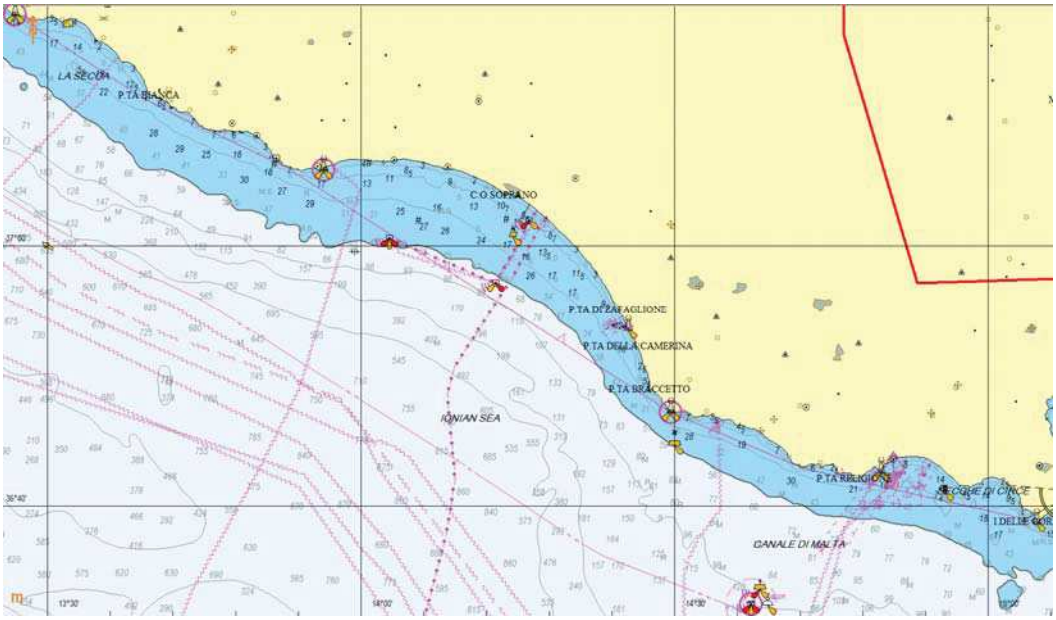

Figure 3-3 C-MAP bathymetry data available in the area of interest

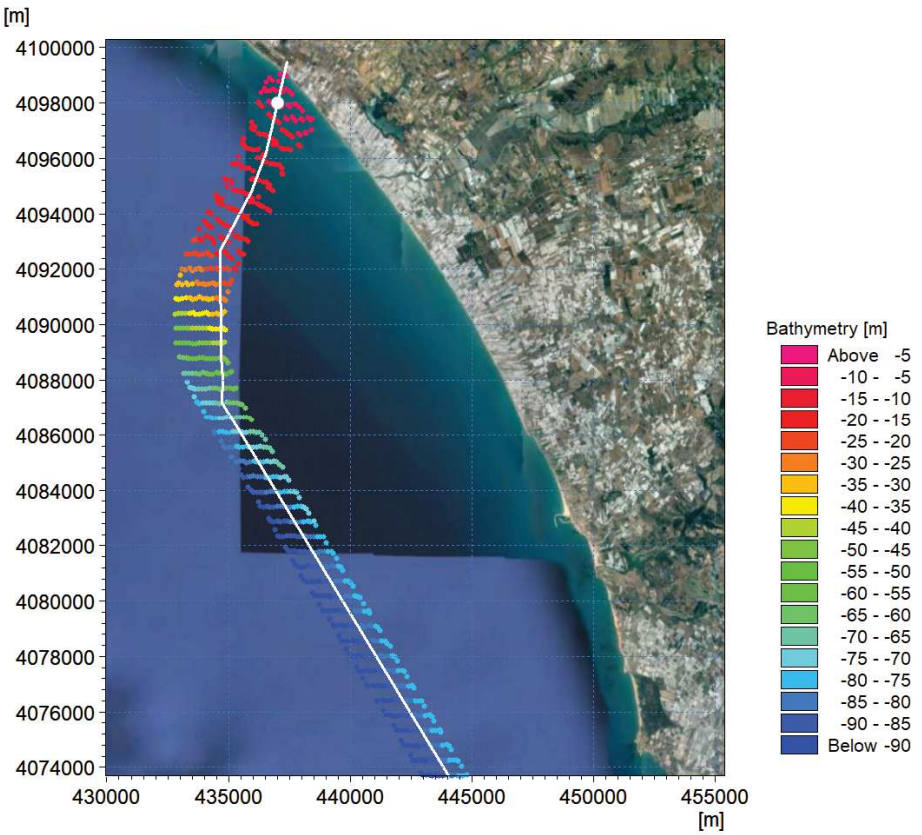

Figure 3-4 Detailed bathymetry survey data near the Italian landfall. The white line indicates the pipeline route, while the white dot indicates the excavation area

3.3 Sediment data

During the period from March to August 2019 the company Lighthouse carried out an environmental campaign in the Sicily Strait, along the planned pipeline route. In October 2019 [9] the company produced a report that summarizes the data collected during the campaign, describing the methodologies and providing an assessment of the results obtained after laboratory analyses. In particular, this report includes an assessment of the physical, biological and chemical characteristics of sediments and water samples collected within the route corridor.

For the purpose of the present study, only the textural analyses results obtained for sediment samples located in the nearshore area of Gela have been considered. This analysis gives the percentages passing through the different diameters and a textural classification as clay, silt, sand and gravel.

Table 3-1 shows results of this grain size analyses, while Figure 3-5 shows the positions of the samples taken into consideration in this study.

Table 3-1 Textural analyses results for samples located in the nearshore area of Gela. In red the sample closest to the trench area

Samples	EASTING (m)	NORTHING (m)	KP (km)	Water depth (m)	top lithology	Clay [%] <0.004mm	Silt [%] 0.004-0.063mm	Sand [%] 0.063-2.0mm	Gravel [%] > 2.0mm
MEW001d_S21	436896.39	4098588.71	0.963	6.5	silty SAND	19.9	39.8	39.7	0.6
MEW001d_S22	437176.64	4098066.94	1.399	7.4	silty SAND	18.8	38.4	42.2	0.6
MEW001d_S23	437479.18	4097565.19	1.81	8.2	silty SAND	17.1	41.7	40.5	0.7
MEW001d_S24	438057.04	4097592.55	1.64	6.3	sandy SILT	21.2	46.4	32.4	< 0.1
MEW001d_S25	436750.45	4098326.81	1.253	7.8	sandy SILT	22.2	43.5	34.3	< 0.1
MEW001d_S26	437043.75	4097813.17	1.678	8.7	silty SAND	19.1	39.9	41	< 0.1
MEW001d_S27	437352.18	4097324.02	2.075	9.3	silty SAND	18.8	37.2	42.8	1.2
MEW001d_S28	437914.28	4097335.79	1.924	7.6	silty SAND	17.3	36.9	44.9	0.9
MEW001d_S29	436621.56	4098087.99	1.516	9	silty SAND	20.2	41.2	38.6	< 0.1
MEW001d_S30	436886.35	4097544.14	1.977	9.8	silty SAND	17.6	37.9	44.1	0.4
MEW001d_S31	437200.26	4097093.24	2.336	10	sandy SILT	21.1	42.8	34.9	1.2
MEW001d_S32	437758.83	4097065.96	2.224	9	silty SAND	19.6	40.2	40.2	< 0.1
MEW001d_S33	436458.81	4097800.62	1.835	10	silty SAND	18.8	39.1	42.1	< 0.1
MEW001d_S34	436736.58	4097291.07	2.259	10.4	silty SAND and CLAY	18.4	40.7	40.9	< 0.1
MEW001d_S35	437047.04	4096768.10	2.648	10.7	sandy SILT	23.1	45.8	31.1	< 0.1
MEW001d_S36	437620.39	4096807.35	2.509	9.8	silty SAND	22	38.2	38.9	0.9
MEW001d_S37	435553.90	4095405.27	4.518	13.4	silty SAND	22	39.3	37.6	1.1
MEW001d_S38	436457.90	4096636.74	2.983	11.3	silty SAND	16	38.1	45.9	< 0.1
MEW001d_S39	436835.83	4096427.33	3.042	11.3	silty SAND	23	39.5	37.5	< 0.1
MEW001d_S40	435903.15	4094732.02	4.949	13.8	sandy clayey SILT	22.9	46.5	30.6	< 0.1

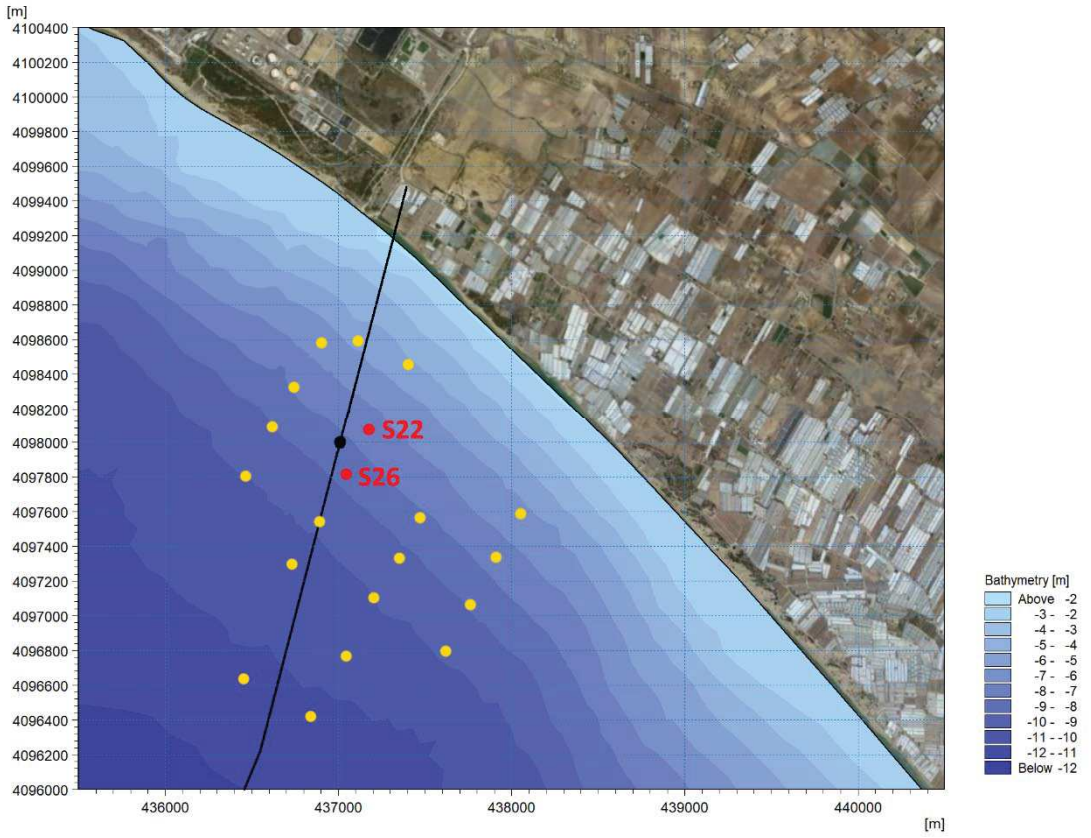

Figure 3-5 Positions of the samples in the nearshore area of Gela. The black dot shows the planned exit point of the HDD and the red dots the closest samples to the excavation area

3.4 Characterization of wind and wave conditions

The characterization of wind and wave conditions has been derived from the metocean study carried out by Lighthouse in April 2019 [10]. The scope of that document was the analysis of the meteo-marine parameters to assess wind and wave conditions as well as the regime of currents in order to estimate the extreme values of these variables required to properly design the submarine pipeline connecting Gela, in Sicily, to Delimara, in Malta.

In the available study wind and wave hindcasted data from 1998 to 2017 had been gathered, validated and carefully analyzed. After the definition of the typical conditions, state-of art numerical models had been used to simulate the distribution of the wave field in order to assess the wave heights affecting the area and to estimate the extreme values.

In the following section, the main results of this analysis have been summarized.

3.4.1 Wind conditions

In the metocean study carried out by Lighthouse, the wind regime has been derived from observation from vessels (KNMI data) as well as from long measurements (at offshore Vega A platform).

The general wind characteristics of the Malta Channel in the past have been derived from KNMI observations from 1960 to 1980. In Table 3-2, the frequency distribution of the wind speed vs incoming direction is presented, while the wind rose is shown in Figure 3-6.

Table 3-2 Frequency distribution (%) of wind speed vs. incoming direction in Malta Channel (KNMI observation, 1960-1980) [10]

DIRECTION (°N)	WIND SPEED (m/s)												
	4	6	8	10	12	14	16	18	20	22	24	>24	TOTAL
0	5.29	1.09	.58	.35	.11	.74	.04	.00	.01	.00	.00	.00	8.21
30	1.34	.87	.41	.26	.13	.07	.08	.02	.01	.01	.00	.00	3.19
60	1.54	1.20	.85	.48	.23	.20	.10	.05	.02	.01	.01	.00	4.69
90	2.68	1.99	1.64	1.12	.57	.40	.26	.09	.06	.01	.01	.00	8.82
120	1.81	1.71	1.35	.90	.50	.28	.15	.06	.04	.01	.00	.00	6.81
150	1.92	1.34	.88	.50	.24	.16	.08	.02	.01	.00	.00	.00	5.17
180	1.54	.97	.59	.38	.15	.12	.02	.01	.00	.00	.00	.00	3.78
210	1.47	.95	.64	.36	.18	.12	.03	.01	.00	.00	.00	.00	3.77
240	2.26	1.44	.82	.56	.27	.25	.08	.04	.02	.01	.00	.01	5.75
270	3.90	2.81	2.43	1.92	1.08	.87	.53	.17	.11	.08	.05	.02	13.96
300	3.64	3.62	3.35	3.13	1.81	1.64	.79	.33	.17	.08	.06	.02	18.64
330	2.63	2.49	2.02	1.43	.69	.63	.27	.10	.06	.03	.03	.02	10.39
TOTAL	30.02	20.49	15.56	11.40	5.96	5.47	2.43	.90	.51	.23	.15	.07	93.18
CALM:	6.82												

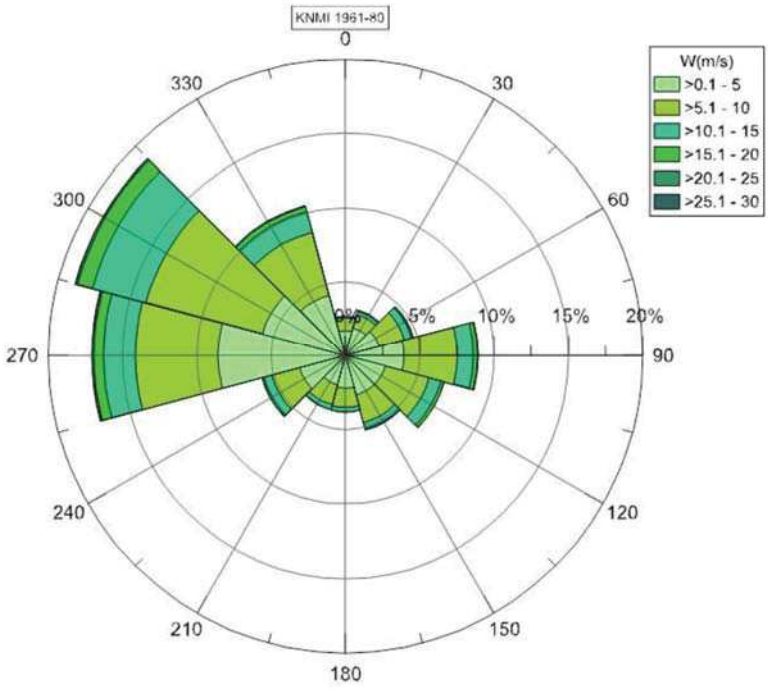

Figure 3-6 Wind rose in Malta Channel (KNMI observations, 1960-1980) [10]

Available wind data has also been collected from measurements at Vega A offshore platform, located at geographical coordinates 36°32'21" N, 14° 37' 39" E at a depth of 122 m, for the period from 2002 to 2017. The anemometer is located 49m above mean sea level, where the wind field is slightly different from the wind field at a standard altitude of 10m above mean sea level. The yearly wind rose at Vega (Figure 3-7) shows that the prevalent wind comes from North-West (IV Quadrant, 270-360°N) with an overall frequency of about 41%, while approximately 30% of wind records come from North-East (I Quadrant, 0-90°N). The wind from South (II and III Quadrant, 90-270°N) is less relevant, with a total frequency of about 29% (Table 3-3).

Table 3-3 Frequency distribution (%) of wind velocity vs incoming direction (Vega A platform data, 2002-2017) [10]

INCOMING DIRECTION (°N)	WIND SPEED (m/s)															
	2	4	6	8	10	12	14	16	18	20	22	24	26	28	30	TOTAL
0	1.13	1.31	.82	.53	.30	.19	.10	.06	.02	.01	*	*	.00	.00	.00	4.48
30	1.13	1.22	1.43	1.34	.86	.49	.28	.13	.05	.02	.01	*	*	.00	.00	6.97
60	1.12	1.73	1.92	1.63	1.49	.95	.47	.20	.09	.02	.01	*	*	*	.00	9.63
90	1.44	1.57	1.93	1.49	.92	.52	.22	.11	.05	.01	*	*	.00	.00	.00	8.28
120	1.06	1.49	1.20	.71	.41	.24	.11	.08	.02	.01	*	.00	.00	.00	.00	5.33
150	1.25	1.34	.72	.33	.20	.10	.05	.02	.01	.01	*	.00	.00	.00	.00	4.03
180	1.66	1.33	.64	.43	.23	.13	.09	.03	.01	*	*	.00	.00	.00	.00	4.55
210	1.38	1.67	1.01	.58	.35	.30	.21	.14	.08	.04	.02	.01	.00	*	.00	5.78
240	1.01	2.09	2.03	1.47	1.00	.78	.60	.47	.33	.13	.07	.02	.01	*	*	10.03
270	1.07	2.80	3.63	2.97	2.56	2.23	1.77	1.40	.92	.44	.19	.09	.02	.01	.00	20.08
300	1.05	2.24	2.66	2.26	1.63	1.36	.96	.66	.38	.16	.07	.02	*	*	.00	13.46
330	1.11	1.74	1.52	1.21	.77	.49	.26	.16	.08	.04	.01	*	*	.00	.00	7.39
TOTAL	14.41	20.54	19.51	14.95	10.72	7.76	5.12	3.46	2.04	.89	.39	.15	.04	.02	.00	100.00

** means < 0.01%

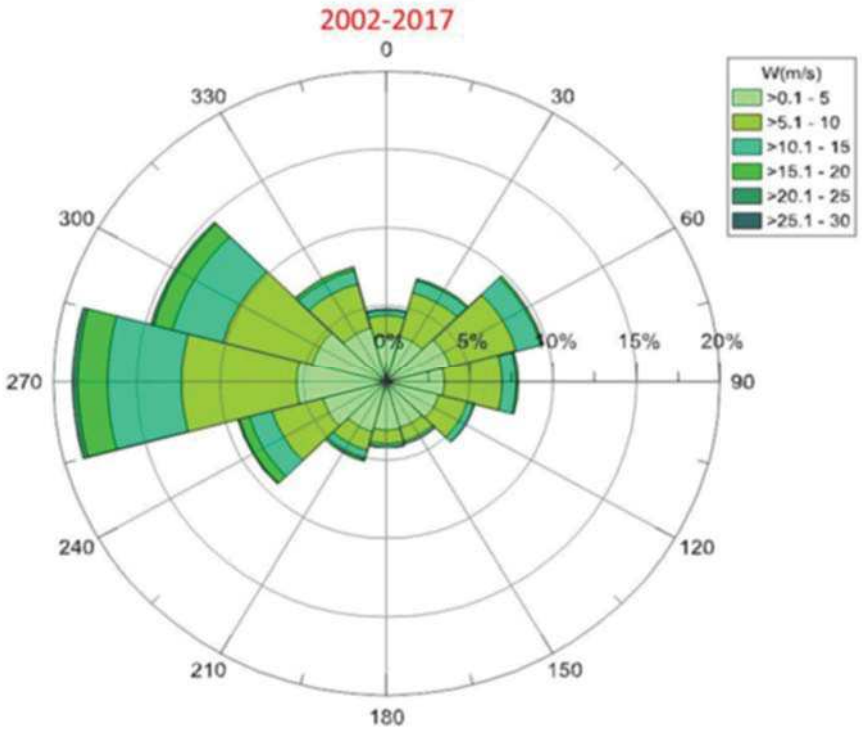

Figure 3-7 Wind rose at Vega A platform (Vega data, 2002-2017) [10]

The seasonal analysis (Figure 3-8) shows that, in all seasons, the zonal flow (from West to East) is always prevalent, with a higher frequency in summer, while the southern fluxes have higher frequencies in autumn-winter. The Balkan flow is present in all seasons with maximum frequency in autumn and minimum in summer; the flow from East also has maximum frequencies in autumn and minimal in summer. The sum of the frequencies of these four wind conditions is on average about 85% of the total; there are obviously other winds, such as Scirocco, with annual frequencies of the order of 9%, and Libeccio, with frequencies of the order of 5-6%.

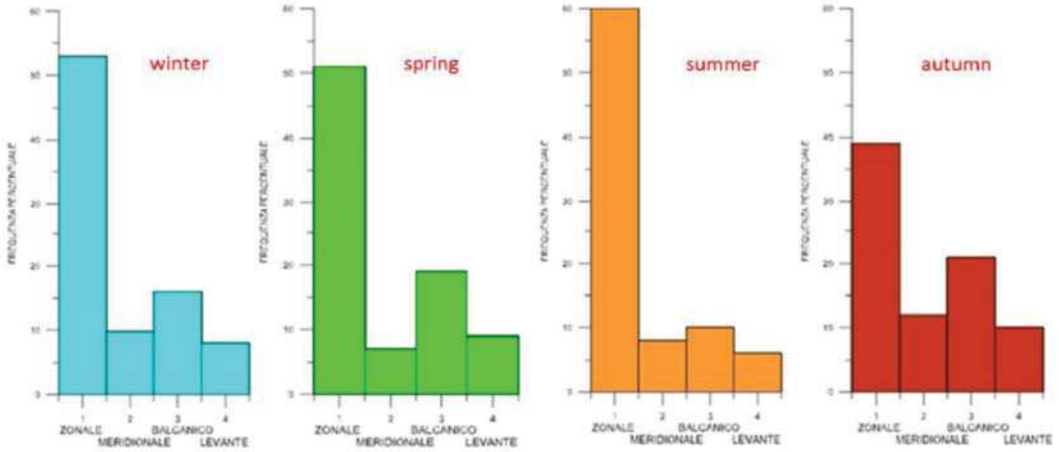

Figure 3-8 Frequency distribution (%) of the main types of flow present in the area in the course of seasons [10]

Finally, the meteomarine study performed by Lighthouse analysed the hindcasted wind data produced by Genoa University, Department of Civil, Chemical and Environmental Engineering (DICCA). These data are available for the period 1998-2017 (20 years) at a standard elevation of 10m above mean sea level. Wind roses (Figure 3-9), presented in 4 points (Figure 3-10), are very similar to the ones obtained from historical KNMI observations and to long term measurement at Vega A platform. Since the points are very distant from each other, the percentages for the directional sector show some variation, but, in any case, within modest limits.

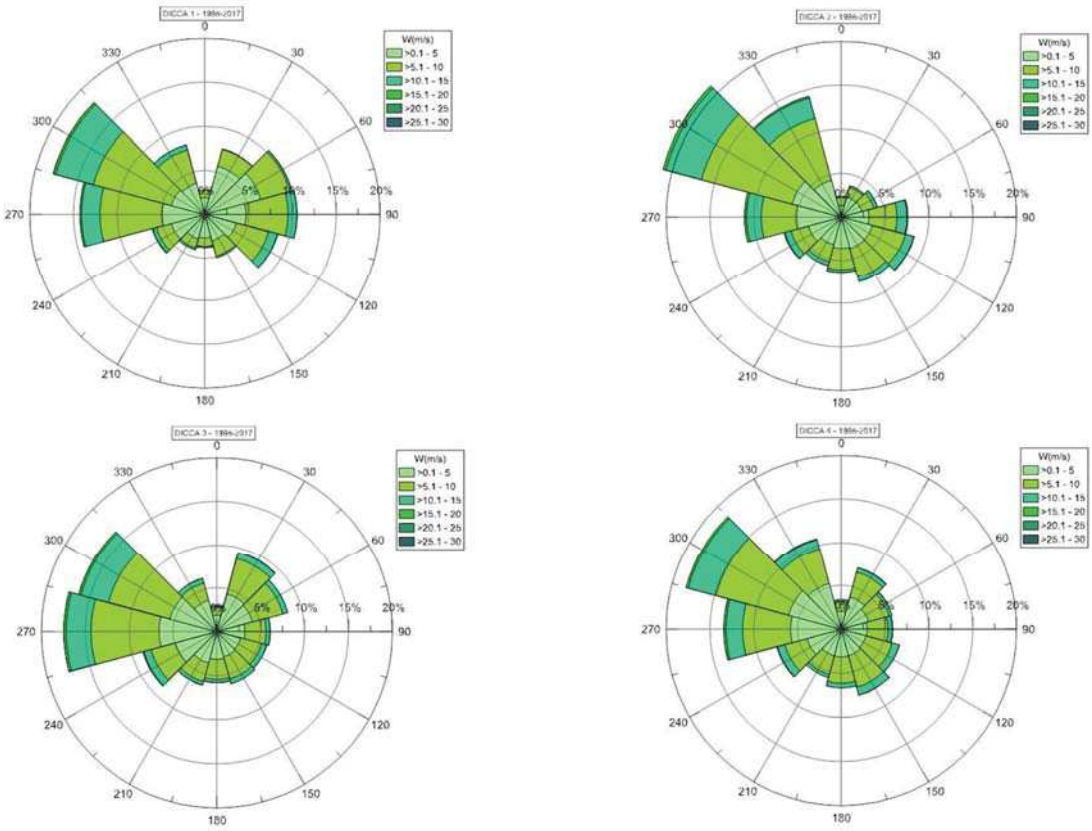

Figure 3-9 Wind roses in 4 points (Figure 3-10 - DICCA hindcasted wind data, 1998-2017) [10]

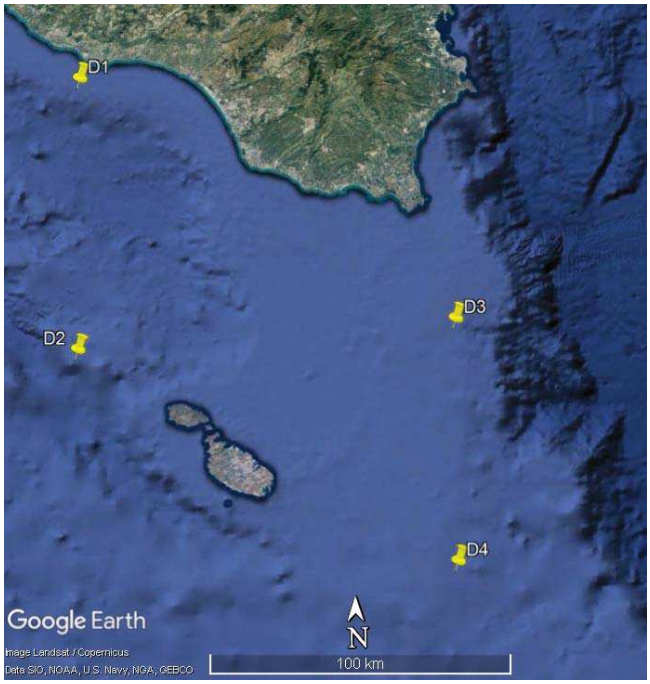

Figure 3-10 Map of locations where DICCA data for the study are available

3.4.2 Wave conditions

Again, a combination of visual observations from vessel (KNMI data) and measurements has been used for waves analysis.

The historical wave data in the Lighthouse study refer to visual observation KNMI from 1960 to 1980. Yearly wave rose obtained from KNMI data is shown in Figure 3-11.

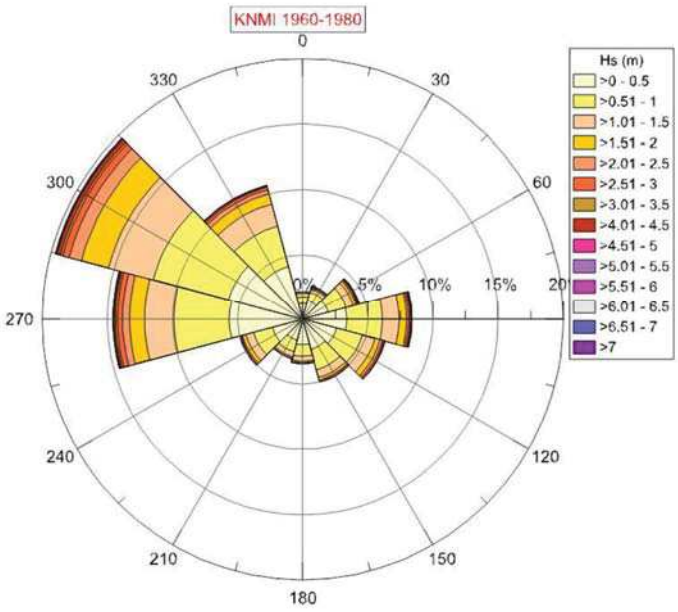

Figure 3-11 Wave rose (KNMI visual observations, 1960-1980) [10]

The Lighthouse study considered also the measurement performed in the Malta Channel in the period 1981-1982 by wavemeters O1-Alfa, O2-Beta and O3-Gamma. The frequency distribution of the significant wave heights recorded during this period is shown in Table 3-4.

Table 3-4 Frequency distribution (%) of significant wave height values at wavemeters O1, O2, O3 [10]

SIGNIFICANT WAVE HEIGHT (m)	O1 -ALFA from JULY 1981 to JULY 1982	O2 - BETA from JULY 1981 to JULY 1982	O3 .GAMMA from JULY 1981 to JULY 1982
0.5	42.1	32.3	34.7
1.0	24.3	26.8	25.5
1.5	16.1	14.5	13.9
2.0	8.2	11.1	9.6
2.5	5.1	6.8	6.7
3.0	1.9	4.2	4.3
3.5	1.3	2.4	2.9
4.0	0.6	1.1	1.4
4.5	0.4	0.4	0.5
5.0	**	0.2	0.2
5.5	-	0.1	0.1
6.0	-	**	0.1
6.5	-	**	**
7.0	-	**	**

** means < 0.1%

Wave data is also measured at Vega A platform, located at geographical coordinates 36°32’21” N, 14° 37’ 39” E at a depth of di 122 m, for the period from 2002 to 2017. The frequency distribution of the significant wave height for incoming direction, displayed in graphical form in Figure 3-12, shows that this long term frequency distribution is very similar to distributions derived from the historical data: W-NW waves are prevailing (about 45%), while approximately 12% of waves comes from NE and approximately 13% from E-SE sectors (Figure 3-12).

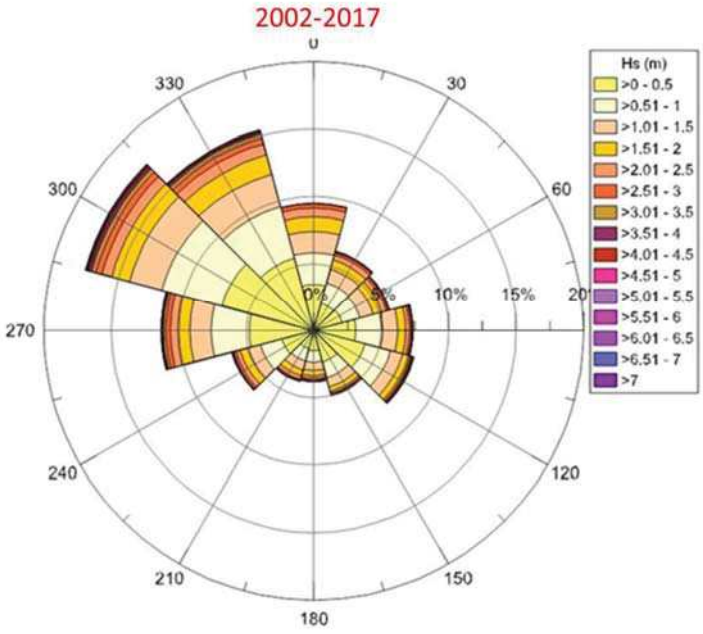

Figure 3-12 Wave rose at Vega A platform (2002-2017) [10]

The seasonal analysis showed that in autumn and winter the highest waves come from W-NW, in spring wave heights are reduced and the frequency from SE increases, in summer wave heights are lower and there is a noticeable increase of waves coming from E-SE sectors.

As for wind, the wave study performed by Lighthouse also analyzed the hindcasted wave data produced by Genoa University, Department of Civil, Chemical and Environmental Engineering (DICCA) in 4 points (Figure 3-10).

In Figure 3-13 the wave roses at the points are shown for the years 1998-2017.

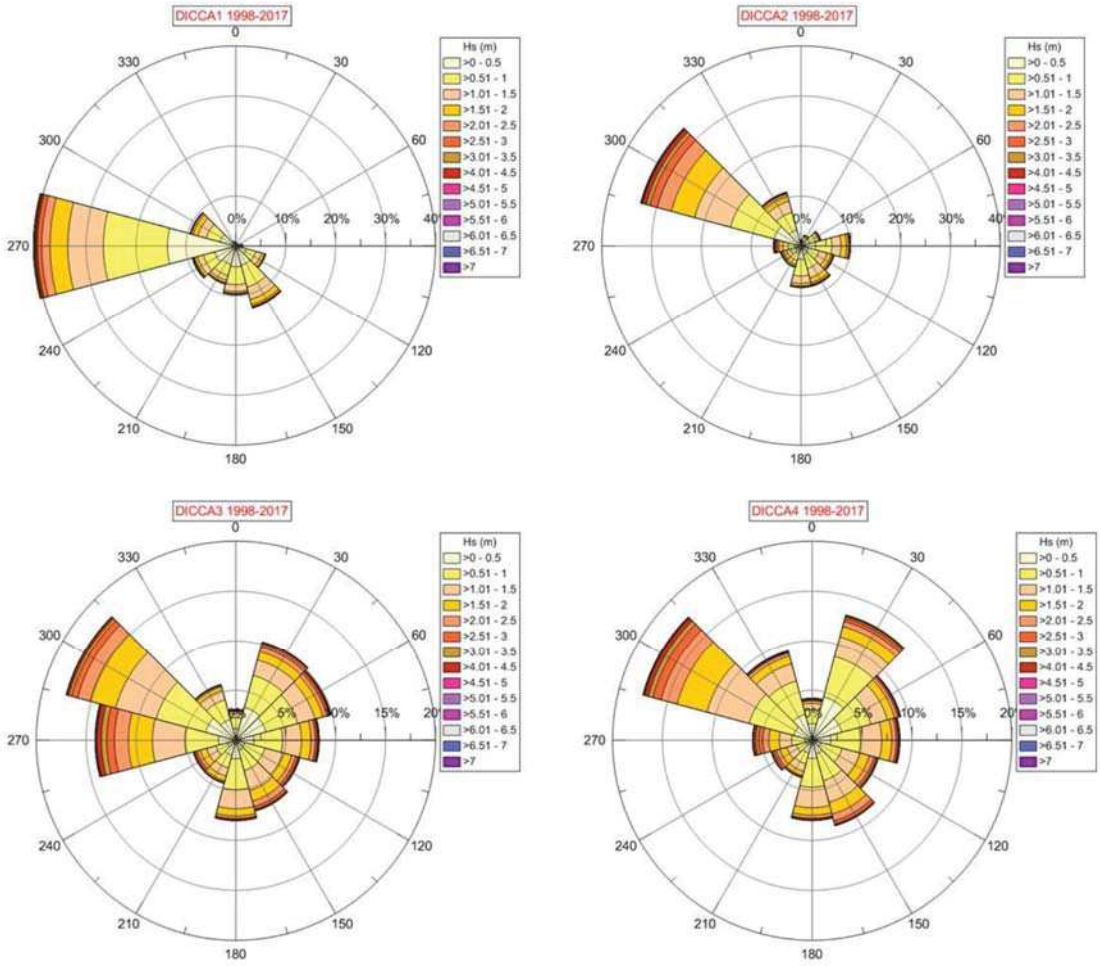

Figure 3-13 Wave roses in 4 points (Figure 3-10 - DICCA hindcasted wave data, 1998-2017) [10]

For point D1, due to the proximity of the coast, the directions from 330° to 90°N are absent, while the waves from the directions 255-295°N are prevalent (approximately 35%). The other sectors, each of them 30° wide, are characterized by a frequency from approximately 7% for the sector 105-135°N, to approximately 17% for the sector 285-315°N.

The other three points, located offshore in deep water, are in general characterized by a prevalent sector from NW (directions between 285°N and 315°N have a frequency of about 37% - point D2 - and 20% - point D4). In points D3 and D4 also the NE and SSE sectors are important.

Wave data provided by University of Genoa had been used in the Lighthouse study as boundary conditions for a local wave model (SWAN). Results have been provided in several points identified along the route of the pipeline. In order to present the details of the wave motion, a number of 25 points had been selected, shown in Figure 3-14, taking into account the depth of the point and its exposure. In the present study, the main parameters (H_s, T_p) of the extreme omnidirectional waves, for different return period (1, 5, 10, 50 and 100 years), obtained from the analysis performed by Lighthouse, are shown in Table 3-5. In this table also the depths and progressive distances, in kilometres, from the Italian landfall are specified.

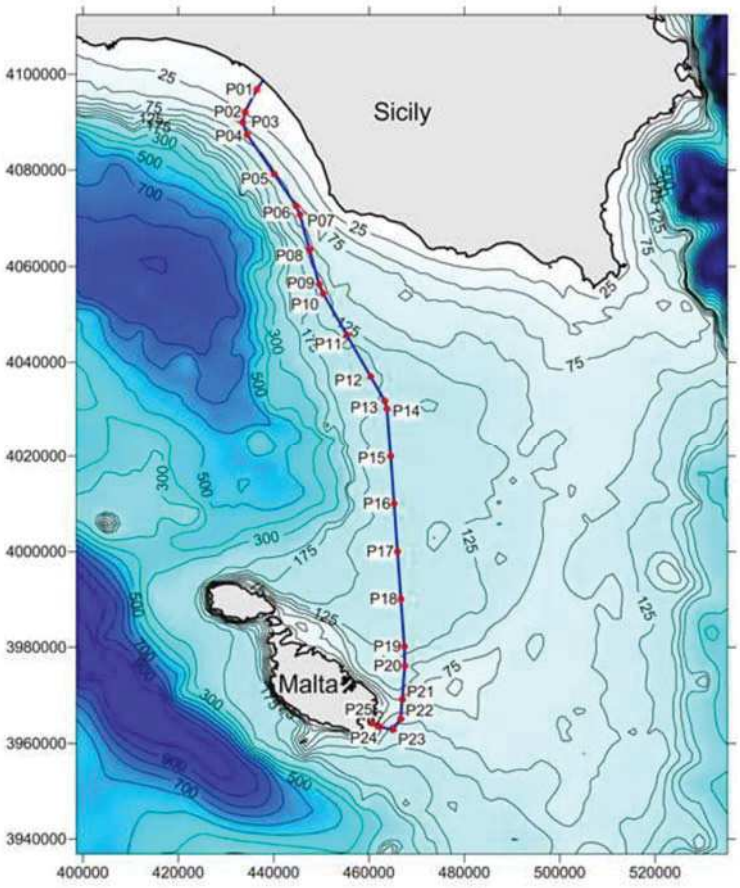

Figure 3-14 Selected points along the pipeline route [10]

Table 3-5 Extreme values (Return Period = 1, 5, 10, 50, 100 years) of omnidirectional wave parameters (Hs, Tp) at 25 points along the pipeline route [10]

			RETURN PERIOD 1 Year		RETURN PERIOD 5 Years		RETURN PERIOD 10 Years		RETURN PERIOD 50 Years		RETURN PERIOD 100 Years	
POINT	Depth (m)	KP (Km)	Hs (m)	Tp (s)	Hs (m)	Tp (s)	Hs (m)	Tp (s)	Hs (m)	Tp (s)	Hs (m)	Tp (s)
P1	11.1	3	3.5	8.8	3.9	9.2	4.1	9.4	4.5	9.7	4.7	9.9
P2	23.4	8	4.3	9.5	4.9	10.0	5.1	10.0	5.7	10.7	5.9	10.9
P3	41.5	10	4.7	9.9	5.3	10.4	5.6	10.6	6.2	11.1	6.5	11.4
P4	57.9	13	5.0	10.1	5.7	10.7	6.0	10.9	6.7	11.5	7.0	11.7
P5	76.8	23	5.4	10.4	6.2	11.1	6.5	11.4	7.3	12.0	7.6	12.3
P6	79.3	31	5.5	10.5	6.4	11.2	6.7	11.5	7.5	12.2	7.8	12.4
P7	85.8	32	5.6	10.6	6.4	11.3	6.8	11.6	7.6	12.2	7.9	12.5
P8	116.7	41	5.8	10.8	6.6	11.5	7.0	11.8	7.9	12.5	8.2	12.7
P9	144.5	48	5.9	10.9	6.9	11.6	7.2	12.0	8.1	12.6	8.5	12.9
P10	129.7	50	5.9	10.9	6.9	11.7	7.2	12.0	8.1	12.7	8.5	13.0
P11	140.0	60	6.0	11.0	7.0	11.7	7.3	12.0	8.2	12.8	8.6	13.1
P12	154.3	70	6.1	11.0	7.0	11.8	7.4	12.1	8.3	12.8	8.7	13.1
P13	149.2	76	6.1	11.0	7.0	11.8	7.4	12.1	8.3	12.8	8.7	13.1
P14	147.9	78	6.1	11.0	7.0	11.8	7.4	12.1	8.3	12.8	8.7	13.1
P15	145.0	88	6.2	11.1	7.1	11.9	7.5	12.2	8.4	12.9	8.8	13.2
P16	142.0	98	6.2	11.1	7.1	11.8	7.5	12.2	8.4	12.9	8.8	13.2
P17	138.6	108	6.1	11.0	7.0	11.8	7.4	12.1	8.3	12.8	8.7	13.1
P18	136.8	118	5.9	10.9	6.8	11.6	7.1	11.9	8.0	12.6	8.3	12.8
P19	132.9	128	5.6	10.6	6.4	11.3	6.8	11.6	7.6	12.2	7.9	12.5
P20	106.5	132	5.4	10.5	6.2	11.2	6.6	11.4	7.4	12.1	7.7	12.3
P21	70.1	139	5.3	10.3	6.2	11.1	6.6	11.5	7.6	12.2	8.0	12.5
P22	89.3	143	5.3	10.4	6.4	11.3	6.8	11.6	7.8	12.4	8.3	12.8
P23	109.7	146	5.3	10.4	6.3	11.2	6.8	11.6	7.8	12.4	8.2	12.8
P24	87.6	149	5.0	10.2	5.9	10.9	6.3	11.2	7.2	11.9	7.5	12.2
P25	35.2	151	4.8	9.9	5.5	10.7	5.9	10.9	6.7	11.5	7.1	11.8

3.5 Atmospheric data used for the 3D hydrodynamic model

The atmospheric data used within the 3D high-resolution hydrodynamic model described in chapter 6.0 is derived from the reanalyses of the Climate Forecast System (CFSR) [11] [12] produced and delivered by the National Centre for Environmental Prediction (NCEP).

The CFSR was designed as a global, high-resolution, coupled atmosphere-ocean-land surface-sea ice system to provide the best estimate of the state of these coupled domains. It uses synoptic data for initialization. The atmospheric model included in the CFSR modelling complex is GFS.

CFSR hindcast data cover the period from January 1979 to December 2010 (31 years) and, since then to present, the operational data set (denoted CFSRv2) was applied. Hence, being operational, there is the possibility to update the database continuously in a consistent manner. The underlying model in CFSRv2 is the same as for CFSR; however, the spatial resolution of wind, cloud cover and air temperature was increased from 0.3° to 0.2° (corresponding to 18 km approximately), while the resolution of relative humidity and precipitation was 0.5° (corresponding to 55 km approximately) for the entire period. Hereafter, CSFR will refer to the combined CFSR and CFSv2 data set. Further details of CFSR are given in [11] and [13].

The specific data used in the study as forcing for the circulation model is the operational analyses of the zonal and meridional components of wind speed and direction, precipitation, cloud cover, 2-meter temperature and relative humidity in the air. The atmospheric data cover

the entire period of the hydrodynamic simulations, to guarantee a dynamic and realistic implementation of the circulation model.

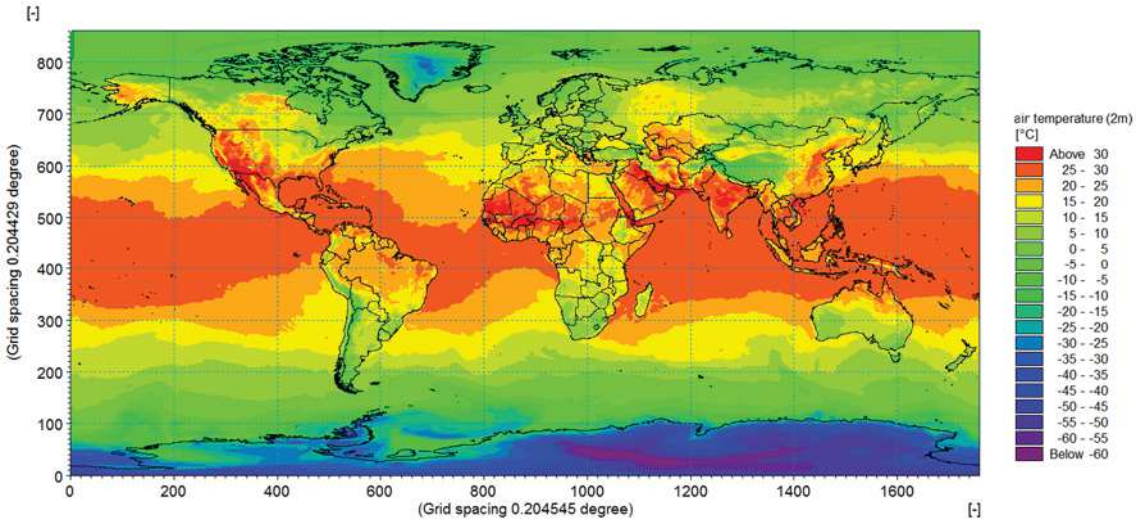

Figure 3-15 Example of air temperature at 2 meters on the global domain of the Climate Forecast System (CFSRv2)

3.6 Oceanographic data used for the 3D hydrodynamic model

[14] Dynamically, the circulation in the Sicilian Channel can be described as an exchange of three main water masses (Figure 3-16):

- the upper layer fresh Modified Atlantic Water (MAW), which enters through the Sicily Channel as an extension of the north African Algerian coastal current and flows eastward; its northernmost branch is generally known as Atlantic-Ionian Stream (AIS), while its southernmost branch is generally known as Atlantic Tunisian Current (ATC);
- the Levantine Intermediate Water (LIW) that flows in the opposite direction mainly entering through the Medina sill to the southeast of Malta;
- the Eastern Mediterranean Deep Water (EMDW) which, together with the LIW, forms the deeper Eastern Overflow Water (EOW).

The general circulation is dictated by the slow basin scale (vertical) thermohaline structure of the Mediterranean and carries a significant seasonal and inter-annual variability. In the upper thermocline the AIS characterizes the circulation by energetic meandering. The circulation is further modified by strong mesoscale signals in the form of eddy, meander and filament patterns.

These mesoscale processes are triggered by the synoptic scale atmospheric forcing. The heat and momentum fluxes at the air-sea interface represent the dominant factor in the mixing and pre-conditioning of the MAW on its way to the eastern Mediterranean.

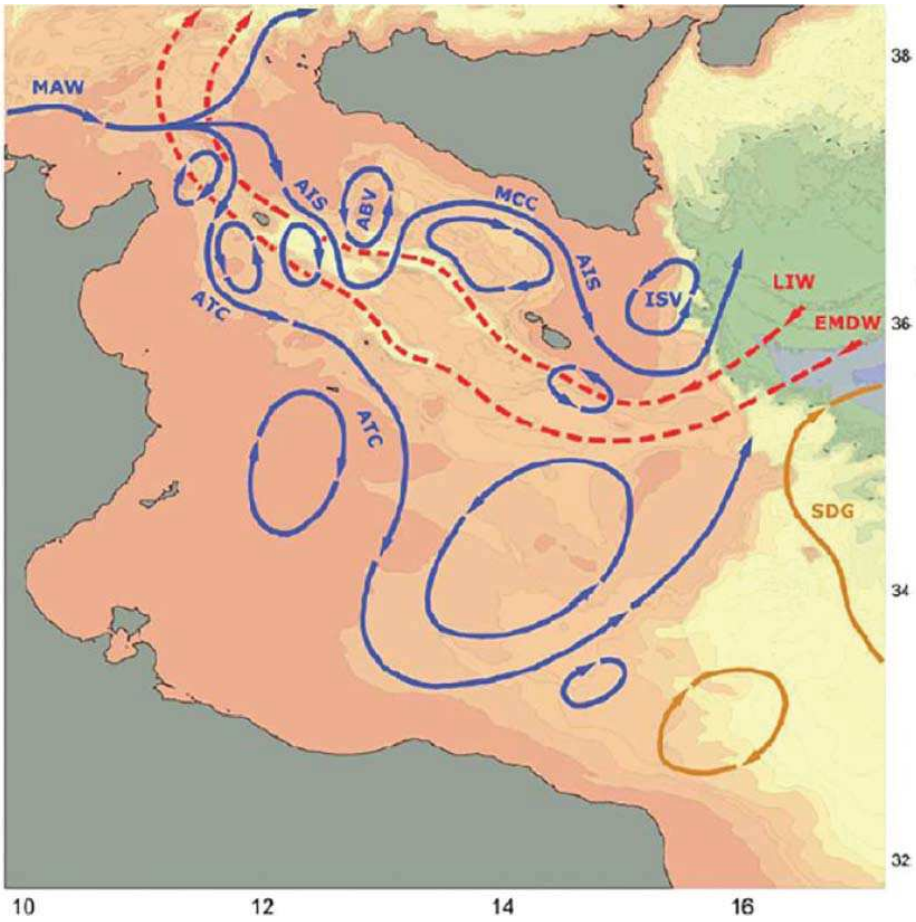

Figure 3-16 Patterns of circulation within the Strait of Sicily. MAW: Modified Atlantic Water; AIS: Atlantic Ionian Stream; ATC: Atlantic Tunisian Current; ABV: Adventure Bank Vortex; MCC: Maltese Channel Crest; ISV: Ionian Chef Break Vortex; SDG: Sidra Gyre; LIW: Levantine Intermediate Water; EMDW: Eastern Mediterranean Deep Water [14]

In the present study, for the specific hydrodynamic analysis, HYCOM, a global system of observations, communications, modelling and assimilation that delivers regular, comprehensive information on the state of the oceans, has been used. The global nowcast / forecast system is a demonstration product of the HYCOM Consortium for data-assimilative ocean modelling sponsored by the National Ocean Partnership Program and partnering projects funded by the Office of Naval Research, the National Science Foundation, the Department of Energy, and the National Oceanic and Atmospheric Administration. It is run operationally at the Naval Oceanographic Office (NAVOCEANO) Major Shared Resource Centre. The model uses atmospheric forcing from the NAVy Global Environmental Model (NAVGEM).

HYCOM is designed as a generalized (hybrid isopycnal/σ/z) coordinate ocean model. It is isopycnal in the open stratified ocean, but it reverts to a terrain-following coordinate in shallow coastal regions and to z-level coordinates near the surface in the mixed layer. The global model has 1/12° of horizontal resolution and is defined on 32 coordinate surfaces in the vertical. The data assimilation is performed using the Navy Coupled Ocean Data Assimilation (NCODA) [15], and it assimilates available satellite altimeter observations (along track obtained via the NAVOCEANO Altimeter Data Fusion Center), satellite, and in situ sea surface temperature (SST), as well as in situ vertical temperature and salinity profiles from XBTs, ARGO floats and moored buoys.

Available data are daily averages of temperature, salinity and half-hourly mean of sea surface height and currents. The HYCOM model does not include tides.

Figure 3-17, Figure 3-18 and Figure 3-19 provide an example of currents, temperature and salinity for the extended area of interest of the present study at the surface layer.

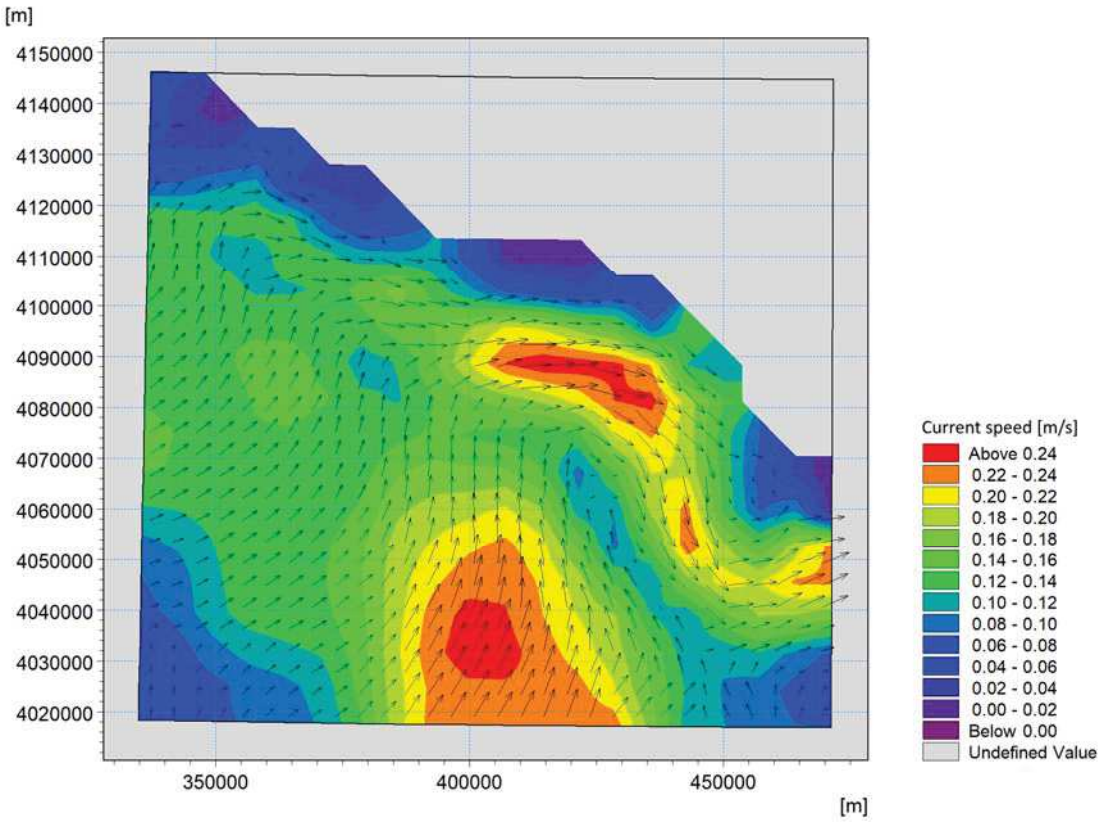

Figure 3-17 Example of current field from the HYCOM global dataset in the area of interest at surface layer

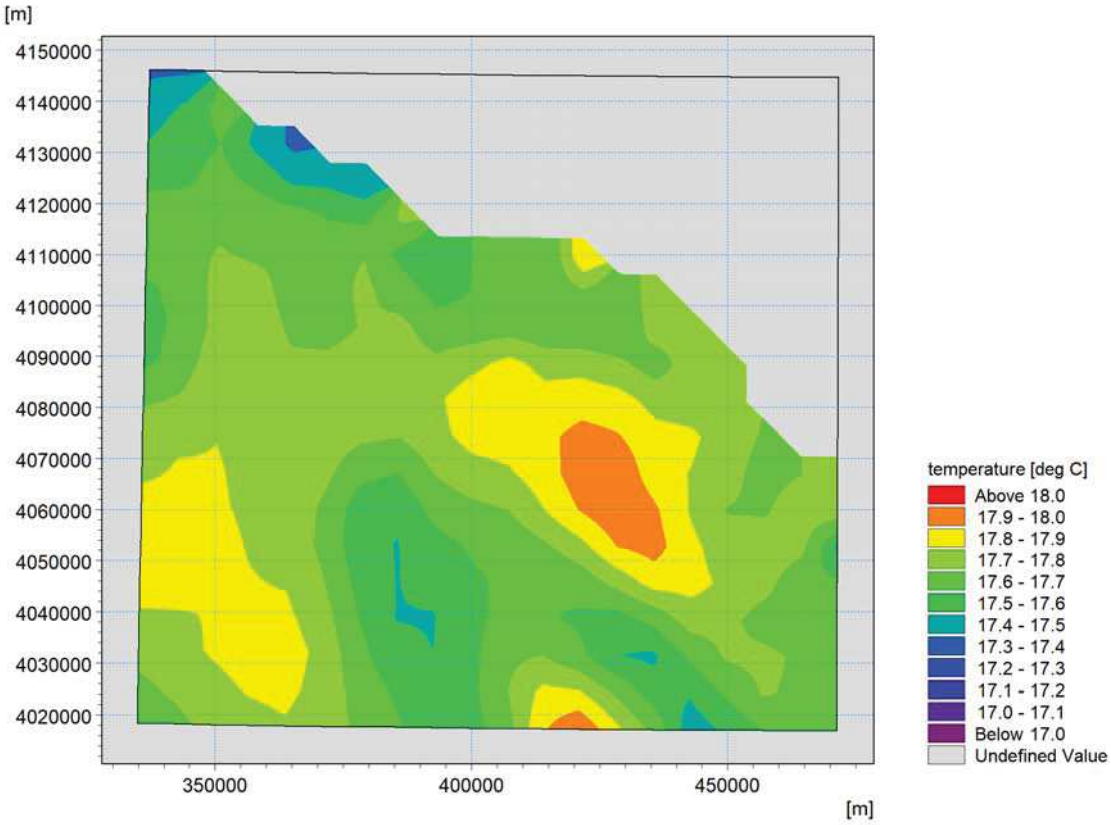

Figure 3-18 Example of temperature field from the HYCOM global dataset in the area of interest at surface layer

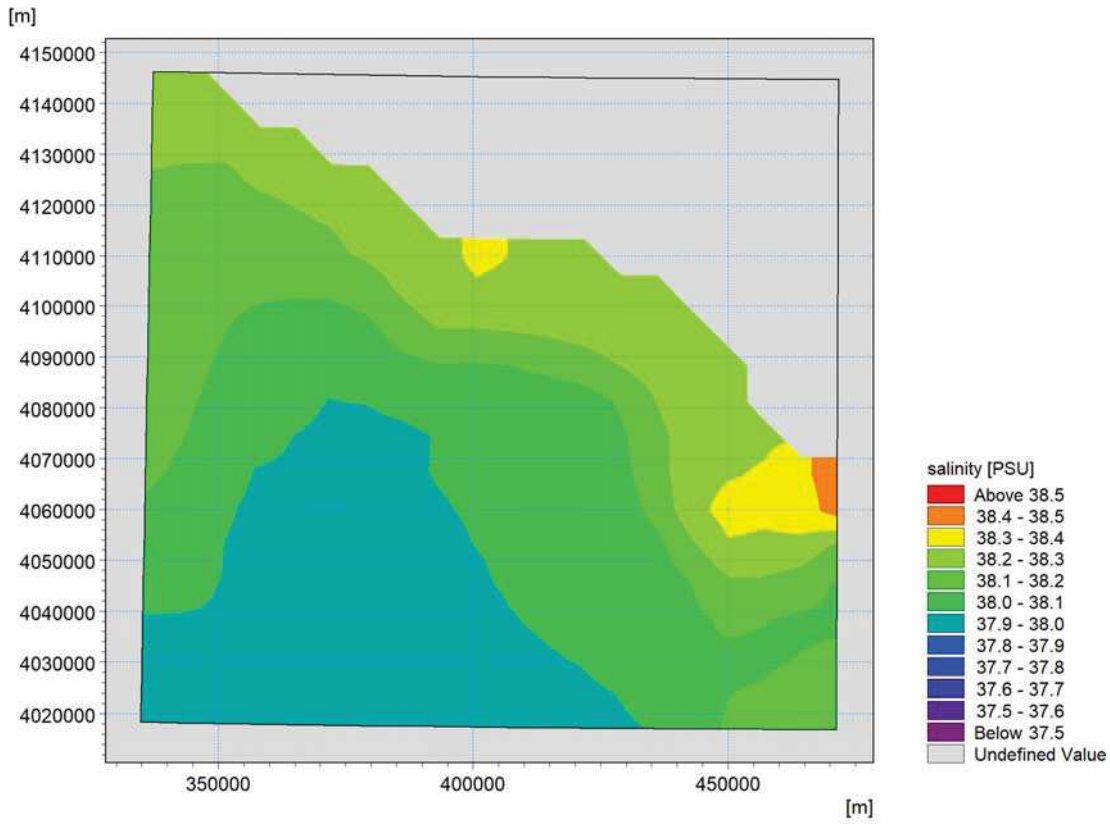

Figure 3-19 Example of salinity field from the HYCOM global dataset in the area of interest at surface layer

3.6.1 Tidal dataset

As tides are not included in HYCOM model, for the tidal analysis, the global ocean tide model DTU10 (Technical University of Denmark) [16] has been applied. This model is developed based on FES2004 (Finite Element Solutions) and the 'response method' (Munk and Cartwright, 1966). Using the latest seventeen years multi-mission measurements from TOPEX/POSEIDON [17] (phase A and phase B), Jason 1 (phase A and phase B) and Jason 2 satellite altimetry for sea level residuals analysis, the harmonic coefficients corresponding to the new global ocean tide model are developed.

The new model is validated with coastal tide gauge measurements over the Northwest European Shelf region and Eastern China Sea. The spatial resolution is 0.125º x 0.125º, including the 12 major tidal constituents.

In order to include the tidal signal in the high-resolution model, these tidal data has been added to sea surface height derived from HYCOM dataset, for initial and boundaries conditions.

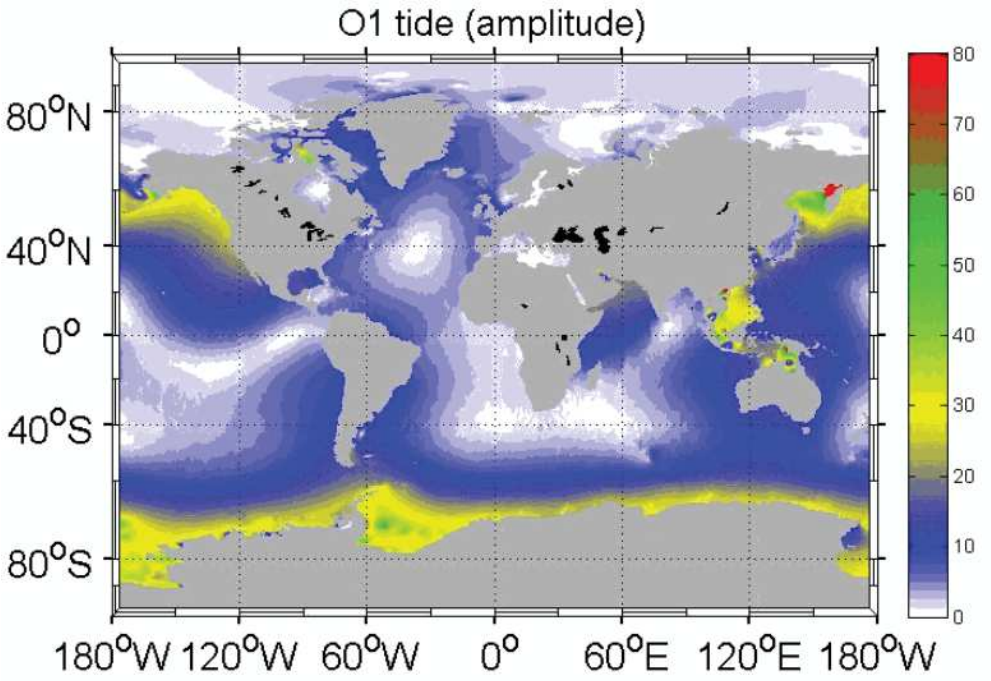

Figure 3-20 Example of tidal constituent O1 in the global ocean tide model DTU10

4.0 SELECTION OF HYDRODYNAMIC SIMULATION PERIODS

One of the most important steps in the setup of a numerical model is the selection of a suitable period which is at the same time long enough to be representative of the meteo-marine variability in the area and able to guarantee reasonable computational efforts.

As suggested by the ISPRA guidelines "Mathematical modelling in the assessment of physical effects induced by sediment handling in marine-coastal areas" [1], the methodology that considers a real period, long enough, instead of different scenarios, allows to take into consideration the infra-annual variations of the main forcing that influence the hydrodynamics and consequently the transport and fate of the plume after the release of fine sediments in the water column during dredging operations.

In order to select a representative period, a specific multi-yearly analysis of the HYCOM dataset has been carried out to identify a specific year without significant anomalies in the area offshore Gela. Results of this analysis showed that year 2017 is well representative of standard conditions, without extreme values of currents and sea temperature (the most relevant variables for the present scope of work). So, year 2017 has been considered as the reference year for the present study.

As the specific period of dredging operations is not yet known, two periods of one month have been taken into account: one is representative for the summer/spring season (higher thermal stratification, lower current speed) and the other one for the winter/autumn period (weaker thermal stratification, higher current speed).

In particular, HYCOM data of current speed for year 2017, averaged throughout the water column, has been analyzed in order to calculate the mean and maxima values in the area where the trench is planned. The results of the analysis, shown in Table 4-1, allowed to select two specific months, January and June, characterized respectively by the most intense currents (January, the average and the maximum values being the highest of the year) and one by a general slow current (June, the average and the maximum values being the lowest of the year).

Table 4-1 Mean and maximum values of current speed, averaged throughout the water column, at the point E 437010m, N 4097990m for the year 2017

	Current speed [m/s]	
Month	**mean**	**maximum**
January	**0.105**	**0.402**
February	0.069	0.359
March	0.089	0.491

April	0.076	0.227
May	0.076	0.299
June	**0.061**	**0.194**
July	0.085	0.320
August	0.071	0.308
September	0.064	0.232
October	0.072	0.307
November	0.085	0.287
December	0.083	0.309

These two months have been considered to implement the high-resolution 3D hydrodynamic model, described in chapter 6.0 , which forms the basis for the fine sediment transport and fate model, described in chapter 7.0.

As aforementioned, the simulation of a long period hydrodynamics (in the order of months or more) allows to study the dispersion and transport of the sediment according to a fully realistic approach, thus overcoming the limits of synthetic / most probable scenarios approach. Through a “moving time-windows” approach, the dredging operations can be simulated several times under different hydrodynamic conditions, in full compliance with the indications provided by ISPRA in its guidelines [1].

The “moving window” approach essentially implies that the dredging operations (which are very fast, i.e. about 2 days – details are illustrated in section 6.0) might take place in a number of sub-periods within the representative period of 1 month. Hence, 10 simulations of sediment transport and fate (i.e. moving time windows) have been carried out for each of the two representative months. Each simulation is independent. The results of the 10 simulations in January and of the 10 simulations in June have been then post-processed in order to assess the most probable extension of the sediment plume, the maximum values of suspended sediment concentration, the persistence of sediment concentration over specific thresholds around the trench area and the mostly subjected areas to high sediment deposition within the domain.

5.0 PROJECT DETAILS

The trench is located at HDD exit at the Gela landfall of the pipeline, at a distance from the coastline of approximately 1.2km, at a depth of about 8.4m. It will be excavated before jack-up mobilization and rig set up and the dredging operations will be carried out starting from land. The geometry of the planned trench can be summarized as follows:

- bottom width: 3 m;
- lateral slope: variable with the characteristics of the soil (assuming 1:3);
- longitudinal length: 100 m;
- depth: variable from 4.4 m at punch out to the natural seabed;
- volume of sediment to be excavated: 2'500 m^3.

The plan view and the cross section of the trench are illustrated in Figure 5-1 and Figure 5-2, respectively.

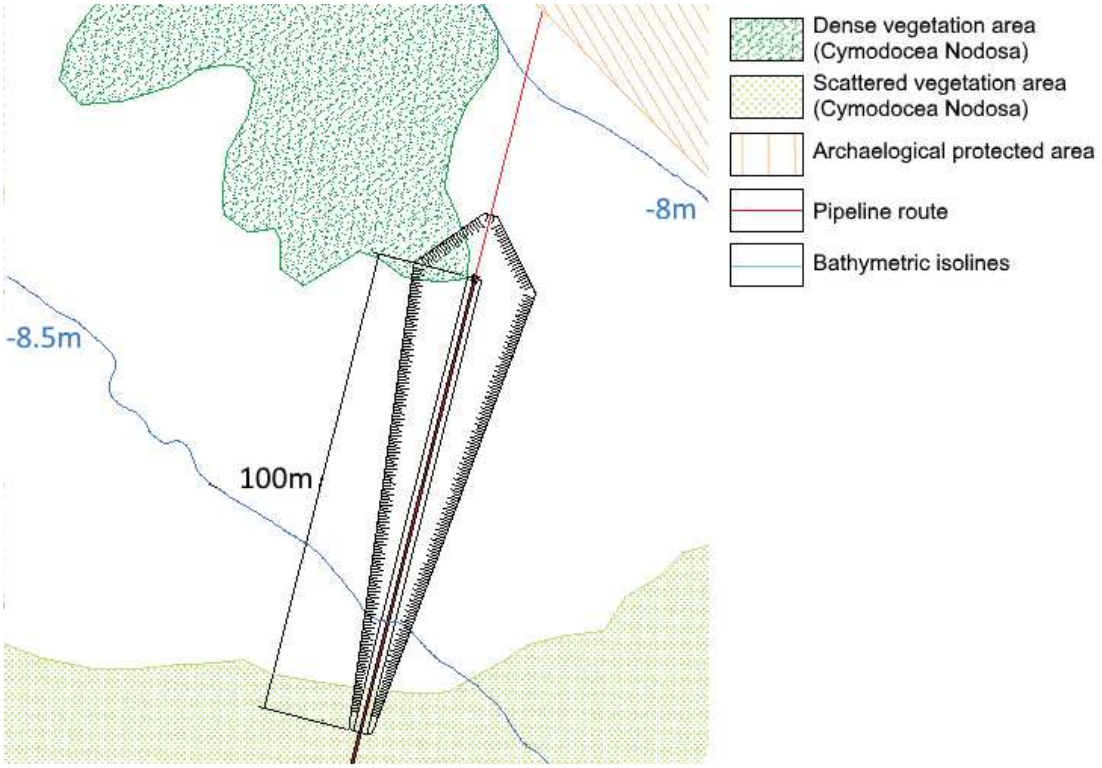

Figure 5-1 Transition trench (in black) at HDD exit at the Gela landfall site – plan view

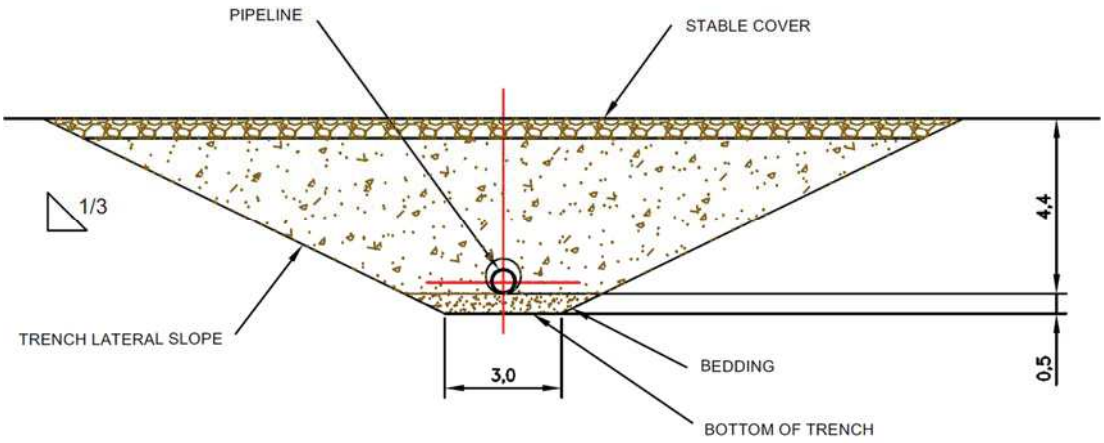

Figure 5-2 Example of trench cross section at HDD exit point at the Gela landfall site

The methodologies planned for the dredging operations are based on the use of a Backhoe Dredger (BHD – an example is shown in Figure 5-3), that has been considered as the most suitable equipment to perform such work considering the availability, speed of execution and costs. The dredger will remain in the area during the entire duration of the activities, to maintain the required depth of the bottom trench and / or the stability of the lateral slopes, in case of possible seabed variations induced by the actions of wave and / or current.

This kind of dredger generates quantitative of fine sediments spilled out of the bucket, and thus dispersed along the water column during the dredging operations, leaving out the load / transport phases and the potential overflow, in the order of 5% of the total fines, as suggested in literature [18] [19] [20]. Besides, the use of Backhoe Dredger suggests considering the release of sediment uniformly along the entire column of water, as it is normally advised in literature [20].

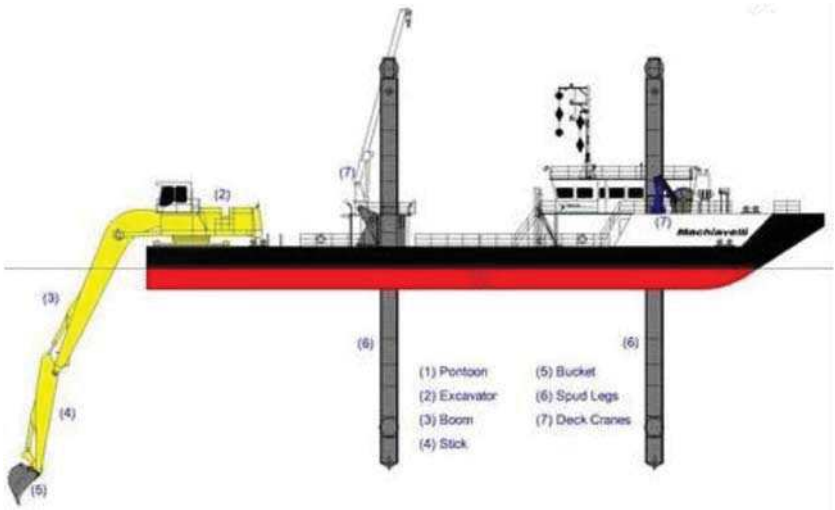

Figure 5-3 Example of Backhoe Dredger (BHD)

The backhoe dredger that will be used can dig 50-60m^3/hr, in case the soil is not stronger than 3-5MPa, and 24/24 hours operability. Given the expected productivity, the assumed duration of the operations is in the order of 40-50 h.

6.0 HIGH-RESOLUTION CIRCULATION MODEL

A high-resolution model of the Gulf of Gela has been implemented through a realistic nesting within the larger scale ocean circulation model HYCOM, introduced in the section 3.6. The downscaling is fully realistic, meaning that all the most important parameters involved in the numerical resolution of the primitive equations of the ocean (atmospheric forcing and boundary conditions) come from deterministic operational models.

The high-resolution numerical model used is MIKE 3 HD [2]. The model is based on a flexible mesh approach (Figure 6-1 and Figure 6-2 show an example of a horizontal and a vertical mesh respectively in a sample domain) and it has been developed for applications within oceanographic, coastal and estuarine environments.

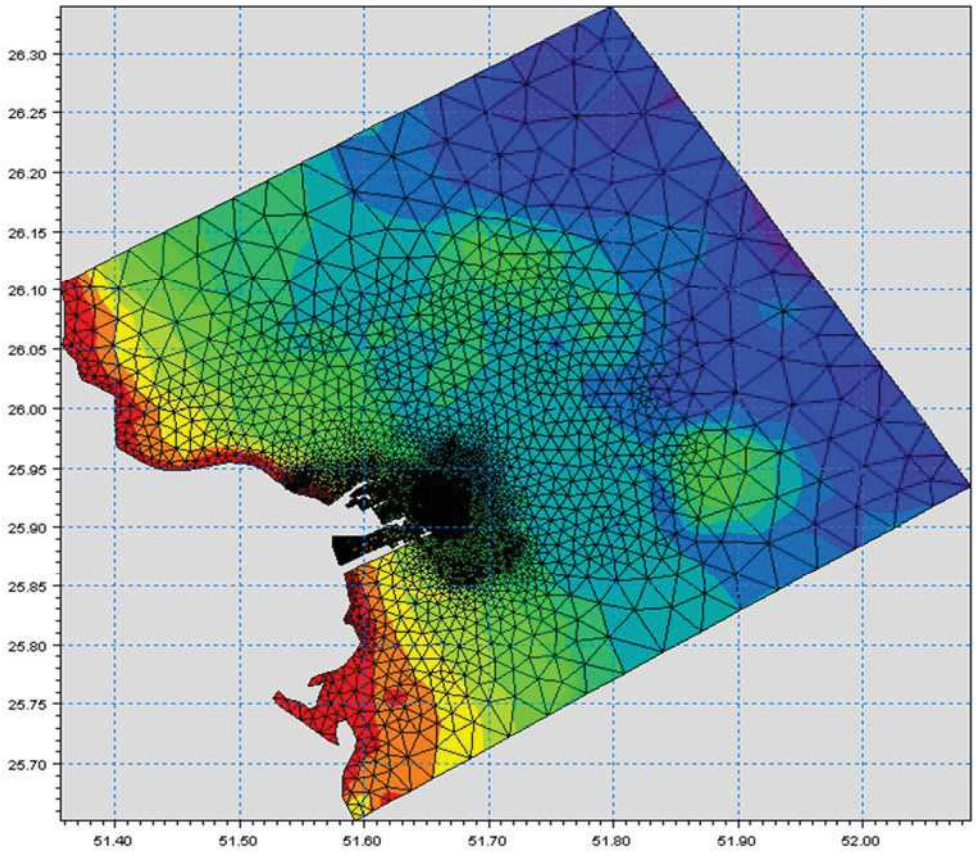

Figure 6-1 Example of horizontal mesh for a general domain

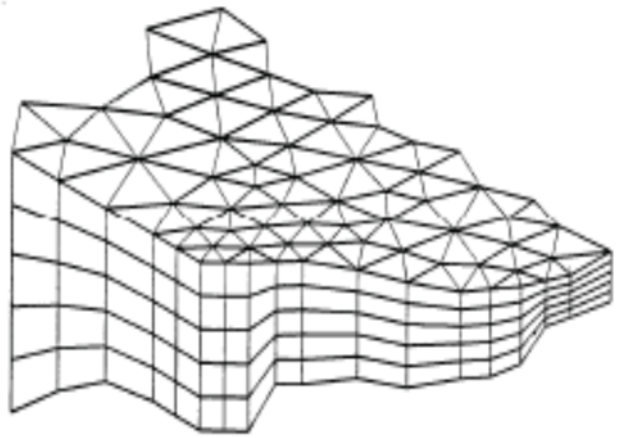

Figure 6-2 Example of vertical mesh for a general domain

The computational code solves the primitive equations of motion under hydrostatic conditions numerically. Density does not depend on pressure, but exclusively on water temperature and salinity.

As for the numerical discretization approach, MIKE 3 is based on finite volumes centred on the single element. In the horizontal direction, a flexible mesh approach is adopted, with the possibility of triangular and quadrilateral elements, whereas along the vertical a threefold approach is possible: σ levels, z levels or hybrid σ-z.

A short description of MIKE 3 FM model is illustrated in Appendix A.

6.1 Model bathymetry and computational grid

As introduced in section 3.2, the digitization of bathymetric data and the import procedures within MIKE environment has been carried out through using two different datasets. In particular, where the different sources of available data may be overlapping, a higher priority has been assigned to the detailed survey.

Figure 6-3 shows the model bathymetry and domain of the high-resolution model resulting from the digitization of the bathymetric datasets.

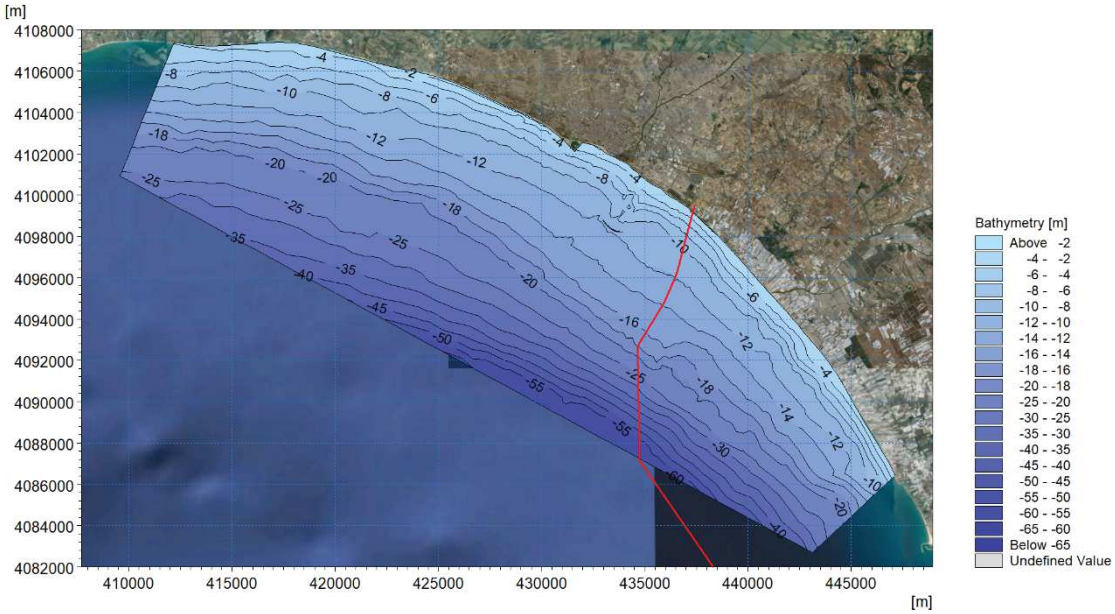

Figure 6-3 Model bathymetry used for high-resolution 3D circulation model. In red the planned route of the pipeline

The computational mesh has an extension of approximately 38km and 6-12km along the directions respectively parallel and perpendicular to the coastline. The maximum water depth in the domain is about 60m. The total number of horizontal elements is approximately 17'000. In the area around the planned trench, the computational mesh has a horizontal resolution of approximately 10m (the highest within the domain). The horizontal resolution decreases gradually leaving this area spanning four more areas with variable resolution from 30m to 850m, at the nesting boundary line with the HYCOM model. Figure 6-4 shows the computational mesh of the model, superimposed on the bathymetry, while Figure 6-5 shows a detail around the trench.

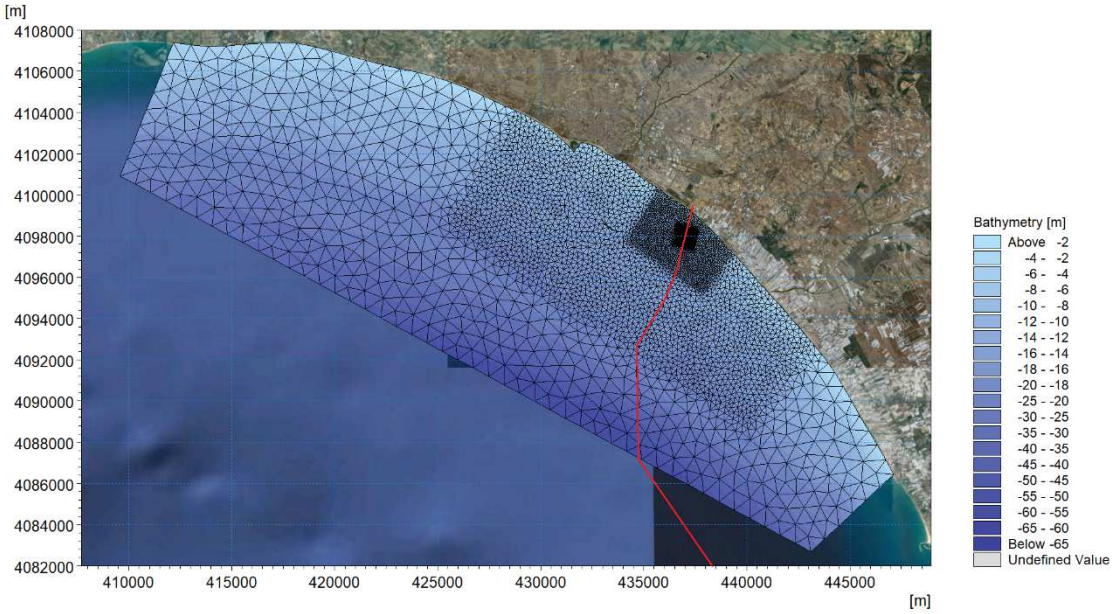

Figure 6-4 Computational mesh used for high-resolution 3D circulation model. The planned route of the pipeline is indicated in red

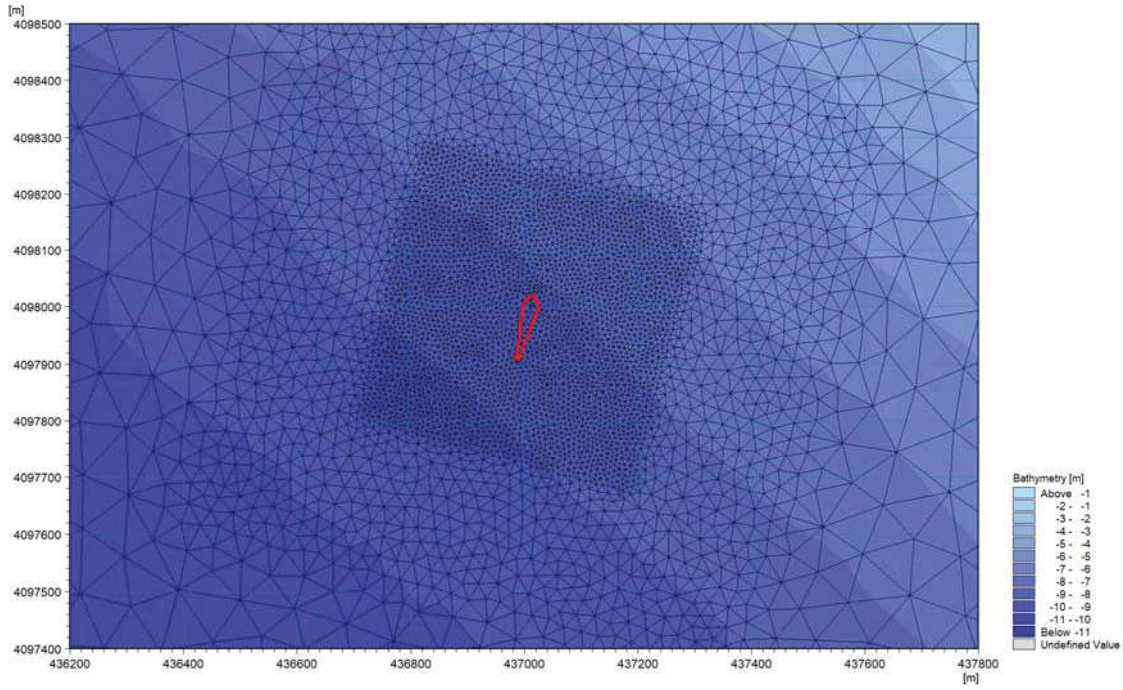

Figure 6-5 Detail of the computational mesh. The excavation area, at the exit point of the HDD is highlighted in red

For what concerns the vertical direction, the model is discretised by 8 vertical sigma σ or *terrain-follow* coordinates equidistant levels (Figure 6-6).

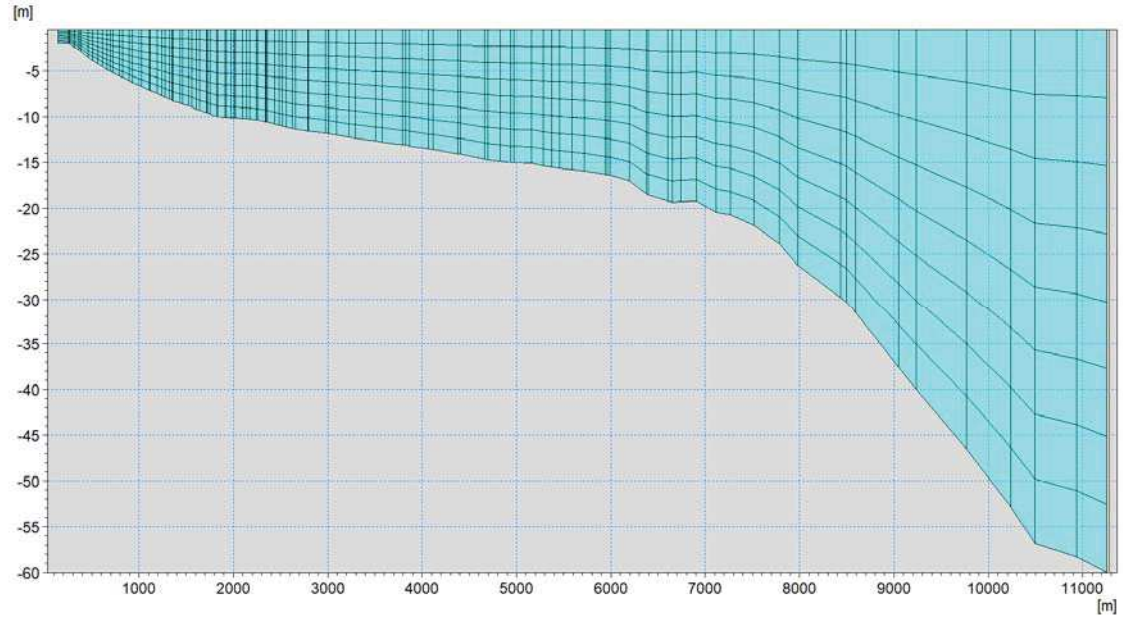

Figure 6-6 Vertical discretization of the 3D high-resolution model

6.2 Forcing data and model characteristics

The forcing data used for the atmospheric component of the 3D high-resolution model come from the reanalyses of the Climate Forecast System (CFSR) [11], described in section 3.5. The variables used in the implementation of the downscaling procedures aiming at building the 3D model of the Gulf of Gela are:

- wind intensity and direction at 10m;

- precipitation;
- mean Sea Level Pressure;
- cloud cover;
- air temperature at 2m;
- relative humidity.

At the open boundary lines, the high resolution 3D model is forced by the HYCOM data of temperature, salinity, meridional and zonal velocities and sea surface height (section 3.6). Sea surface height includes also tides from the Global Tide Model developed by DTU Space (section 3.6.1). Rivers are not included in the model.

The 3D high-resolution model has been implemented and run for two different periods, each one long 1 month (January 2017 and June 2017), as described in chapter 0.

The results have been saved every 15 minutes over the entire domain and over all the 8 vertical levels.

The below table summarizes the main characteristics of the implemented 3D high resolution model.

Table 6-1Characteristics of the implementation of the 3D high-resolution hydrodynamic model

Numerical model	MIKE 3 FM
Horizontal resolution (min/max)	10m/850m
Typology of computational grid	Finite volumes
Vertical resolution	8 equidistant σ levels
Integration period	January 2017 and June 2017
Temporal frequency of output	15-minutes snapshots
Atmospheric forcing	CFS (Climate Forecast System): – Horizontal resolution 0.2° – Time frequency: hourly – Available data: U, V, MSLP, T2m, Precipitation, Relative Humidity, Cloud Cover.
Initial conditions	Instantaneous from HYCOM (U, V, T, S, SSH)
Open Boundary data	Realistic from HYCOM model at 1/12° horizontal resolution
Open Boundary Condition	Flather boundary condition [21] [22]
Rivers	No
Air-sea fluxes	Momentum: yes Heat: yes Mass: yes
Data assimilation	No
Tides	Yes

6.2.1 Results of the high-resolution 3D hydrodynamic model

In this section some examples of the results of the 3D hydrodynamic model as instantaneous maps during January and June 2017 are shown. As maps are only representative of some specific snapshots captured during the overall studied period of 2 months, the roses of current speed in the trench area, for the two months, have also been reported.

Roses are useful to better understand the main pattern of circulation in the zone of the dredging operations and, consequently, to support the proper selection of the most

representative snapshots (maps). The roses of current have been plotted at surface and at the sea bottom.

The roses at surface (Figure 6-7 and Figure 6-9) show that in general the current flows parallel to the coastline. The prevailing direction, i.e. the most frequent directional sector characterized by the highest velocities, is from North-West to South-East, both in winter and summer seasons. In particular, in January the most significant current direction is between 120°N and 135°N, characterized by a very high frequency, of about 50%, and a maximum value of current speed of about 0.4m/s. In June, the main sector is wider: the most frequent directions are between 105°N and 150°N, and between 300°N and 315°N, while the maximum velocities are approximately equal to 0.3m/s to the directions 120-135°N, as during the winter scenario.

At the bottom layer, during winter (Figure 6-8), the trend is very similar to the one described for the surface, but it is characterized by smaller current intensities (maximum velocity is about 0.25m/s). During summer (Figure 6-10), velocities at the sea bottom layer are very low, always below 0.1m/s and the circulation pattern is more chaotic. The most frequent fluxes are however from North-West to South-East, as it happens at surface, but with a lower frequency.

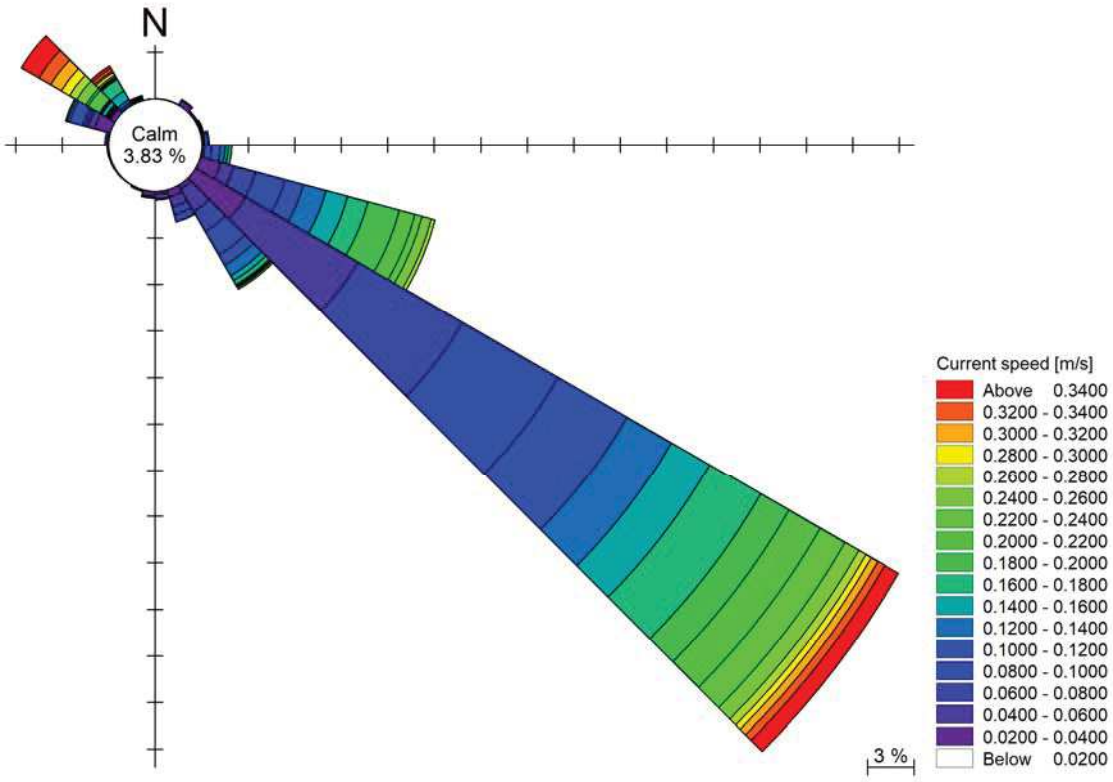

Figure 6-7 Roses of modelled currents at surface in January 2017. Direction is "flowing to"

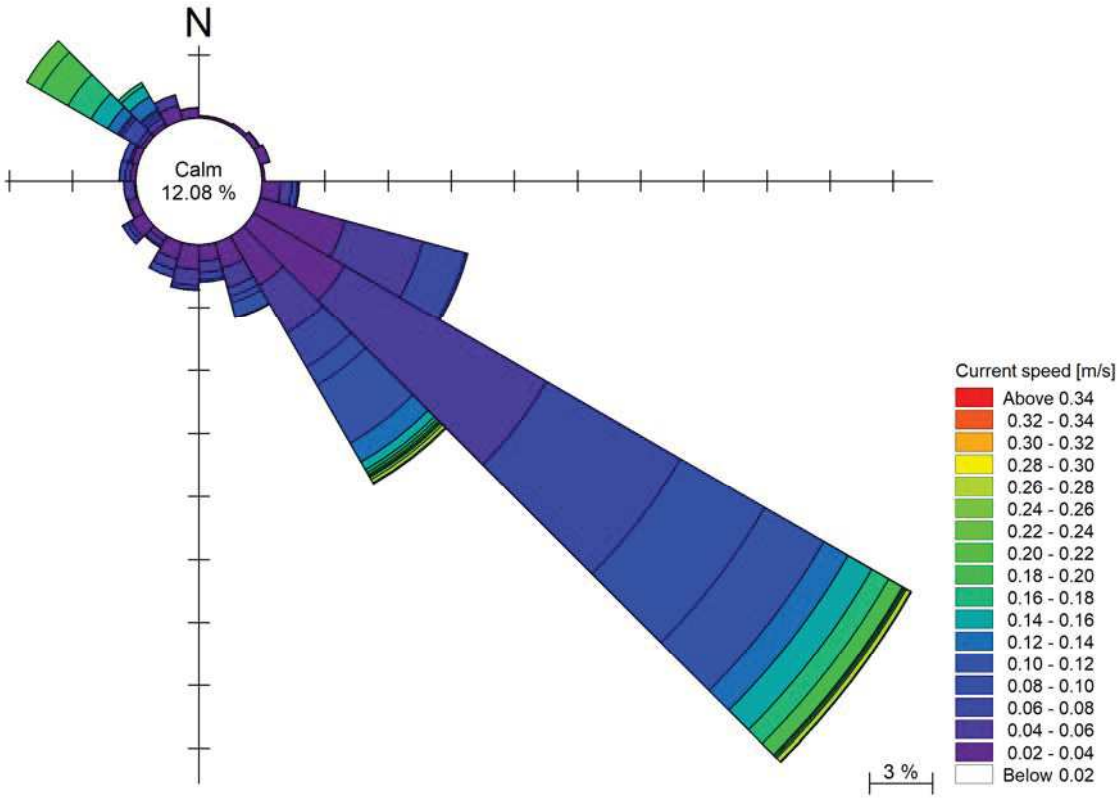

Figure 6-8 Roses of modelled currents at the sea bottom in January 2017. Direction is "flowing to"

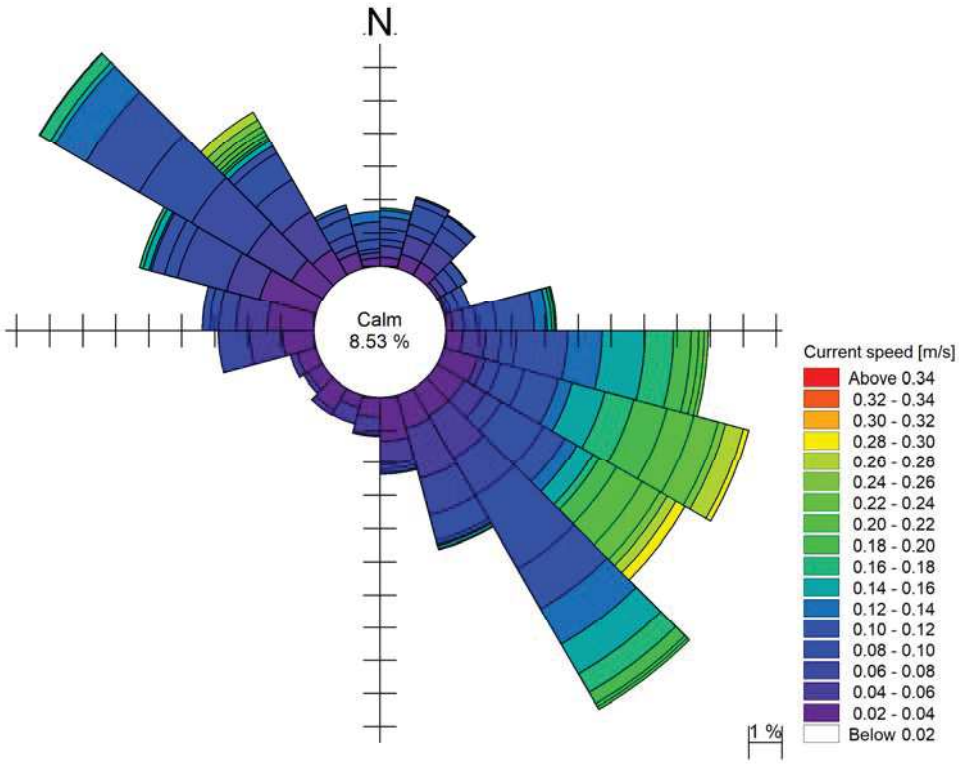

Figure 6-9 Roses of modelled currents at surface in June 2017. Direction is "flowing to"

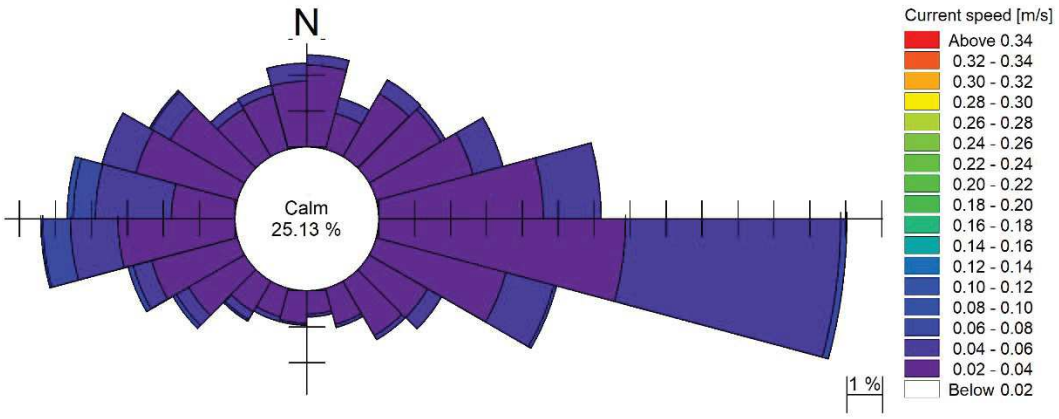

Figure 6-10 Roses of modelled currents at the sea bottom in June 2017. Direction is "flowing to"

The following maps represent the fields of intensity (coloured background) and direction (superimposed arrows) of the currents at three different depths along the water column: surface, intermediate depth and sea bottom. To properly visualize the results in the area of interest, the figures show the current field in a zoomed area of the whole calculation domain.

Maps from Figure 6-11 to Figure 6-13 and from Figure 6-17 to Figure 6-19 represent a specific snapshot during the simulation, respectively in January and in June, characterized by a main current, at surface in the dredged area, from North-West to South-East.

The maps from Figure 6-14 to Figure 6-16 and from Figure 6-20 to Figure 6-22 represent a specific snapshot during the simulation, respectively in January and in June, characterized by a main current, at surface in the dredged area, from South-East to North-West.

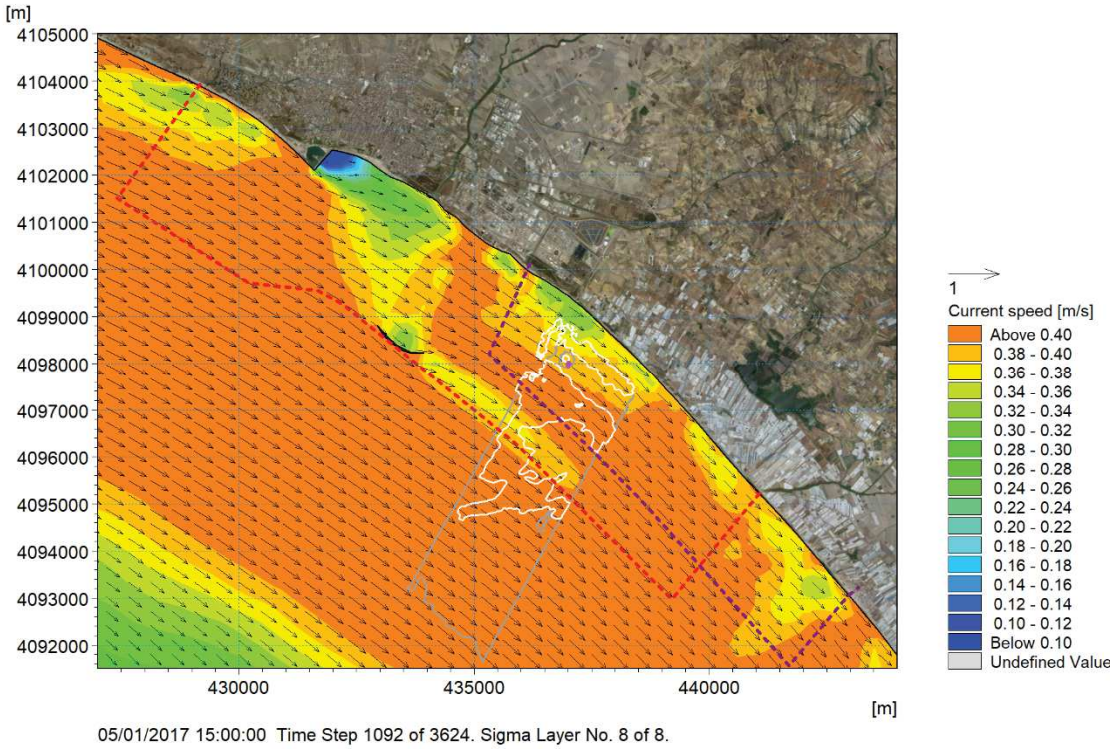

Figure 6-11 Example of surface currents in winter (05.01.2017 h.15:00). Coloured lines indicate: SIN limits (dashed red), ZPS limits (dashed purple), Cymodocea Nodosa meadows limits (in grey the scattered and in white the dense presence). The dot in magenta indicates the trench area

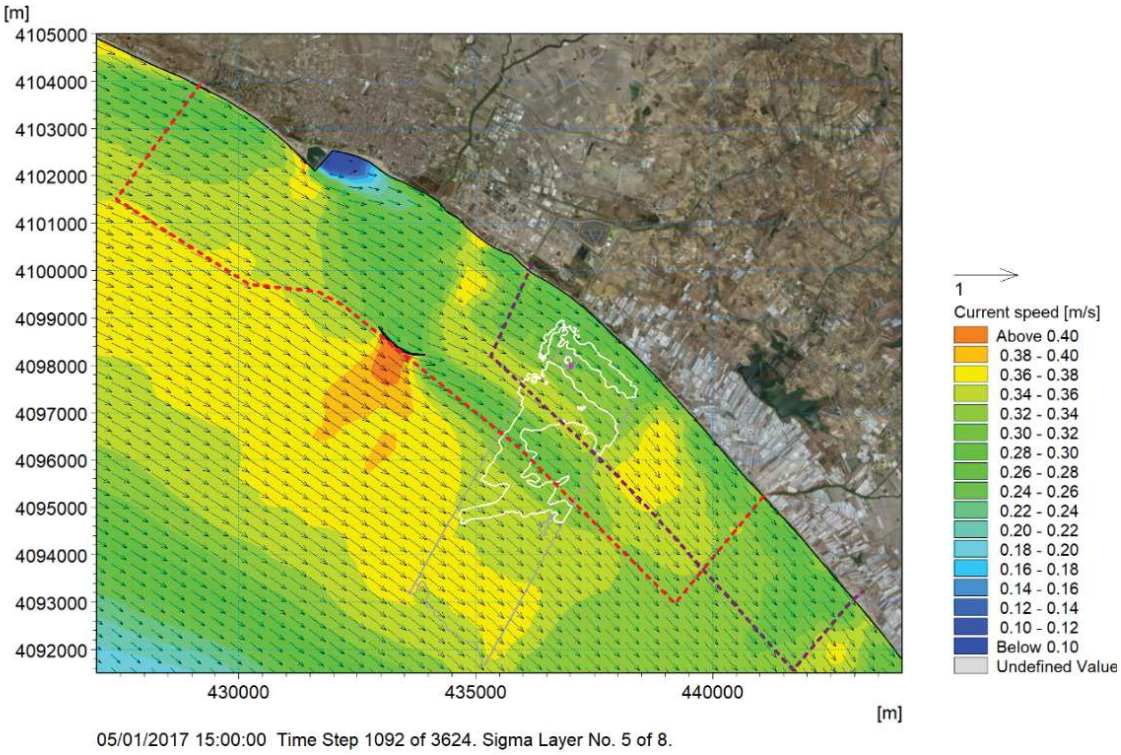

Figure 6-12 Example of mid-depth currents in winter (05.01.2017 h.15:00). Coloured lines indicate: SIN limits (dashed red), ZPS limits (dashed purple), Cymodocea Nodosa meadows limits (in grey the scattered and in white the dense presence). The dot in magenta indicates the trench area

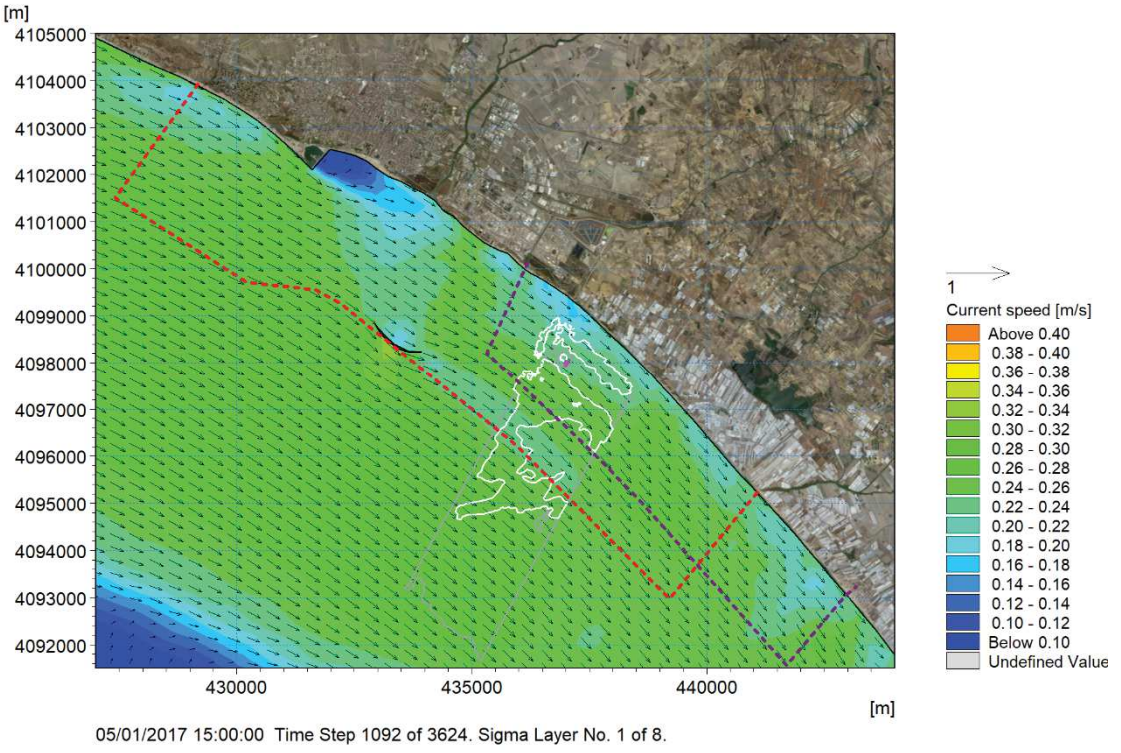

Figure 6-13 Example of bottom currents in winter (05.01.2017 h.15:00). Coloured lines indicate: SIN limits (dashed red), ZPS limits (dashed purple), Cymodocea Nodosa meadows limits (in grey the scattered and in white the dense presence). The dot in magenta indicates the trench area

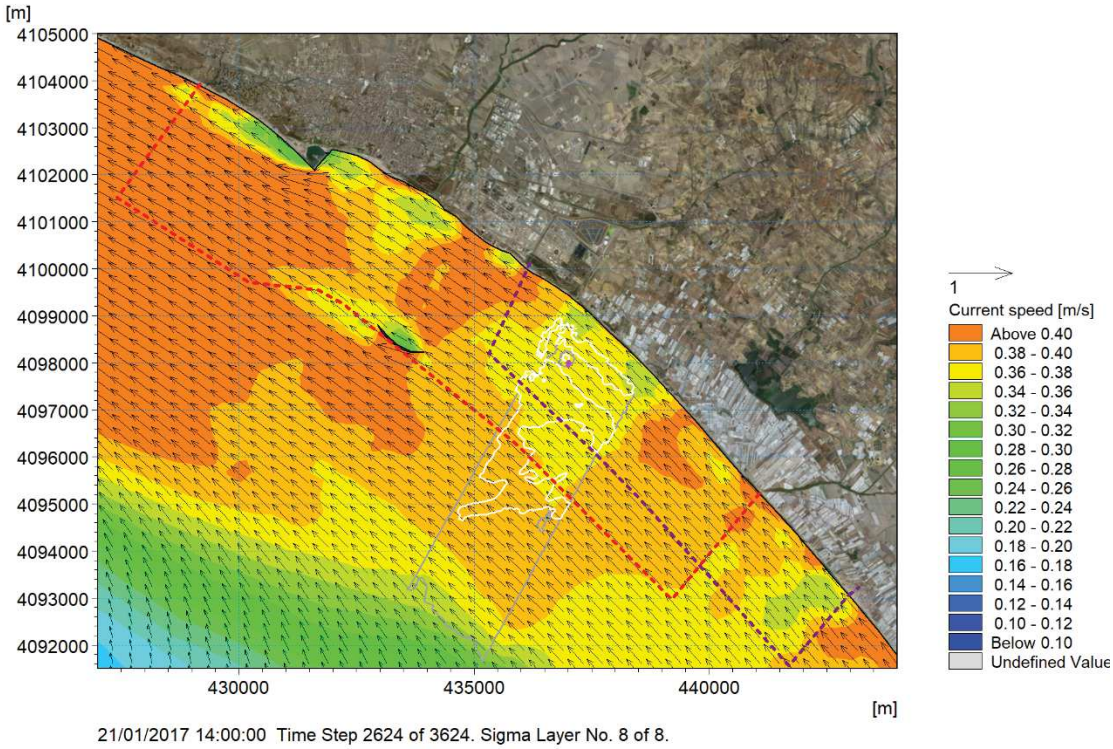

Figure 6-14 Example of surface currents in winter (21.01.2017 h.14:00). Coloured lines indicate: SIN limits (dashed red), ZPS limits (dashed purple), Cymodocea Nodosa meadows limits (in grey the scattered and in white the dense presence). The dot in magenta indicates the trench area

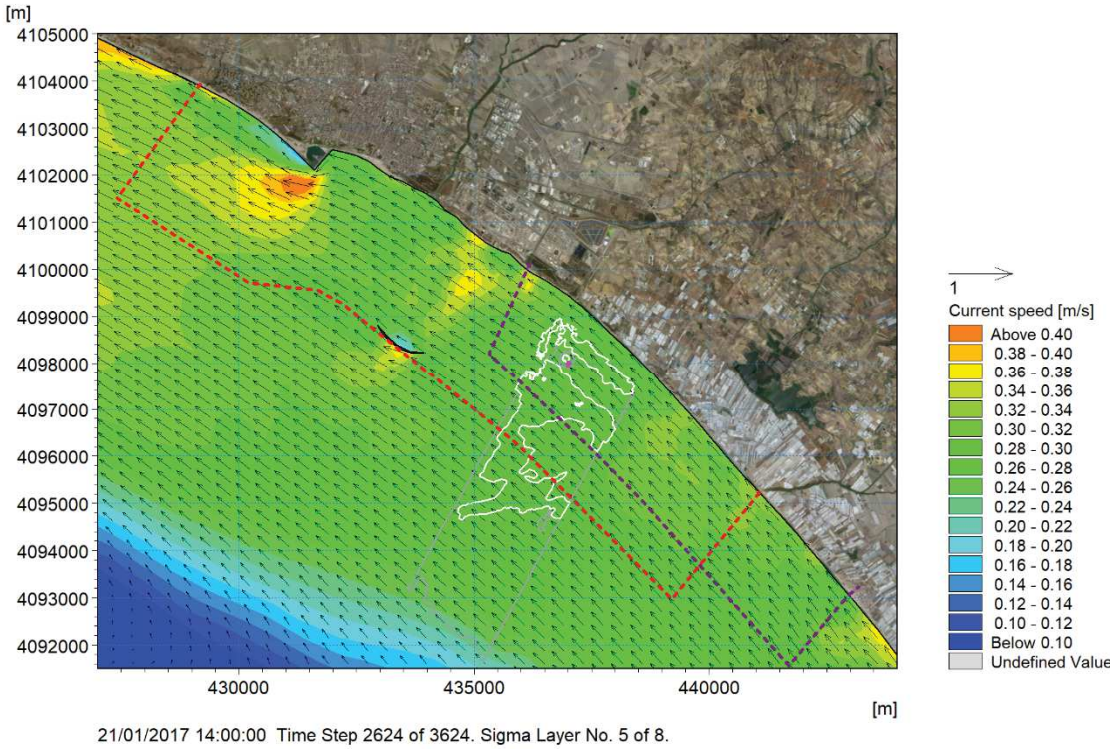

Figure 6-15 Example of mid-depth currents in winter (21.01.2017 h.14:00). Coloured lines indicate: SIN limits (dashed red), ZPS limits (dashed purple), Cymodocea Nodosa meadows limits (in grey the scattered and in white the dense presence). The dot in magenta indicates the trench area

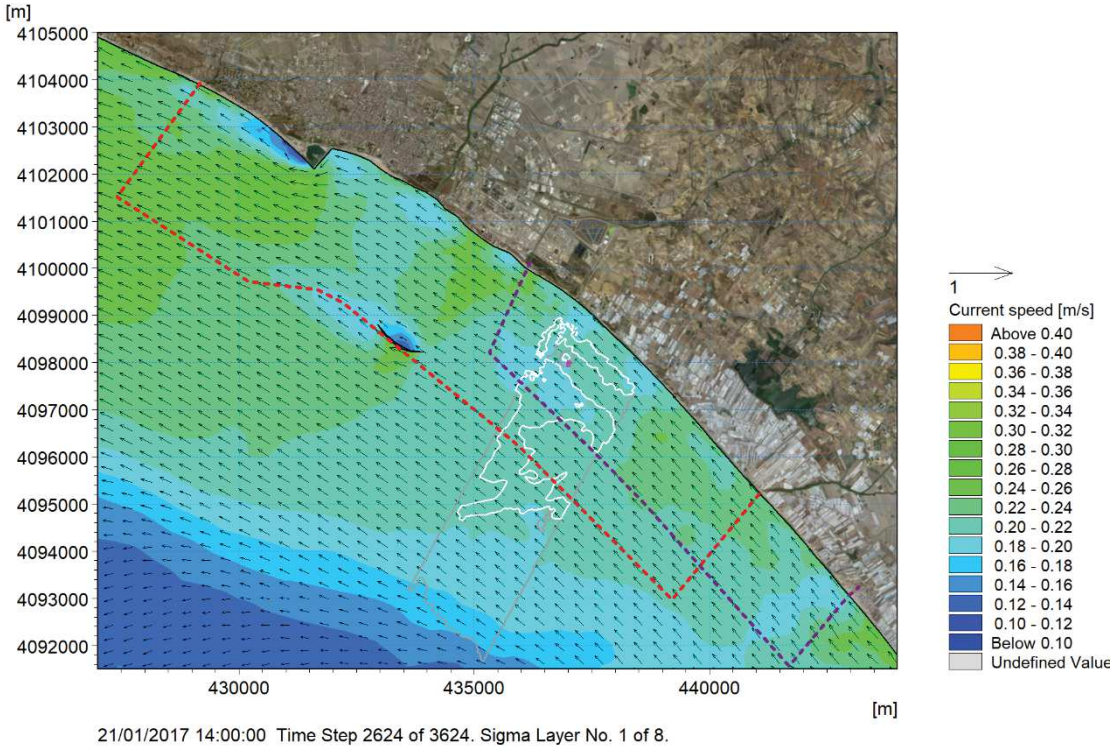

Figure 6-16 Example of bottom currents in winter (21.01.2017 h.14:00). Coloured lines indicate: SIN limits (dashed red), ZPS limits (dashed purple), Cymodocea Nodosa meadows limits (in grey the scattered and in white the dense presence). The dot in magenta indicates the trench area

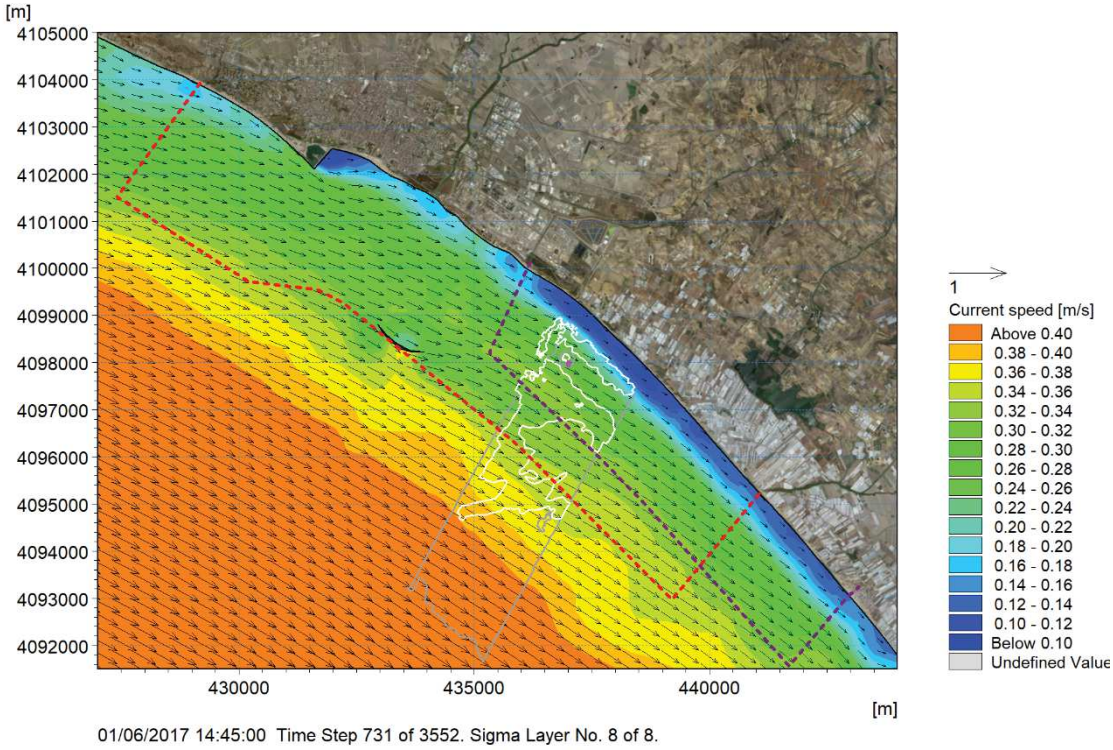

Figure 6-17 Example of surface currents in summer (01.06.2017 h.15:00). Coloured lines indicate: SIN limits (dashed red), ZPS limits (dashed purple), Cymodocea Nodosa meadows limits (in grey the scattered and in white the dense presence). The dot in magenta indicates the trench area

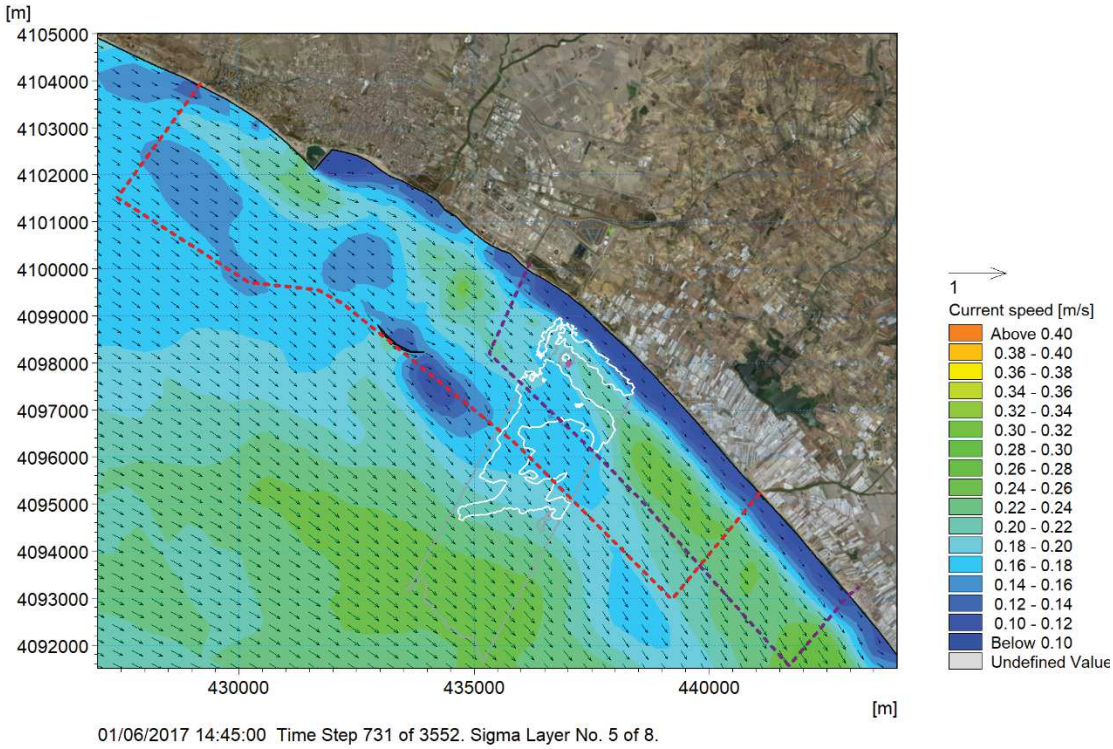

Figure 6-18 Example of mid-depth currents in summer (01.06.2017 h.15:00). Coloured lines indicate: SIN limits (dashed red), ZPS limits (dashed purple), Cymodocea Nodosa meadows limits (in grey the scattered and in white the dense presence). The dot in magenta indicates the trench area

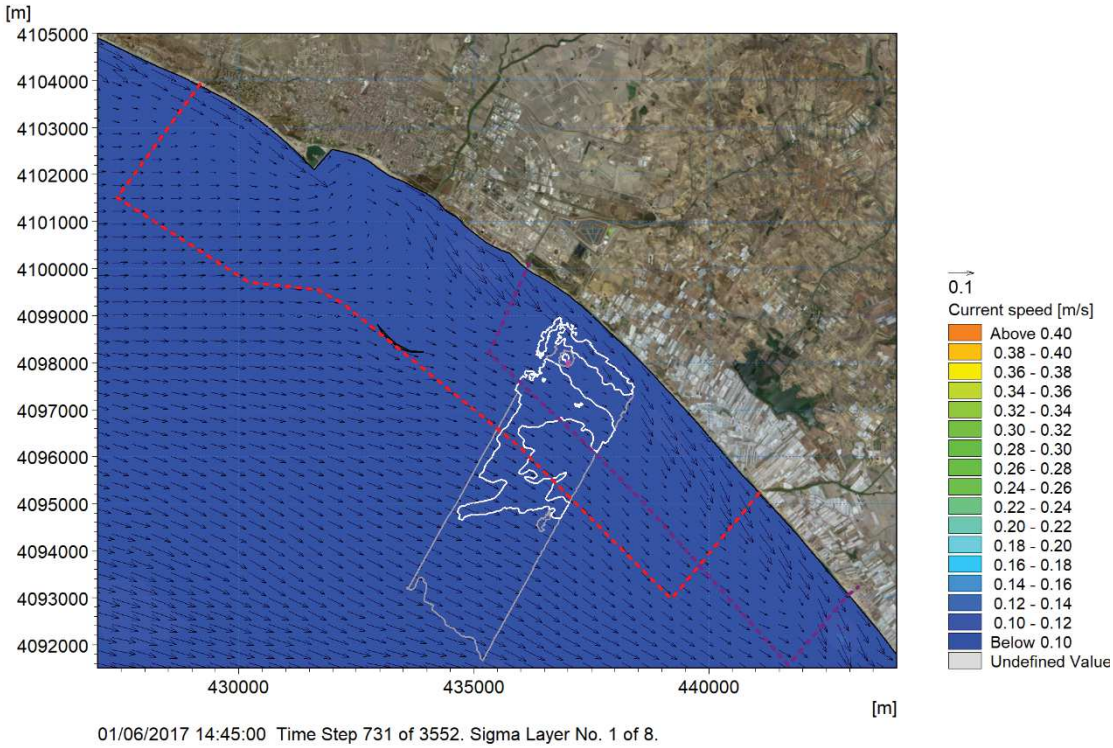

Figure 6-19 Example of bottom currents in summer (01.06.2017 h.15:00). Coloured lines indicate: SIN limits (dashed red), ZPS limits (dashed purple), Cymodocea Nodosa meadows limits (in grey the scattered and in white the dense presence). The dot in magenta indicates the trench area

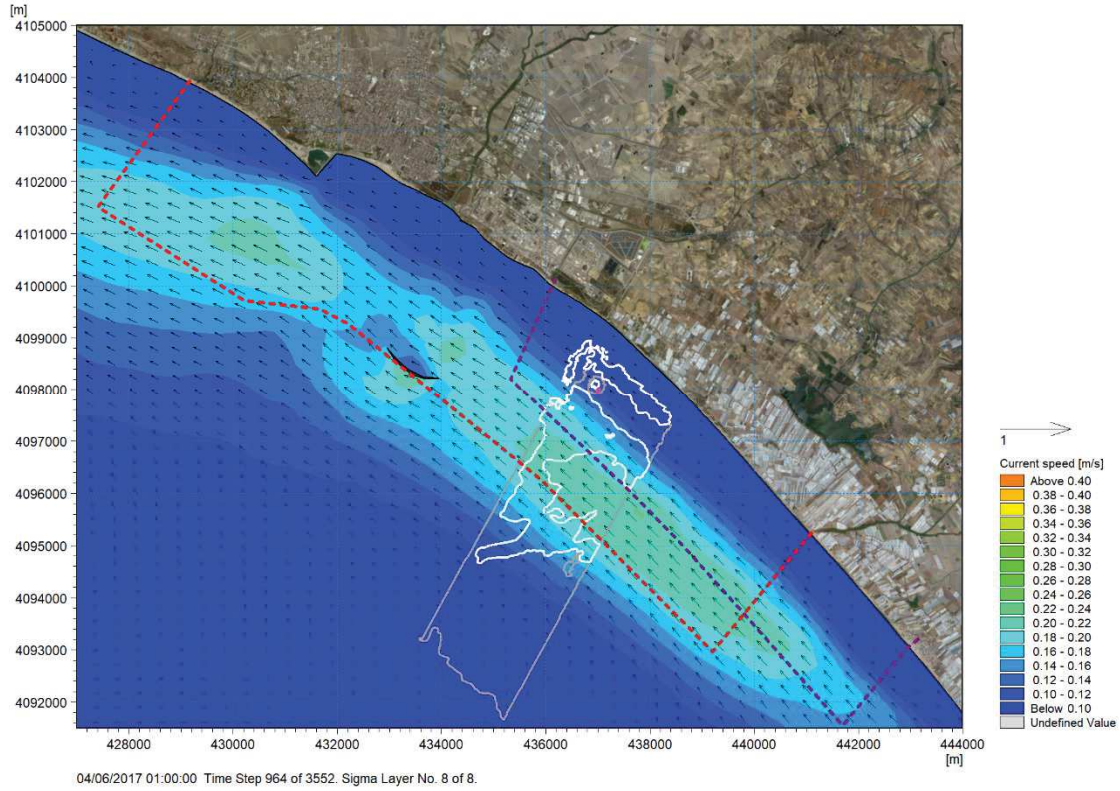

Figure 6-20 Example of surface currents in summer (04.06.2017 h.01:00). Coloured lines indicate: SIN limits (dashed red), ZPS limits (dashed purple), Cymodocea Nodosa meadows limits (in grey the scattered and in white the dense presence). The dot in magenta indicates the trench area

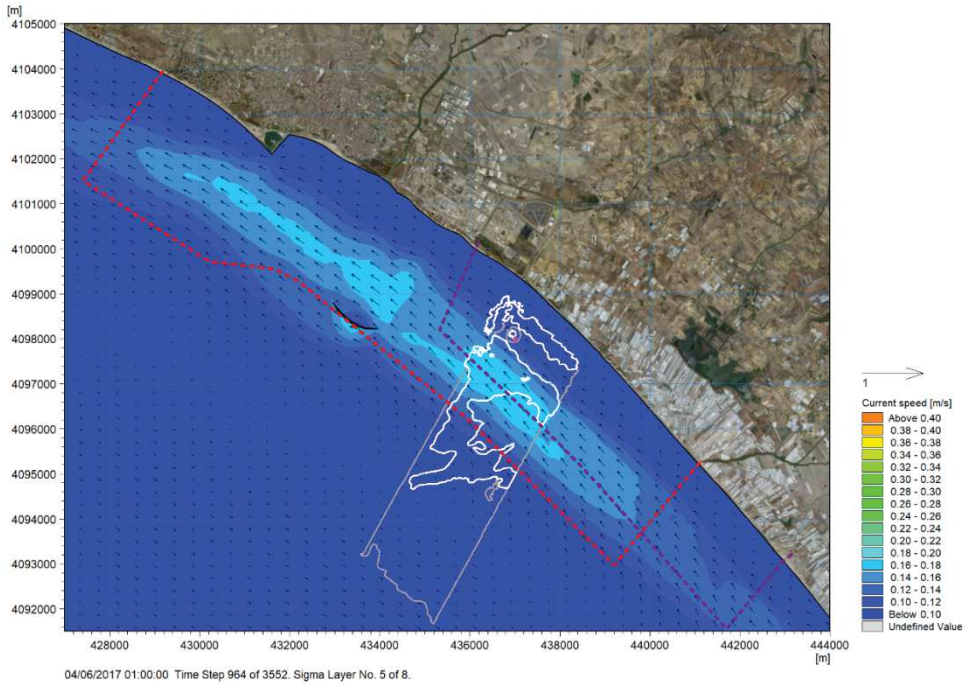

Figure 6-21 Example of mid-depth current in summer (04.06.2017 h.01:00). Coloured lines indicate: SIN limits (dashed red), ZPS limits (dashed purple), Cymodocea Nodosa meadows limits (in grey the scattered and in white the dense presence). The dot in magenta indicates the trench area

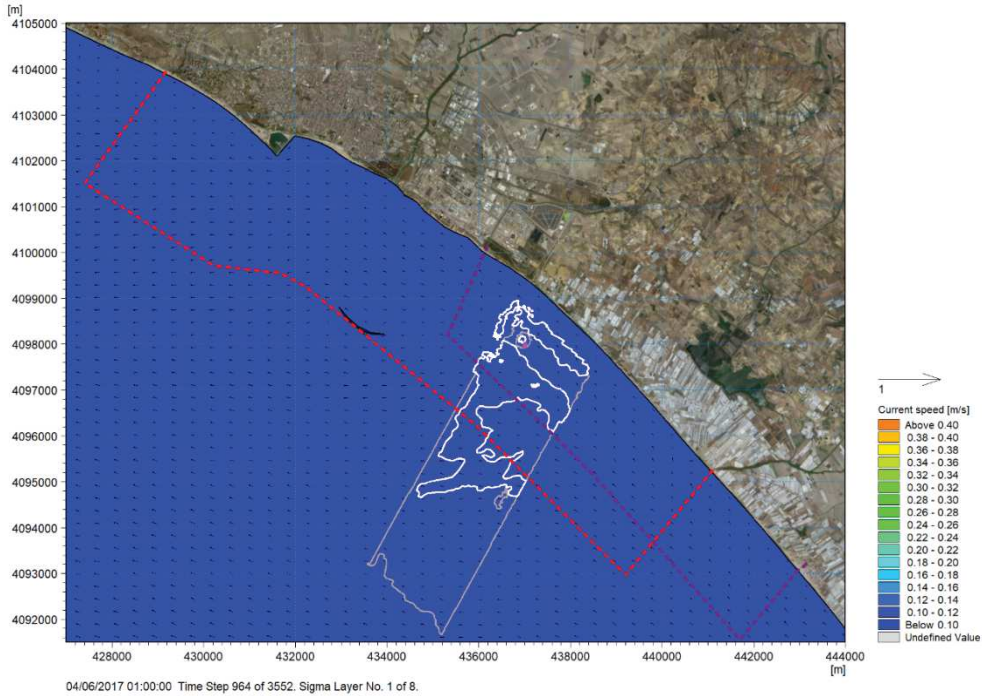

Figure 6-22 Example of bottom current in summer (04.06.2017 h.01:00). Coloured lines indicate: SIN limits (dashed red), ZPS limits (dashed purple), Cymodocea Nodosa meadows limits (in grey the scattered and in white the dense presence). The dot in magenta indicates the trench area

The well mixed temperature throughout the water column, typical of winter conditions, as well as the high thermal stratification, typical of summer conditions, can be clearly derived from the two vertical temperature profiles in Figure 6-23: in the zone of the trench, the average temperature is homogeneous in January, while during June throughout the 8m of water column, a gradient of about 2.5°C can be appreciated.

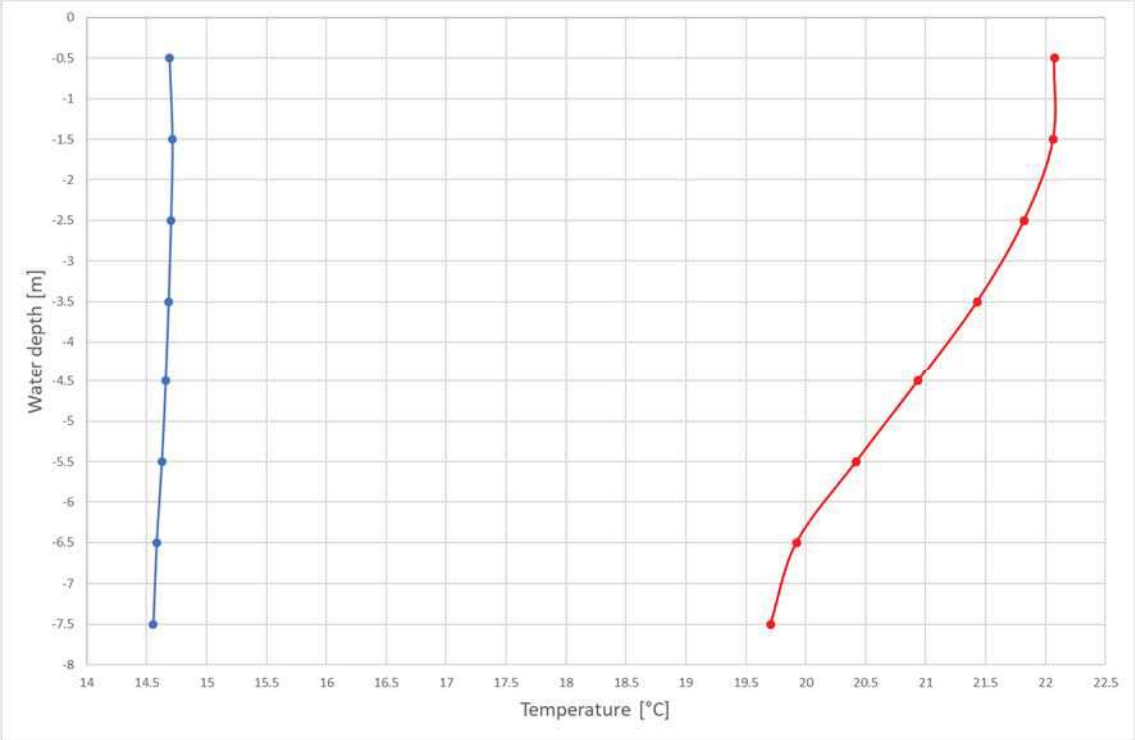

Figure 6-23 Average vertical profile of temperature in January (blue line) and in June (red line)

The following maps represent the fields of temperature at three different depths along the water column (surface, intermediate depth and bottom) for a specific snapshot during the month of January (Figure 6-24, Figure 6-25 and Figure 6-26) and June (Figure 6-27, Figure 6-28 and Figure 6-29).

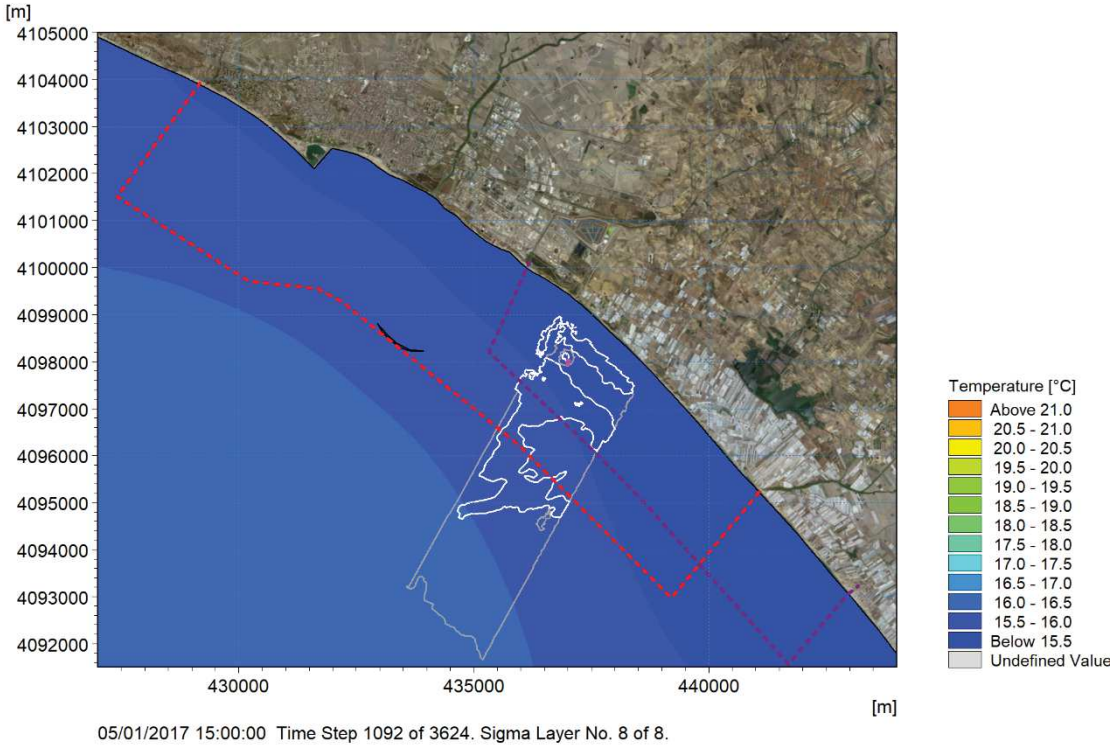

Figure 6-24 Example of surface temperature in winter (05.01.2017 h.15:00). Coloured lines indicate: SIN limits (dashed red), ZPS limits (dashed purple), Cymodocea Nodosa meadows limits (in grey the scattered and in white the dense presence). The dot in magenta indicates the trench area

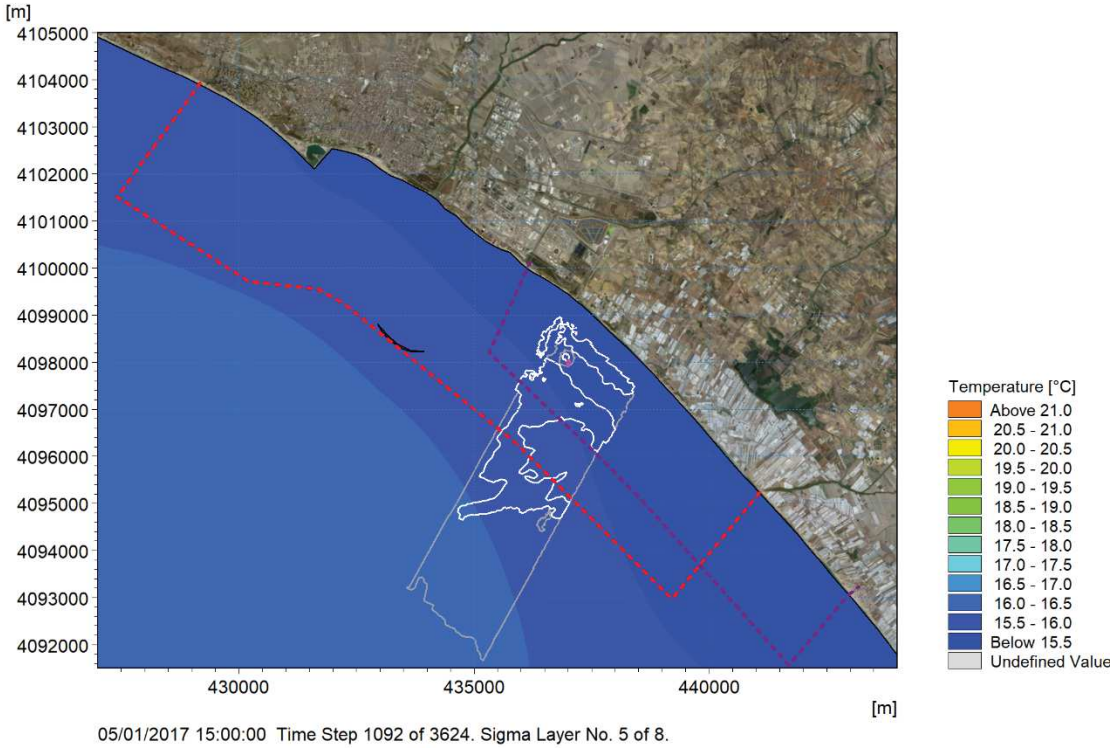

Figure 6-25 Example of mid-depth temperature in winter (05.01.2017 h.15:00). Coloured lines indicate: SIN limits (dashed red), ZPS limits (dashed purple), Cymodocea Nodosa meadows limits (in grey the scattered and in white the dense presence). The dot in magenta indicates the trench area

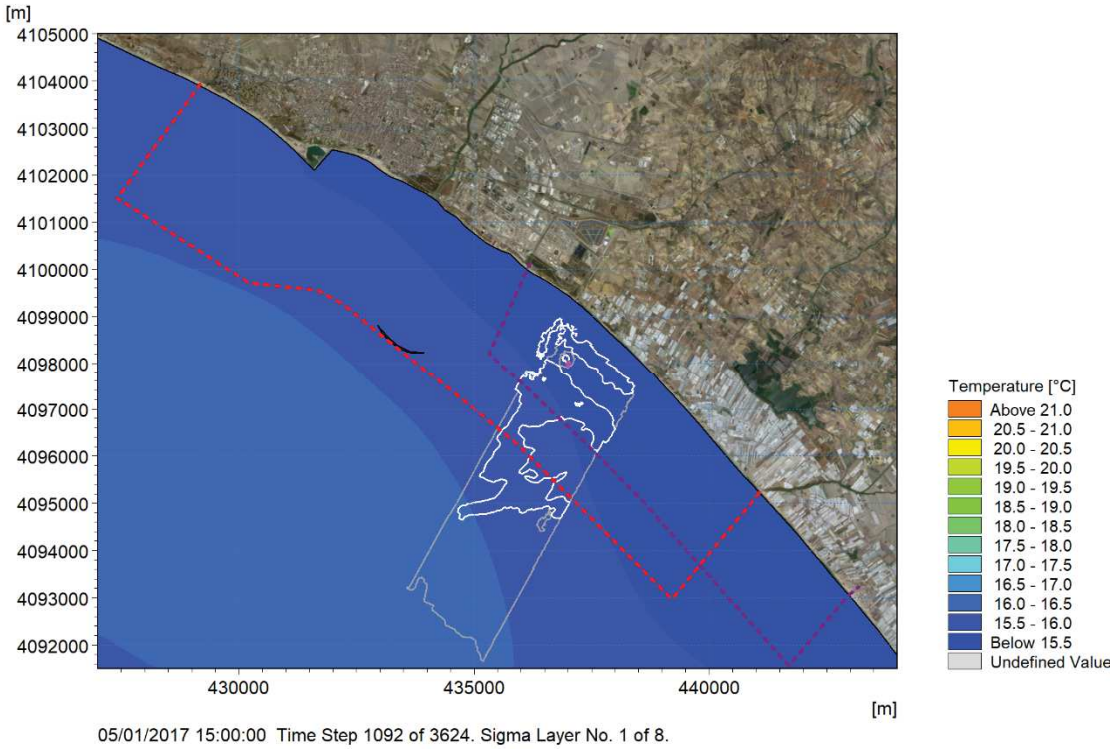

Figure 6-26 Example of bottom temperature in winter (05.01.2017 h.15:00). Coloured lines indicate: SIN limits (dashed red), ZPS limits (dashed purple), Cymodocea Nodosa meadows limits (in grey the scattered and in white the dense presence). The dot in magenta indicates the trench area

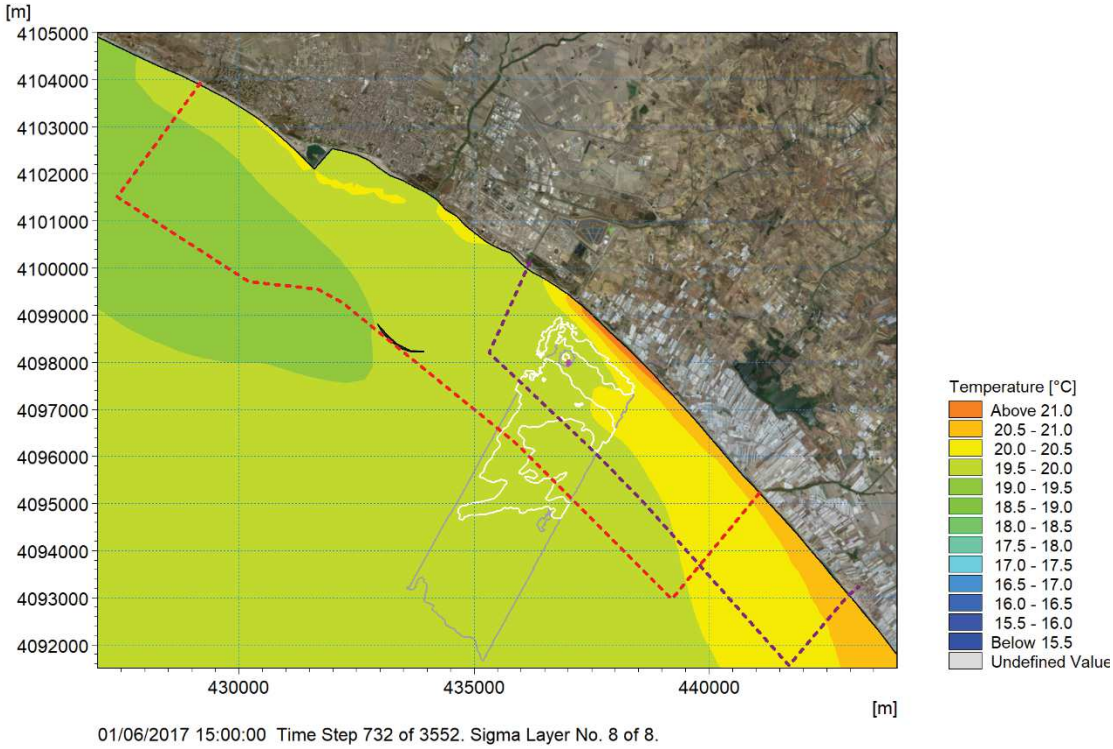

Figure 6-27 Example of surface temperature in summer (18.06.2017 h.12:00). Coloured lines indicate: SIN limits (dashed red), ZPS limits (dashed purple), Cymodocea Nodosa meadows limits (in grey the scattered and in white the dense presence). The dot in magenta indicates the trench area

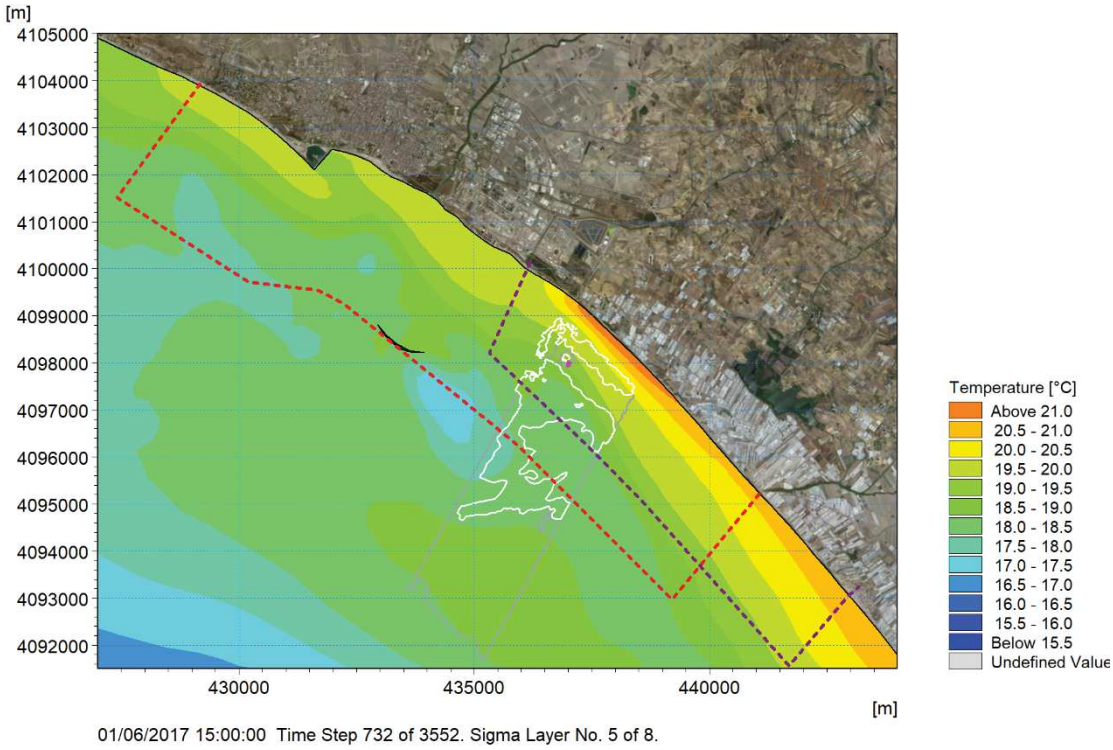

Figure 6-28 Example of mid-depth temperature in summer (18.06.2017 h.12:00). Coloured lines indicate: SIN limits (dashed red), ZPS limits (dashed purple), Cymodocea Nodosa meadows limits (in grey the scattered and in white the dense presence). The dot in magenta indicates the trench area

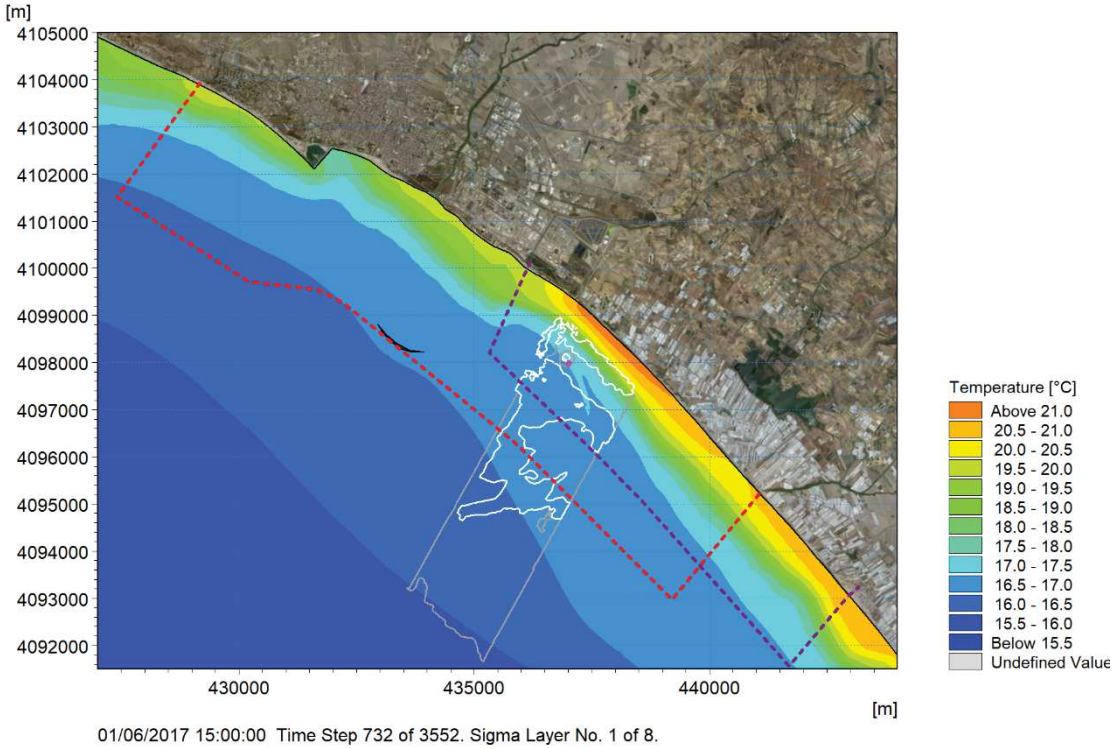

Figure 6-29 Example of bottom temperature in summer (18.06.2017 h.12:00). Coloured lines indicate: SIN limits (dashed red), ZPS limits (dashed purple), Cymodocea Nodosa meadows limits (in grey the scattered and in white the dense presence). The dot in magenta indicates the trench area

7.0 3D SEDIMENT TRANSPORT MODEL

The model applied to study the transport and fate of sediments resulting from the trench dredging operations is the MIKE 3 MT – Mud Transport [3]. The model simulates the erosion, the transport and the deposition of silt and silt-sand mixtures under the effects of currents and waves. As described in chapter 0, the effect of wave action has been studied separately (see chapter 8.0), while in the present section the general circulation has been taken into account.

The application of the MT module includes the possibility of accounting for different fractions of sediment and representing the following processes:

- flocculation;
- turbidity flows;
- hindered settling;
- seabed consolidation;
- morphological variations of the bottom;
- continuous update of the bottom morphology.

A detailed description of the MIKE 3 MT module is reported in Appendix B.

Figure 7-1 shows the main processes managed by MIKE 3 MT.

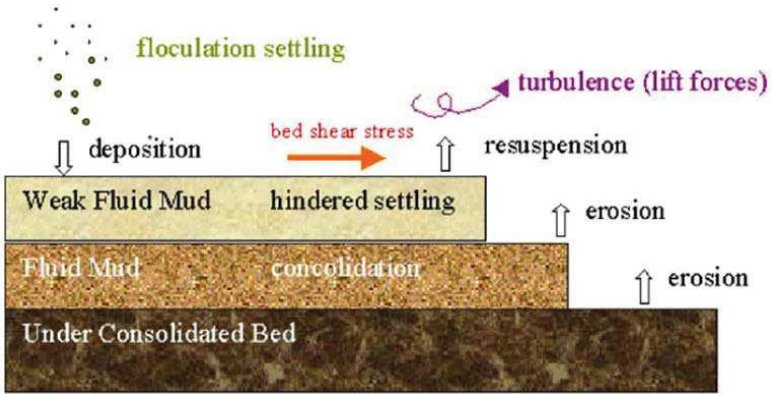

Figure 7-1 Schematic representation of the main processes managed by MIKE 3 MT

7.1 Implementation of the 3D sediment transport model

The computational domain of the sediment transport model has the same characteristics in terms of model extension and bathymetry as the MIKE 3 HD module, as described in section 6.1.

To setup the MT module, the following characteristics of sediments have been assumed:

- **Sediment texture and composition**. For this study the sample MEW001d_S26 (Table 3-1) has been considered. It represents the closest sediment sample to the trench area and it guarantees the most conservative approach (as the silt and clay percentages are higher than the percentages of the other samples near the trench

area). So, the considered texture is composed by 19.1% of clay (diameter less than 4µm), 39.9% of silt (diameter between 4µm and 63µm) and 41% of sand (diameter between 63µm and 200µm). The numerical model has been applied without considering the sand fraction, whose contribution in terms of Suspended Sediment Concentration (SSC) will be negligible at short distance from the release point, in consideration of its high settling velocities that will induce sand to deposit fast and close to the excavation point. This kind of approach is suggested also by ISPRA Manual and Guidelines [1].

- **Settling velocities of the different sediment fractions**. The settling velocities have been calculated through the Stokes formulation, which correlates them to the mean diameter of the grains as follows:

$$w_s = \frac{2R^2(d_e - d_i)g}{9\eta}$$

where: w_s = settling velocity [m/s]; R = suspended particle radius [m]; d_i = sediment density [kg/m^3]; d_e = sea water density [kg/m^3]; g = gravity acceleration [m/s^2]; η = viscosity of the continuous phase [m^2/s]. In this study, the settling velocities for the two fractions of sediments resulted as follows: W_{s_clay}=0.014 mm/s, W_{s_silt}=0.214 mm/s.

- **Sediment density**, that is 2650kg/m^3, and density of freshly deposited sediments. This value, that considers the presence of porosity, has been set equal to 1150kg/m^3, that correspond to a weakly (few days) consolidated mud;
- **Limit for flocculation**: based on the decade-long experience of DHI in similar studies, the activation of flocculation has been imposed for concentrations of cohesive sediment above 10 mg/l. In fact, for higher concentrations the probability of collision of the individual sediment particles increases consequently triggering the process of flocculation;
- **Limit for hindered settling**: again, based on DHI's experience in similar studies, the activation of the hindered settling has been imposed for cohesive sediment concentrations higher than 10'000 mg/l. In fact, this process activates when, due to high concentration, the particles come in contact with each other preventing an undisturbed deposition;
- **The bottom is assumed un-erodible** in order to prevent that the assessment of the turbidity and deposition related to the operations might be influenced by the possible natural resuspension of the natural seabed.

Since the excavated volumes are not spatially uniform (the dredged volumes in the vicinity of the exit point, at the beginning of the trench, are much larger than those dredged at the end of the trench, both due to a greater width and higher depth of the excavations) while, on the contrary, the hourly rate of productivity is constant in time (assumed 50 m^3/h, as described in section 3.1), a variable speed of the dredger has been assumed, proportionally to the excavated volumes.

It is important to underline that the total volume excavated is equal 2'500 m^3 (see chapter 5.0). But, considering that the 41% of this volume is sand (see paragraph 3.3) and, as previously explained, the sand fraction has not been modelled, a total volume of 1'475 m^3 has been considered for the simulations. This volume is constituted for 32.4% by clay and for 67.6% by silt.

Given the operational technologies planned for the trench excavation, the sediment release along the water column is assumed as uniformly distributed throughout the water column.

At the boundaries of the MIKE 3 MT model, a Dirichlet condition has been prescribed, i.e. open boundaries with specified values. In the present study, the boundaries of the model are placed far away from the area interested by the operations of excavation; moreover, the natural turbidity is not a specific object of the analysis. For these reasons, along the open boundaries a value of sediment concentration equal to zero has been assumed.

As initial conditions, a null value for suspended sediment concentration has been set. Therefore, a negligible natural turbidity has been assumed and only the turbidity generated by the dredging operations has been accounted for.

As anticipated at chapter 0, the one month long realistic simulation of the hydrodynamics allowed to adopt a "moving window" approach for the study of the dispersion of the fine solid matter [23]: the sediment transport module has been run 10 times for each month, coupled to the MIKE 3 HD realistic simulations, assuming for each run a window of 3 days (the first 50 hours for the dredging operations and the last 22 hours for the plume fate). These 10 runs are independent, in order to avoid mutual interference. Then, the resulting number of simulations of sediment transport is 20 (10 for each month).

This approach allows on one side to capture the natural variability of the system – which would have been otherwise impossible through a classical scenario-based approach – and on the other side, to carry out a much more significant post-processing of the output from a statistical point of view. This allows also to identify, at different depths, the maximum concentration of sediment reached during all the simulations, and the time of persistence of sediment concentration over a specific threshold. As regulations about maximum suspended sediment concentrations admissible in presence of sensitive marine habitat don't exist, reference values already used in similar studies have been applied. In particular, the thresholds have been set to be 10mg/l and 50mg/l, reference values already used in the modelling study of the transport and deposition processes during dredging and backfilling operations for the Trans Adriatic Pipeline, that represents one of the documents required by the Ministry for Environment, Land and Sea Protection for the EIA Screening [24]. The 10mg/l value is significant because surveys undertaken during natural conditions show background concentrations confined between approximately 6mg/l and 17mg/l [9]. 50mg/l value has been set "*a-posteriori*" because simulations showed that the highest modelled concentration over the *Cymodocea nodosa* (albeit on an extremely limited portion) are of this order of magnitude.

The analysis of these two parameters (maximum concentrations and persistence over threshold values for concentration) provide a comprehensive picture of the effect of the operations on the surrounding marine environment in terms of resulting sediment plumes.

Last, the maximum bottom deposition averaged over all the simulations has been provided.

The main characteristics of the sediment transport model are reported in Table 7-1.

Table 7-1 Main characteristics of the sediment transport model and input data

Clay average diameter **Silt average diameter**	4 µm 15.6 µm
$W_{s\ clay}$ **$W_{s\ silt}$**	0.014 mm/s 0.214 mm/s
$\%_{clay}$ **$\%_{silt}$**	32.4% 67.6%
Sediment density	2'650 kg/m^3
Threshold for flocculation	10 mg/l
Threshold for hindered settling	10'000 mg/l
Critical shear stress for deposition	0.07 N/m^2
Critical shear stress for erosion	high enough to prevent erosion
Typology of release of the sediment	Uniform throughout the water column Moving in time Continuous
Total volume of dredged material	1'475 m^3
Duration of operations	50 hours
Sediment release rate	50 m^3/hr
% of dispersed sediments	5%
Number of simulations	10 simulations per month, i.e. 20 simulations in total
Duration of the simulations	72 hour (50 hours for dredging operations + 22 hours for plume fate)

7.2 Results of the 3D sediment transport model

The following plots refer to the results obtained by the MIKE 3 MT simulations for the whole set of moving windows runs (10 in summer and 10 in winter). In particular, the following maps are shown and analysed:

- maps of maximum suspended sediment concentration (SSC) referred to all fractions (clay and silt), at the bottom layer, in an intermediate layer and at surface level (from Figure 7-1 to Figure 7-6). Maxima are calculated as the maximum value of the highest concentrations recorded during each simulation throughout the entire period of the operations (50 hours);
- maps of persistence in time of sediment concentration exceeding 10mg/l (from Figure 7-7 to Figure 7-12) and 50mg/l (from Figure 7-13 to Figure 7-18), refer to the entire period of the operations (50 hours). The persistence is calculated for each simulation and finally the maxima values over the number of simulations (10 in summer and 10 in winter) have been calculated;

- maps of maximum sediment deposition at the bottom (Figure 7-19 and Figure 7-20). This value is calculated for each simulation and finally the maxima values over the number of simulations (10 in summer and 10 in winter) have been calculated.

It is important to underline that the values in the following maps don't represent a specific temporal moment during the simulations (snapshot), but a set of the worst conditions that could be reached in different times during the operations. This is the reason for the odd shape of the distribution of concentration / deposition.

The choice of the minimum value of suspended sediment concentration in the colour palette is not straightforward. At international level [25] [26], the value of 2mg/l is usually considered as the threshold for clear waters, thus implying a healthy environment for any natural species. Therefore, in the following maps a minimum value of 2mg/l has been used.

Results of suspended sediment concentration show that during the winter period the plume of maximum SSC is elongated and its major axis runs parallel to the coast (consistently to the prevailing current directions), and it is approximately symmetrical (in the NW-SE direction) with respect to the excavation area. The plume is larger at the bottom (Figure 7-3), where it has a length of about 10km, parallel to coast, and about 1.6km, perpendicular to the coast, if we refer to a minimum SSC value of 2mg/l. The plume decreases moving towards the surface (Figure 7-1), where the dimensions are approximately 7km parallel to the coast, and 1.2km perpendicular to the coast. Referring to a concentration of 10mg/l the plume has a length parallel to the coast approximately from 2.4km, at the bottom, to 1.8km, at surface level, and perpendicular to the coast approximately from 1km, at the bottom, to 0.5km, at surface level.

During summer period, the current speed is generally slower than in winter and more evenly distributed along the water column. Therefore, the plume of maximum SSC has a quite circular shape (the differences between the axis parallel and perpendicular to the coast are smaller than in winter), centred on the dredging area, and concentrations are similar throughout the water column (Figure 7-4, Figure 7-5 and Figure 7-6). In particular, the plume of maximum SSC is characterized by an axis parallel to the coast of approximately 4.5km, if we refer to a SSC value of 2mg/l, and of approximately 1.5km if we refer to a value of 10mg/l. The axis perpendicular to the coast is slightly smaller: it is about 1.5km, considering 2mg/l, and about 1km considering 10mg/l. In general, concentrations higher than 100mg/l can be found in the dredging area only, where fine sediments are released.

Results in terms of persistence in time of prescribed sediment concentration show that, in general, during the whole period of dredging operations (50 hours) the concentration exceeds 10mg/l for not more than 30 hours (from Figure 7-7 to Figure 7-12) and 50mg/l (from Figure 7-13 to Figure 7-18) for a maximum time of 21 hours (so, less than half of the duration of dredging operations). Again, these maxima values of persistence are reached in the area close to the trench. As described above, in winter the area where a concentration of 10mg/l is exceeded for more than 3 hours is elongated parallel to the coast, while in summer this area shows a circular shape.

As described in section 3.1, the trench will be dredged in a zone where there are scattered meadows of *Cymodocea nodosa*: these meadows take up a corridor, parallel to the coast, approximately 250m wide. Beyond this corridor, nearshore and offshore, there are dense meadows of *Cymodocea nodosa* as well as in a very small area near the trench. The analysis

highlights that small zones of dense meadows of *Cymodocea nodosa* are affected by concentrations higher than 10mg/l, only for a maximum duration of about 6 hours during the dredging operations, while concentrations higher than 50mg/l are not reached. In the small area of dense meadow of *Cymodocea nodosa*, near the trench, concentrations of 10mg/l are reached for about half of the total duration of dredging operations (approximately 25 hours). The threshold of 50mg/l is reached only around the dredged trench, having a diameter of about 500m.

The sediment deposition at the sea bottom during dredging operations involves a confined portion of the domain (Figure 7-19 and Figure 7-20). Only in the proximity of the dredged trench, up to approximately 200-300m, the deposition is larger than 1cm. The deposition decreases as soon as the distance from the dredged area grows: it is indeed only 1mm at a distance from the dredged area of approximately 2600m parallel to the coast and 800m perpendicular to the coast. Starting from a distance from the focus area of 500-600m in NW-SE direction and of 200-300m in SW-NE direction, the deposition is lower than 0.1mm.

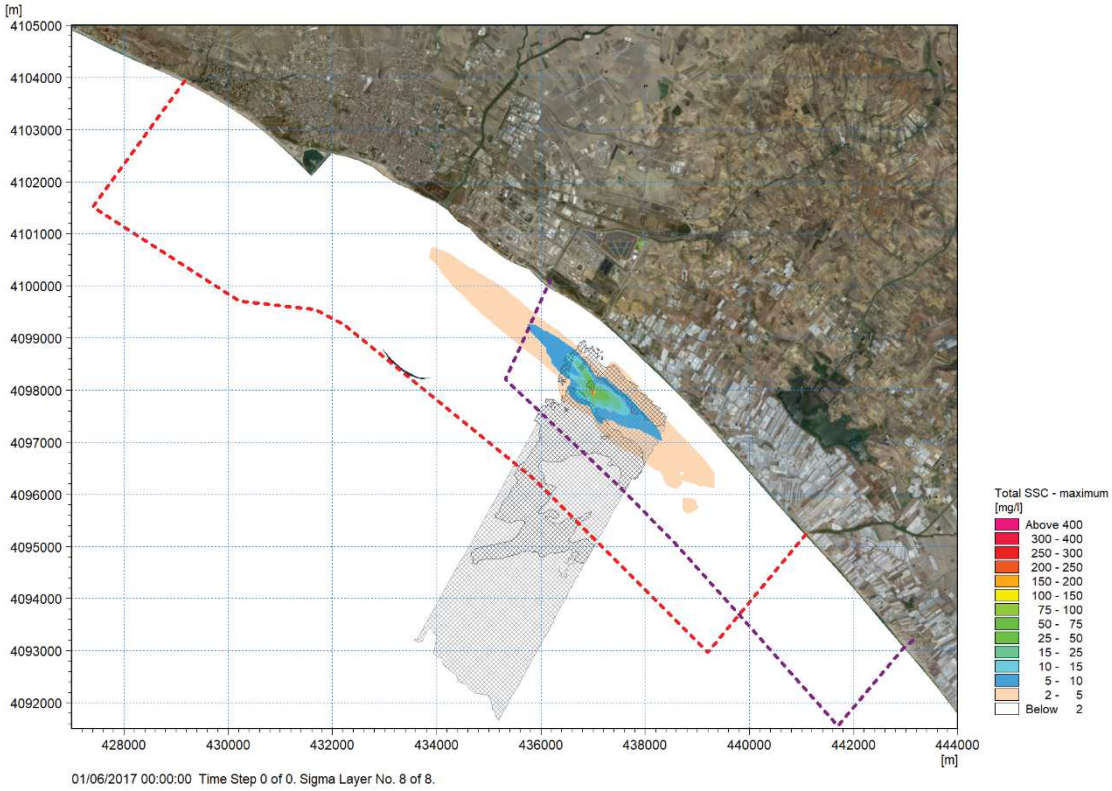

Figure 7-1 Maximum concentration during dredging operation (50 hours) on monthly basis at surface – winter period (January 2017)

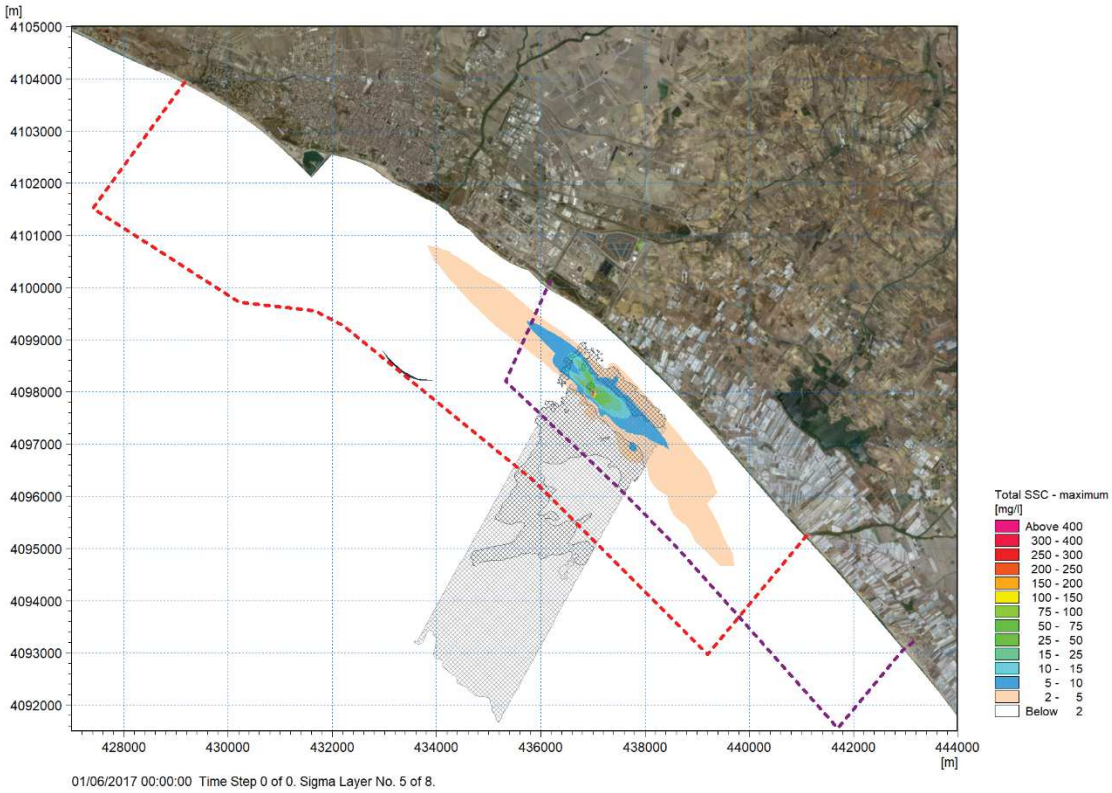

Figure 7-2 Maximum concentration during dredging operation (50 hours) on monthly basis at intermediate depth – winter period (January 2017)

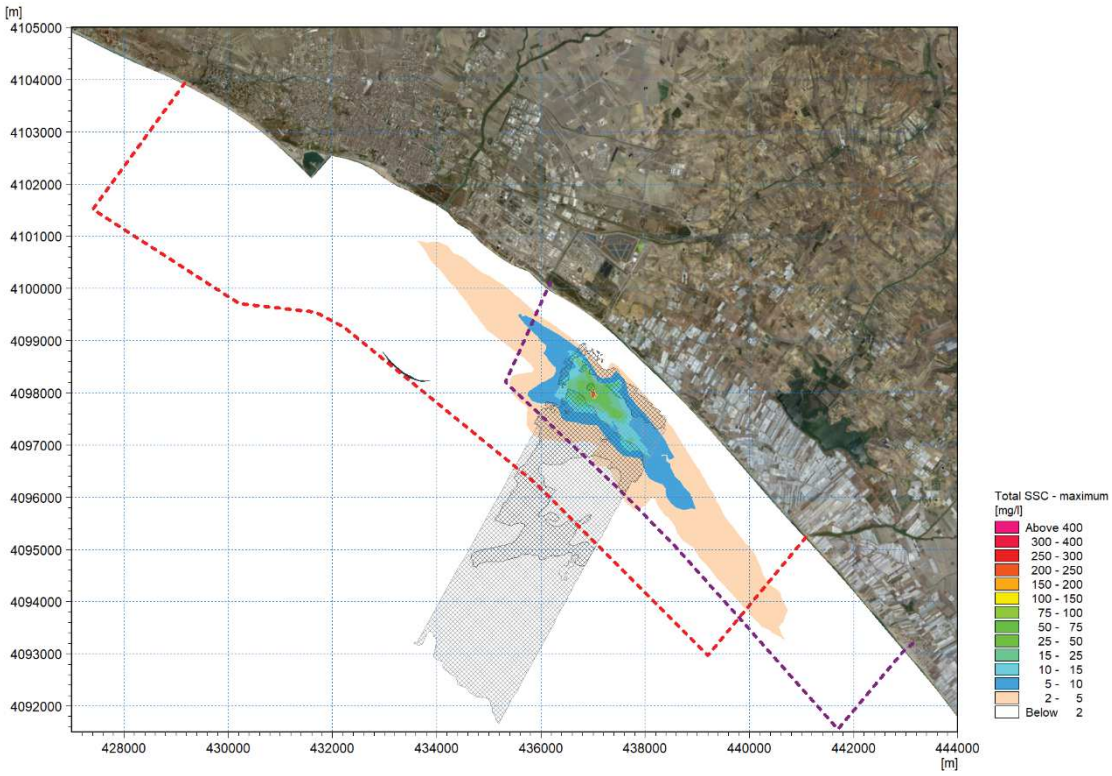

Figure 7-3 Maximum concentration during dredging operation (50 hours) on monthly basis at the sea bottom – winter period (January 2017)

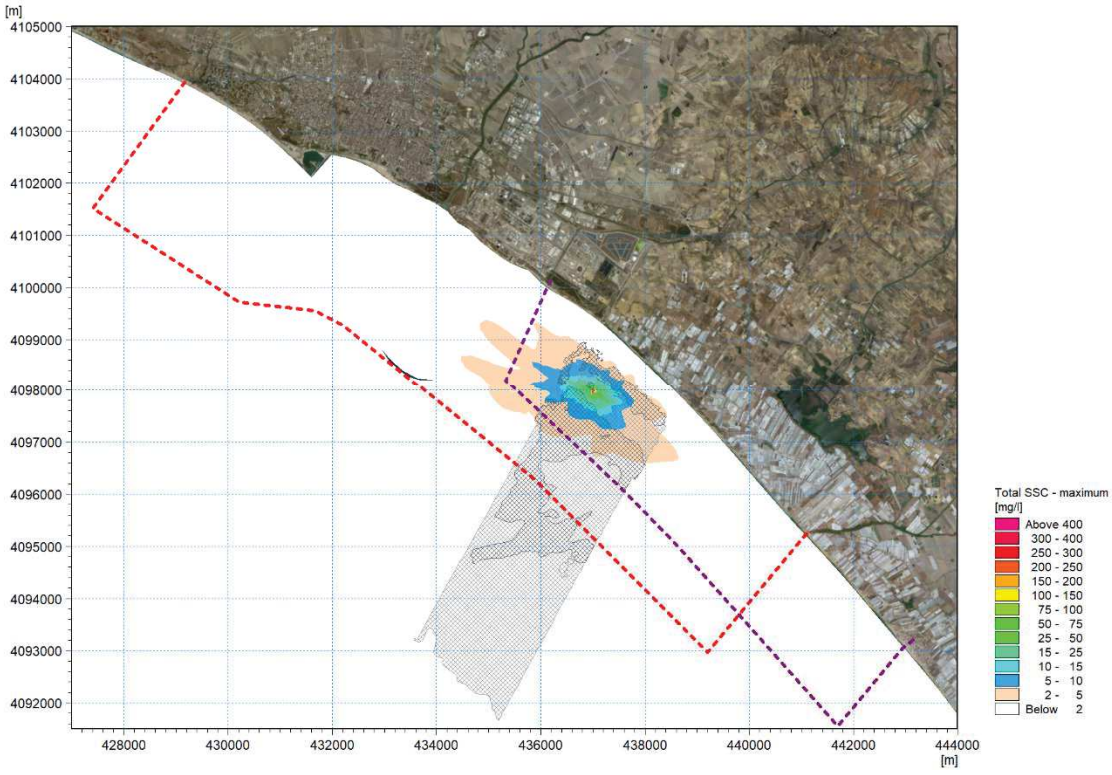

Figure 7-4 Maximum concentration during dredging operation (50 hours) on monthly basis at surface – summer period (June 2017)

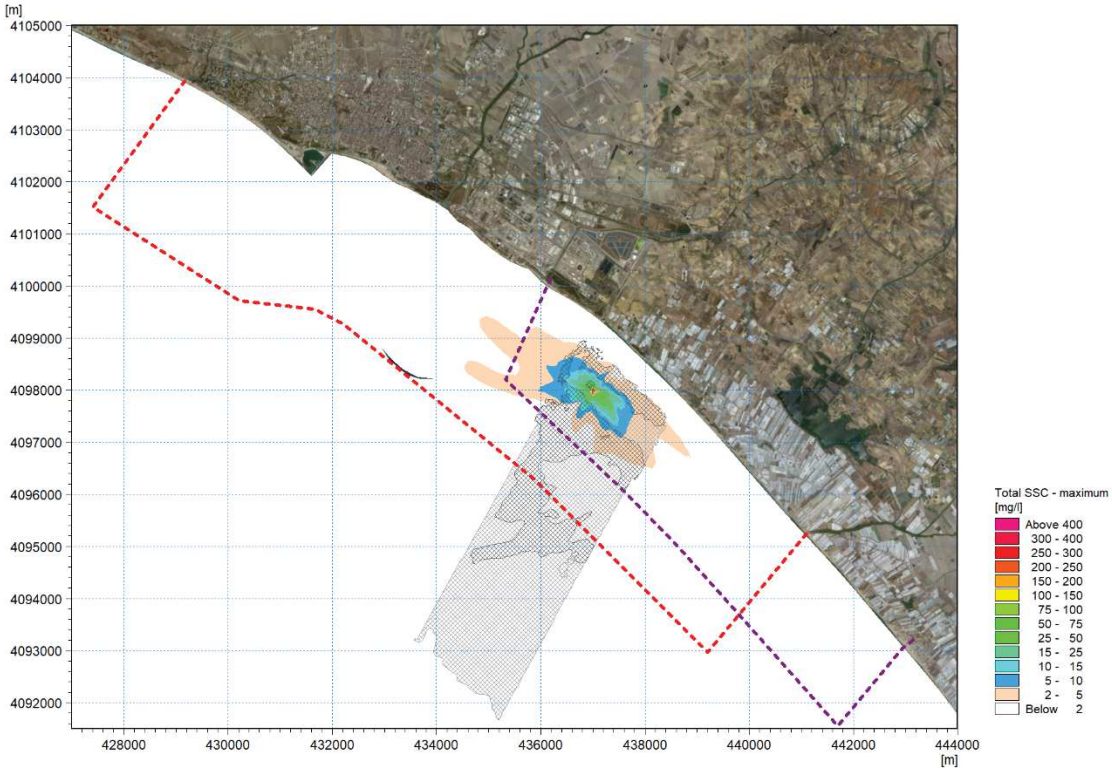

Figure 7-5 Maximum concentration during dredging operation (50 hours) on monthly basis at intermediate depth – summer period (June 2017)

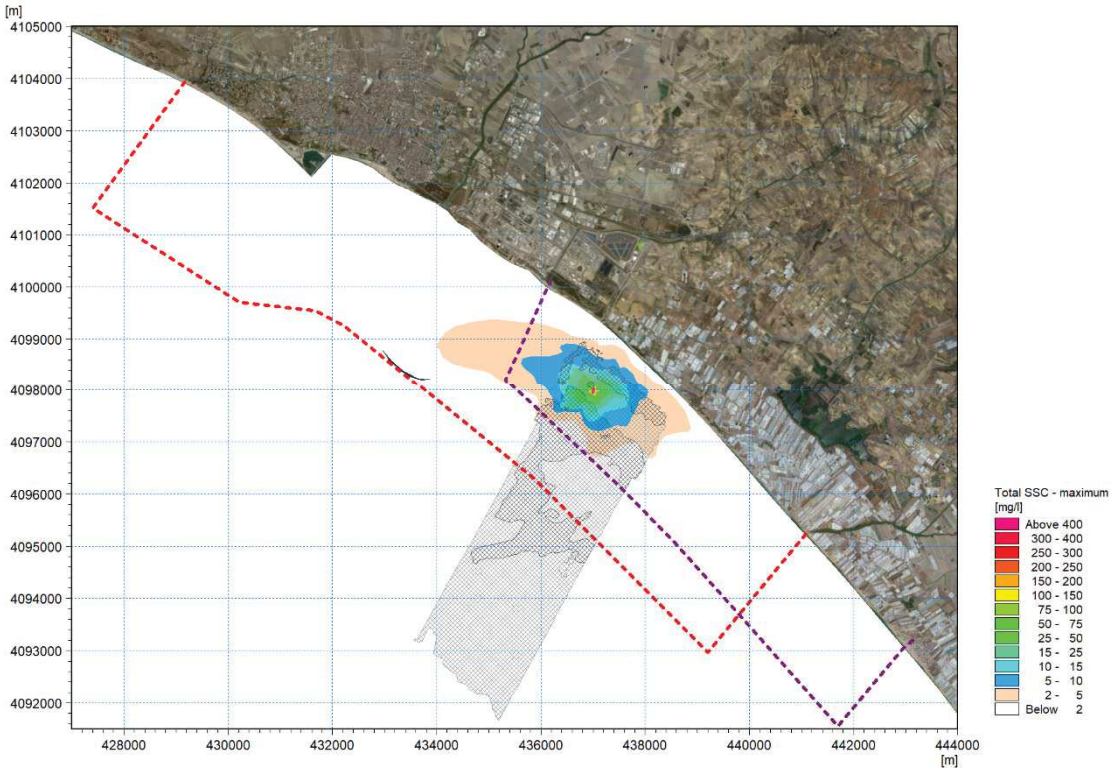

Figure 7-6 Maximum concentration during dredging operation (50 hours) on monthly basis at the sea bottom – summer period (June 2017)

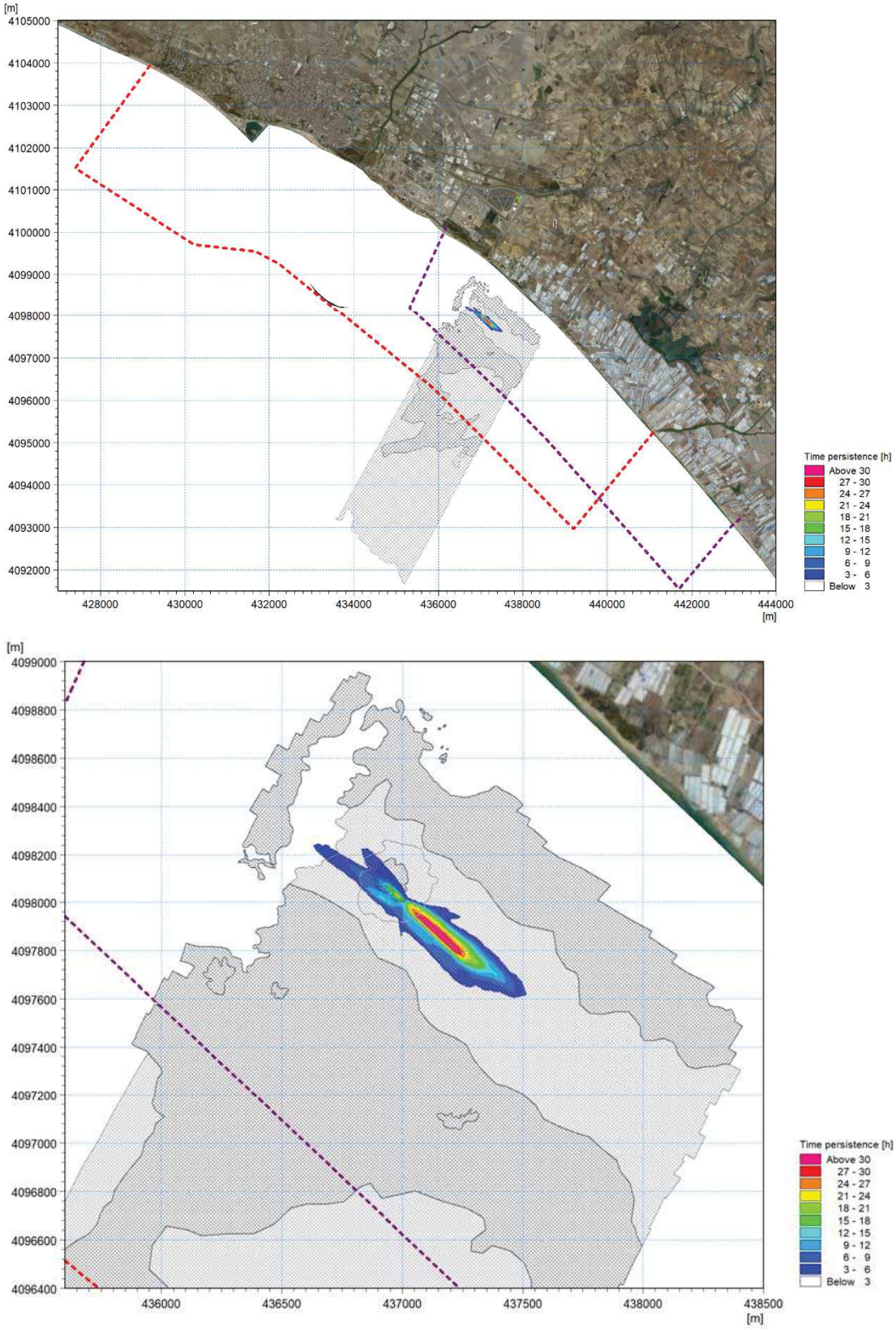

Figure 7-7 Persistence in time, during dredging operation (50 hours), of concentration exceeding 10mg/l on monthly basis at surface – winter period (January 2017). Whole domain (upper panel) and detail on the excavation area (lower panel)

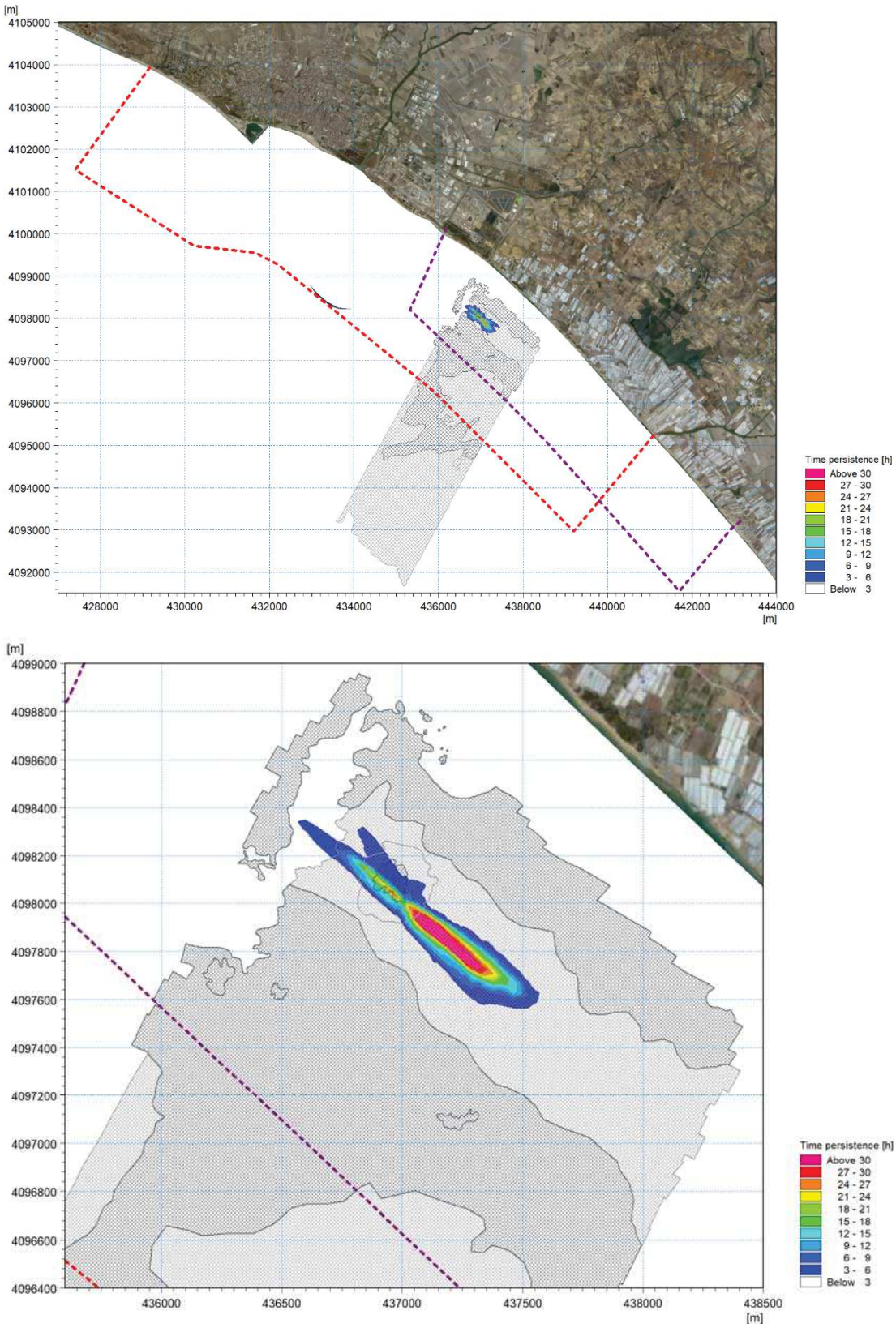

Figure 7-8 Persistence in time, during dredging operation (50 hours), of concentration exceeding 10mg/l on monthly basis at intermediate depth – winter period (January 2017). Whole domain (upper panel) and detail on the excavation area (lower panel)

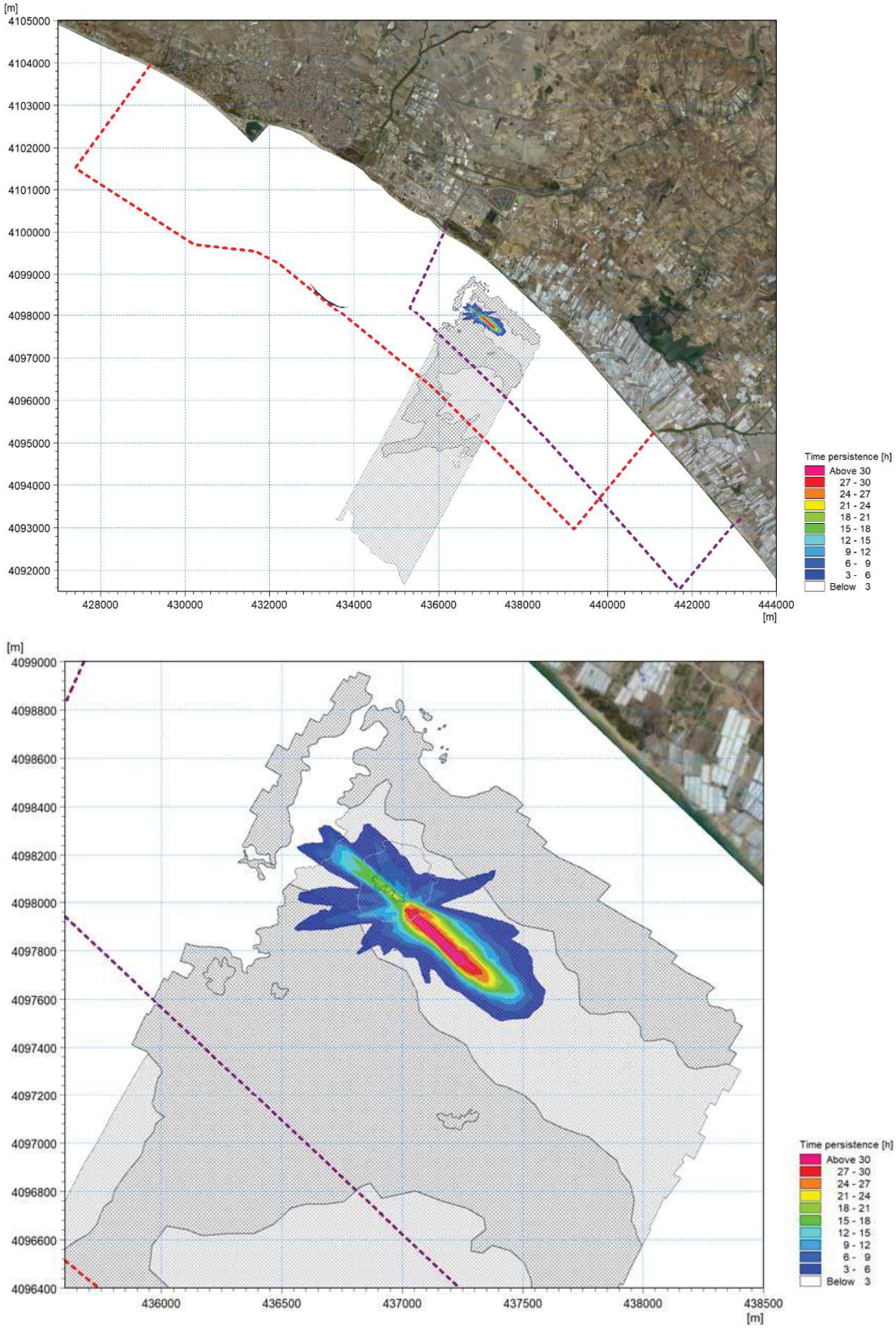

Figure 7-9 Persistence in time, during dredging operation (50 hours), of concentration exceeding 10mg/l on monthly basis at the sea bottom – winter period (January 2017). Whole domain (upper panel) and detail on the excavation area (lower panel)

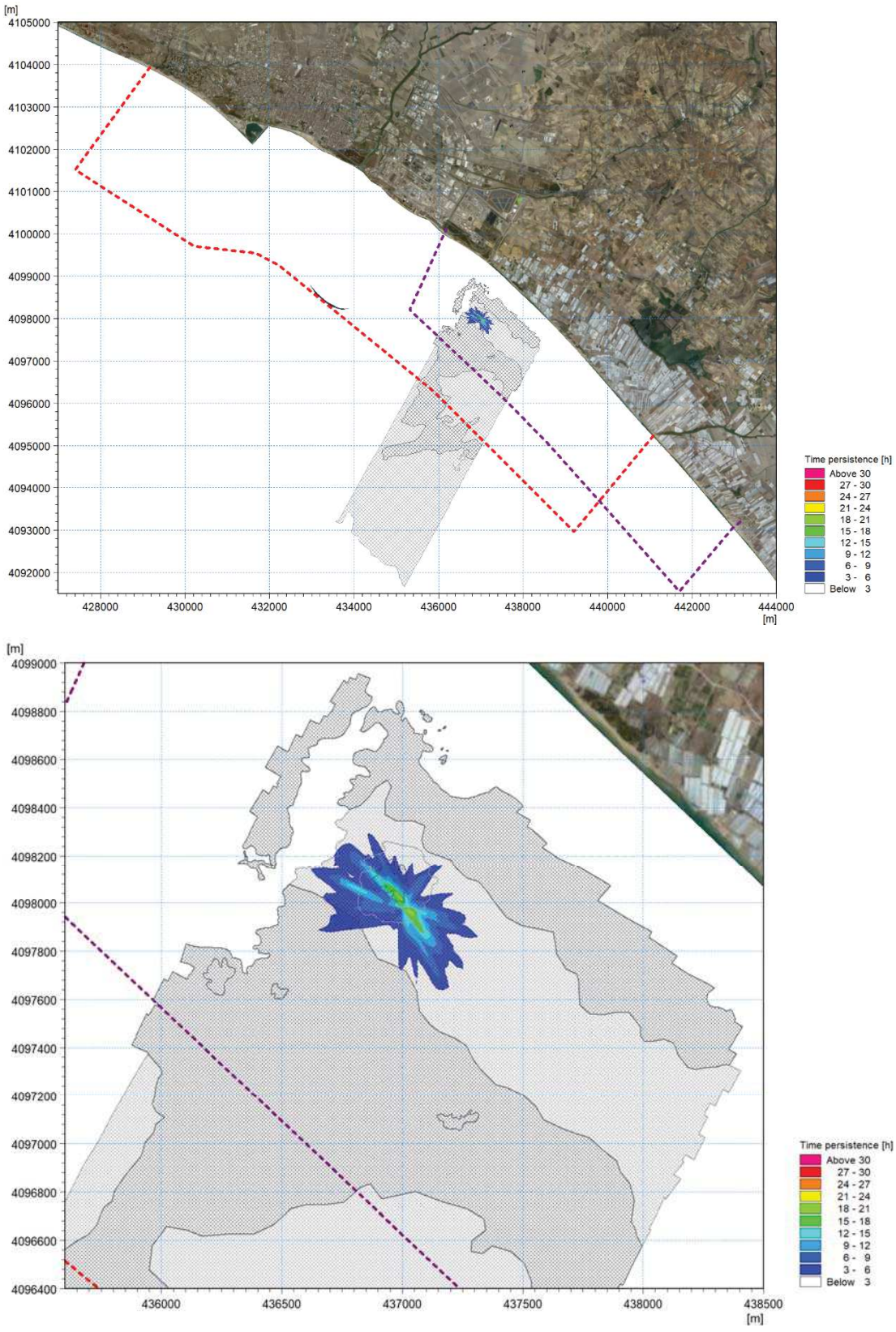

Figure 7-10 Persistence in time, during dredging operation (50 hours), of concentration exceeding 10mg/l on monthly basis at surface – summer period (June 2017). Whole domain (upper panel) and detail on the excavation area (lower panel)

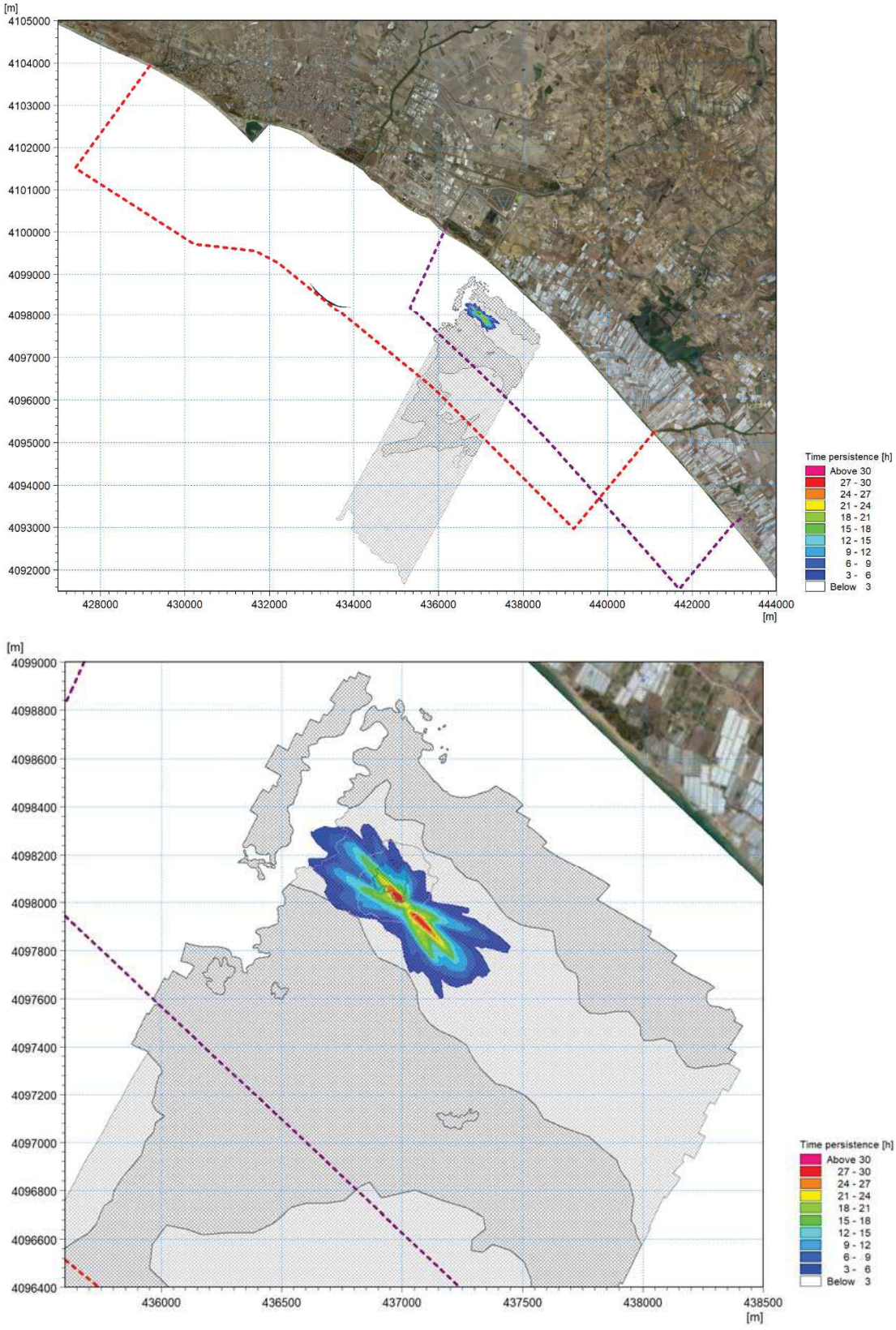

Figure 7-11 Persistence in time, during dredging operation (50 hours), of concentration exceeding 10mg/l on monthly basis at intermediate depth – summer period (June 2017). Whole domain (upper panel) and detail on the excavation area (lower panel)

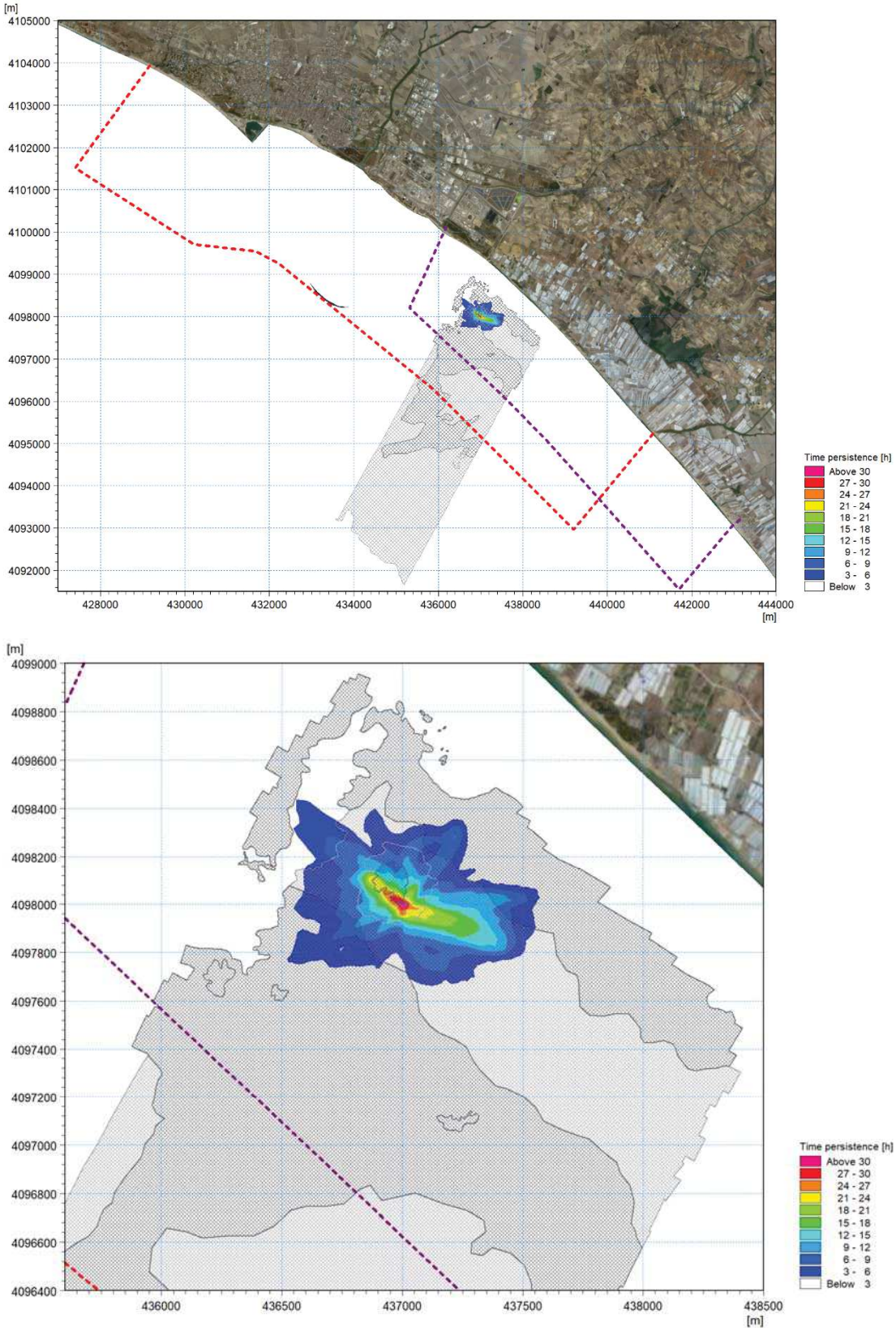

Figure 7-12 Persistence in time, during dredging operation (50 hours), of concentration exceeding 10mg/l on monthly basis at the sea bottom – summer period (June 2017). Whole domain (upper panel) and detail on the excavation area (lower panel)

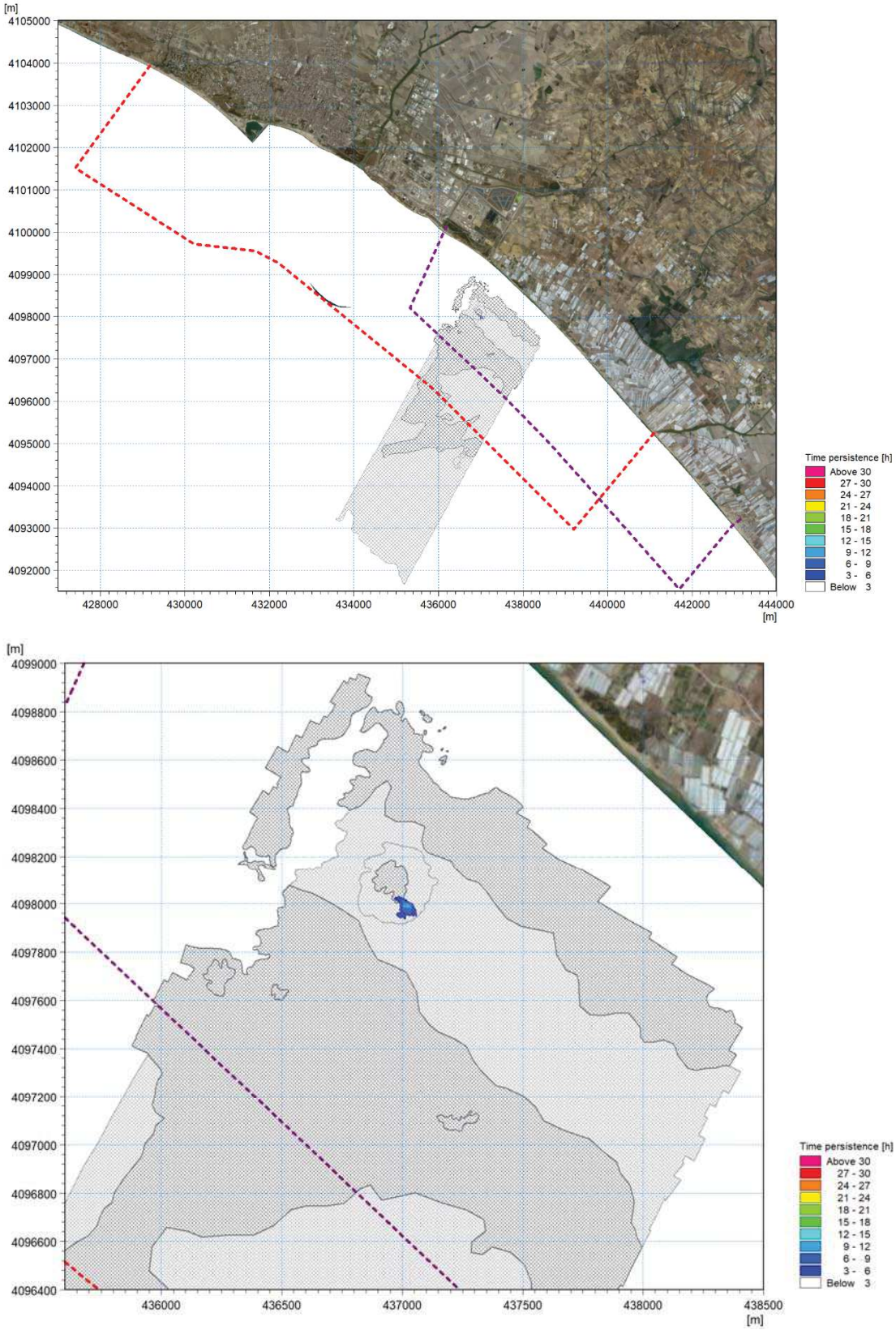

Figure 7-13 Persistence in time, during dredging operation (50 hours), of concentration exceeding 50mg/l on monthly basis at surface – winter period (January 2017). Whole domain (upper panel) and detail on the excavation area (lower panel)

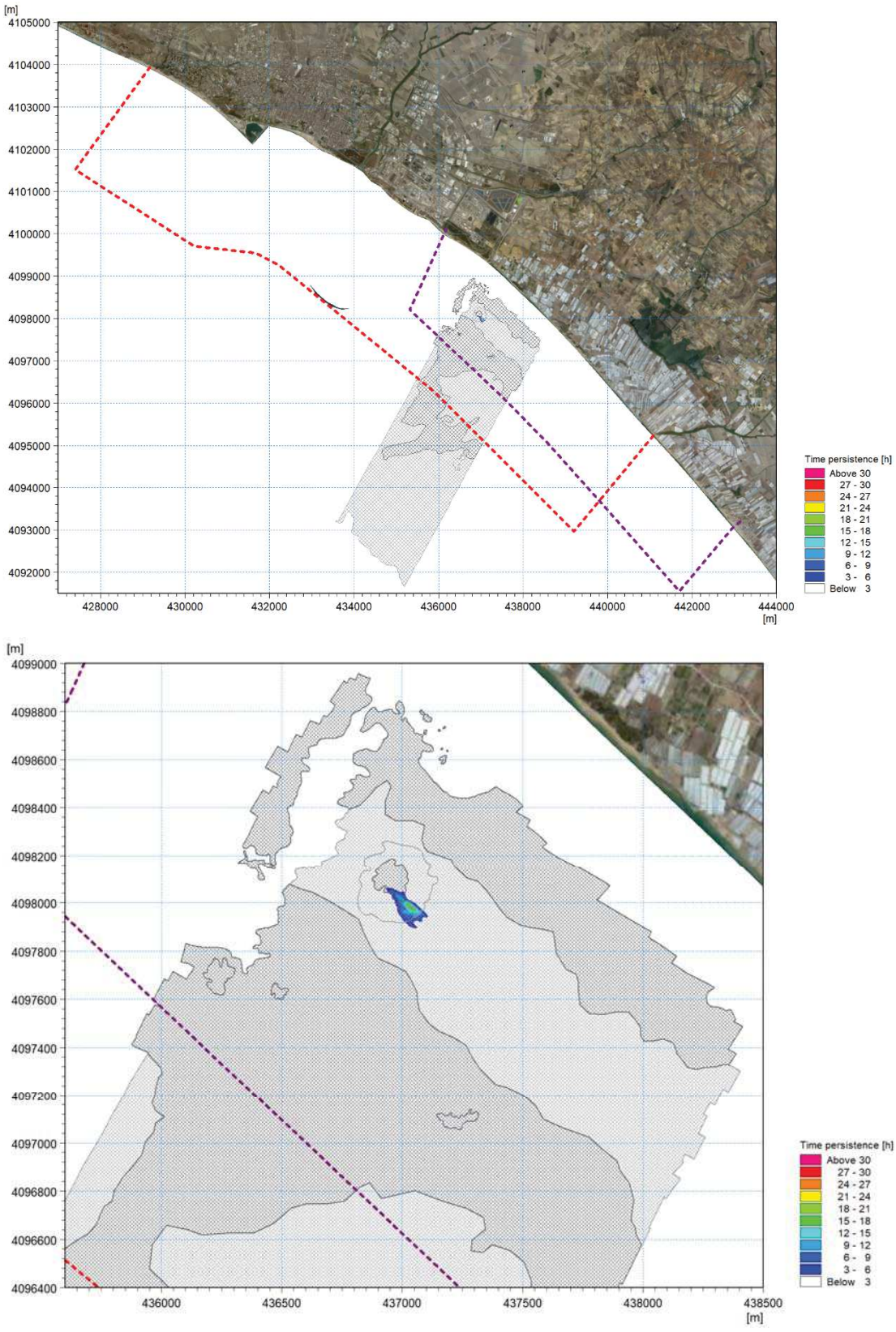

Figure 7-14 Persistence in time, during dredging operation (50 hours), of concentration exceeding 50mg/l on monthly basis at intermediate depth – winter period (January 2017). Whole domain (upper panel) and detail on the excavation area (lower panel)

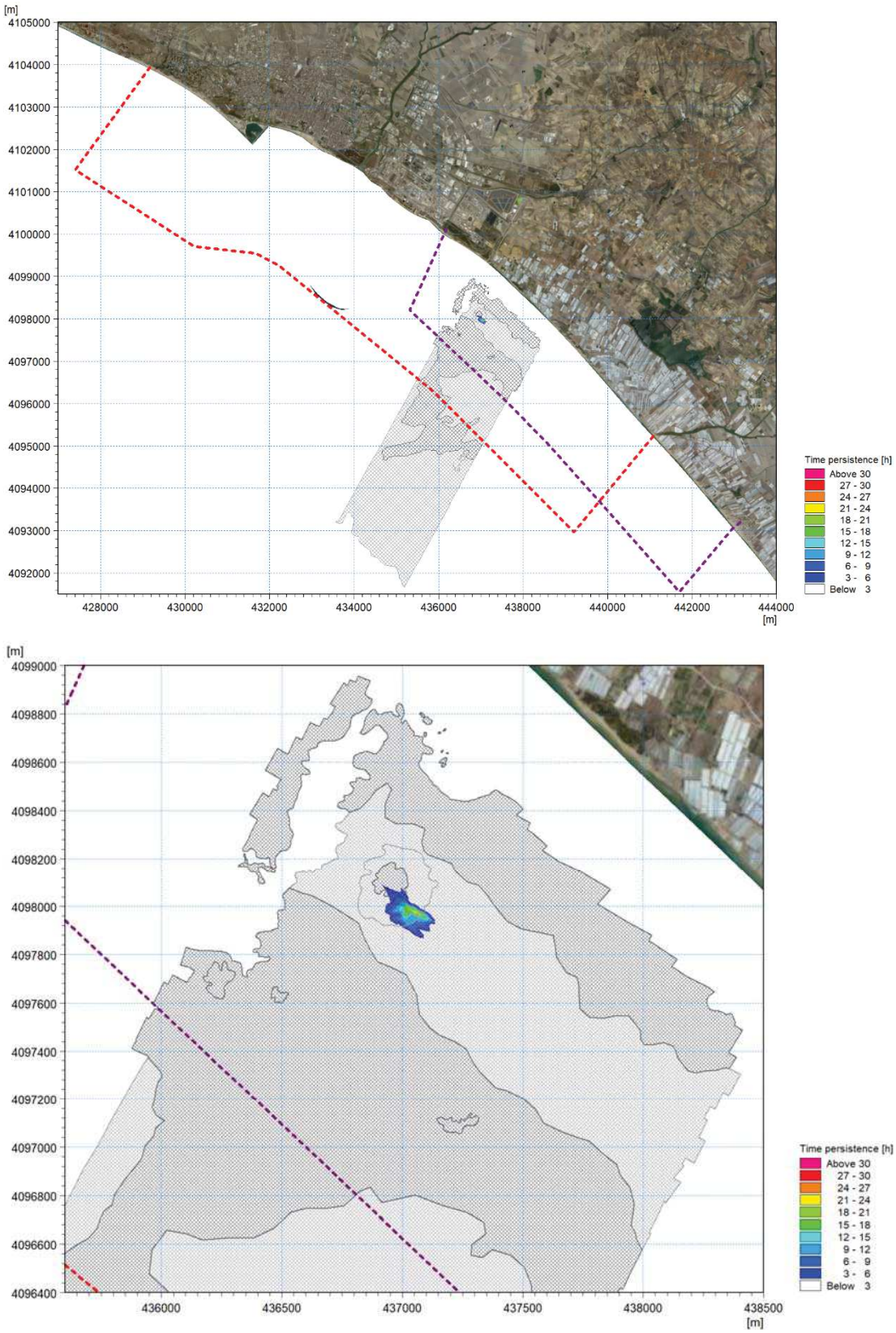

Figure 7-15 Persistence in time, during dredging operation (50 hours), of concentration exceeding 50mg/l on monthly basis at the sea bottom – winter period (January 2017). Whole domain (upper panel) and detail on the excavation area (lower panel)

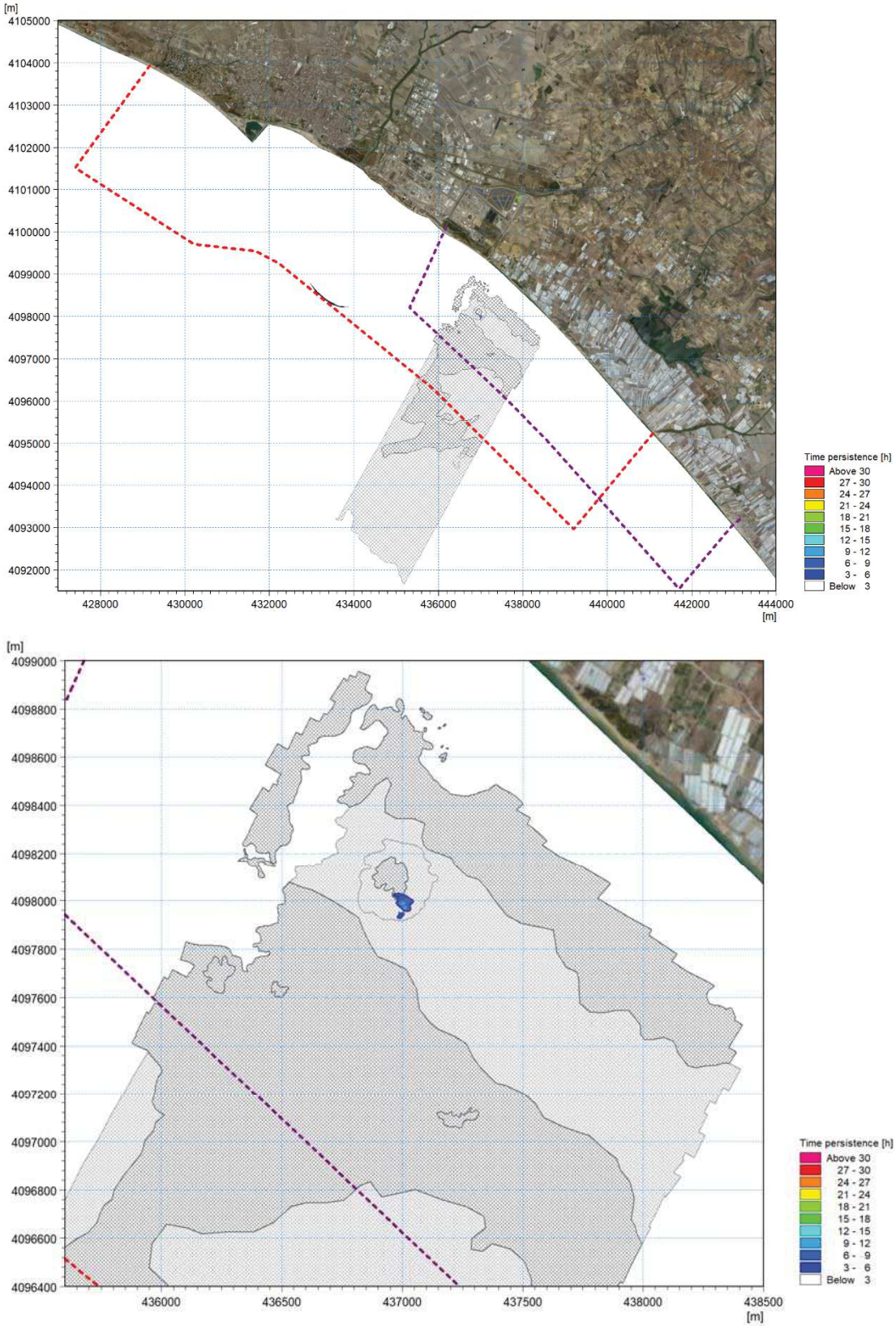

Figure 7-16 Persistence in time, during dredging operation (50 hours), of concentration exceeding 50mg/l on monthly basis at surface – summer period (June 2017). Whole domain (upper panel) and detail on the excavation area (lower panel)

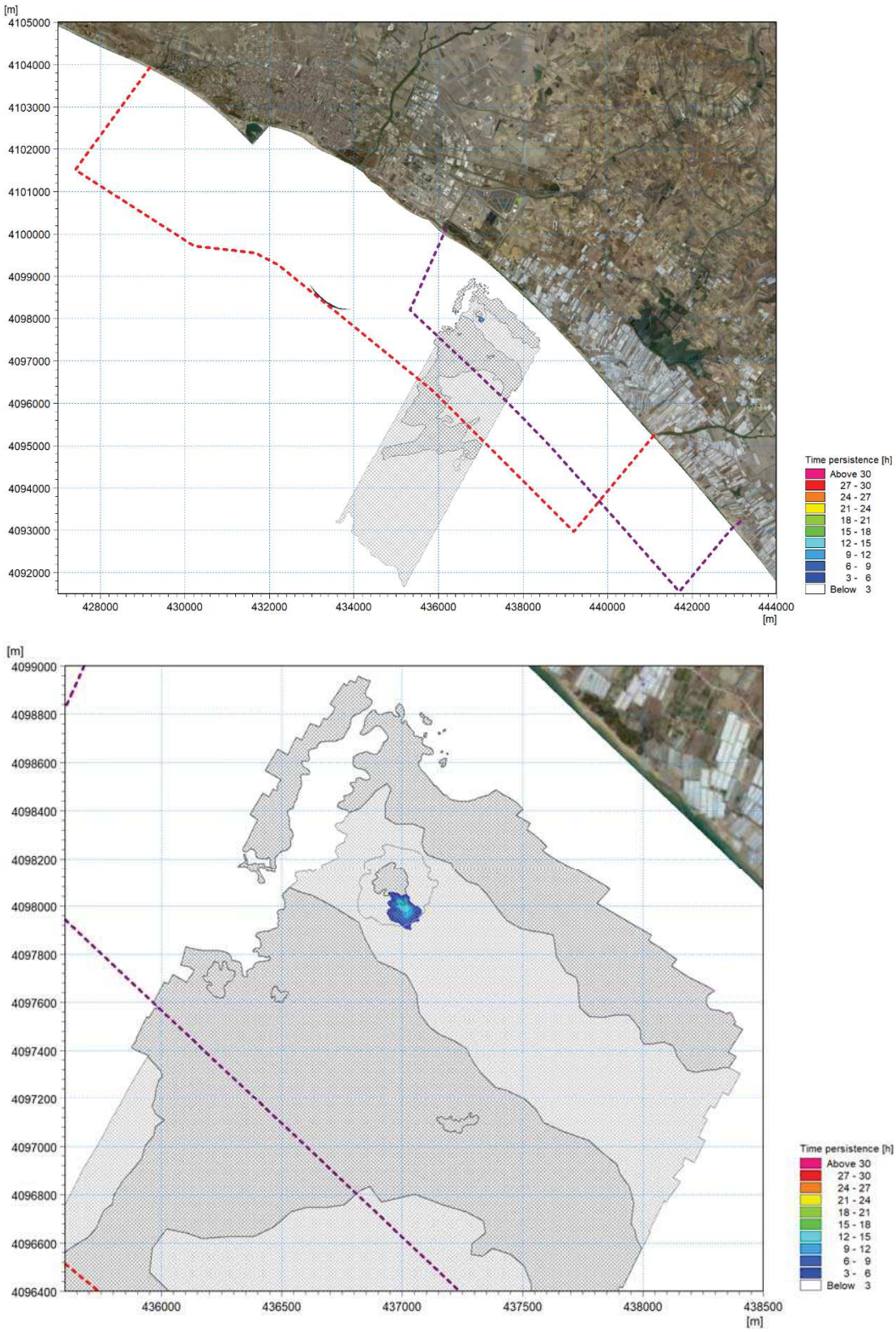

Figure 7-17 Persistence in time, during dredging operation (50 hours), of concentration exceeding 50mg/l on monthly basis at intermediate depth – summer period (June 2017). Whole domain (upper panel) and detail on the excavation area (lower panel)

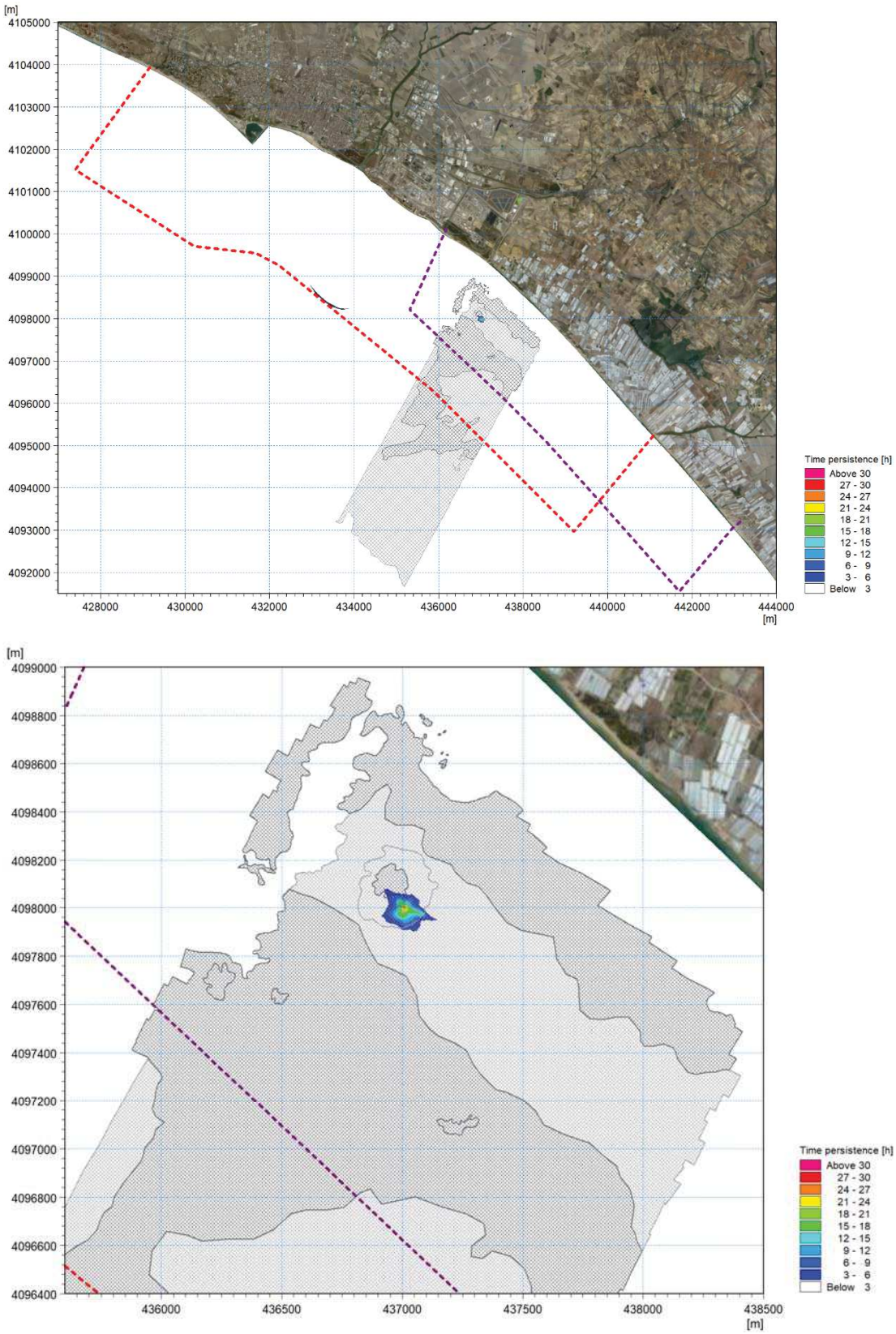

Figure 7-18 Persistence in time, during dredging operation (50 hours), of concentration exceeding 50mg/l on monthly basis at the sea bottom – summer period (June 2017). Whole domain (upper panel) and detail on the excavation area (lower panel)

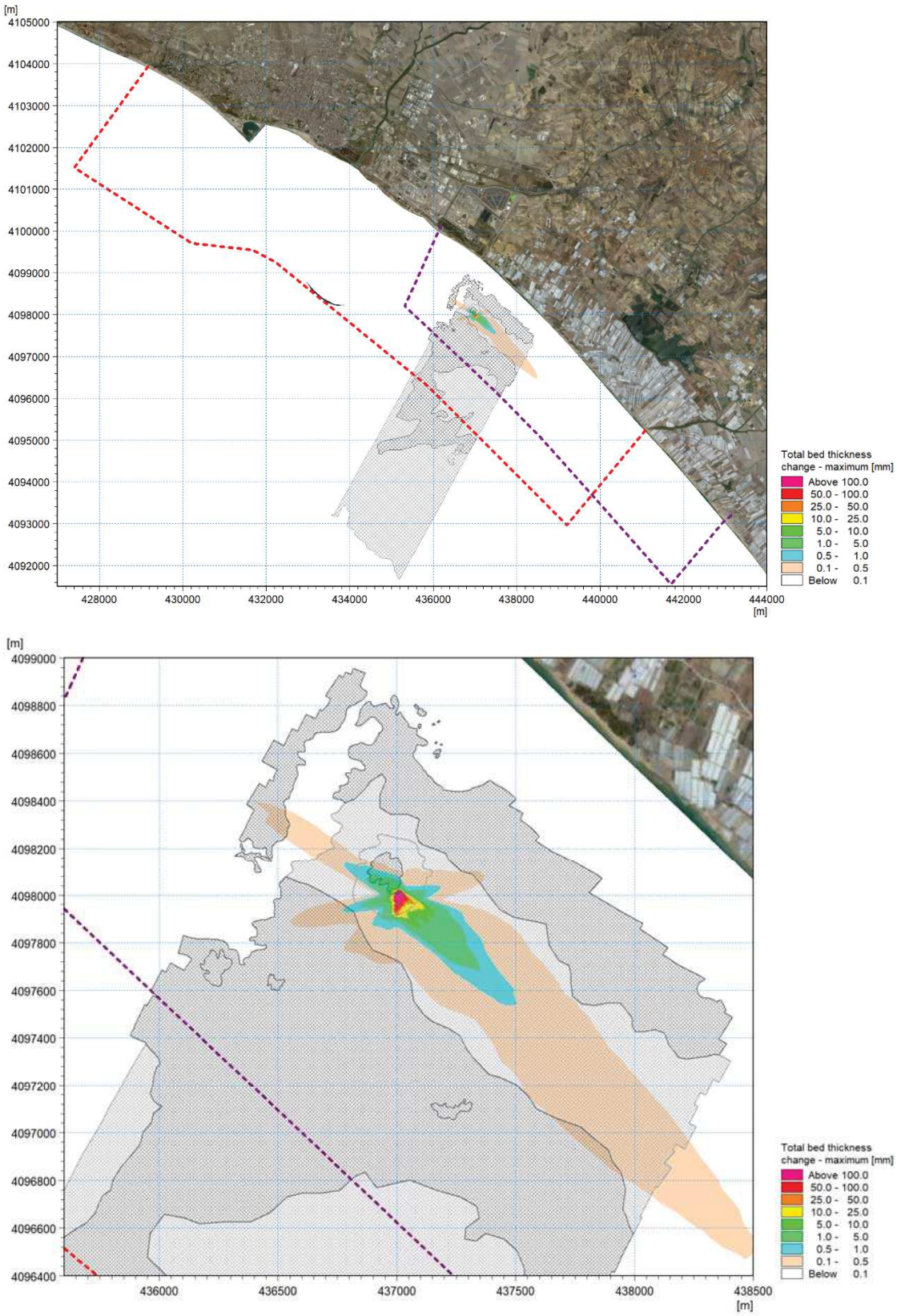

Figure 7-19 Maximum deposition 22 hours after the end of dredging operations (50 hours) on monthly basis – winter period (January 2017). Whole domain (upper panel) and detail on the excavation area (lower panel)

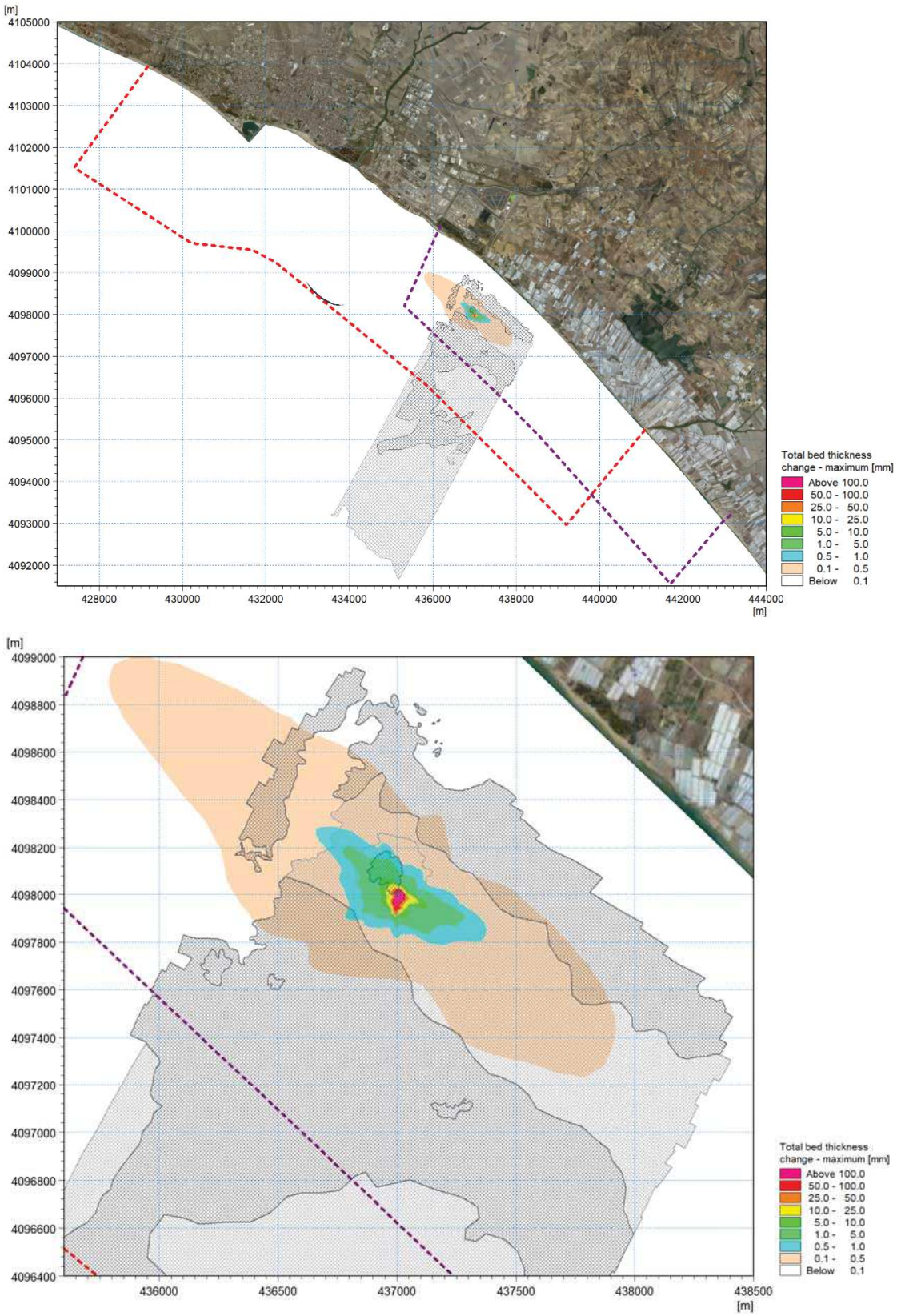

Figure 7-20 Maximum deposition 22 hours after the end of dredging operations (50 hours) on monthly basis – summer period (June 2017). Whole domain (upper panel) and detail on the excavation area (lower panel)

8.0 EFFECTS OF WAVES ON THE SUSPENDED SEDIMENT CONCENTRATION

As anticipated in chapter 2.0, the effect of incoming waves at the seabed has also been studied, while the wave generated currents (*longshore currents*) is assumed to be negligible.

Longshore currents are generated by the shore component of the stresses associated to wave breaking, shoaling and refraction processes, the so-called *radiation stresses*. This current is the dominant component in the nearshore area, with the highest values laying within the wave breaking zone ("surf zone"). Longshore currents are generally parallel to the coastline and their magnitude vary according to the wave height and direction at breaking. As the position of wave breaking constantly shifts due to the irregularity of natural wave fields, the distribution of the longshore current in the coastal profile will vary accordingly. The width of the wave breaking zone is limited by the so-called *closure depth*, i.e. the depth of a beach profile where the wave generated sediment transport becomes negligible. In a previous study developed in this area to meet the environmental prescriptions of the Ministry for Environment, Land and Sea Protection [4], the closure depths in the Gulf of Gela have been estimated around 3.5m. Considering that the trench is planned at a depth of about 8-9m (chapter 5.0), it is possible to assume that wave generated currents are not relevant for the dispersion and fate of the sediment released during dredging operations.

The main contribution of waves here is therefore associated to the orbital velocities at the seabed, that in case of storms can be strong enough to resuspend sediments after deposition. Given the very limited period of dredging operations (about 2 days), it can be assumed that storm conditions will be avoided with proper short-term planning. At the same time, after operations, for a period in the order of weeks / months a storm might easily put in suspension the fine sediment released during operations. The effect of an intense but not extreme real storm (7 March 2017) has been therefore modelled, in order to compare the natural turbidity generated by high waves resuspending the whole sediment at the seabed and the contribution of the sediment "freshly" deposited after operations.

8.1 Modelling study of a wave storm

For the wave analysis, the hindcast wave data from MWM (Mediterranean Wind Wave Model) [27] have been used. The database is the result of a high-resolution numerical hindcast study of wind and wave conditions in the Mediterranean Sea performed by DHI in Italy in partnership with HyMOLab (Hydrodynamics and Met-Ocean Laboratory) of the University of Trieste, Italy. The MWM database is the result of a modelling chain implementation which benefits from two state-of-the-art models for atmospheric modelling (WRF-ARW [28], [12] – a widely used non-hydrostatic model, open source) and wave modelling (MIKE 21 SW-Spectral Waves [29] – developed by DHI and widely used in a large number of coastal and offshore applications worldwide). The database covers about 40 years and it is composed by hourly wind and wave data over the whole Mediterranean basin at a resolution of approximately 10 km for the wind, and a variable resolution for the waves. These latter ranges from around 10 km at open sea, up to approximately 3 km in shallow water areas, near the coasts and around islands. For further details, see Appendix D.

In the present analysis, the timeseries of wave parameters for the year 2017 has been extracted from the database MWM in order to select a storm characterized by high waves but also high frequency of occurrence. It has been therefore decided to refer to a storm characterized by a 1 year return period. As highlighted within the metocean study [10] and reported in Table 3-5, a storm characterized by a return period of approximately 1 year is associated to a significant wave height equal to 3.5m at a depth of 11m; therefore, a similar wave has been selected from the available timeseries.

In particular, the storm occurred at the beginning of March 2017 (peak time at 07/03/2017, 15:00 h) has been analyzed. In order to study the wave conditions in the area of interest, the selected storm have been simulated through numerical modelling using the MIKE 21 SW - Spectral Wave [29]. The wave model is based on an unstructured, cell-centred finite volume method and uses an unstructured mesh in geographical space. MIKE 21 SW simulates the growth, decay and transformation of wind-generated waves and swells in offshore and coastal areas.

MIKE 21 SW includes the following physical phenomena:

- wave growth by action of wind;
- non-linear wave-wave interaction (quadruplet and triad-wave interactions);
- dissipation due to white-capping;
- dissipation due to bottom friction;
- dissipation due to depth-induced wave breaking;
- refraction and shoaling due to depth variations and currents;
- wave-current interaction;
- wave diffraction;
- wave reflection

For further details, see Appendix C.

The MIKE 21 SW model has been implemented using the same bathymetry and computational domain described at section 6.1 and, as boundary conditions, the wave parameters extract from the MWM database.

The characteristics of the simulated storm, in terms of wave field at the peck of the storm and of timeseries offshore and at 11m water depth, are shown respectively in Figure 8-1 Figure 8-2.

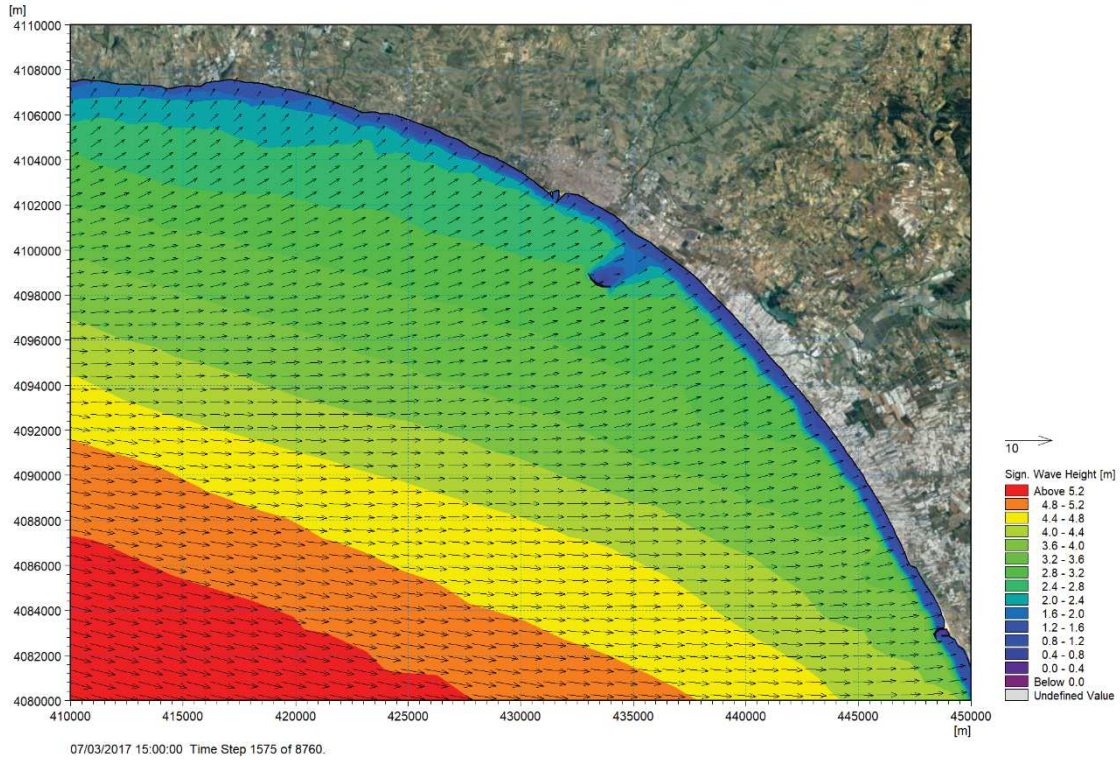

Figure 8-1 Field of significant wave height at the peak of the selected storm (07/03/2017, 15:00 h)

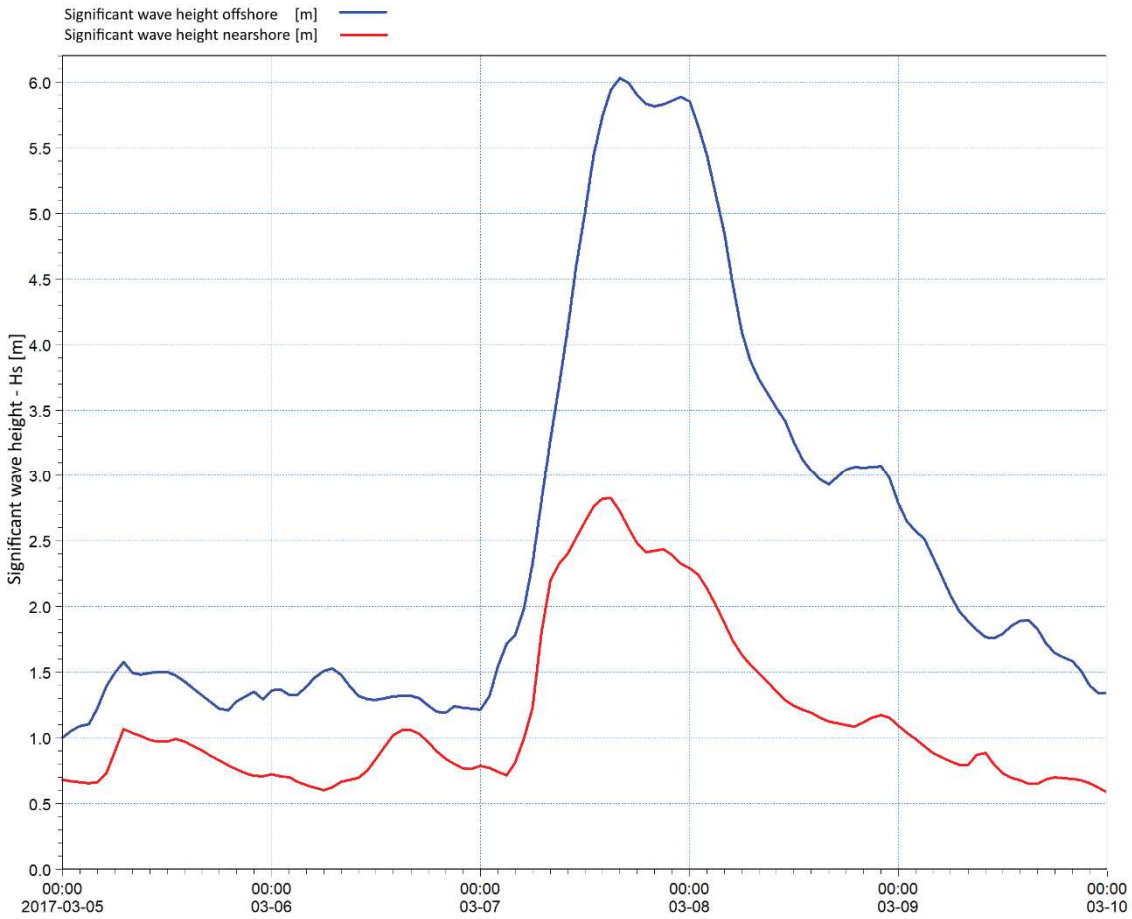

Figure 8-2 Significant wave height offshore (blue line) and at 11m water depth (red line), during the selected storm. Period: 05.03.2017-10.03.2017

8.2 Modelling study of turbidity due to a wave storm

The MIKE 3 MT model has been implemented using the same bathymetry, computational domain and sediments properties described at section 7.1. The critical bed shear stress for erosion has been here set equal to 0.3 N/ m^2, to let the seabed erode under wave conditions.

Figure 8-3 shows the values of bed shear stress (induced by wave orbital velocities) during the storm in the area of interest at different depths, from 8m, where the dredging of the trench is planned, to 50m: it's possible to observe that the maxima values are between 4N/m^2, at -8m, and approximately 0.2N/m^2, at -50m. Therefore, assuming that erosion can occur above 0.3N/m^2, the depth of about 35-40m can be indicated as the limit for the natural resuspension of sediments in severe storm conditions.

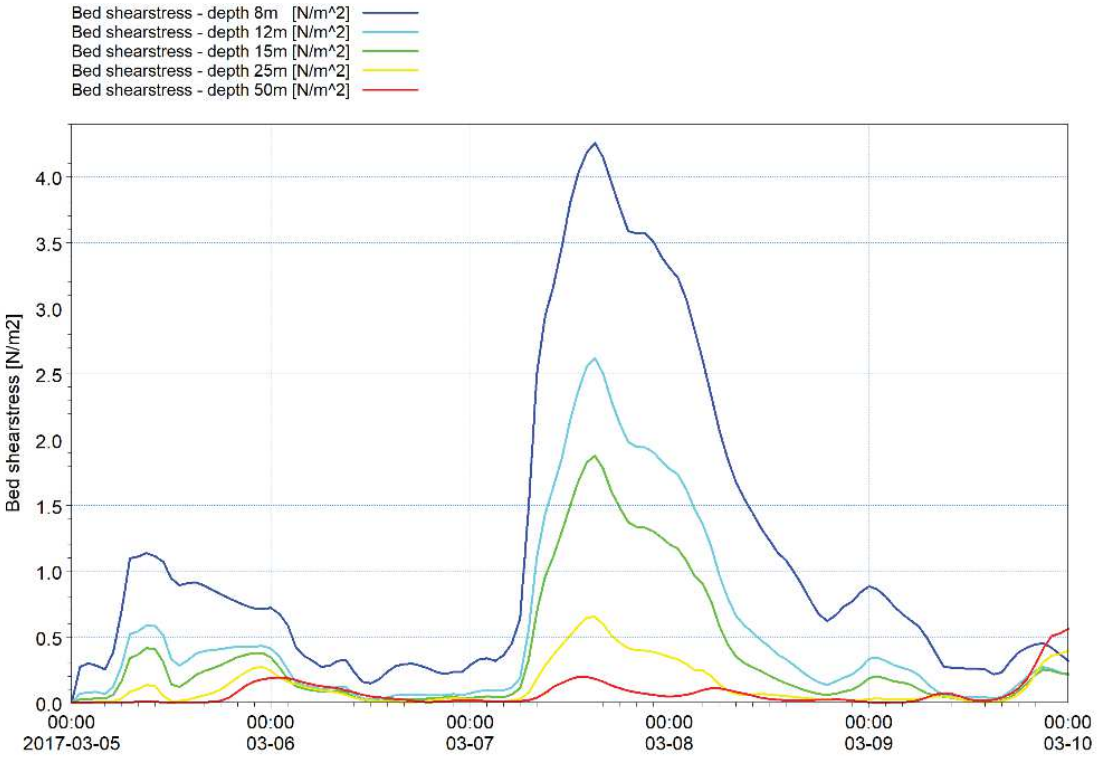

Figure 8-3 Bed shear stress during the storm (Figure 8-2) at 5 different depths (8m – where the dredging of the trench is planned - 12m, 15m, 25m, 50m)

In order to compare the natural turbidity generated by high waves resuspending the whole sediment at the seabed and the contribution of the sediment "freshly" deposited after operations, the following two conditions have been simulated:

- natural seabed: in order to quantify the turbidity due to the wave actions in "natural" conditions, in absence of dredging operations, the whole seabed has been considered potentially erodible. Therefore, the results show the "natural" concentration of suspended sediment resuspended by waves during a storm;
- deposited sediment only: in order to quantify the contribution of dredging operations to suspended sediment concentration due to resuspension of the deposited sediments, only the deposited sediment from dredging operations has been considered available for erosion. Conservatively, the thickness of deposited sediment

has been set equal to the maximum deposition reached at the end of the 20 simulations, characterized by a density corresponding to a weakly (few days) consolidated mud.

This approach allows to demonstrate the negligible contribution to the turbidity of the water column of the deposited sediment following dredging operations, if compared to natural storm conditions.

It is indeed the volume of deposited sediment to be negligible: the concentration is always below 5 mg/l even in the area where dredging operations will take place (Figure 8-4). On the other hand, during a storm, at a water depth of about 10m, values of 500mg/l of suspended sediment concentration could be easily reached, as shown in Figure 8-5.

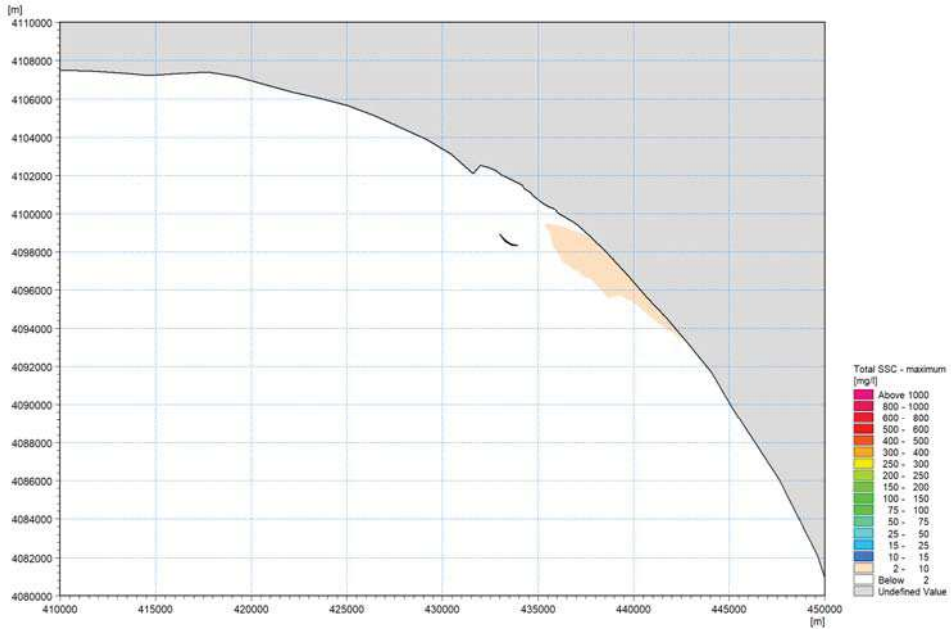

Figure 8-4 Map of suspended sediment concentrations at the seabed during a storm - deposited sediment only

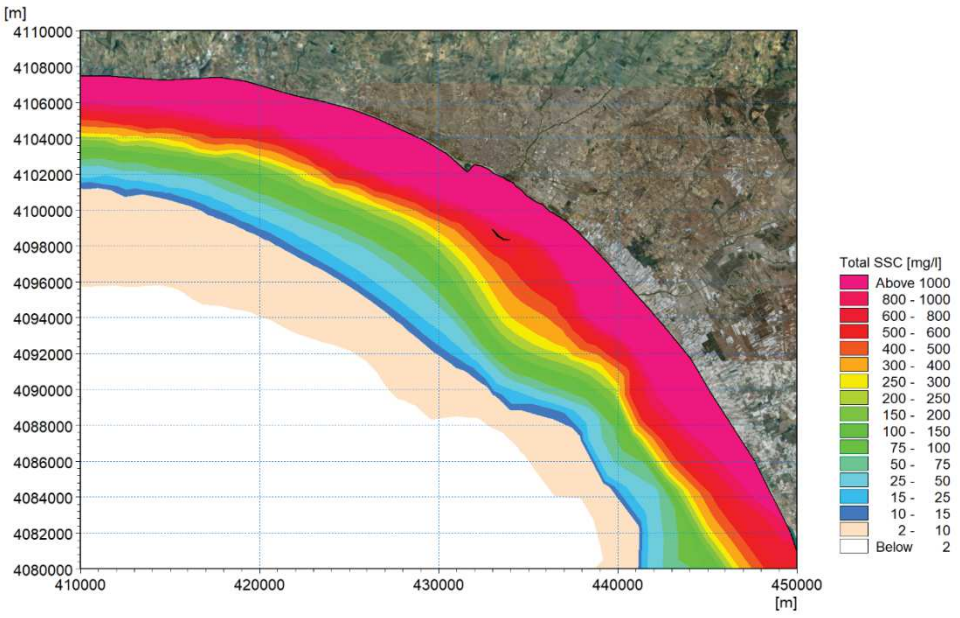

Figure 8-5 Map of suspended sediment concentrations at the seabed during a storm - natural seabed

9.0 SUMMARY AND CONCLUSIONS

Within the planned connection of Malta to the European Gas Network through a Gas Pipeline, the present numerical modelling study has been carried out to quantify the effects, during the laying operations of the pipeline, of the excavation at the Italian landfall in terms of suspended sediment concentration and sediment deposition at the seabed. The methodology adopted for the shore approach (Horizontal Directional Drilling - HDD) requires, indeed, the dredging of a small volume of sediment (around 2'500 m^3) at the exit point of the HDD.

The study is carried out through the implementation and coupling of MIKE 3 HD (Hydrodynamics) and MT (Mud Transport) three-dimensional models, state-of-the-art in the framework of marine circulation and sediment transport.

The approach followed to simulate the hydrodynamic component (circulation) is based on a three-dimensional realistic nesting of the regional scale model HYCOM. The resulting, high resolution, nested model starts from a resolution of 850m in the offshore area and, through a flexible mesh approach, reaches the highest resolution of 10m in the area where the excavation works will take place. After a detailed meteomarine characterization for the site, two periods of 1 month each have been simulated: one is representative for the summer/spring season (higher thermal stratification, lower current speed) and the other one for the winter/autumn period (weaker thermal stratification, higher current speed).

The results of the circulation component of the study show a regime of currents at surface with prevailing flux parallel to the coastline along the directions NW-SE; during the summer season the main directional sector is wider than in winter period. In general, the directions between 120°N and 135°N are the most frequent as well as the ones characterized by the highest velocities. At the sea bottom, during the winter period the trend is very similar to the one described at surface level, but it is characterized by smaller current intensities. During summer season, velocities at the sea bottom are very low and the circulation pattern is more chaotic.

The effect of incoming waves at the seabed has also been studied and the analysis put in evidence that the wave contribution is negligible, in consideration of the depth where dredging operations will take place and of the very small volumes that will be dredged.

The simulation of a long period hydrodynamics (in the order of months or more) allows to study the dispersion and transport of the sediment according to a fully realistic approach, thus overcoming the limits of synthetic / most probable scenarios approach. Through a "moving time-windows" approach, the dredging operations can be simulated several times under different hydrodynamic conditions, in full compliance with the indications provided by ISPRA in its guidelines [1].

The results have been then elaborated and provided in terms of (i) maps of maximum concentration of sediments within the model domain, (ii) maps of persistence in time of sediment concentration over specific thresholds (10mg/l and 50mg/l), and (iii) maps of

deposition of sediment at the seabed. All the statistical analyses have been conducted on monthly basis and analysed on three different reference levels: surface, mid water column and sea bottom.

Model results show that the distribution of maximum suspended sediment concentration resulting from dredging operations presents an elongated elliptic shape whose major axis is parallel to the coast (consistently with the prevailing current directions) and approximately centred along the trench area (minor axis of the ellipse). This elongated shape is more evident during the winter period, when the plume is larger at the sea bottom than at surface level. In summer the extension of the sediment plume is quite similar throughout the water column.

In general, a concentration of 10mg/l is reached at a maximum distance of approximately 1.2km from the dredged area, along the direction parallel to the coastline, and of 800m in the perpendicular direction. The concentration value of 50mg/l is reached only in an area around the dredged trench having a diameter of about 500m. Results in terms of persistence in time of given concentration values put in evidence that during the whole period of dredging operations (50 hours) the concentration exceeds 10mg/l for not more than 30 hours and 50mg/l for a maximum time of 21 hours and the highest persistence time is reached in the area close to the trench. The dense meadows of *Cymodocea nodosa* around the dredged area are affected by concentrations higher than 10mg/l only for a maximum duration of about 6 hours during the dredging operations, and only for a very limited portion, while concentrations higher than 50mg/l are not reached.

The sediment deposition at the sea bottom during dredging operations involves a confined portion of the domain. Only in the proximity of the dredged trench, up to approximately 200-300m, the deposition is larger than 1cm. The deposition decreases as soon as the distance from the dredged area grows: it is indeed only 1mm at a distance from the dredged area of approximately 2600m parallel to the coast and 800m perpendicular to the coast. Starting from a distance from the focus area of 500-600m in NW-SE direction and of 200-300m in SW-NE direction, the deposition is lower than 0.1mm.

10.0 REFERENCES

[1] I. Lisi, A. Feola, A. Bruschi, M. Di Risio, A. Pedroncini, D. Pasquali and E. Romano, “Mathematical modelling in the assessment of physical effects induced by sediment handling in marine-coastal areas,” ISPRA Manual and Guidelines, vol. 169, p. 144, 2017.

[2] DHI, “MIKE 3 Flow Model HD FM, Hydrodynamics Flexible Mesh, Scientific Documentation,” MIKE by DHI, Hørsholm, 2019.

[3] DHI, “MIKE 3 MT FM, Mud Transport Flexible Mesh, Scientific Documentation,” MIKE by DHI, Hørsholm, 2019.

[4] DHI, “Studio delle Dinamiche Costiere nel tratto di litorale prospiciente l'area di intervento,” Exploitation concession d.3G.C.-A.G. resulting from the exploration permits G.R13.AG and G.R14.AG https://va.minambiente.it/en-GB/Oggetti/Documentazione/526/3210, 29 11 2016.

[5] Lighthouse, “Environmental and biodiversity baseline report,” in Gas pipeline interconnection Malta-Italy post survey assessment, October 2019.

[6] DHI, “MIKE C-MAP, Extraction of World Wide Bathymetry Data and Tidal Information, Scietific Documentation,” MIKE by DHI, Hørsholm, 2019.

[7] Jeppesen Marine, “CM-93, Global Electronic Chart Database Professional+,” Jeppesen Marine, Norway, 2019.

[8] Lighthouse, “Geophysical survey - North-Up Bathy-Morphological Chart,” in Gas pipeline interconnection Malta-Italy project, June 2019.

[9] Lighthouse, “Environmental campaigns,” in Gas pipeline interconnection Malta-Italy pipeline reconaissance survey, October 2019.

[10] Lighthouse, “Metocean Study,” in Malta-Italy gas pipeline interconnection, April 2019.

[11] S. Saha, S. Moorthi, H. Pan and e. al., “The NCEP Climate Forecast System Reanalysis,” Bull. Amer. Meteor. Soc, vol. 91, pp. 1015 -1057, 2010.

[12] J. Michalakes, J. Dudhia, D. Gill, T. Henderson, J. Klemp, W. Skamarock and W. Wang, “The Weather Research and Forecast Model: Software Architecture and Performance,” in Proceedings of the 11th ECMWF Workshop on the Use of High Performance Computing in Meteorology, 2004.

[13] NCEP - National Centre for Environmental Prediction, “The GFS Atmospheric Model,” 28 August 2003. [Online]. Available: http://www.emc.ncep.noaa.gov/gmb/moorthi/gam.html.

[14] United Nations, “Sicily Channel/Tunisian Plateau: Topography, circulation and their effects on biological component,” in United Nations Environment Programme Mediterranean Action Plan - UNEP(DEPI)/MED WG.408/Inf.23, Athens, Greece, 2015.

[15] J. A. Cummings, “Operational multivariate ocean data assimilation,” Quarterly Journal of the royal meteorological society, vol. 131, no. 613, pp. 3583-3604, 2005.

[16] C. Yongcun and O. Baltazar Andersen, “Improvement in global ocean tide model in shallow water regions,” in Poster, SV.1-68 45, OSTST, Lisbon, Oct.18-22, 2010.

[17] A. Bennet and M. Foreman, “TOPEX/Poseidon tides estimated using a global inverse model.,” Journal of Geophysical Research, vol. 99, no. 24, pp. 821-852, 1994.

[18] J. G. S. Pennekamp, R. J. C. Epskamp, W. F. Rosenbrand, A. Mullié, G. L. Wessel, T. Arts and I. K. Deibel, “Turbidity Caused by Dredging; Viewed in Perspective,” Terra et Aqua - Number 64, September 1996.

[19] S. A. John, S. L. Challinor, M. Simpson, T. N. Burt and J. Spearman, “Scoping the assessment of sediment plumes from dredging,” in CIRIA Report C547, London, 2000.

[20] J. Becker, E. Van Elke, J. Van Wiechen, W. De Lange, T. Damsma, T. Smolders and M. Van Koningsveld, “Estimating source terms for far field dredge plume modelling,” Journal of Environmental Management, vol. 149, pp. 282-293, 2015.

[21] R. Flather, “A tidal model of the northwest European continental shelf,” Memories de la Societe Royale des Sciences de Liege, vol. 6, no. 10, p. 141–164, 1976.

[22] M. Tsimplis, R. Proctor and R. Flather, “A two-dimensional tidal model for the Mediterranean Sea,” Journal of Geophysical Research, vol. 100, Agosto 1995.

[23] A. Feola, I. Lisi, A. Salmeri, F. Venti, A. Pedroncini, M. Gabellini and E. Romano, “Platform of integrated tools to support environmental studies and management of dredging activities,” Journal of Environmental Management, vol. 166, pp. 357-373, 2016.

[24] DHI, “Studio Modellistico dei processi di trasporto e deposizione dei sedimenti nelle fasi di dragaggio e successivo riempimento,” in Trans Adriatic Pipeline - Albania-Italy pipeline - https://va.minambiente.it/en-GB/Oggetti/Documentazione/625/2852, 2017.

[25] DHI, “Øresund Link Environmental Impact Assessment,” 1990-2000.

[26] DHI, “Feedback Monitoring, Environmental Monitoring and Management,” Øresund, Denmark, 1995-2000.

[27] A. Pedroncini, G. Contento, L. Donatini, L. Cusati, G. Lupieri, H. Hansen and R. Bolanos Sanches, “Mediterranean Wind Wave Model (MWM): a 40 year hindcast database of wind and wave conditions and a base for relocatable operational forecast models,” 2019.

[28] J. Michalakes, S. Chen, J. Dudhia, L. Hart, J. Klemp, J. Middlecoff and W. Skamarock, “Development of a Next Generation Regional Weather Research and Forecast Model,” in Proceedings of the 9th ECMWF Workshop on the Use of High Performance Computing in Meteorology., 2001.

[29] DHI, “MIKE 21 SW - Spectral Wave Module, Scientific Documentation,” MIKE by DHI, Hørsholm, 2019.

APPENDIX A – MIKE 3 HD FM

MIKE
Powered by DHI

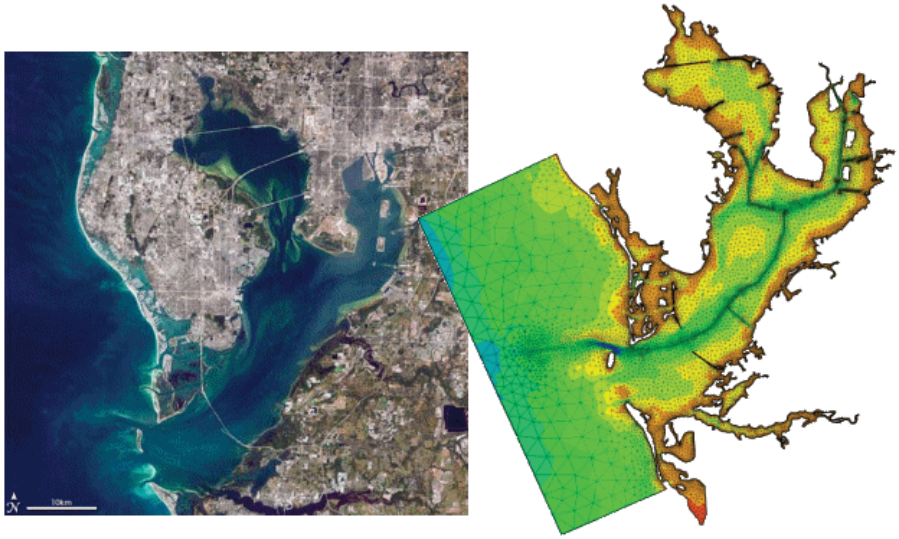

MIKE 21 & MIKE 3 Flow Model FM

Hydrodynamic Module

Short Description

MIKE 21 & MIKE 3 Flow Model FM

The Flow Model FM is a comprehensive modelling system for two- and three-dimensional water modelling developed by DHI. The 2D and 3D models carry the same names as the classic DHI model versions MIKE 21 & MIKE 3 with an 'FM' added referring to the type of model grid - Flexible Mesh.

The modelling system has been developed for complex applications within oceanographic, coastal and estuarine environments. However, being a general modelling system for 2D and 3D free-surface flows it may also be applied for studies of inland surface waters, e.g. overland flooding and lakes or reservoirs.

MIKE 21 & MIKE 3 Flow Model FM is a general hydrodynamic flow modelling system based on a finite volume method on an unstructured mesh

The Modules of the Flexible Mesh Series

DHI's Flexible Mesh (FM) series includes the following modules:

Flow Model FM modules

- Hydrodynamic Module, HD
- Transport Module, TR
- Ecology Modules, MIKE ECO Lab/AMB Lab
- Oil Spill Module, OS
- Mud Transport Module, MT
- Particle Tracking Module, PT
- Sand Transport Module, ST
- Shoreline Morphology Module, SM

Wave module

- Spectral Wave Module, SW

The FM Series meets the increasing demand for realistic representations of nature, both with regard to 'look alike' and to its capability to model coupled processes, e.g. coupling between currents, waves and sediments. Coupling of modules is managed in the Coupled Model FM.

All modules are supported by advanced user interfaces including efficient and sophisticated tools for mesh generation, data management, 2D/3D visualization, etc. In combination with comprehensive documentation and support, the FM series forms a unique professional software tool for consultancy services related to design, operation and maintenance tasks within the marine environment.

An unstructured grid provides an optimal degree of flexibility in the representation of complex geometries and enables smooth representations of boundaries. Small elements may be used in areas where more detail is desired, and larger elements used where less detail is needed, optimising information for a given amount of computational time.

The spatial discretisation of the governing equations is performed using a cell-centred finite volume method. In the horizontal plane, an unstructured grid is used while a structured mesh is used in the vertical domain (3D).

This document provides a short description of the Hydrodynamic Module included in MIKE 21 & MIKE 3 Flow Model FM.

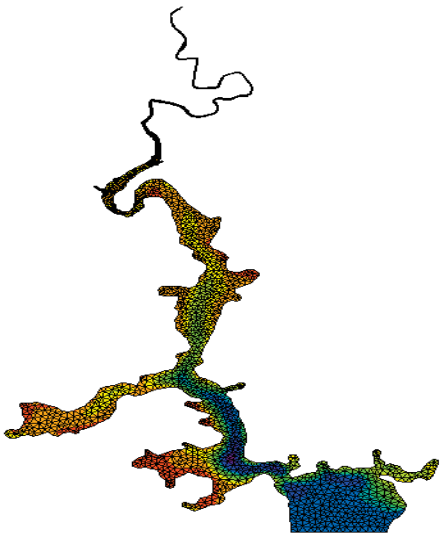

Example of computational mesh for Tamar Estuary, UK

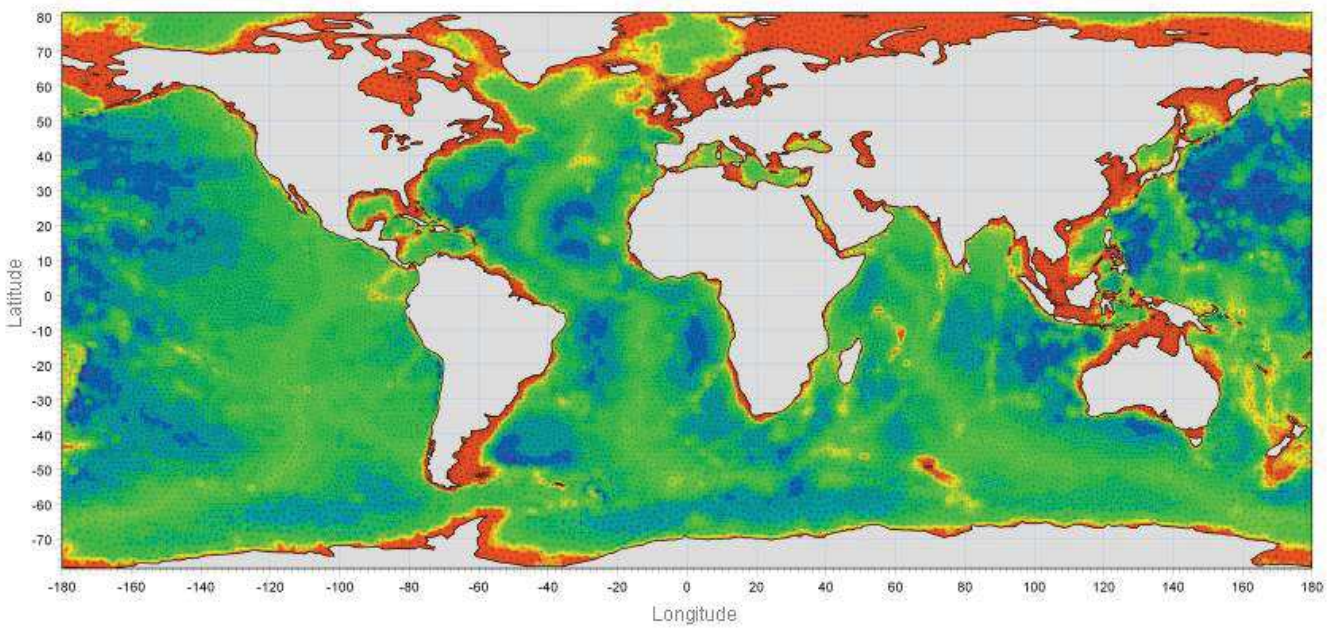

MIKE 21 & MIKE 3 FLOW MODEL FM supports both Cartesian and spherical coordinates. Spherical coordinates are usually applied for regional and global sea circulation applications. The chart shows the computational mesh and bathymetry for the planet Earth generated by the MIKE Zero Mesh Generator

MIKE 21 & MIKE 3 Flow Model FM - Hydrodynamic Module

The Hydrodynamic Module provides the basis for computations performed in many other modules, but can also be used alone. It simulates the water level variations and flows in response to a variety of forcing functions on flood plains, in lakes, estuaries and coastal areas.

Application Areas

The Hydrodynamic Module included in MIKE 21 & MIKE 3 Flow Model FM simulates unsteady flow taking into account density variations, bathymetry and external forcings.

The choice between 2D and 3D model depends on a number of factors. For example, in shallow waters, wind and tidal current are often sufficient to keep the water column well-mixed, i.e. homogeneous in salinity and temperature. In such cases a 2D model can be used. In water bodies with stratification, either by density or by species (ecology), a 3D model should be used. This is also the case for enclosed or semi-enclosed waters where wind-driven circulation occurs.

Typical application areas are

- Assessment of hydrographic conditions for design, construction and operation of structures and plants in stratified and non-stratified waters
- Environmental impact assessment studies
- Coastal and oceanographic circulation studies
- Optimization of port and coastal protection infrastructures
- Lake and reservoir hydrodynamics
- Cooling water, recirculation and desalination
- Coastal flooding and storm surge
- Inland flooding and overland flow modelling
- Forecast and warning systems

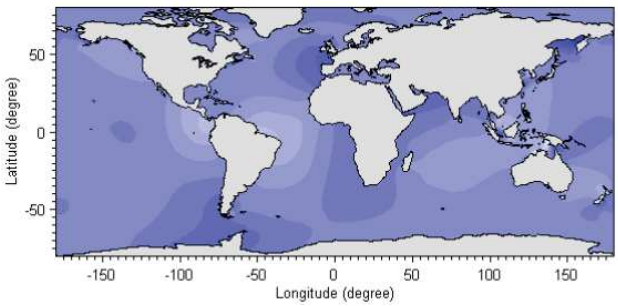

Example of a global tide application of MIKE 21 Flow Model FM. Results from such a model can be used as boundary conditions for regional scale forecast or hindcast models

The MIKE 21 & MIKE 3 Flow Model FM also support spherical coordinates, which makes both models particularly applicable for global and regional sea scale applications.

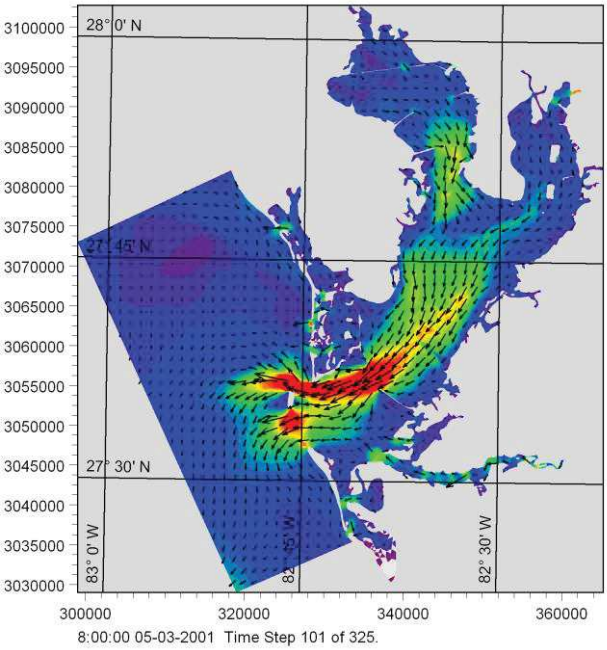

Example of a flow field in Tampa Bay, Florida, simulated by MIKE 21 Flow Model FM

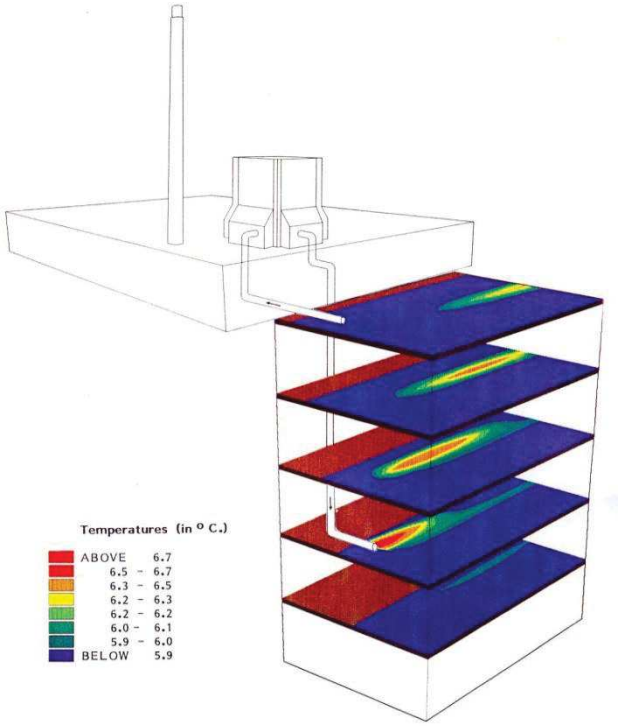

Study of thermal plume dispersion

Typical applications with the MIKE 21 & MIKE 3 Flow Model FM include cooling water recirculation and ecological impact assessment (eutrophication)

The Hydrodynamic Module is together with the Transport Module (TR) used to simulate the spreading and fate of dissolved and suspended substances. This module combination is applied in tracer simulations, flushing and simple water quality studies.

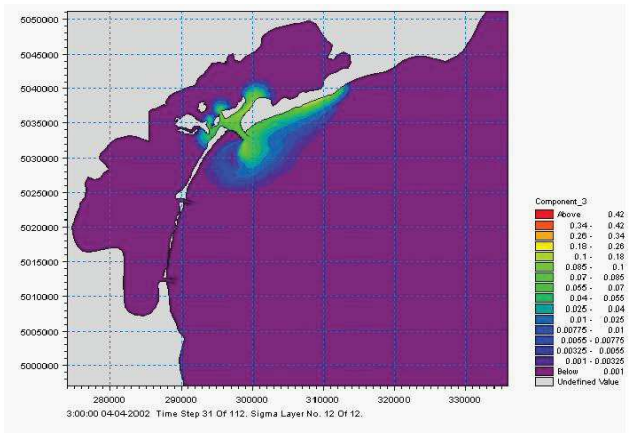

Tracer simulation of single component from outlet in the Adriatic, simulated by MIKE 21 Flow Model FM HD+TR

Prediction of ecosystem behaviour using the MIKE 21 & MIKE 3 Flow Model FM together with MIKE ECO Lab

The Hydrodynamic Module can be coupled to the Ecological Module (MIKE ECO Lab) to form the basis for environmental water quality studies comprising multiple components.

Furthermore, the Hydrodynamic Module can be coupled to sediment models for the calculation of sediment transport. The Sand Transport Module and Mud Transport Module can be applied to simulate transport of non-cohesive and cohesive sediments, respectively.

In the coastal zone the transport is mainly determined by wave conditions and associated wave-induced currents. The wave-induced currents are generated by the gradients in radiation stresses that occur in the surf zone. The Spectral Wave Module can be used to calculate the wave conditions and associated radiation stresses.

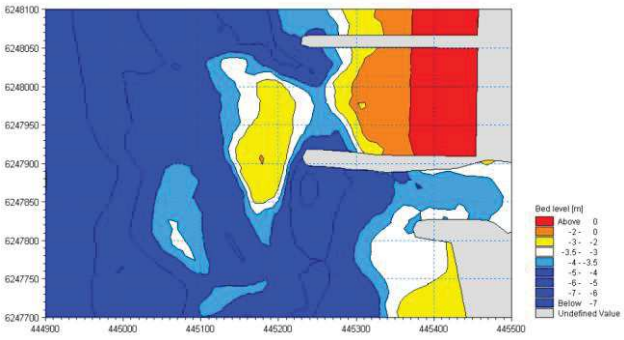

Coastal application (morphology) with coupled MIKE 21 HD, SW and ST, Torsminde harbour Denmark

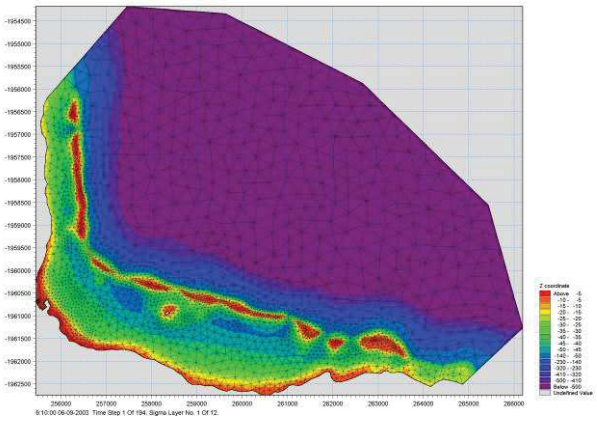

Model bathymetry of Taravao Bay, Tahiti

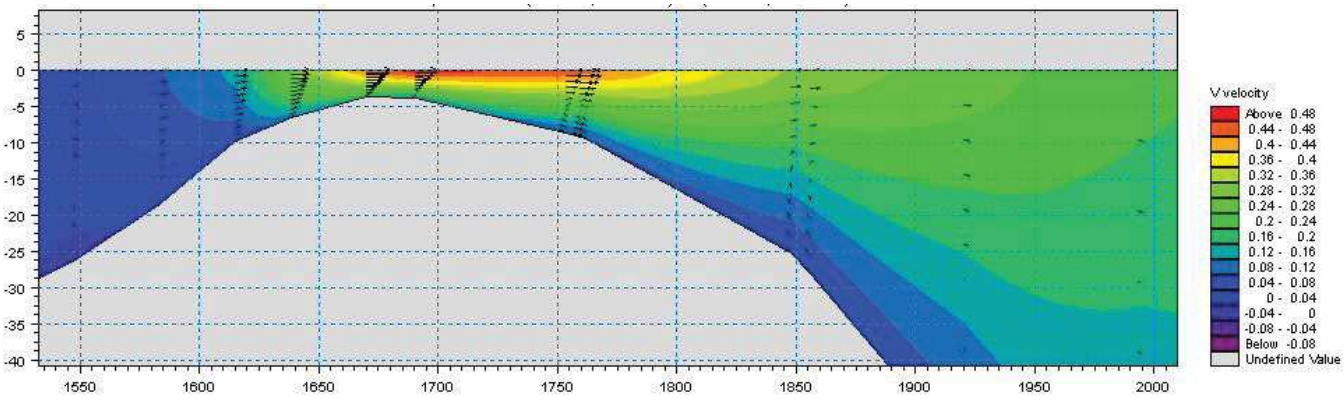

Example of vertical profile of cross reef currents in Taravao Bay, Tahiti simulated with MIKE 3 Flow Model FM. The circulation and renewal of water inside the reef is dependent on the tides, the meteorological conditions and the cross reef currents, thus the circulation model includes the effects of wave induced cross reef currents

Computational Features

The main features and effects included in simulations with the MIKE 21 & MIKE 3 Flow Model FM – Hydrodynamic Module are the following:

- Flooding and drying
- Momentum dispersion
- Bottom shear stress
- Coriolis force
- Wind shear stress
- Barometric pressure gradients
- Ice coverage
- Tidal potential
- Precipitation/evaporation
- Infiltration
- Heat exchange with atmosphere
- Wave radiation stresses
- Sources and sinks, incl. jet
- Structures

Model Equations

The modelling system is based on the numerical solution of the two/three-dimensional incompressible Reynolds averaged Navier-Stokes equations subject to the assumptions of Boussinesq and of hydrostatic pressure. Thus, the model consists of continuity, momentum, temperature, salinity and density equations and it is closed by a turbulent closure scheme. The density does not depend on the pressure, but only on the temperature and the salinity.

For the 3D model, the free surface is taken into account using a sigma-coordinate transformation approach or using a combination of a sigma and z-level coordinate system.

Below the governing equations are presented using Cartesian coordinates.

The local continuity equation is written as

$$\frac{\partial u}{\partial x}+\frac{\partial v}{\partial y}+\frac{\partial w}{\partial z}=S$$

and the two horizontal momentum equations for the x- and y-component, respectively

$$\frac{\partial u}{\partial t}+\frac{\partial u^2}{\partial x}+\frac{\partial vu}{\partial y}+\frac{\partial wu}{\partial z}=fv-g\frac{\partial \eta}{\partial x}-\frac{1}{\rho_0}\frac{\partial p_a}{\partial x}-\frac{g}{\rho_0}\int_z^\eta \frac{\partial \rho}{\partial x}dz+F_u+\frac{\partial}{\partial z}\left(\nu_t\frac{\partial u}{\partial z}\right)+u_sS$$

$$\frac{\partial v}{\partial t}+\frac{\partial v^2}{\partial y}+\frac{\partial uv}{\partial x}+\frac{\partial wv}{\partial z}=-fu-g\frac{\partial \eta}{\partial y}-\frac{1}{\rho_0}\frac{\partial p_a}{\partial y}-\frac{g}{\rho_0}\int_z^\eta \frac{\partial \rho}{\partial y}dz+F_v+\frac{\partial}{\partial z}\left(\nu_t\frac{\partial v}{\partial z}\right)+v_sS$$

Temperature and salinity

In the Hydrodynamic Module, calculations of the transports of temperature, *T*, and salinity, *s* follow the general transport-diffusion equations as

$$\frac{\partial T}{\partial t}+\frac{\partial uT}{\partial x}+\frac{\partial vT}{\partial y}+\frac{\partial wT}{\partial z}=F_T+\frac{\partial}{\partial z}\left(D_v\frac{\partial T}{\partial z}\right)+\hat{H}+T_sS$$

$$\frac{\partial s}{\partial t}+\frac{\partial us}{\partial x}+\frac{\partial vs}{\partial y}+\frac{\partial ws}{\partial z}=F_s+\frac{\partial}{\partial z}\left(D_v\frac{\partial s}{\partial z}\right)+s_sS$$

Unstructured mesh technique gives the maximum degree of flexibility, for example: 1) Control of node distribution allows for optimal usage of nodes 2) Adoption of mesh resolution to the relevant physical scales 3) Depth-adaptive and boundary-fitted mesh. Below is shown an example from Ho Bay, Denmark with the approach channel to the Port of Esbjerg

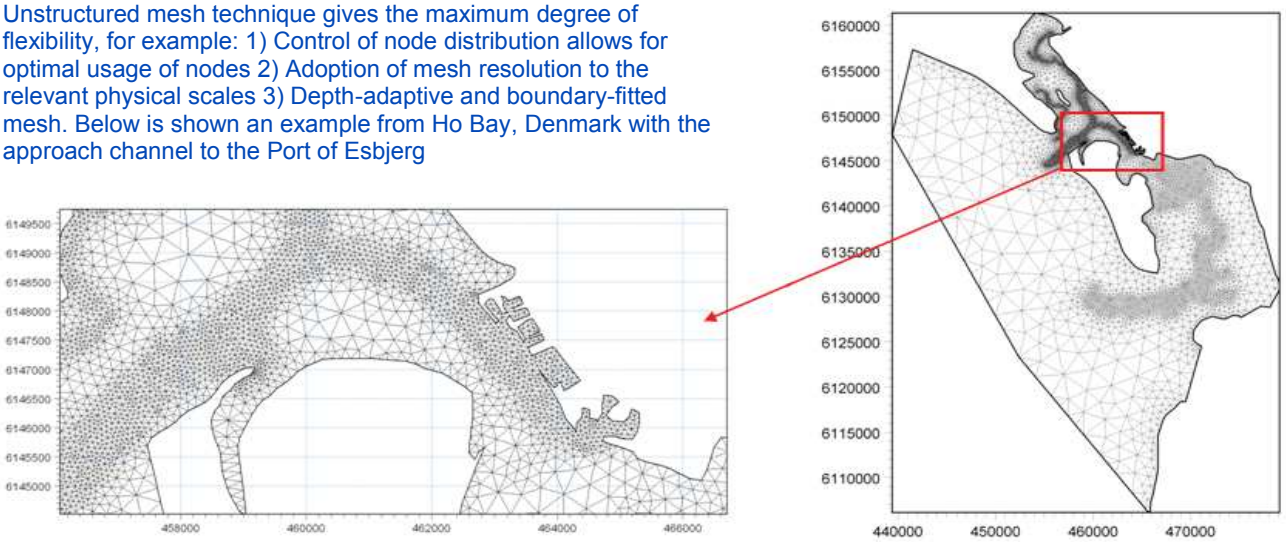

The horizontal diffusion terms are defined by

$$(F_T, F_s) = \left[\frac{\partial}{\partial x}\left(D_h \frac{\partial}{\partial x}\right) + \frac{\partial}{\partial y}\left(D_h \frac{\partial}{\partial y}\right)\right](T, s)$$

The equations for two-dimensional flow are obtained by integration of the equations over depth.

Heat exchange with the atmosphere is also included.

Symbol list

t	time
x, y, z	Cartesian coordinates
u, v, w	flow velocity components
T, s	temperature and salinity
D_v	vertical turbulent (eddy) diffusion coefficient
$\hat{H}$	source term due to heat exchange with atmosphere
S	magnitude of discharge due to point sources
T_s, s_s	temperature and salinity of source
F_T, F_s, F_c	horizontal diffusion terms
D_h	horizontal diffusion coefficient
h	depth

Solution Technique

The spatial discretisation of the primitive equations is performed using a cell-centred finite volume method. The spatial domain is discretised by subdivision of the continuum into non-overlapping elements/cells.

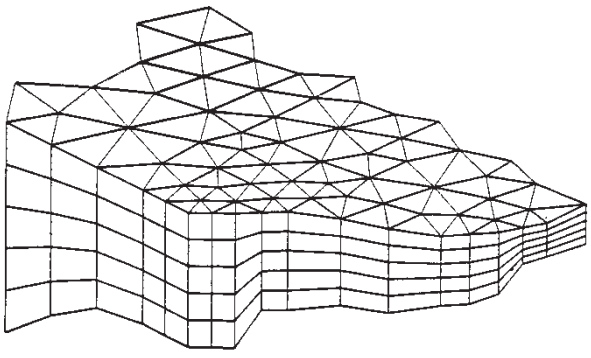

Principle of 3D mesh

In the horizontal plane an unstructured mesh is used while a structured mesh is used in the vertical domain of the 3D model. In the 2D model the elements can be triangles or quadrilateral elements. In the 3D model the elements can be prisms or bricks whose horizontal faces are triangles and quadrilateral elements, respectively.

The effect of a number of structure types (weirs, culverts, dikes, gates, piers and turbines) with a horizontal dimension which usually cannot be resolved by the computational mesh is modelled by a subgrid technique.

Model Input

Input data can be divided into the following groups:

- Domain and time parameters:
  - computational mesh (the coordinate type is defined in the computational mesh file) and bathymetry
  - simulation length and overall time step
- Calibration factors
  - bed resistance
  - momentum dispersion coefficients
  - wind friction factors
  - heat exchange coefficients
- Initial conditions
  - water surface level
  - velocity components
  - temperature and salinity
- Boundary conditions
  - closed
  - water level
  - discharge
  - temperature and salinity
- Other driving forces
  - wind speed and direction
  - tide
  - source/sink discharge
  - wave radiation stresses
- Structures
  - Structure type
  - location
  - structure data

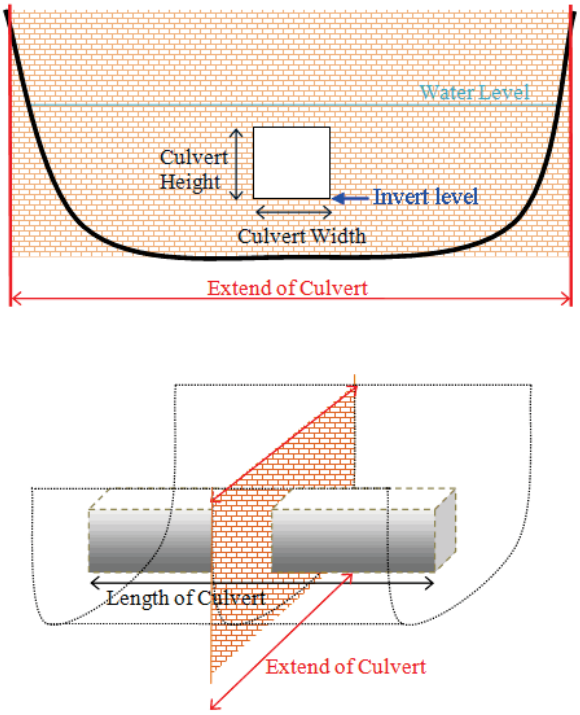

Setup definition of culvert structure

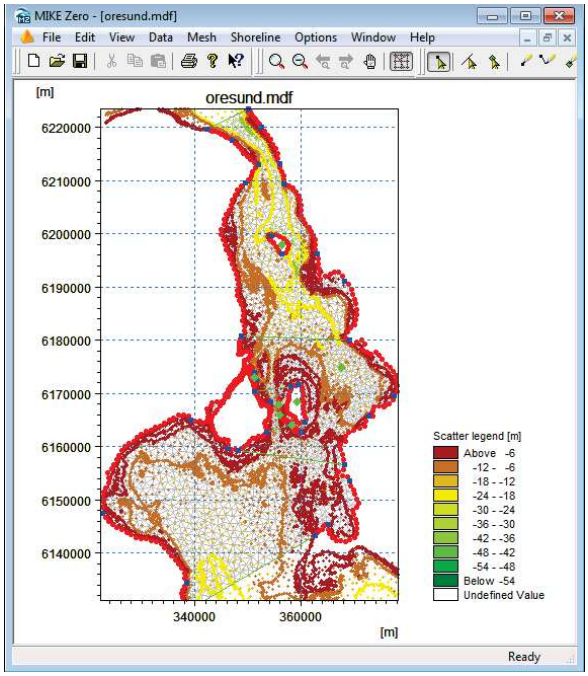

The Mesh Generator is an efficient MIKE Zero tool for the generation and handling of unstructured meshes, including the definition and editing of boundaries

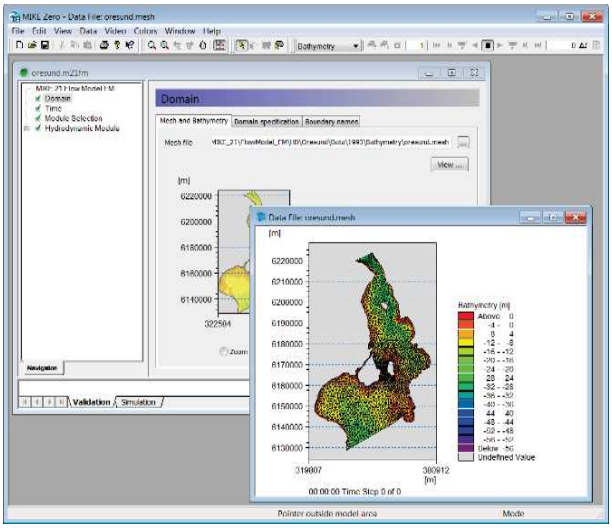

View button on all the GUIs in MIKE 21 & MIKE 3 FM HD for graphical view of input and output files

Providing MIKE 21 & MIKE 3 Flow Model FM with a suitable mesh is essential for obtaining reliable results from the models. Setting up the mesh includes the appropriate selection of the area to be modelled, adequate resolution of the bathymetry, flow, wind and wave fields under consideration and definition of codes for defining boundaries.

2D visualization of a computational mesh (Odense Estuary)

Bathymetric values for the mesh generation can e.g. be obtained from the MIKE Powered by DHI product MIKE C-Map. MIKE C-Map is an efficient tool for extracting depth data and predicted tidal elevation from the world-wide Electronic Chart Database CM-93 Edition 3.0 from C-MAP Norway.

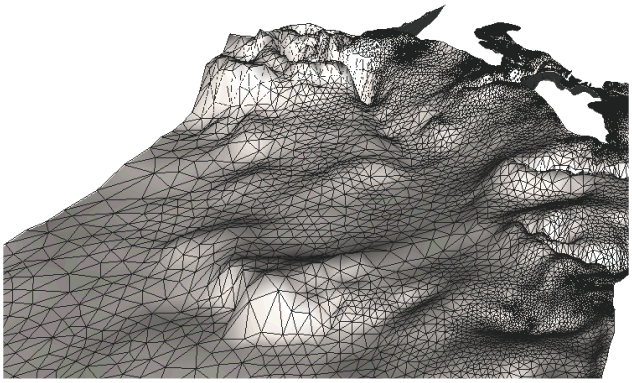

3D visualization of a computational mesh

If wind data is not available from an atmospheric meteorological model, the wind fields (e.g. cyclones) can be determined by using the wind-generating programs available in MIKE 21 Toolbox.

Global winds (pressure & wind data) can be downloaded for immediate use in your simulation. The sources of data are from GFS courtesy of NCEP, NOAA. By specifying the location, orientation and grid dimensions, the data is returned to you in the correct format as a spatial varying grid series or a time series. The link is:

http://www.waterforecast.com/hindcastdataproducts

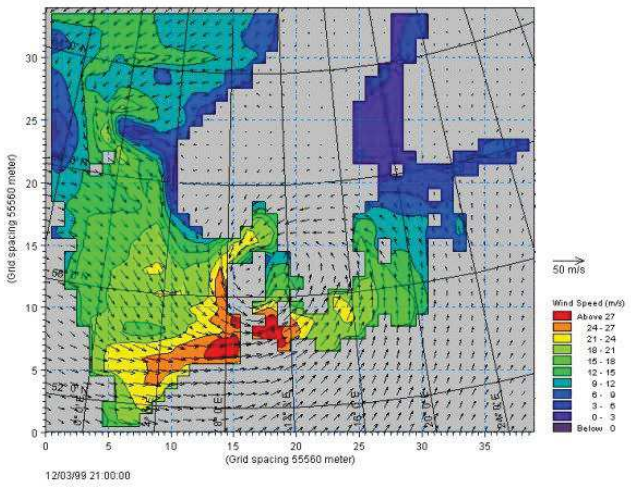

The chart shows a hindcast wind field over the North Sea and Baltic Sea as wind speed and wind direction

Model Output

Computed output results at each mesh element and for each time step consist of:

- Basic variables
  - water depths and surface elevations
  - flux densities in main directions
  - velocities in main directions
  - densities, temperatures and salinities
- Additional variables
  - Current speed and direction
  - Wind velocity
  - Air pressure
  - Drag coefficient
  - Precipitation/evaporation
  - Courant/CFL number
  - Eddy viscosity
  - Element area/volume

The output results can be saved in defined points, lines and areas. In the case of 3D calculations, the results are saved in a selection of layers.

Output from MIKE 21 & MIKE 3 Flow Model FM is typically post-processed using the Data Viewer available in the common MIKE Zero shell. The Data Viewer is a tool for analysis and visualization of unstructured data, e.g. to view meshes, spectra, bathymetries, results files of different format with graphical extraction of time series and line series from plan view and import of graphical overlays.

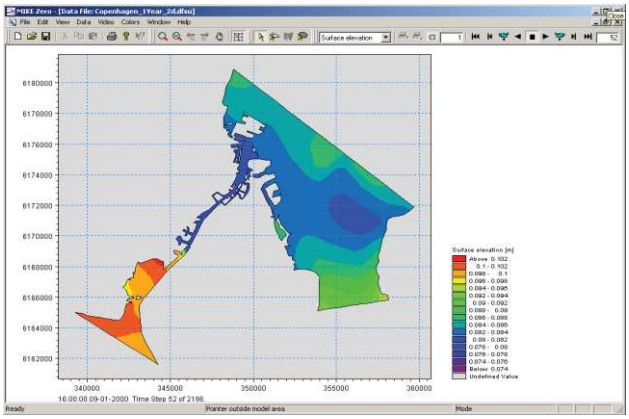

The Data Viewer in MIKE Zero – an efficient tool for analysis and visualization of unstructured data including processing of animations. Above screen dump shows surface elevations from a model setup covering Port of Copenhagen

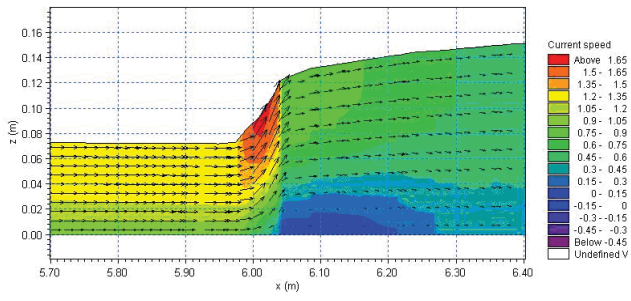

Vector and contour plot of current speed at a vertical profile defined along a line in Data Viewer in MIKE Zero

Validation

Prior to the first release of MIKE 21 & MIKE 3 Flow Model FM in year 19xx the model has successfully been applied to a number of basic idealized situations for which the results can be compared with analytical solutions or information from the literature.

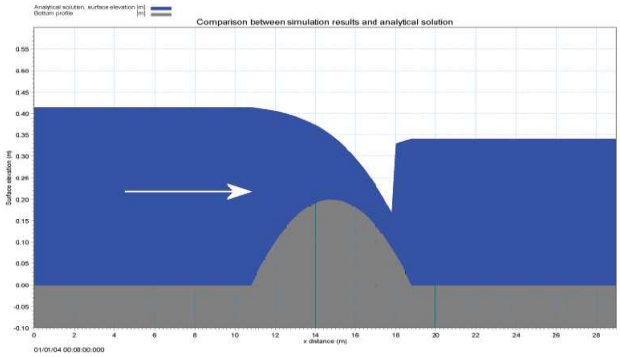

The domain is a channel with a parabola-shaped bump in the middle. The upstream (western) boundary is a constant flux and the downstream (eastern) boundary is a constant elevation. Below: the total depths for the stationary hydraulic jump at convergence. Red line: 2D setup, green line: 3D setup, black line: analytical solution

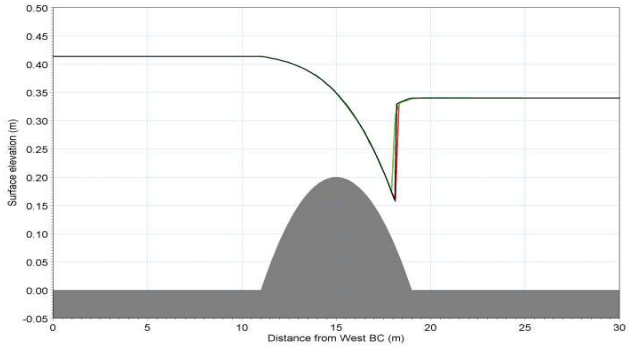

A dam-break flow in an L-shaped channel (a, b, c):

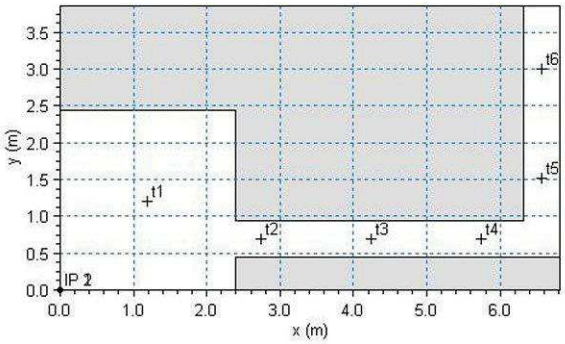

a) Outline of model setup showing the location of gauging points

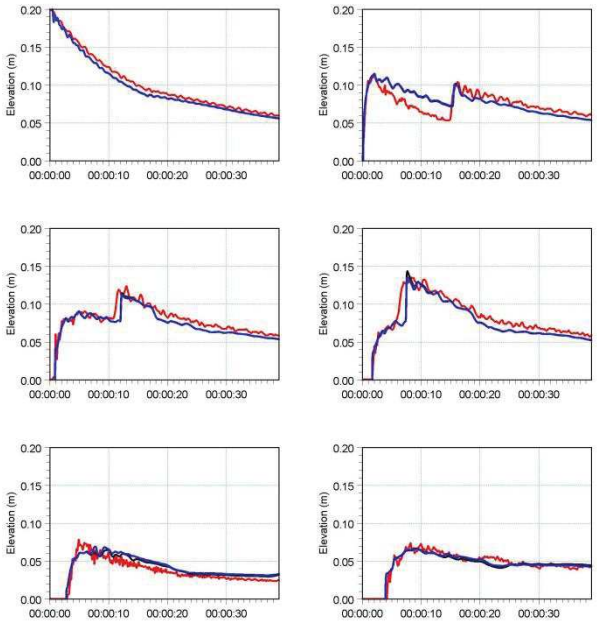

b) Comparison between simulated and measured water levels at the six gauge locations.
(Blue) coarse mesh solution (black) fine mesh solution and (red) measurements

The model has also been applied and tested in numerous natural geophysical conditions; ocean scale, inner shelves, estuaries, lakes and overland, which are more realistic and complicated than academic and laboratory tests.

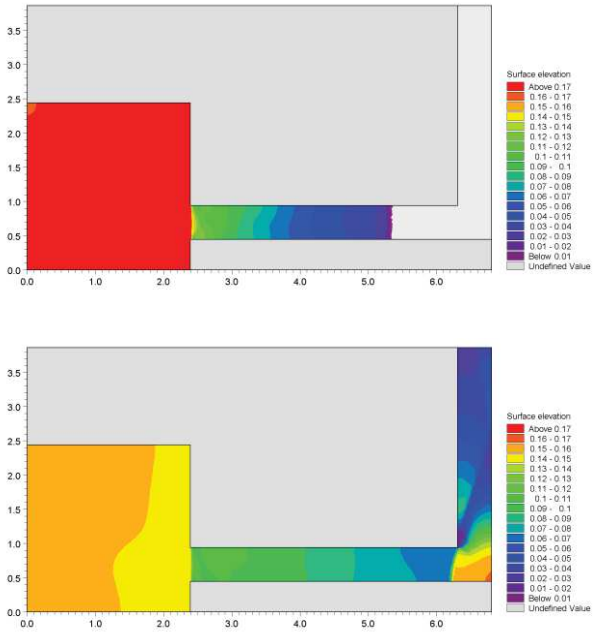

c) Contour plots of the surface elevation at T = 1.6 s (top) and T = 4.8 s (bottom)

Example from Ho Bay, a tidal estuary (barrier island coast) in South-West Denmark with access channel to the Port of Esbjerg.

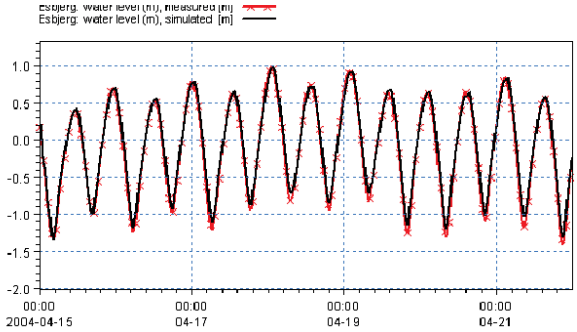

Comparison between measured and simulated water levels

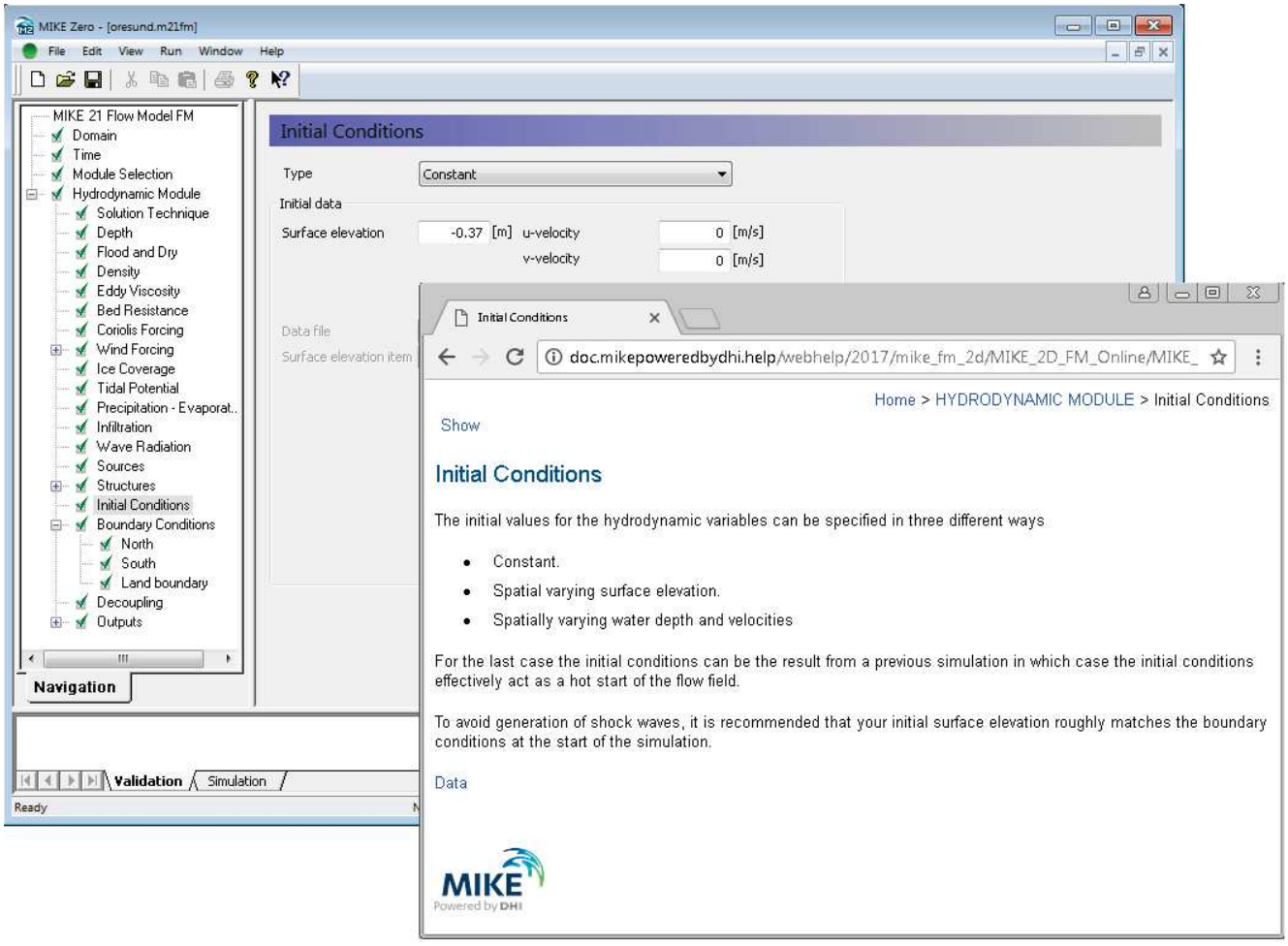

The user interface of the MIKE 21 and MIKE 3 Flow Model FM (Hydrodynamic Module), including an example of the extensive Online Help system

Graphical User Interface

The MIKE 21 & MIKE 3 Flow Model FM Hydrodynamic Module is operated through a fully Windows integrated graphical user interface (GUI). Support is provided at each stage by an Online Help system.

The common MIKE Zero shell provides entries for common data file editors, plotting facilities and utilities such as the Mesh Generator and Data Viewer.

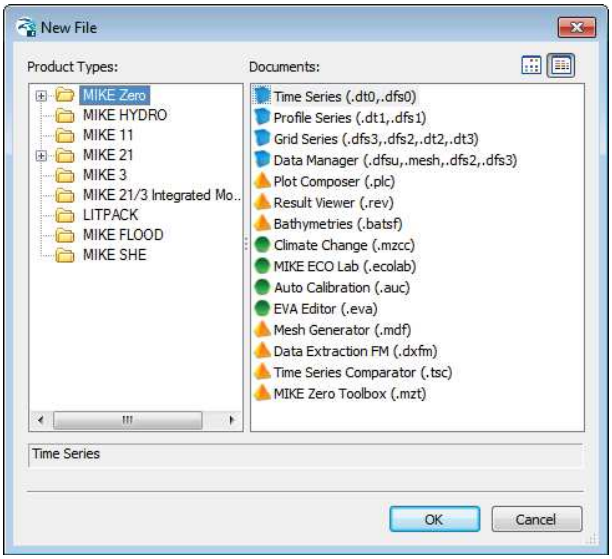

Overview of the common MIKE Zero utilities

Parallelisation

The computational engines of the MIKE 21 & MIKE 3 FM series are available in versions that have been parallelised using both shared memory as well as distributed memory architecture. The latter approach allows for domain decomposition. The result is much faster simulations on systems with multiple cores. It is also possible to use a graphics card (GPU) to perform computational intensive hydrodynamic computations.

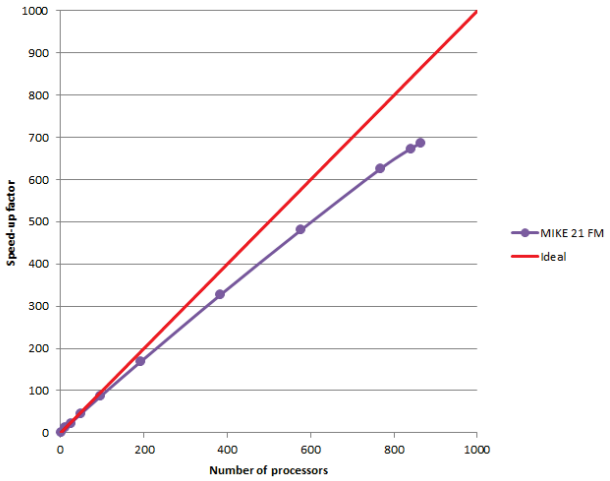

Example of MIKE 21 HD FM speed-up using a HPC Cluster with distributed memory architecture (purple)

Hardware and Operating System Requirements

The MIKE Zero Modules support Microsoft Windows 7 Professional Service Pack 1 (64 bit), Windows 10 Pro (64 bit), Windows Server 2012 R2 Standard (64 bit) and Windows Server 2016 Standard (64 bit).

Microsoft Internet Explorer 9.0 (or higher) is required for network license management. An internet browser is also required for accessing the web-based documentation and online help.

The recommended minimum hardware requirements for executing the MIKE Zero modules are:

Processor:	3 GHz PC (or higher)
Memory (RAM):	2 GB (or higher)
Hard disk:	40 GB (or higher)
Monitor:	SVGA, resolution 1024x768
Graphics card: (GUI and visualisation)	64 MB RAM (256 MB RAM or higher is recommended)
Graphics card: (for GPU computation)	1 GB RAM (or higher). requires a NVIDIA graphics card with compute capability 2.0 or higher

Support

News about new features, applications, papers, updates, patches, etc. are available here:

www.mikepoweredbydhi.com/Download/DocumentsAndTools.aspx

For further information on MIKE 21 and MIKE 3 Flow Model FM software, please contact your local DHI office or the support centre:

MIKE Powered by DHI Client Care
Agern Allé 5
DK-2970 Hørsholm
Denmark

Tel: +45 4516 9333
Fax: +45 4516 9292

mike@dhigroup.com
www.mikepoweredbydhi.com

Further Reading

Petersen, N.H., Rasch, P. “Modelling of the Asian Tsunami off the Coast of Northern Sumatra”, presented at the 3rd Asia-Pacific DHI Software Conference in Kuala Lumpur, Malaysia, 21-22 February, 2005

French, B. and Kerper, D. Salinity Control as a Mitigation Strategy for Habitat Improvement of Impacted Estuaries. 7th Annual EPA Wetlands Workshop, NJ, USA 2004.

DHI Note, “Flood Plain Modelling using unstructured Finite Volume Technique” January 2004 – download from

http://www.theacademybydhi.com/research-and-publications/scientific-publications

Documentation

The MIKE 21 & MIKE 3 Flow Model FM models are provided with comprehensive user guides, online help, scientific documentation, application examples and step-by-step training examples.

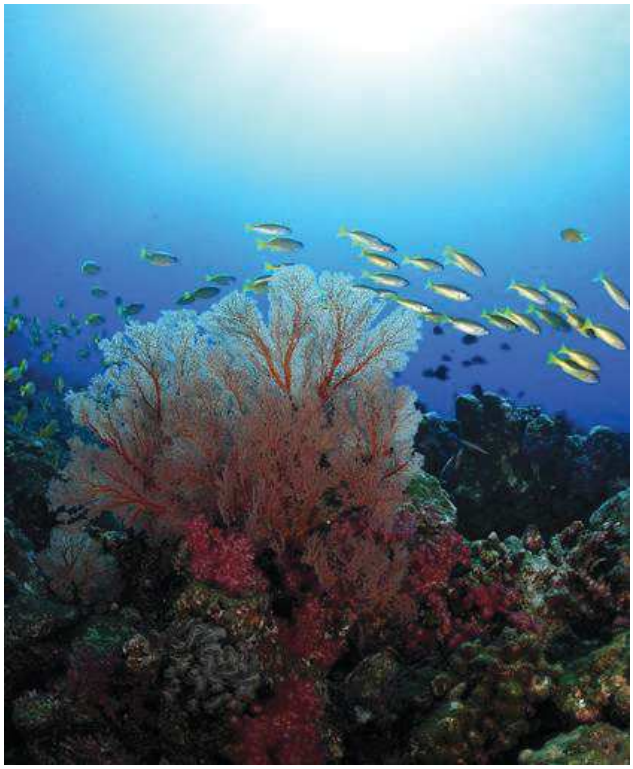

APPENDIX B – MIKE 3 MT FM

MIKE 21 & MIKE 3 Flow Model FM

Mud Transport Module

Short Description

MIKE 21 & MIKE 3 Flow Model FM – Mud Transport Module

This document describes the Mud Transport Module (MT) under the comprehensive modelling system for two- and three-dimensional flows, the Flexible Mesh series, developed by DHI.

The MT module includes a state-of-the-art mud transport model that simulates the erosion, transport, settling and deposition of cohesive sediment in marine, brackish and freshwater areas. The module also takes into account fine-grained non-cohesive material.

Example of spreading of dredged material in Øresund, Denmark

The MT module is an add-on module to MIKE 21 & MIKE 3 Flow Model FM. It requires a coupling to the hydrodynamic solver and to the transport solver for passive components (Advection Dispersion module). The hydrodynamic basis is obtained with the MIKE 21 or MIKE 3 FM HD module. The influence of waves on the erosion/deposition patterns can be included by applying the Spectral Wave module, MIKE 21 FM SW.

With the FM series it is possible to combine and run the modules dynamically. If the morphological changes within the area of interest are within the same order of magnitude as the variation in the water depth, then it is possible to take the morphological impact on the hydrodynamics into consideration. This option for dynamic feedback between update of seabed and flow may be relevant to apply in shallow areas, for example, where long term effects are being considered. Furthermore, it may be relevant in shallow areas where capital or considerable maintenance dredging is planned and similarly at sites where disposal of the dredged material takes place.

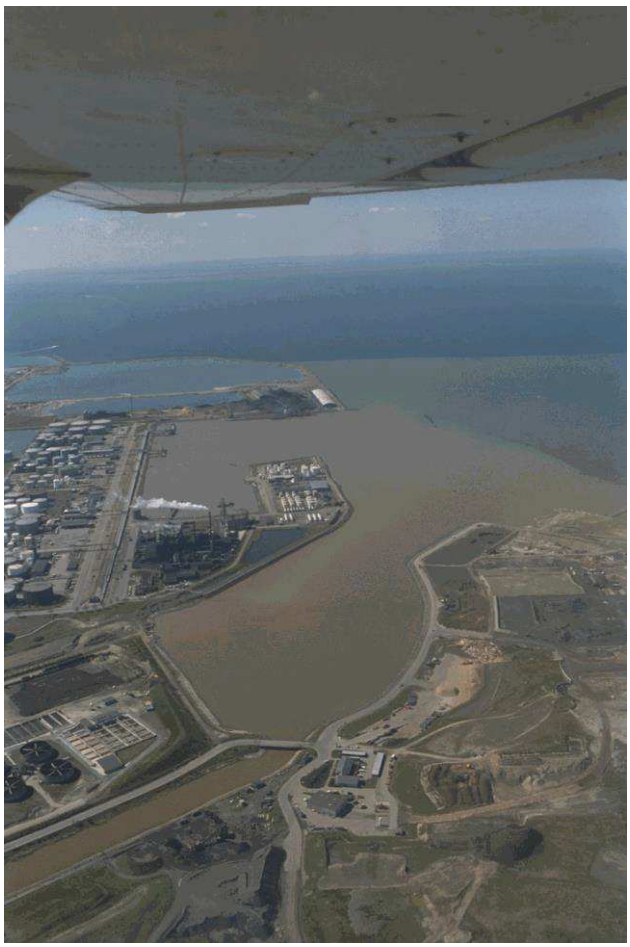

Example of sediment plume from a river near Malmö, Sweden

Application Areas

The MT module is used in a variety of cases where the erosion, dispersion, and deposition of cohesive sediments are of interest. Fine-grained sediment may cause impacts in different ways. In suspension, the fines may shadow areas over a time span, which can be critical for the survival of light-depending benthic fauna and flora. The fine-grained sediment may deposit in areas where deposition is unwanted, for instance in harbour inlets.

Furthermore, pollutants such as heavy metals and TBT are prone to adhere to the cohesive sediment. If polluted sediment is deposited in ecologically sensitive areas it may heavily affect local flora and fauna and water quality in general.

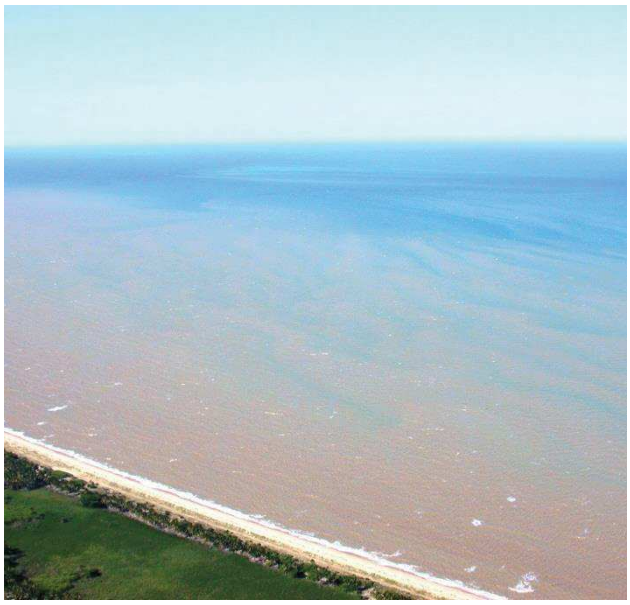

Example of resuspension in the nearshore zone. Caravelas, Brazil. Assessment of resuspension may be relevant in, for example, dredging projects to identify sources and levels of background turbidity

The estimation of siltation rates is an area where the MT module often is applied and also an important aspect to consider when designing new approach channels or deepening existing channels to allow access for larger vessels to the ports. Simulations of fine-grained sediment dynamics may contribute to optimise the design with regard to navigation and manoeuvrability on one hand and minimising the need for maintenance dredging on the other.

The MT module has many application areas and some of the most frequently used are listed below:

- Dispersion of dredged material
- Optimisation of dredging operations
- Siltation of harbours
- Siltation in access channels
- Cohesive sediment dynamics and morphology
- Dispersion of river plumes
- Erosion of fine-grained material under combined waves and currents
- Sediment laden gravity flows and turbidity currents
- Studies of dynamics of contaminated sediments

Example of muddy estuary. Caravelas, Brazil

Computational Features

The main features of the MIKE 21 & MIKE 3 Flow Model FM Mud Transport module are:

- Multiple sediment fractions
- Multiple bed layers
- Flocculation
- Hindered settling
- Inclusion of non-cohesive sediments
- Bed shear stress from combined currents and waves
- Waves included as wave database or 2D time series
- Consolidation
- Morphological update of bed
- Tracking of sediment spills

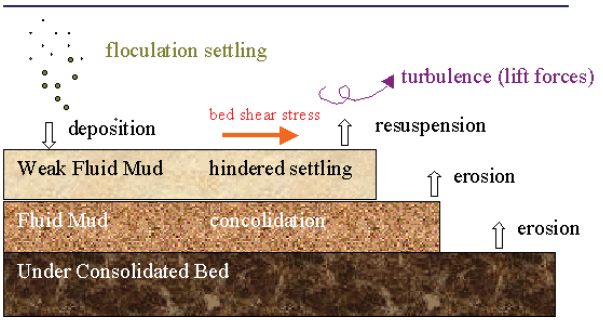

Example of modelled physical processes

Model Equations

The governing equations behind the MT module are essentially based on Mehta et al. (1989). The impact of waves is introduced through the bed shear stress. The cohesive sediment transport module or mud transport (MT) module deals with the movement of mud in a fluid and the interaction between the mud and the bed.

The transport of the mud is generally described by the following equation (e.g. Teisson, 1991):

$$\frac{\partial c^i}{\partial t}+\frac{\partial uc^i}{\partial x}+\frac{\partial vc^i}{\partial y}+\frac{\partial wc^i}{\partial z}-\frac{\partial w_s c^i}{\partial z}=$$

$$\frac{\partial}{\partial x}\left(\frac{\upsilon_{Tx}}{\sigma^i_{Tx}}\frac{\partial c^i}{\partial x}\right)+\frac{\partial}{\partial y}\left(\frac{\upsilon_{Ty}}{\sigma^i_{Ty}}\frac{\partial c^i}{\partial y}\right)+\frac{\partial}{\partial z}\left(\frac{\upsilon_{Tz}}{\sigma^i_{Tz}}\frac{\partial c^i}{\partial z}\right)+S^i$$

The transport of the cohesive sediment is handled by a transport solver for passive components (AD-module). The settling velocity w_s is a sedimentological process and as such it is described separately with the extra term $\frac{\partial w_s C^i}{\partial z}$ using an operator splitting technique.

Symbol list

t	time
x, y, z	Cartesian co-ordinates
u, v, w	flow velocity components
D_v	vertical turbulent (eddy) diffusion coefficient
c^i	the i'th scalar component (defined as the mass concentration)
$w_s{}^i$:	fall velocity
$\sigma_{Tx}{}^j$	turbulent Schmidt number
ν_{Tx}	anisotropic eddy viscosity
S^i	source term

The bed interaction/update and the settling velocity terms are handled in the MT module.

The sedimentological effects on the fluid density and viscosity (concentrated near-bed suspensions) are not considered as part of the mud process module. Instead they are provided as separate sub-modules as they are only relevant for higher suspended sediment concentrations (SSC).

Mud plains in Loire River, France

Settling velocity

The settling velocity of the suspended sediment may be specified as a constant value. Flocculation is described as a relationship with the suspended sediment concentration as given in Burt (1986). Hindered settling can be applied if the suspended sediment concentration exceeds a certain level. To distinguish between three different settling regimes, two boundaries are defined, c_{floc} and $c_{hindered}$, being the concentrations where flocculation and hindered settling begins, respectively.

Constant settling velocity

Below a certain suspended sediment concentration the flocculation may be negligible and a constant settling velocity can be applied:

$$w_s = k \qquad c < c_{floc}$$

where w_s is the settling velocity and k is the constant.

Flocculation

After reaching c_{floc}, the sediment will begin to flocculate. Burt (1986) found the following relationship:

$$w_s = k \times \left(\frac{c}{\rho_{sediment}}\right)^{\gamma} \qquad c_{floc} > c > c_{hindered}$$

In which k is a constant, $\rho_{sediment}$ is the sediment density, and γ is a coefficient termed settling index.

Hindered settling

After a relatively high sediment concentration ($c_{hindered}$) is reached, the settling columns of flocs begin to interfere and hereby reducing the settling velocity. Formulations given by Richardson and Zaki (1954) and Winterwerp (1999) are implemented.

Deposition

The deposition is described as (Krone, 1962):

$$S_D = w_s c_b p_D$$

where w_s is the settling velocity of the suspended sediment (m s^{-1}), c_b is the suspended sediment concentration near the bed, and p_d is an expression of the probability of deposition:

$$p_d = 1 - \frac{\tau_b}{\tau_{cd}}$$

In the three-dimensional model, c_b is simply equal to the sediment concentration in the water cell just above the sediment bed.

In the two-dimensional model, two different approaches are available for computing c_b. If the Rouse profile is applied, the near bed sediment concentration is related to the depth averaged sediment concentration by multiplying with a constant centroid height:

$$c_b = \bar{c} \times (\text{centroid height})$$

Teeter (1986) related the near bed concentrations to the Peclet number (P_e), the bed fluxes, and the depth averaged suspended sediment concentrations. In this case, the near bed sediment concentration is described as:

$$c_b = \bar{c} \times \left(1 + \left(\frac{P_e}{1.25 + 4.75\left(p_d{}^{2.5}\right)}\right)\right)$$

where P_e is the Peclet number:

$$P_e = \frac{w_s h}{D_z}$$

where h is the water depth, D_z is the eddy diffusivity, both computed by the hydrodynamic model.

Erosion

Erosion features the following two modes.

Hard bed

For a consolidated bed the erosion rate can be written as (Partheniades, 1965):

$$S_E = E\left(\frac{\tau_b}{\tau_{ce}} - 1\right)^n \qquad \tau_b > \tau_c$$

Where E is the erodibility (kg m^{-2} s^{-1}), n is the power of erosion, τ_b is the bed shear stress (N m^{-2}) and τ_{ce} is the critical shear stress for erosion (N m^{-2}). S_E is the erosion rate (kg m^{-2} s^{-1}).

Soft bed

For a soft, partly consolidated bed the erosion rate can be written as (Parchure and Mehta, 1985):

$$S_E = E\left(e^{\alpha\sqrt{(\tau_b - \tau_c)}}\right) \qquad \tau_b > \tau_c$$

Consolidation

When long term simulations are performed consolidation of deposited sediment may be an important process. If several bed layers are used a transition rate (T_i) can be applied. This will cause sediment from the top layers to be transferred to the subsequently lower layers.

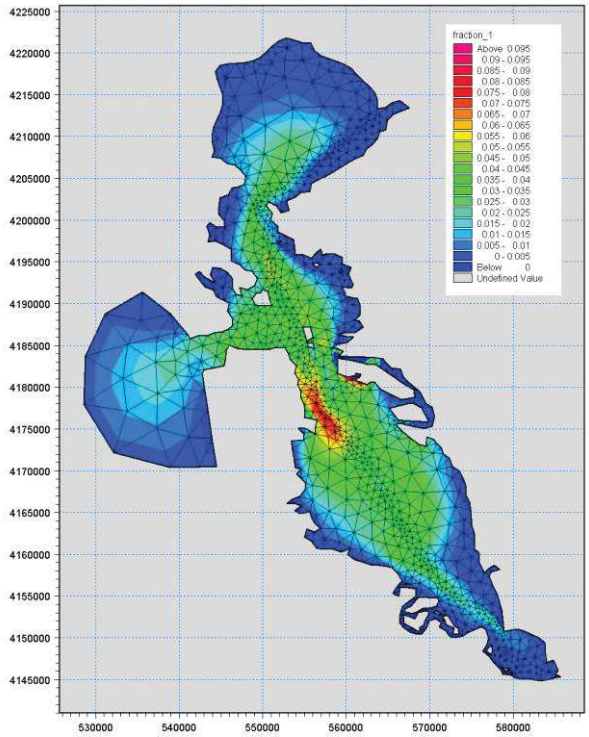

The MT module is a tool for estuary sediment management in complex estuaries like San Francisco bay, California, USA

Solution Technique

The solution of the transport equations is closely linked to the solution of the hydrodynamic conditions.

The spatial discretisation of the primitive equations is performed using a cell-centred finite volume method. The spatial domain is discretised by subdivision of the continuum into non-overlapping elements/cells. In the horizontal plane an unstructured grid is used while in the vertical domain in the 3D model a structured mesh is used. In the 2D model the elements can be triangles or quadrilateral elements. In the 3D model the elements can be prisms or bricks whose horizontal faces are triangles and quadrilateral elements, respectively.

The time integration is performed using an explicit scheme.

Model Input

The generic nature of cohesive sediment dynamics reveals a numerical model that will always call for tremendous field work or calibration due to measurements performed. The following input parameters have to be given:

- Settling velocity
- Critical shear stress for erosion
- Critical shear stress for deposition
- Erosion coefficients
- Power of erosion
- Suspended sediment
- Concentration at open boundaries
- Dispersion coefficients
- Thickness of bed layers or estimate of total amount of active sediment in the system
- Transition coefficients between bed layers
- Dry density of bed layers

Model Output

The main output possibilities are listed below:

- Suspended sediment concentrations in space and time
- Sediment in bed layers given as masses or heights
- Net sedimentation rates
- Computed bed shear stress
- Computed settling velocities
- Updated bathymetry

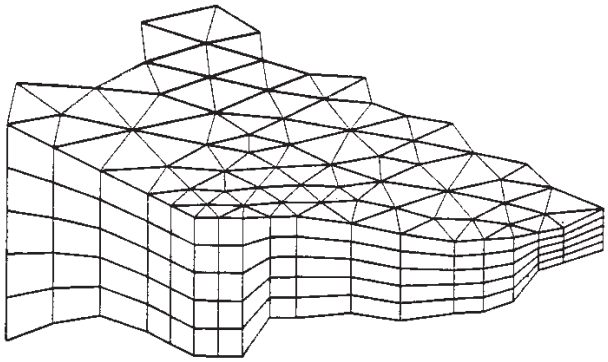

Principle of 3D mesh

Validation

The model engine is well proven in numerous studies throughout the world:

The Rio Grande estuary, Brazil

In 2001, the model was applied for a 3D study in the Rio Grande estuary (Brazil). The study focused on a number of hydrodynamic issues related to changing the Rio Grande Port layout. In addition the possible changes in sedimentation patterns and dredging requirements were investigated.

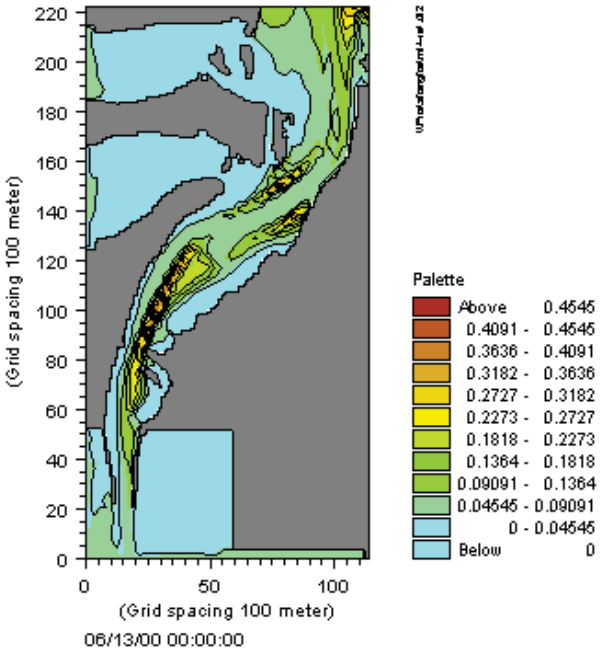

SSC in surface layer (kg/m^3), Rio Grande, Brazil

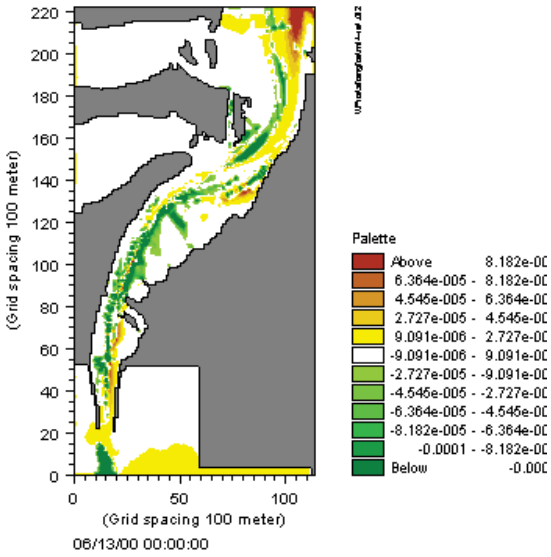

Instantaneous erosion (kg/m^2/s), Rio Grande, Brazil

The figure below shows the most common calibration parameter, which is the suspended sediment concentration (SSC). The results are reasonable given the large uncertainties connected with mud transport modelling.

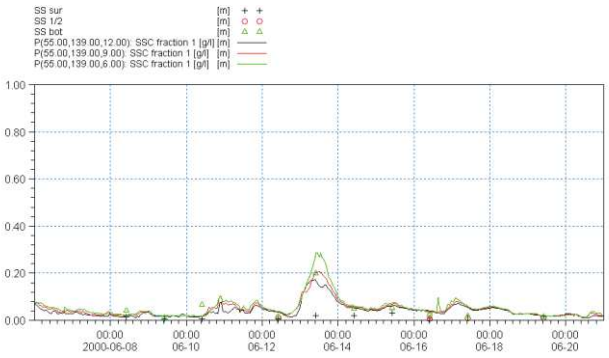

Suspended sediment concentrations, Rio Grande, Brazil

The Graadyb tidal inlet, Denmark

The MT module has also been used in the Graadyb tidal inlet located in the Danish part of the Wadden Sea. In this area, the highest tidal range reaches 1.7 m at springs, but the storm surge in the area can be as high as 2-4 metres.

The maximum current in the navigation channel leading to the harbour of Esbjerg is in the range of 1-2 m/s. The depth in the channel is 10-12 m at mean sea level.

Graadyb tidal inlet (Skallingen), Denmark

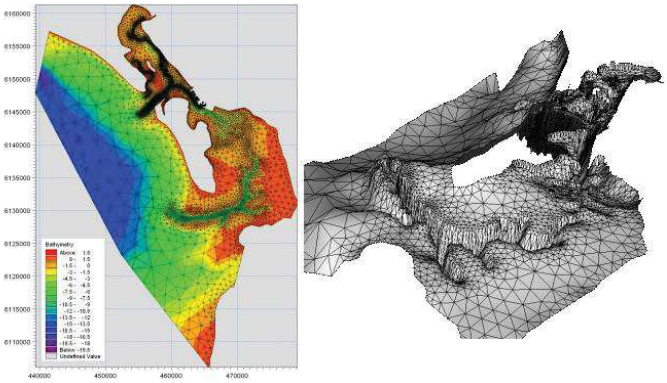

Bathymetry and computational mesh for the Graadyb tidal inlet, Denmark

A comparison between measured and simulated SSC time series is shown below. The overall comparison is excellent.

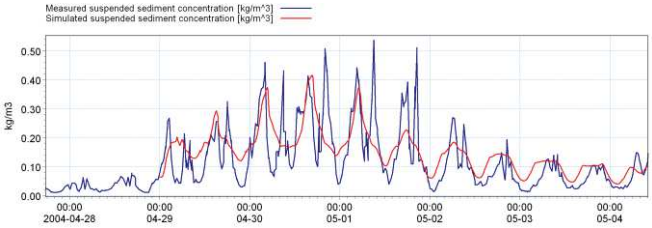

Comparison between measured and simulated suspended sediment concentrations, Graadyb tidal inlet, Denmark

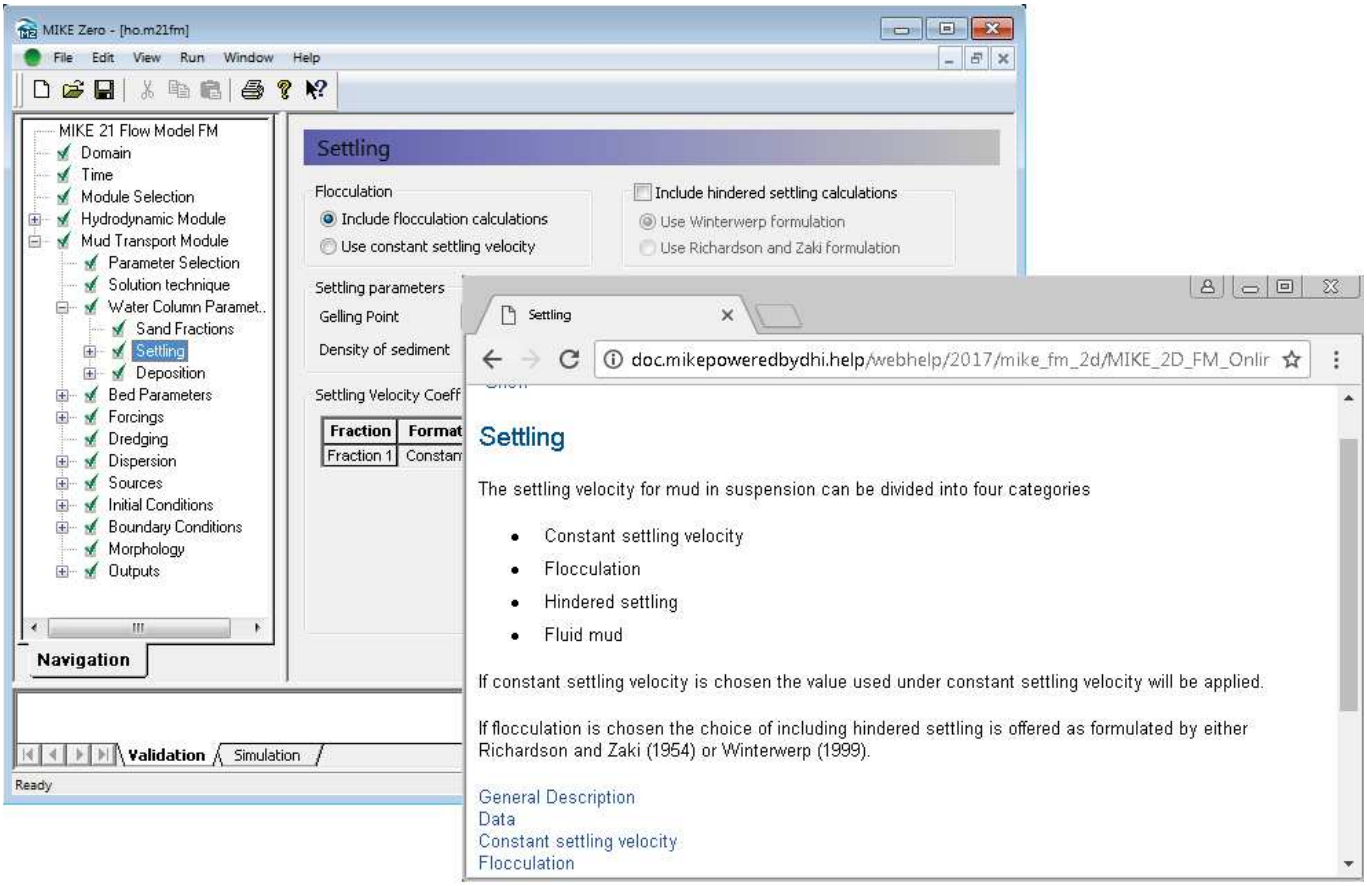

Graphical user interface of the MIKE 21 Flow Model FM, Mud Transport Module, including an example of the Online Help System

Graphical User Interface

The MIKE 21 & MIKE 3 Flow Model FM, Mud Transport Module is operated through a fully Windows integrated Graphical User Interface (GUI). Support is provided at each stage by an Online Help System.

The common MIKE Zero shell provides entries for common data file editors, plotting facilities and a toolbox for/utilities as the Mesh Generator and Data Viewer.

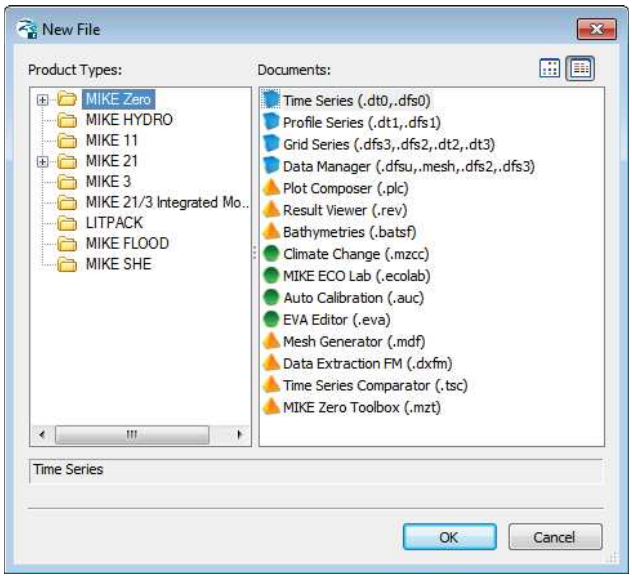

Overview of the common MIKE Zero utilities

Parallelisation

The computational engines of the MIKE 21/3 FM series are available in versions that have been parallelised using both shared memory as well as distributed memory architecture. The latter approach allows for domain decomposition. The result is much faster simulations on systems with many cores.

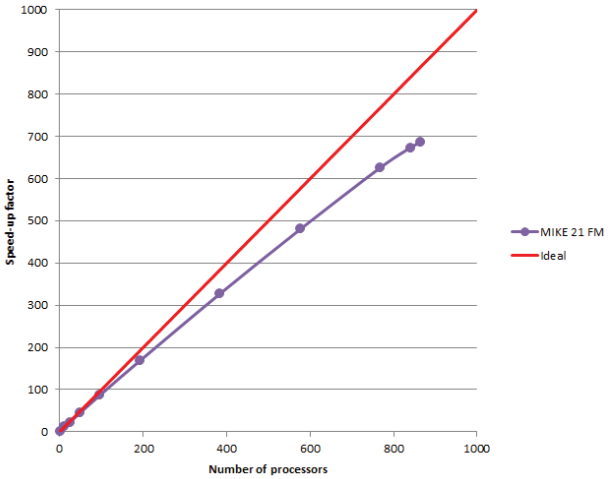

Example of MIKE 21 HD FM speed-up using a HPC Cluster with distributed memory architecture (purple)

Hardware and Operating System Requirements

The MIKE Zero Modules support Microsoft Windows 7 Professional Service Pack 1 (64 bit), Windows 10 Pro (64 bit), Windows Server 2012 R2 Standard (64 bit) and Windows Server 2016 Standard (64 bit).

Microsoft Internet Explorer 9.0 (or higher) is required for network license management. An internet browser is also required for accessing the web-based documentation and online help.

The recommended minimum hardware requirements for executing the MIKE Zero modules are:

Processor:	3 GHz PC (or higher)
Memory (RAM):	2 GB (or higher)
Hard disk:	40 GB (or higher)
Monitor:	SVGA, resolution 1024x768
Graphics card: (GUI and visualisation)	64 MB RAM (256 MB RAM or higher is recommended)

Support

News about new features, applications, papers, updates, patches, etc. are available here:

www.mikepoweredbydhi.com/Download/DocumentsAndTools.aspx

For further information on MIKE 21 & MIKE 3 Flow Model FM software, please contact your local DHI office or the support centre:

MIKE Powered by DHI Client Care
Agern Allé 5
DK-2970 Hørsholm
Denmark

Tel: +45 4516 9333
Fax: +45 4516 9292

mike@dhigroup.com
www.mikepoweredbydhi.com

Documentation

The MIKE 21 & MIKE 3 Flow Model FM models are provided with comprehensive user guides, online help, scientific documentation, application examples and step-by-step training examples.

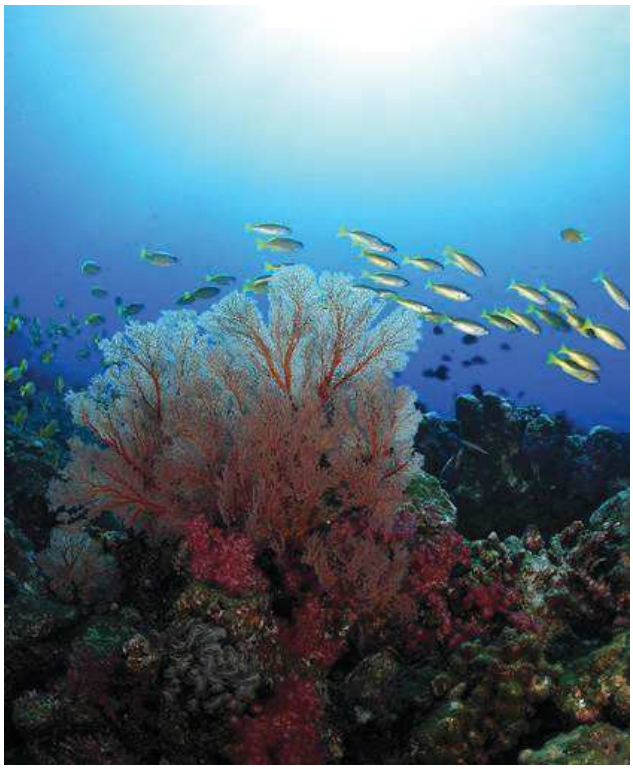

References

Burt, N., 1986. Field settling velocities of estuary muds. In: Estuarine Cohesive Sediment Dynamics, edited by Mehta, A.J. Springer-Verlag, Berlin, Heidelberg, NewYork, Tokyo, 126–150.

Krone, R.B., 1962. Flume Studies of the Transport of Sediment in Estuarine Shoaling Processes. Final Report to San Francisco District U. S. Army Corps of Engineers, Washington D.C.

Mehta, A.J., Hayter, E.J., Parker, W.R., Krone, R.B. and Teeter, A.M., 1989. Cohesive sediment transport. I: Process description. Journal of Hydraulic Engineering – ASCE 115 (8), 1076–1093.

Parchure, T.M. and Mehta, A.J., 1985. Erosion of soft cohesive sediment deposits. Journal of Hydraulic Engineering – ASCE 111 (10), 1308–1326.

Partheniades, E., 1965. Erosion and deposition of cohesive soils. Journal of the hydraulics division Proceedings of the ASCE 91 (HY1), 105–139.

Richardson, J.F and Zaki, W.N., 1954. Sedimentation and fluidization, Part I, Transactions of the institution Chemical Engineers 32, 35–53.

Teeter, A.M., 1986. Vertical transport in fine-grained suspension and newly deposited sediment. In: Estuarine Cohesive Sediment Dynamics, edited by Mehta, A.J. Springer-Verlag, Berlin, Heidelberg, NewYork, Tokyo, 170–191.

Teisson, C., 1991. Cohesive suspended sediment transport: feasibility and limitations of numerical modelling. Journal of Hydraulic Research 29 (6), 755–769.

Winterwerp, J.C., 1999. “Flocculation and settling velocity”, TU delft. pp 10-17.

References on applications

Edelvang, K., Lund-Hansen, L.C., Christiansen, C., Petersen, O.S., Uhrenholdt, T., Laima, M. and Berastegui, D.A., 2002. Modelling of suspended matter transport from the Oder River. Journal of Coastal Research 18 (1), 62–74.

Lumborg, U., Andersen, T.J. and Pejrup, M., 2006. The effect of *Hydrobia ulvae* and microphytobenthos on cohesive sediment dynamics on an intertidal mudflat described by means of numerical modelling. Estuarine, Coastal and Shelf Science 68 (1-2), 208–220.

Lumborg, U. and Pejrup, M., 2005. Modelling of cohesive sediment transport in a tidal lagoon – An annual budget. Marine Geology 218 (1-4), 1–16.

Petersen, O. and Vested, H.J., 2002. Description of vertical exchange processes in numerical mud transport modelling. In: Fine Sediment Dynamics in the Marine Environment, edited by Winterwerp, J.C. and Kranenburg, C. Elsevier, Amsterdam, 375–391.

Petersen, O., Vested, H.J., Manning, A.J., Christie, M. and Dyer, K., 2002. Numerical modelling of mud transport processes in the Tamar Estuary. In: Fine Sediment Dynamics in the Marine Environment, edited by Winterwerp, J.C. and Kranenburg, C. Elsevier, Amsterdam, 643–654.

Valeur, J.R., 2004. Sediment investigations connected with the building of the Øresund bridge and tunnel. Danish Journal of Geography 104 (2), 1–12.

APPENDIX C – MIKE 21 SW FM

MIKE
Powered by DHI

MIKE 21 Wave Modelling

MIKE 21 Spectral Waves FM

Short Description

MIKE 21 SW - SPECTRAL WAVE MODEL FM

MIKE 21 SW is a state-of-the-art third generation spectral wind-wave model developed by DHI. The model simulates the growth, decay and transformation of wind-generated waves and swells in offshore and coastal areas.

MIKE 21 SW includes two different formulations:

- Fully spectral formulation
- Directional decoupled parametric formulation

The fully spectral formulation is based on the wave action conservation equation, as described in e.g. Komen et al (1994) and Young (1999). The directional decoupled parametric formulation is based on a parameterisation of the wave action conservation equation. The parameterisation is made in the frequency domain by introducing the zeroth and first moment of the wave action spectrum. The basic conservation equations are formulated in either Cartesian co-ordinates for small-scale applications and polar spherical co-ordinates for large-scale applications.

The fully spectral model includes the following physical phenomena:

- Wave growth by action of wind
- Non-linear wave-wave interaction
- Dissipation due to white-capping
- Dissipation due to bottom friction
- Dissipation due to depth-induced wave breaking
- Refraction and shoaling due to depth variations
- Wave-current interaction
- Effect of time-varying water depth
- Effect of ice coverage on the wave field

The discretisation of the governing equation in geographical and spectral space is performed using cell-centred finite volume method. In the geographical domain, an unstructured mesh technique is used. The time integration is performed using a fractional step approach where a multi-sequence explicit method is applied for the propagation of wave action.

MIKE 21 SW is a state-of-the-art numerical modelling tool for prediction and analysis of wave climates in offshore and coastal areas. © BIOFOTO/Klaus K. Bentzen

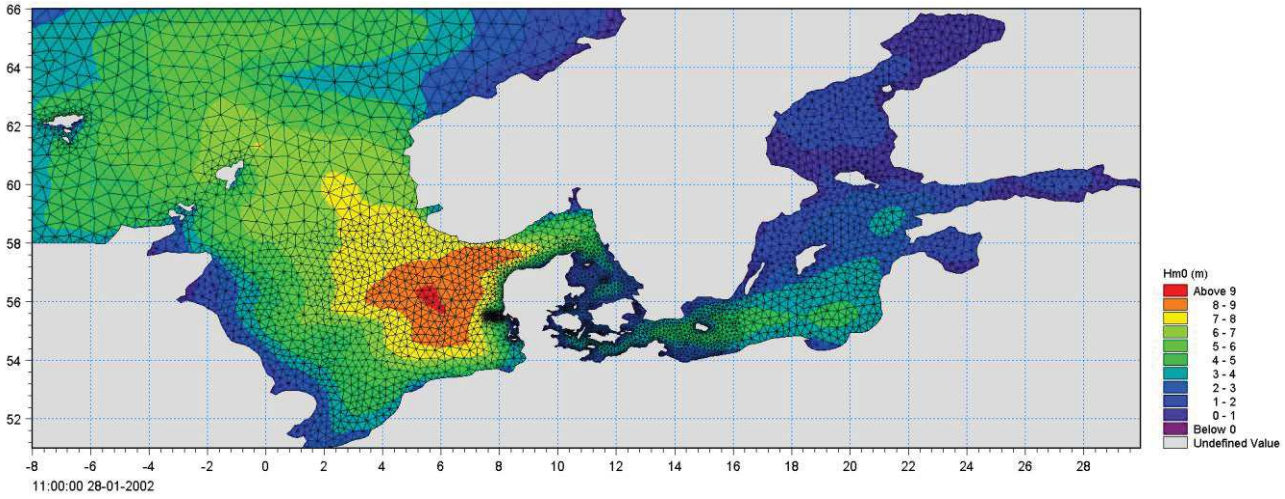

A MIKE 21 SW forecast application in the North Sea and Baltic Sea. The chart shows a wave field (from the NSBS model) illustrated by the significant wave height in top of the computational mesh. See also www.waterforecast.com

Computational Features

The main computational features of MIKE 21 SW - Spectral Wave Model FM are as follows:

- Fully spectral and directionally decoupled parametric formulations
- Source functions based on state-of-the-art 3rd generation formulations
- Instationary and quasi-stationary solutions
- Optimal degree of flexibility in describing bathymetry and ambient flow conditions using depth-adaptive and boundary-fitted unstructured mesh
- Coupling with hydrodynamic flow model for modelling of wave-current interaction and time-varying water depth
- Flooding and drying in connection with time-varying water depths
- Cell-centred finite volume technique
- Fractional step time-integration with an multi-sequence explicit method for the propagation
- Extensive range of model output parameters (wave, swell, air-sea interaction parameters, radiation stress tensor, spectra, etc.)

Application Areas

MIKE 21 SW is used for the assessment of wave climates in offshore and coastal areas - in hindcast and forecast mode.

A major application area is the design of offshore, coastal and port structures where accurate assessment of wave loads is of utmost importance to the safe and economic design of these structures.

Illustrations of typical application areas of DHI's MIKE 21 SW – Spectral Wave Model FM

Measured data are often not available during periods long enough to allow for the establishment of sufficiently accurate estimates of extreme sea states.

In this case, the measured data can then be supplemented with hindcast data through the simulation of wave conditions during historical storms using MIKE 21 SW.

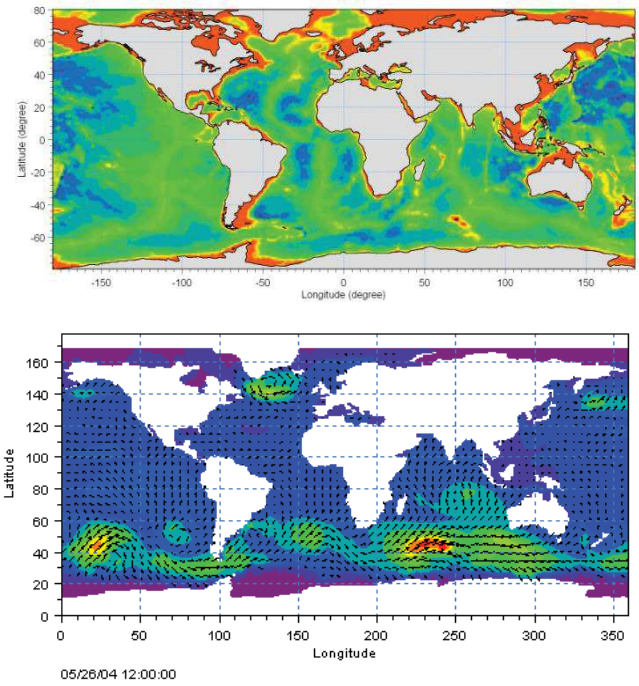

Example of a global application of MIKE 21 SW. The upper panel shows the bathymetry. Results from such a model (cf. lower panel) can be used as boundary conditions for regional scale forecast or hindcast models. See http://www.waterforecast.com for more details on regional and global modelling

MIKE 21 SW is particularly applicable for simultaneous wave prediction and analysis on regional scale and local scale. Coarse spatial and temporal resolution is used for the regional part of the mesh and a high-resolution boundary and depth-adaptive mesh is describing the shallow water environment at the coastline.

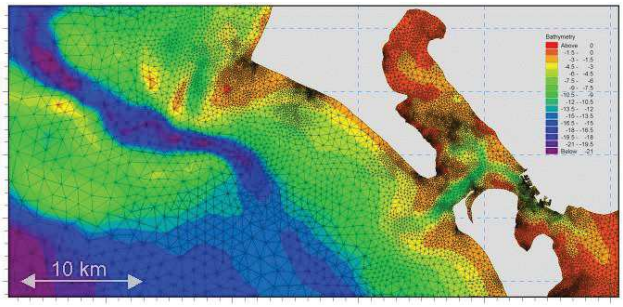

Example of a computational mesh used for transformation of offshore wave statistics using the directionally decoupled parametric formulation

MIKE 21 SW is also used for the calculation of the sediment transport, which for a large part is determined by wave conditions and associated wave-induced currents. The wave-induced current is generated by the gradients in radiation stresses that occur in the surf zone.

MIKE 21 SW can be used to calculate the wave conditions and associated radiation stresses. The long-shore currents and sediment transport are then calculated using the flow and sediment transport models available in the MIKE 21 package. For such type of applications, the directional decoupled parametric formulation of MIKE 21 SW is an excellent compromise between the computational effort and accuracy.

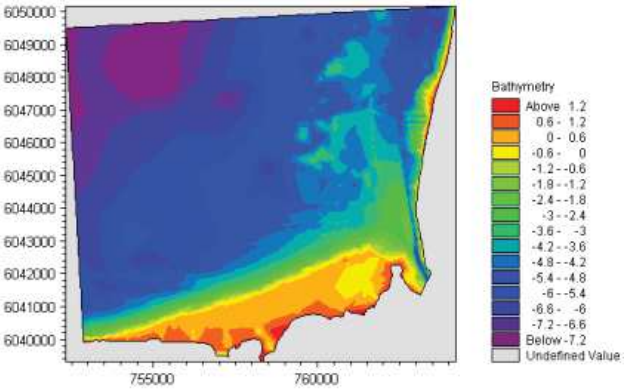

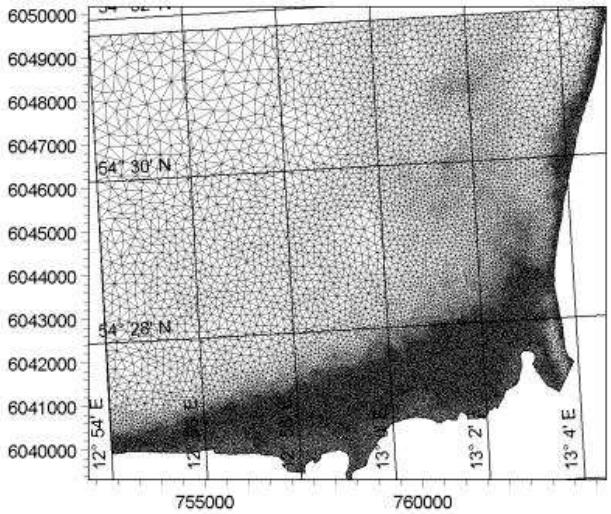

Bathymetry (upper) and computational mesh (lower) used in a MIKE 21 SW application on wave induced currents in Gellen Bay, Germany

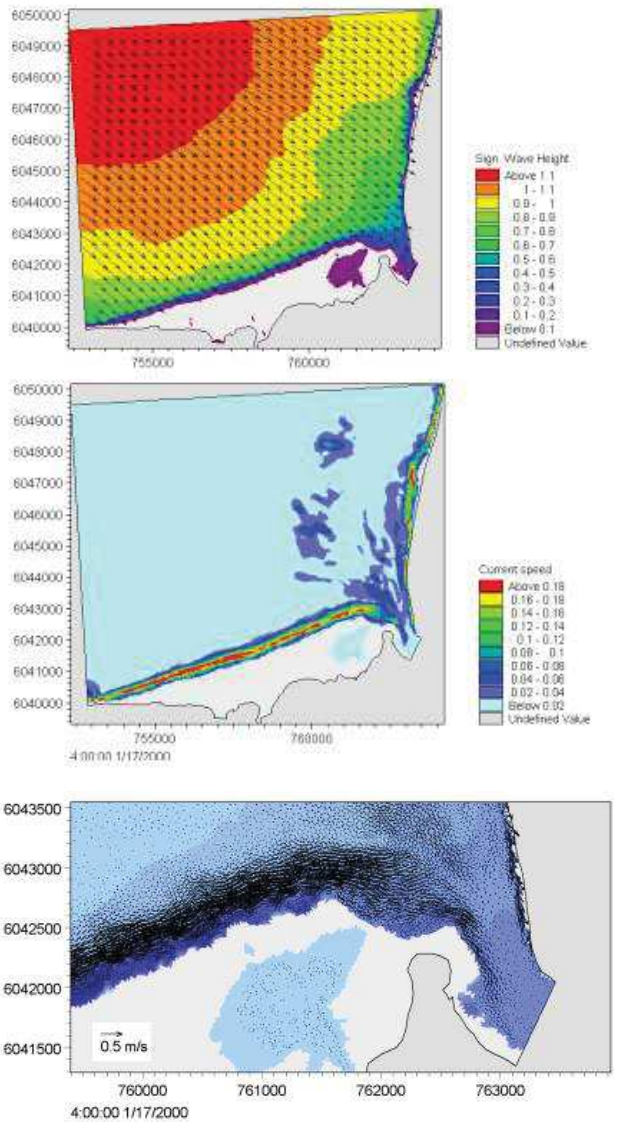

Map of significant wave height (upper), current field (middle) and vector field (lower). The flow field is simulated by DHI's MIKE 21 Flow Model FM, which is dynamically coupled to MIKE 21 SW

Model Equations

In MIKE 21 SW, the wind waves are represented by the wave action density spectrum $N(\sigma,\theta)$. The independent phase parameters have been chosen as the relative (intrinsic) angular frequency, $\sigma = 2\pi f$ and the direction of wave propagation, θ. The relation between the relative angular frequency and the absolute angular frequency, ω, is given by the linear dispersion relationship

$$\sigma = \sqrt{gk\tanh(kd)} = \omega - \bar{k}\cdot\bar{U}$$

where *g* is the acceleration of gravity, *d* is the water depth and $\bar{U}$ is the current velocity vector and $\bar{k}$ is the wave number vector with magnitude *k* and direction θ. The action density, $N(\sigma,\theta)$, is related to the energy density $E(\sigma,\theta)$ by

$$N = \frac{E}{\sigma}$$

Fully Spectral Formulation

The governing equation in MIKE 21 SW is the wave action balance equation formulated in either Cartesian or spherical co-ordinates. In horizontal Cartesian co-ordinates, the conservation equation for wave action reads

$$\frac{\partial N}{\partial t} + \nabla\cdot(\bar{v}N) = \frac{S}{\sigma}$$

where $N(\bar{x},\sigma,\theta,t)$ is the action density, *t* is the time, $\bar{x} = (x,y)$ is the Cartesian co-ordinates, $\bar{v} = (c_x, c_y, c_\sigma, c_\theta)$ is the propagation velocity of a wave group in the four-dimensional phase space $\bar{x}$, σ and θ. *S* is the source term for energy balance equation. ∇ is the four-dimensional differential operator in the $\bar{x}$, σ, θ-space. The characteristic propagation speeds are given by the linear kinematic relationships

$$(c_x, c_y) = \frac{d\bar{x}}{dt} = \bar{c}_g + \bar{U} = \frac{1}{2}\left(1 + \frac{2kd}{\sinh(2kd)}\right)\frac{\sigma}{k} + \bar{U}$$

$$c_\sigma = \frac{d\sigma}{dt} = \frac{\partial\sigma}{\partial d}\left[\frac{\partial d}{\partial t} + \bar{U}\cdot\nabla_{\bar{x}} d\right] - c_g\bar{k}\cdot\frac{\partial\bar{U}}{\partial s}$$

$$c_\theta = \frac{d\theta}{dt} = -\frac{1}{k}\left[\frac{\partial\sigma}{\partial d}\frac{\partial d}{\partial m} + \bar{k}\cdot\frac{\partial\bar{U}}{\partial m}\right]$$

Here, *s* is the space co-ordinate in wave direction θ and *m* is a co-ordinate perpendicular to *s*. $\nabla_{\bar{x}}$ is the two-dimensional differential operator in the $\bar{x}$-space.

Source Functions

The source function term, *S*, on the right hand side of the wave action conservation equation is given by

$$S = S_{in} + S_{nl} + S_{ds} + S_{bot} + S_{surf}$$

Here S_{in} represents the momentum transfer of wind energy to wave generation, S_{nl} the energy transfer due non-linear wave-wave interaction, S_{ds} the dissipation of wave energy due to white-capping (deep water wave breaking), S_{bot} the dissipation due to bottom friction and S_{surf} the dissipation of wave energy due to depth-induced breaking.

The default source functions S_{in}, S_{nl} and S_{ds} in MIKE 21 SW are similar to the source functions implemented in the WAM Cycle 4 model, see Komen et al (1994).

The wind input is based on Janssen's (1989, 1991) quasi-linear theory of wind-wave generation, where the momentum transfer from the wind to the sea not only depends on the wind stress, but also the sea state itself. The non-linear energy transfer (through the resonant four-wave interaction) is approximated by the DIA approach, Hasselmann et al (1985). The source function describing the dissipation due to white-capping is based on the theory of Hasselmann (1974) and Janssen (1989). The bottom friction dissipation is modelled using the approach by Johnson and Kofoed-Hansen (2000), which depends on the wave and sediment properties. The source function describing the bottom-induced wave breaking is based on the well-proven approach of Battjes and Janssen (1978) and Eldeberky and Battjes (1996).

A detailed description of the various source functions is available in Komen et al (1994) and Sørensen et al (2003), which also includes the references listed above.

Directional Decoupled Parametric Formulation

The directionally decoupled parametric formulation is based on a parameterisation of the wave action conservation equation. Following Holthuijsen et al (1989), the parameterisation is made in the frequency domain by introducing the zeroth and first moment of the wave action spectrum as dependent variables.

A similar formulation is used in the MIKE 21 NSW Near-shore Spectral Wind-Wave Model, which is one of the most popular models for wave transformation in coastal and shallow water environment. However, with MIKE 21 SW it is not necessary to set up a number of different orientated bathymetries to cover varying wind and wave directions.

The parameterisation leads to the following coupled equations

$$\frac{\partial(m_0)}{\partial t}+\frac{\partial(c_x m_0)}{\partial x}+\frac{\partial(c_y m_0)}{\partial y}+\frac{\partial(c_\theta m_0)}{\partial \theta}=T_0$$

$$\frac{\partial(m_1)}{\partial t}+\frac{\partial(c_x m_1)}{\partial x}+\frac{\partial(c_y m_1)}{\partial y}+\frac{\partial(c_\theta m_1)}{\partial \theta}=T_1$$

where $m_0(x, y, \theta)$ and $m_1(x, y, \theta)$ are the zeroth and first moment of the action spectrum $N(x, y, \sigma, \theta)$, respectively. $T_0(x, y, \theta)$ and $T_1(x, y, \theta)$ are source functions based on the action spectrum. The moments $m_n(x, y, \theta)$ are defined as

$$m_n(x,y,\theta)=\int_0^\infty \omega^n N(x,y,\omega,\theta)d\omega$$

The source functions T_0 and T_1 take into account the effect of local wind generation (stationary solution mode only) and energy dissipation due to bottom friction and wave breaking. The effects of wave-current interaction are also included. The source functions for the local wind generation are derived from empirical growth relations, see Johnson (1998) for details.

Numerical Methods

The frequency spectrum (fully spectral model only) is split into a prognostic part for frequencies lower than a cut-off frequency σ_{max} and an analytical diagnostic tail for the high-frequency part of the spectrum

$$E(\sigma,\theta)=E(\sigma_{\max},\theta)\left(\frac{\sigma}{\sigma_{\max}}\right)^{-m}$$

where m is a constant (= 5) as proposed by Komen et al (1994).

The directional decoupled parametric formulation in MIKE 21 SW is used extensively for calculation of the wave transformation from deep-water to the shoreline and for wind-wave generation in local areas

Space Discretisation

The discretisation in geographical and spectral space is performed using cell-centred finite volume method. In the geographical domain an unstructured mesh is used. The spatial domain is discretised by subdivision of the continuum into non-overlapping elements. Triangle and quadrilateral shaped polygons are presently supported in MIKE 21 SW. The action density, $N(\sigma,\theta)$ is represented as a piecewise constant over the elements and stored at the geometric centres.

In frequency space either an equidistant or a log-arithmic discretisation is used. In the directional space, an equidistant discretisation is used for both types of models. The action density is represented as piecewise constant over the discrete intervals, $\Delta\sigma$ and $\Delta\theta$, in the frequency and directional space.

Integrating the wave action conservation over an area A_i, the frequency interval $\Delta\sigma_l$ and the directional interval $\Delta\theta_m$ gives

$$\frac{\partial}{\partial t}\int_{\Delta\theta_m}\int_{\Delta\sigma_l}\int_{A_i} N d\Omega d\sigma d\theta - \int_{\Delta\theta_m}\int_{\Delta\sigma_l}\int_{A_i}\frac{S}{\sigma}d\Omega d\sigma d\theta$$
$$= \int_{\Delta\theta_m}\int_{\Delta\sigma_l}\int_{A_i}\nabla\cdot(\bar{v}N)d\Omega d\sigma d\theta$$

where Ω is the integration variable defined on A_i. Using the divergence theorem and introducing the convective flux $\bar{F} = \bar{v}N$, we obtain

$$\frac{\partial N_{i,l,m}}{\partial t} = -\frac{1}{A_i}\left[\sum_{p=1}^{NE}(F_n)_{p,l,m}\Delta l_p\right]$$
$$-\frac{1}{\Delta\sigma_l}\left[(F_\sigma)_{i,l+1/2,m} - (F_\sigma)_{i,l-1/2,m}\right]$$
$$-\frac{1}{\Delta\theta_m}\left[(F_\theta)_{i,l,m+1/2} - (F_\theta)_{i,l,m-1/2}\right] + \frac{S_{i,l,m}}{\sigma_l}$$

where NE is the total number of edges in the cell, $(F_n)_{p,l,m} = (F_x n_x + F_y n_y)_{p,l,m}$ is the normal flux trough the edge p in geographical space with length Δl_p. $(F_\sigma)_{i,l+1/2,m}$ and $(F_\theta)_{i,l,m+1/2}$ is the flux through the face in the frequency and directional space, respectively.

The convective flux is derived using a first-order upwinding scheme. In that

$$F_n = c_n\left(\frac{1}{2}(N_i + N_j) - \frac{1}{2}\frac{c}{|c|}(N_i - N_j)\right)$$

where c_n is the propagation speed normal to the element cell face.

Time Integration

The integration in time is based on a fractional step approach. Firstly, a propagation step is performed calculating an approximate solution N^* at the new time level $(n+1)$ by solving the homogenous wave action conservation equation, i.e. without the source terms. Secondly, a source terms step is performed calculating the new solution N^{n+1} from the estimated solution taking into account only the effect of the source terms.

The propagation step is carried out by an explicit Euler scheme

$$N^*_{i,l,m} = N^n_{i,l,m} + \Delta t\left(\frac{\partial N_{i,l,m}}{\partial t}\right)^n$$

To overcome the severe stability restriction, a multi-sequence integration scheme is employed. The maximum allowed time step is increased by employing a sequence of integration steps locally, where the number of steps may vary from point to point.

A source term step is performed using an implicit method (see Komen et al, 1994)

$$N^{n+1}_{i,l,m} = N^*_{i,l,m} + \Delta t\left[\frac{(1-\alpha)S^*_{i,l,m} + \alpha S^{n+1}_{i,l,m}}{\sigma_l}\right]$$

where α is a weighting coefficient that determines the type of finite difference method. Using a Taylor series to approximate S^{n+1} and assuming the off-diagonal terms in $\partial S/\partial E = \gamma$ are negligible, this equation can be simplified as

$$N^{n+1}_{i,l,m} = N^n_{i,l,m} + \frac{(S^*_{i,l,m}/\sigma_l)\Delta t}{(1-\alpha\gamma\Delta t)}$$

For growing waves ($\gamma > 0$) an explicit forward difference is used ($\alpha = 0$), while for decaying waves ($\gamma < 0$) an implicit backward difference ($\alpha = 1$) is applied.

MIKE 21 SW is also applied for wave forecasts in ship route planning and improved service for conventional and fast ferry operators

Model Input

The necessary input data can be divided into following groups:

- Domain and time parameters:
  - computational mesh
  - co-ordinate type (Cartesian or spherical)
  - simulation length and overall time step
- Equations, discretisation and solution technique
  - formulation type
  - frequency and directional discretisation
  - number of time step groups
  - number of source time steps
- Forcing parameters
  - water level data
  - current data
  - wind data
  - ice data
- Source function parameters
  - non-linear energy transfer
  - wave breaking (shallow water)
  - bottom friction
  - white capping
- Structures
  - location and geometry
  - approach
  - structures coefficients
- Initial conditions
  - zero-spectrum (cold-start)
  - empirical data
  - data file
- Boundary conditions
  - closed boundaries
  - open boundaries (data format and type)

Providing MIKE 21 SW with a suitable mesh is essential for obtaining reliable results from the model. Setting up the mesh includes the appropriate selection of the area to be modelled, adequate resolution of the bathymetry, flow, wind and wave fields under consideration and definition of codes for essential and land boundaries.

Furthermore, the resolution in the geographical space must also be selected with respect to stability considerations.

As the wind is the main driving force in MIKE 21 SW, accurate hindcast or forecast wind fields are of utmost importance for the wave prediction.

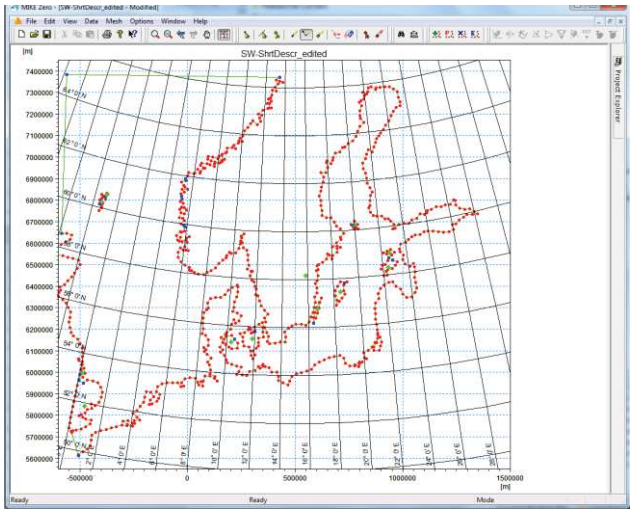

The Mesh Generator is an efficient MIKE Zero tool for the generation and handling of unstructured meshes, including the definition and editing of boundaries

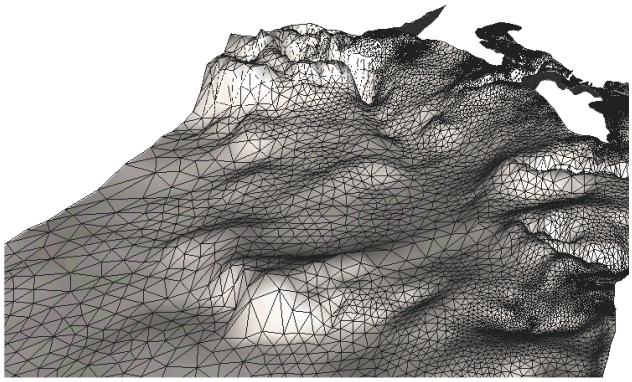

3D visualisation of a computational mesh

If wind data is not available from an atmospheric meteorological model, the wind fields (e.g. cyclones) can be determined by using the wind-generating programs available in MIKE 21 Toolbox.

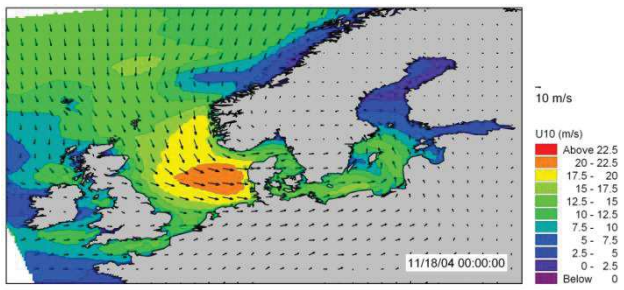

The chart shows an example of a wind field covering the North Sea and Baltic Sea as wind speed and wind direction. This is used as input to MIKE 21 SW in forecast and hindcast mode

Model Output

At each mesh point and for each time step four types of output can be obtained from MIKE 21 SW:

- Integral wave parameters divided into wind sea and swell such as
  - significant wave height, H_{m0}
  - peak wave period, T_p
  - averaged wave period, T_{01}
  - zero-crossing wave period, T_{02}
  - wave energy period, T_{-10}
  - peak wave direction, θ_p
  - mean wave direction, θ_m
  - directional standard deviation, σ
  - wave height with dir., $H_{m0} \cos\theta_m$, $H_{m0} \sin\theta_m$
  - radiation stress tensor, S_{xx}, S_{xy} and S_{yy}
  - particle velocities, *horizontal/vertical*
  - wave power, P, P_x *and* P_y

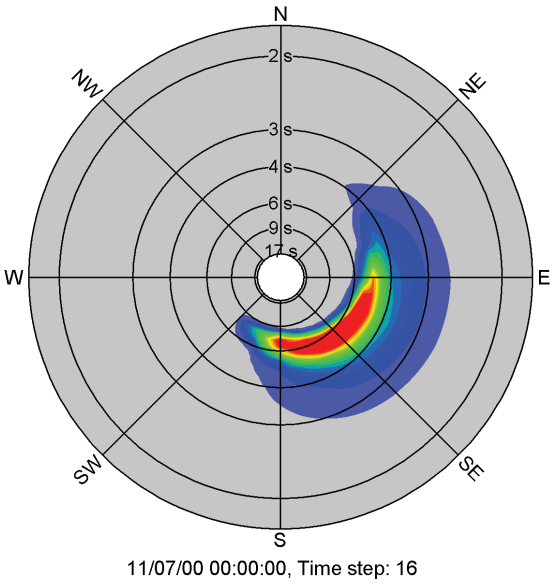

Example of model output (directional-frequency wave spectrum) processed using the Polar Plot control in the MIKE Zero Plot Composer

The distinction between wind-sea and swell can be calculated using either a constant threshold frequency or a dynamic threshold frequency with an upper frequency limit.

- Input parameters
  - water level, *WL*
  - water depth, *h*
  - current velocity, $\overline{U}$
  - wind speed, U_{10}
  - wind direction, θ_w
  - Ice concentration
- Model parameters
  - bottom friction coefficient, C_f
  - breaking parameter, γ
  - Courant number, *Cr*
  - time step factor, α
  - characteristic edge length, Δl
  - area of element, *a*
  - wind friction speed, u_*
  - roughness length, z_0
  - drag coefficient, C_D
  - Charnock parameter, z_{ch}
- Directional-frequency wave spectra at selected grid points and or areas as well as direction spectra and frequency spectra

Output from MIKE 21 SW is typically post-processed using the Data Viewer available in the common MIKE Zero shell. The Data Viewer is a tool for analysis and visualisation of unstructured data, e.g. to view meshes, spectra, bathymetries, results files of different format with graphical extraction of time series and line series from plan view and import of graphical overlays.

Various other editors and plot controls in the MIKE Zero Composer (e.g. Time Series Plot, Polar Plot, etc.) can be used for analysis and visualisation.

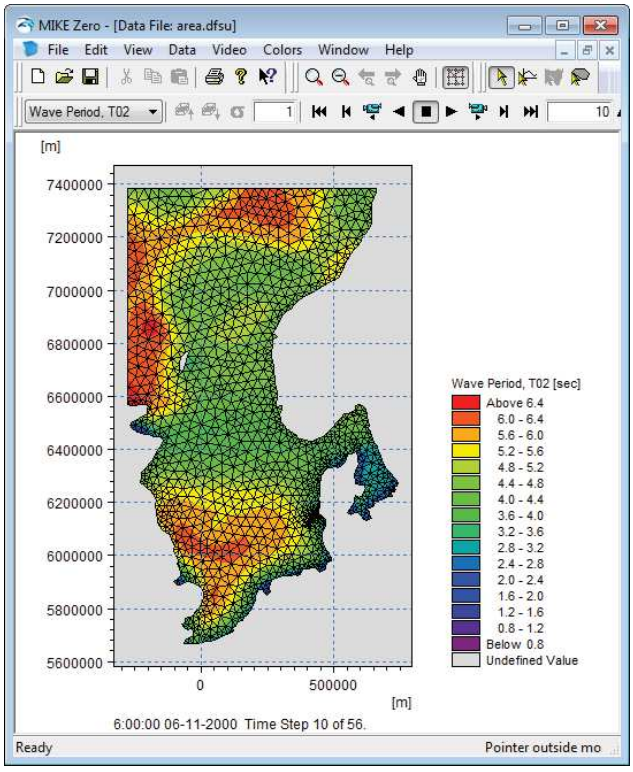

The Data Viewer in MIKE Zero – an efficient tool for analysis and visualisation of unstructured data including processing of animations

Validation

The model has successfully been applied to a number of rather basic idealised situations for which the results can be compared with analytical solutions or information from the literature. The basic tests covered fundamental processes such as wave propagation, depth-induced and current-induced shoaling and refraction, wind-wave generation and dissipation.

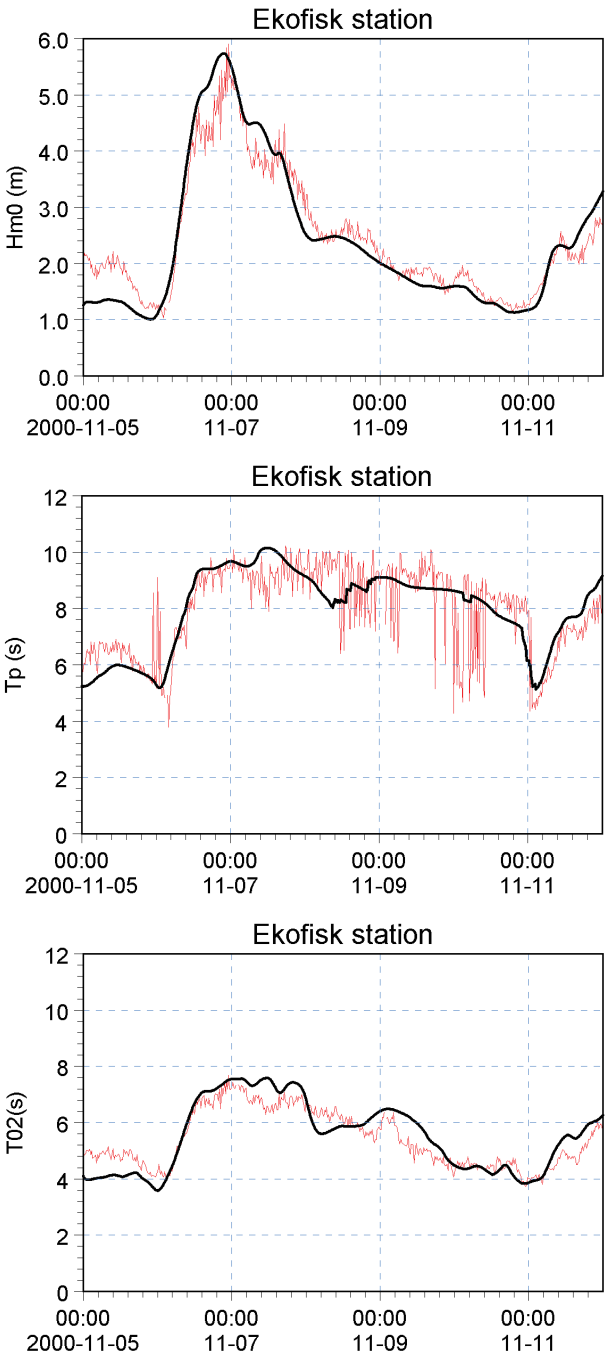

Comparison between measured and simulated significant wave height, peak wave period and mean wave period at the Ekofisk offshore platform (water depth 70 m) in the North Sea). (——) calculations and (——) measurements

A major application area of MIKE 21 SW is in connection with design and maintenance of offshore structures

The model has also been tested in natural geophysical conditions (e.g. in the North Sea, the Danish West Coast and the Baltic Sea), which are more realistic and complicated than the academic test and laboratory tests mentioned above.

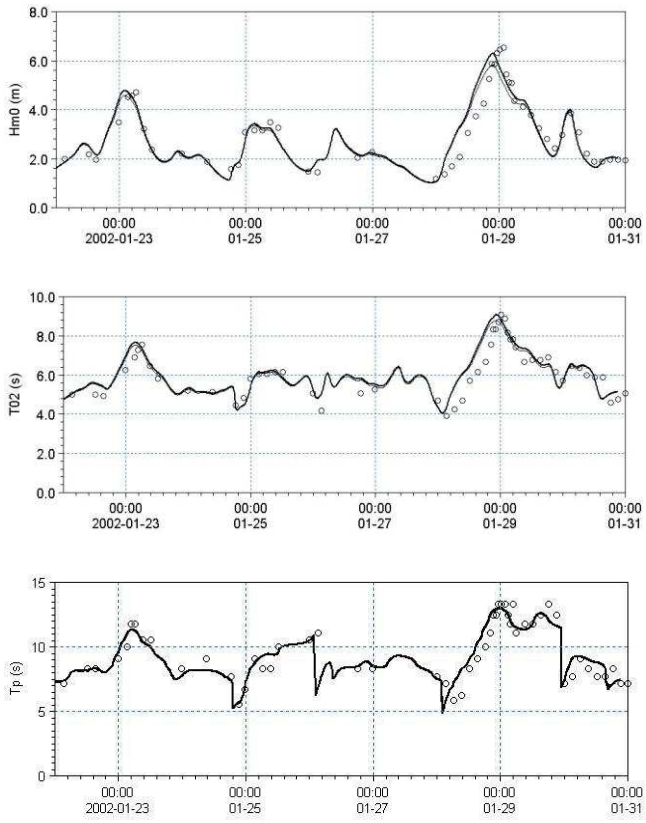

Comparison between measured and simulated significant wave height, peak wave period and mean wave period at Fjaltring located at the Danish west coast (water depth 17.5 m).(——) calculations and (o) measurements

The Fjaltring directional wave rider buoy is located offshore relative to the depicted arrow

MIKE 21 SW is used for prediction of the wave conditions at the complex Horns Rev (reef) in the southeastern part of the North Sea. At this site, a 168 MW offshore wind farm with 80 turbines has been established in water depths between 6.5 and 13.5 m.

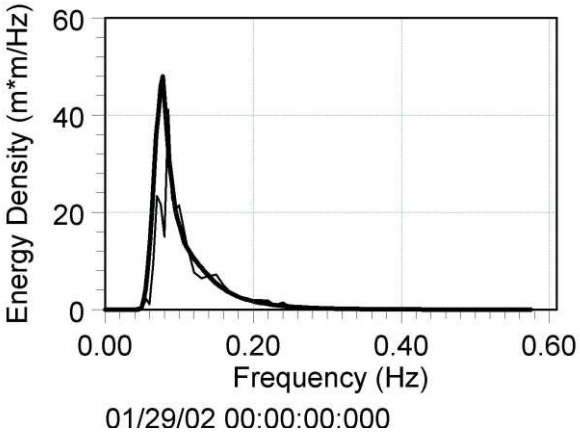

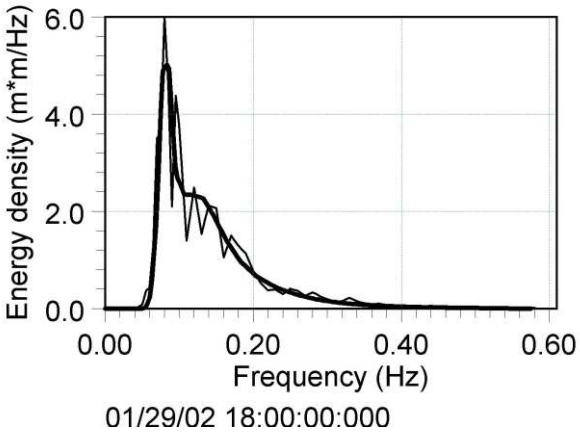

Comparison of frequency spectra at Fjaltring. (——) calculations and (——)measurements

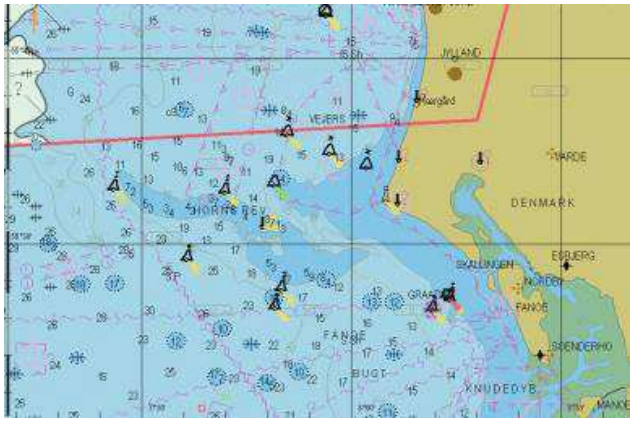

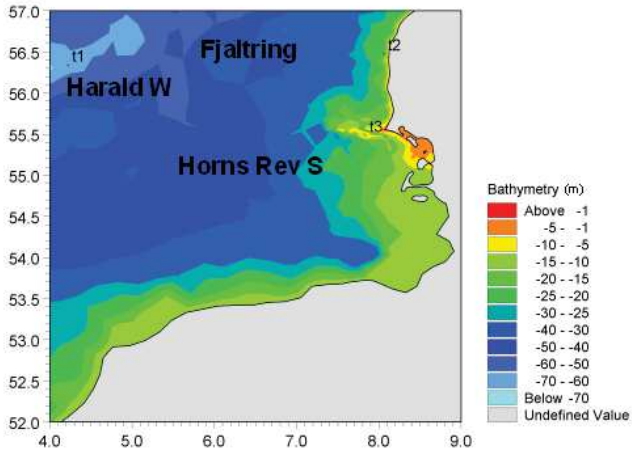

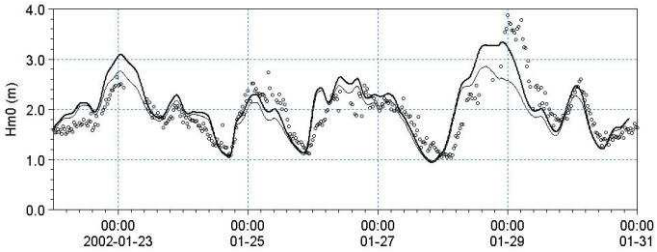

The upper panels show the Horns Rev offshore wind farm and MIKE C-map chart. 'The middle panel shows a close-up of the mesh near the Horns Rev S wave rider buoy (t3, 10 m water depth. The lower panel shows a comparison between measured and simulated significant wave height at Horns Rev S, (——) calculations including tide and surge and (——-) calculations excluding including tide and surge, (o) measurements

The predicted nearshore wave climate along the island of Hiddensee and the coastline of Zingst located in the micro-tidal Gellen Bay, Germany have been compared to field measurements (Sørensen et al, 2004) provided by the MORWIN project. From the illustrations it can be seen that the wave conditions are well reproduced both offshore and in more shallow water near the shore. The RMS values (on significant wave height) are less than 0.25m at all five stations.

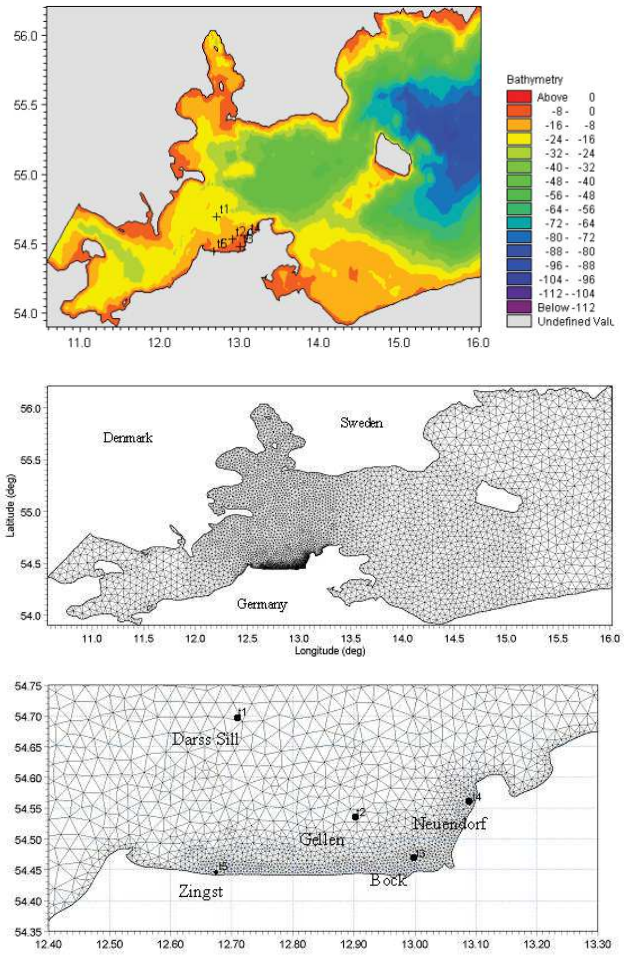

A MIKE 21 SW hindcast application in the Baltic Sea. The upper chart shows the bathymetry and the middle and lower charts show the computational mesh. The lower chart indicates the location of the measurement stations

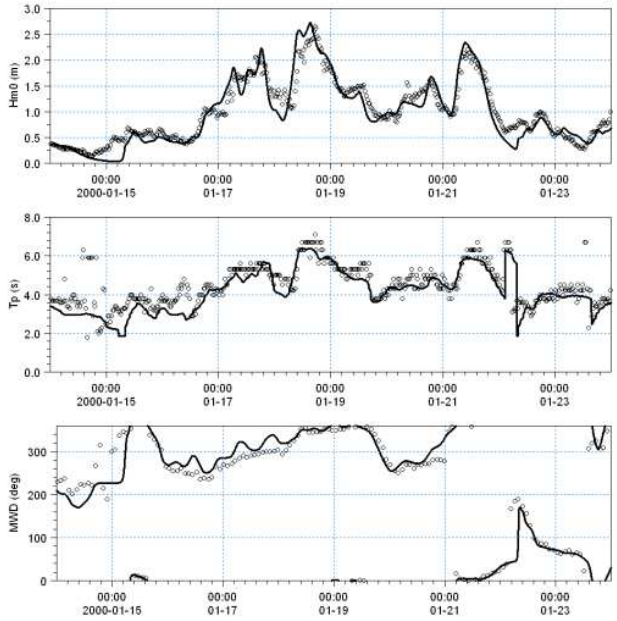

Time series of significant wave height, H_{m0}, peak wave period, T_p , and mean wave direction, MWD, at Darss sill (Offshore, depth 20.5 m). (——) Calculation and (o) measurements. The RMS value on H_{m0} is approximately 0.2 m

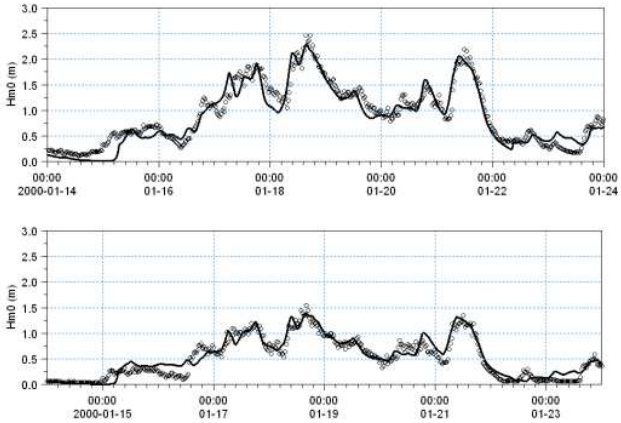

Time series of significant wave height, H_{m0}, at Gellen (upper, depth 8.3m) and Bock (lower, depth 5.5 m). (——) Calculation and (o) measurements. The RMS value on H_{m0} is approximately 0.15 m

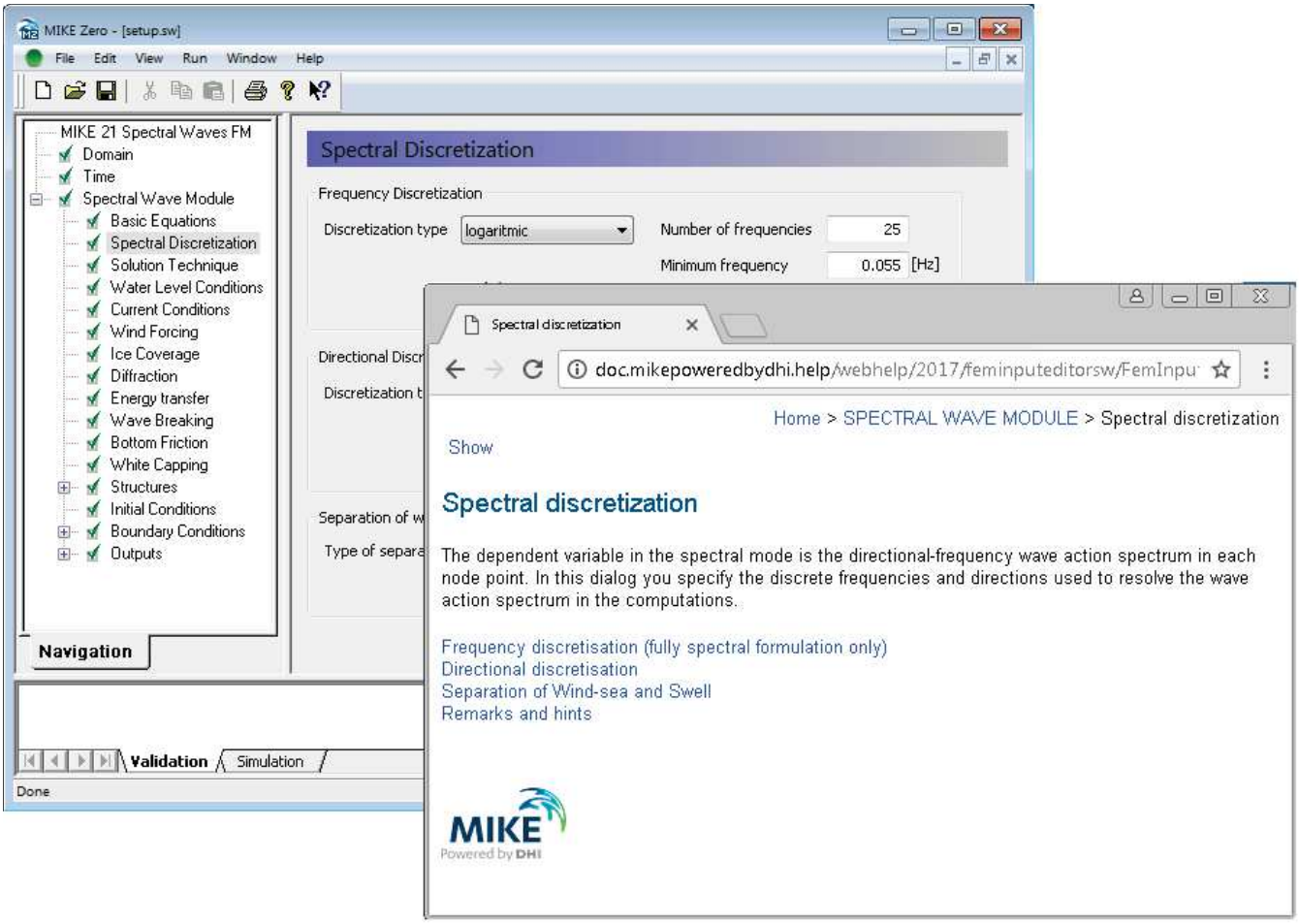

Graphical user interface of MIKE 21 SW, including an example of the Online Help System

Graphical User Interface

MIKE 21 SW is operated through a fully Windows integrated Graphical User Interface (GUI). Support is provided at each stage by an Online Help System.

The common MIKE Zero shell provides entries for common data file editors, plotting facilities and a toolbox for/utilities as the Mesh Generator and Data Viewer.

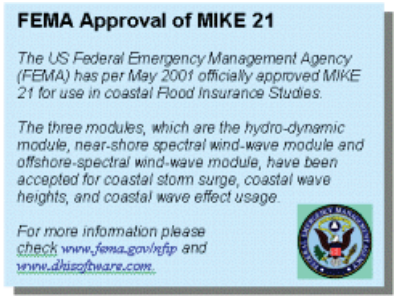

FEMA approval of the MIKE 21 package

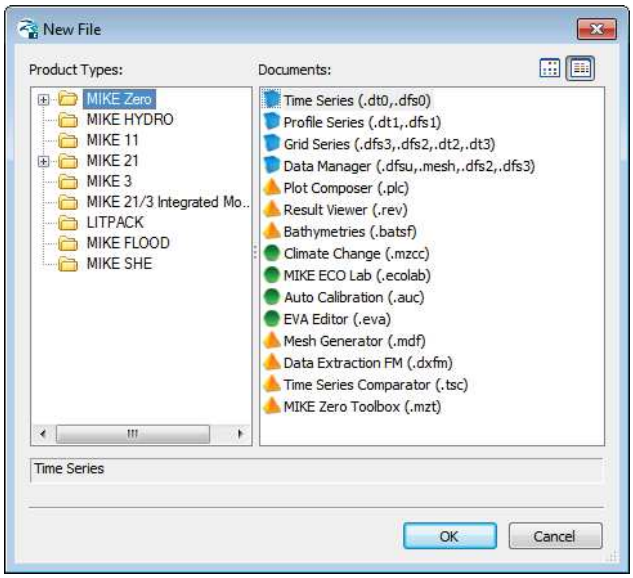

Overview of the common MIKE Zero utilities

Parallelisation

The computational engines of the MIKE 21/3 FM series are available in versions that have been parallelised using both shared memory as well as distributed memory architecture. The latter approach allows for domain decomposition. The result is much faster simulations on systems with many cores.

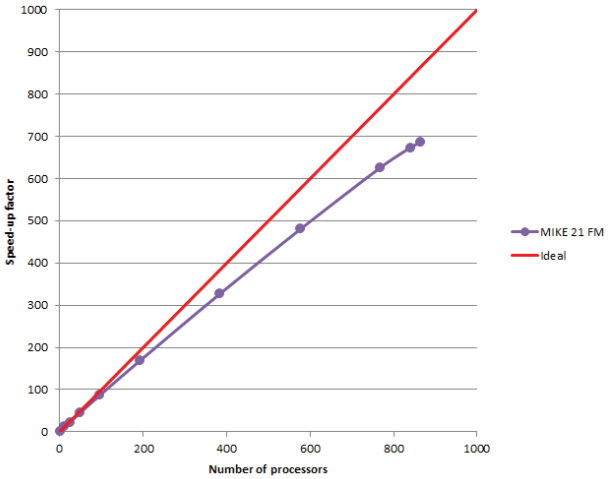

Example of MIKE 21 HD FM speed-up using a HPC Cluster with distributed memory architecture (purple)

Hardware and Operating System Requirements

The MIKE Zero Modules support Microsoft Windows 7 Professional Service Pack 1 (64 bit), Windows 10 Pro (64 bit), Windows Server 2012 R2 Standard (64 bit) and Windows Server 2016 Standard (64 bit).

Microsoft Internet Explorer 9.0 (or higher) is required for network license management. An internet browser is also required for accessing the web-based documentation and online help.

The recommended minimum hardware requirements for executing the MIKE Zero modules are:

Processor:	3 GHz PC (or higher)
Memory (RAM):	2 GB (or higher)
Hard disk:	40 GB (or higher)
Monitor:	SVGA, resolution 1024x768
Graphics card: (GUI and visualisation)	64 MB RAM (256 MB RAM or higher is recommended)

Support

News about new features, applications, papers, updates, patches, etc. are available here:

www.mikepoweredbydhi.com/Download/DocumentsAndTools.aspx

For further information on MIKE 21 SW, please contact your local DHI office or the support centre:

MIKE Powered by DHI Client Care
Agern Allé 5
DK-2970 Hørsholm
Denmark

Tel: +45 4516 9333
Fax: +45 4516 9292

mike@dhigroup.com
www.mikepoweredbydhi.com

Documentation

The MIKE 21 & MIKE 3 FM models are provided with comprehensive user guides, online help, scientific documentation, application examples and step-by-step training examples.

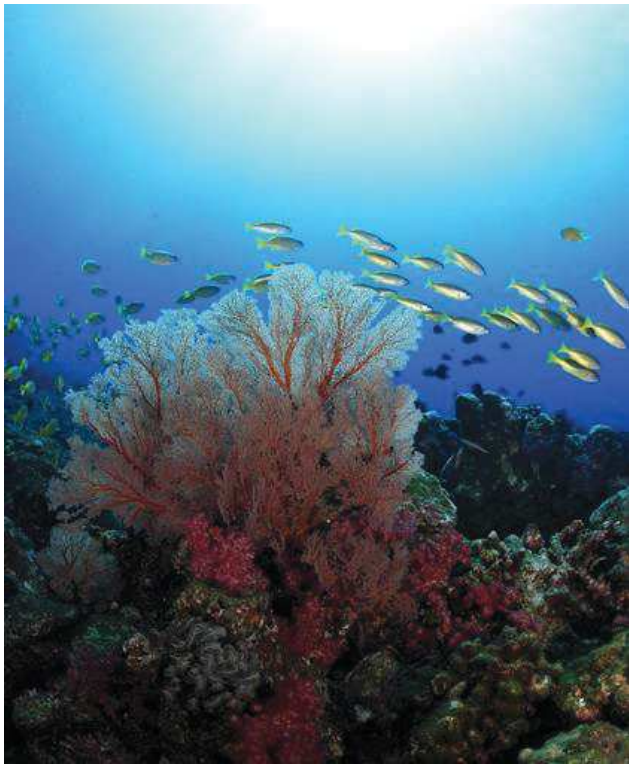

References

Sørensen, O. R., Kofoed-Hansen, H., Rugbjerg, M. and Sørensen, L.S., (2004): A Third Generation Spectral Wave Model Using an Unstructured Finite Volume Technique. In Proceedings of the 29th International Conference of Coastal Engineering, 19-24 September 2004, Lisbon, Portugal.

Johnson, H.K., and Kofoed-Hansen, H., (2000). Influence of bottom friction on sea surface roughness and its impact on shallow water wind wave modelling. *J. Phys. Oceanog.,* **30,** 1743-1756.

Johnson, H.K., Vested, H.J., Hersbach, H. Højstrup, J. and Larsen, S.E., (1999). On the coupling between wind and waves in the WAM model. *J. Atmos. Oceanic Technol.,* **16,** 1780-1790.

Johnson, H.K. (1998). On modeling wind-waves in shallow and fetch limited areas using the method of Holthuijsen, Booij and Herbers. *J. Coastal Research,* **14**, 3, 917-932.

Young, I.R., (1999). Wind generated ocean waves, in Elsevier Ocean Engineering Book Series, Volume 2, Eds. R. Bhattacharyya and M.E. McCormick, Elsevier.

Komen, G.J., Cavaleri, L., Doneland, M., Hasselmann, K., Hasselmann S. and Janssen, P.A.E.M., (1994). Dynamics and modelling of ocean waves. Cambridge University Press, UK, 560 pp.

Holthuijsen, L.H, Booij, N. and Herbers, T.H.C. (1989). A prediction model for stationary, short-crested waves in shallow water with ambient currents, *Coastal Engr.*, **13**, 23-54.

References on Applications

Kofoed-Hansen, H., Johnson, H.K., Højstrup, J. and Lange, B., (1998). Wind-wave modelling in waters with restricted fetches. In: Proc of 5th International Workshop on Wave Hindcasting and Forecasting, 27-30 January 1998, Melbourne, FL, USA, pp. 113-127.

Kofoed-Hansen, H, Johnson, H.K., Astrup, P. and Larsen, J., (2001). Prediction of waves and sea surface roughness in restricted coastal waters. In: Proc of 27th International Conference of Coastal Engineering, pp.1169-1182.

Al-Mashouk, M.A., Kerper, D.R. and Jacobsen, V., (1998). Red Sea Hindcast study: Development of a sea state design database for the Red Sea.. *J Saudi Aramco Technology*, **1**, 10 pp.

Rugbjerg, M., Nielsen, K., Christensen, J.H. and Jacobsen, V., (2001). Wave energy in the Danish part of the North Sea. In: Proc of 4th European Wave Energy Conference, 8 pp.

APPENDIX D – Mediterranean Wind Wave Model (MWM)

MWM: Mediterranean Wind Wave Model

General description of the models' chain

The models and datasets used for the development of the MWM database are:

- the *CFSR* (*Climate Forecast System Reanalysis*) global re-analysis dataset, produced and freely published by NCEP (*National Centers for Environmental Prediction*) (Saha et al, 2010; http://rda.ucar.edu/datasets/ds093.0/index.html#description), hourly (re-forecast) data with a space resolution of 0.5°; these data are used as initial (IC) and boundary conditions (BC) of the *WRF-ARW model* (below);

- the atmospheric model *WRF-ARW – version 3.4.1* (*Weather Research and Forecast - Advanced Research WRF*), model developed by NCAR (*National Center for Atmospheric Research*) (Skamarock and Klemp, 2007; Michalakes et al, 2001; Michalakes et al, 2005); *WRF-ARW* is presently considered among the best state-of-the-art non-hydrostatic meteorological models; it is supported by a massive worldwide community that contributes to its local use and development (http://www.mmm.ucar.edu/wrf/OnLineTutorial/index.htm; http://www.wrf-model.org/index.php);

- the wave model MIKE 21 Spectral Waves (SW) developed by DHI (former Danish Hydraulic Institute) (Sorensen, O.R., Kofoed-Hansen, H., Rugbjerg, M. and Sorensen, L.S., 2004). MIKE 21 SW is among the state of the art wave models, widely used in thousands of offshore and coastal applications worldwide.

In the following a description of the CFSR dataset, the WRF-ARW and the MIKE 21 SW model is given, with specific interest to the implementation adopted in MWM.

CFSR Dataset

The CFSR dataset (Fig. A.1) is the result of a long and complex process performed by NCEP, an ensemble of nine weather prediction centers in the United States belonging to the NWS (*National Weather Service*) of the NOAA (*National Oceanic and Atmospheric Administration*). The simulation, completed in 2011, is based on a global atmospheric numerical model including atmosphere-ocean and sea-ice couplings, with a systematic ingestion of both conventional (point) and satellite observations with data assimilation procedures.

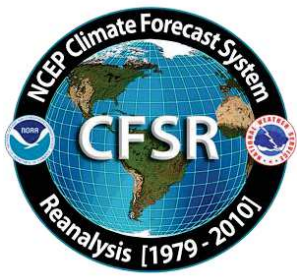

Figure A.1

The CFSR now covers a 35-year period from 1979 to 2013 (included) and is continuously updated with new recent data. The simulations were performed as 9 hours forecast simulations, initialized 4 times a day (at 00:00, 06:00, 12:00 and 18:00) between the 6-hourly re-analysis frames. The

results of these simulations, gathered in the CFSR dataset, consist in complete atmospheric data over ocean and lands with a one hour time resolution and a 0.5° horizontal resolution, while the vertical resolution changes greatly amongst the atmospheric variables, spanning from the single surface value up to values at 64 different isobaric levels.

MWM dataset ingest the 6-hourly CFSR data, specifically the *ds093.0* dataset.

Chawla et al (2013) presented a thorough analysis of the *CFSR* dataset against satellite and oceanic buoys data. The final goal of that study is the use of the U_{10} wind data from the *CFSR* dataset as the forcing term of *WWIII* to generate wave fields at global scale, without any assimilation of wave data. The analysis of the *CFSR* dataset shown in that paper includes the intrinsic performance of the model in terms of the seasonal and annual variability of the percentiles. A moving average is applied to smooth the altimeter data from the satellites and from the buoys. The normalized percentiles ("...normalized with the wind speeds at corresponding percentiles from the altimeters") computed over the satellite tracks exhibit an oscillatory behavior, never below 0.93 or 0.90 in the Northern and Southern hemisphere respectively. From that analysis, the wind and wave *CFSR* and *WWIII* data compare very well with satellite data in terms of normalized percentiles. The Q-Q plots at selected offshore buoys are generally good or very good, with some unexpected variations from case to case for some buoys close to the coast, with even a contradictory behavior between U_{10} and H_s in some locations.

The analysis of the wind field of the *CFSR* dataset is far beyond the scope of the present work but still some checks have been done in specific cases, like the event of November 1999 in Trieste (Italy). The performance of a local area model is directly related to the information contained in the global model used as boundary and initial conditions; Fig. A.2 after Contento et al (2014) shows the wind speed for the case of November 1999 in Trieste (Northern Adriatic Sea - Italy); the red dots are experimental data by NOAA (http://gis.ncdc.noaa.gov/map/viewer/#app=cdo&cfg=cdo&theme=hourly&layers=1&node=gis); the yellow line corresponds to the re-analysis data *CFSR d093.0* (Saha et al, 2010; http://rda.ucar.edu/datasets/ds093.0/index.html#description) interpolated at the same position of the station; the blue dots are related to a fully certified and verified measurement station of the Regional Agency for the Environment Protection (ARPA FVG-OSMER, http://www.osmer.fvg.it/home.php) located few meters far from the station used by NOAA (http://gis.ncdc.noaa.gov/map/viewer/#app=cdo&cfg=cdo&theme=hourly&layers=1&node=gis); the cyan line corresponds to the present hindcast dataset (model *WRF-ARW*). It is rather evident that the CFSR dataset ingests the experimental data from NOAA but there are some non-negligible discrepancies between the two experimental datasets (private communication with ARPA FVG-OSMER - Regional Agency for the Environment Protection – Friuli Venezia Giulia Region, Italy). In this case the local model *WRF-ARW* is able to develop the local wind field and matches correctly the measurement by ARPA, irrespective of the wrong assimilated data as BC and IC; this, however, cannot be always guaranteed.

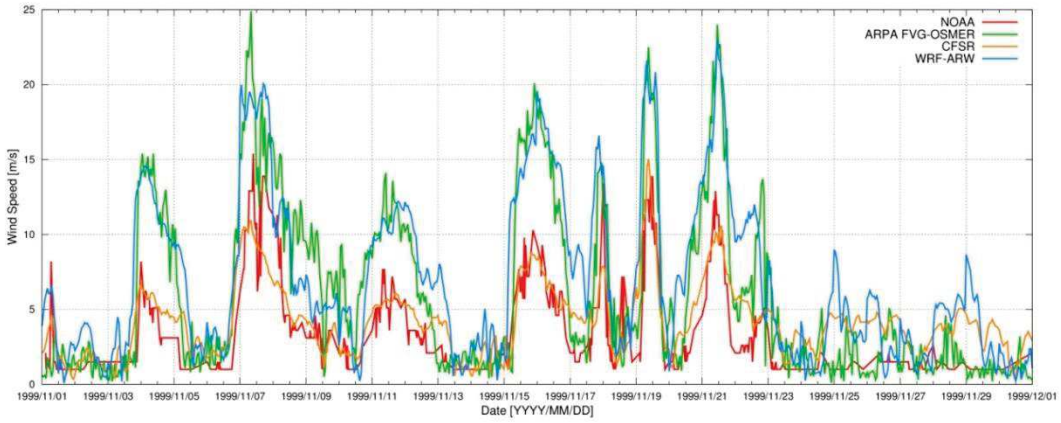

Figure A.2 Comparison between measured wind speed at two ground neighbor (few meters from each other) stations in Trieste (Italy - Northern Adriatic Sea) from the database of NOAA

(http://gis.ncdc.noaa.gov/map/viewer/#app=cdo&cfg=cdo&theme=hourly&layers=1&node=gis) (red line) and from ARPA-FVG OSMER (http://www.osmer.fvg.it/home.php) (blue line). Model data from *CFSR* (Saha et al, 2010) (yellow line) and the present simulations with *WRF-ARW* (cyan line) are overlapped.

The scope of these checks was solely to verify the sensitivity of the *CFSR* wind pattern to a complex steep geographic area facing the sea. The eastern coast of the Adriatic Sea is just an example among many others. The availability of certified wind data from the local Regional Agency for the Environment Protection – Friuli Venezia Giulia (ARPA FVG-OSMER, http://www.osmer.fvg.it/home.php) related to ground stations and to a fixed station in the middle of the Gulf of Trieste (Northern Adriatic Sea *http://www.ts.ismar.cnr.it/node/84*]), helped a lot in defining the set-up of the local area meteorological model. The aim of the set-up process was to let the model *WRF-ARW* develop mesoscale and local weather structures, thus using a domain large enough to develop these structures, but at the same time avoiding the use of too large a domain that may lead to a model drift from the experimental data. These undesired effects were observed along the entire Adriatic Sea, specifically on the eastern side (Contento et al, 2011; Contento et al, 2014).

WRF-ARW meteorological model

The WRF model is an open source mesoscale to microscale atmospheric model developed by the American atmospheric research center NCAR in cooperation with many other meteorological institutions. It is largely used worldwide for both atmospheric research and forecast or hindcast purposes due to its ability to perform atmospheric simulations over a wide range of length scales spanning from less then 1 kilometer to thousands of kilometers. This flexibility is further increased by its capability of performing two way coupled nested runs.

The WRF modelling system includes a pre-processor system (WPS), a data assimilation system (WRF-DA) and the dynamic solver. During this work the ARW dynamic solver, developed and maintained by the Mesoscale and Microscale Meteorology Division of NCAR, has been used. The ARW dynamic core is a fully compressible and non-hydrostatic model, based on a terrain-following hydrostatic pressure vertical coordinate system and on an Arakawa C-grid staggered evaluation of the vector quantities. The solver uses high order time integration and 3-D advection schemes.

The WRF model works internally with NetCDF files, a self-describing and machine-independent data format particularly suitable for the manipulation of long arrays of scientific data.

A WRF-ARW model run is a quite complex process, since it involves several different steps to be run in a precise order. First of all, WRF requires boundary and initial conditions; these conditions can be supplied by the GRIB files obtained from the CFSR dataset files described in CISL RDA: NCEP Climate Forecast System Re-analysis (CFSR) 6-hourly Products, January 1979 to December 2010." [Online] Available at http://rda.ucar.edu/datasets/ds093.0/index.html#description

GRIB files needed to cover completely the whole simulated period must be fed to the model to complete the simulation process successfully.

Moreover, since the atmosphere behaviour is strongly dependent on the soil characteristics, detailed data about these characteristics must be fed to the model too in order to let it develop the local weather phenomena correctly. However, there is no need to produce this type of data since suitable 30" resolved geographic data are included in the default WRF pre-processing (WPS). Since these data are time-independent they need to be downloaded only once, and they remain valid for every simulation unlike the GRIB files. Actually, some of the parameters contained in the geographic data cannot be considered as completely time-independent; in fact, some of the parameters show a time dependence which, however, is limited to seasonal changes, e.g. the

reduced vegetation cover in winter. The possible seasonal variability of the geographical parameters is included in the geographical data archive of WPS.

A complete WRF-ARW simulation needs the WPS (*WRF Pre-processor System*) to be run before the numerical solver (*wrf.exe*). The WPS pre-processor system deals with both the domain set-up and the preliminary input manipulations; it is composed by three main executables carrying out different tasks:

- *geogrid.exe* is responsible for the definition of the horizontal grid as well as for the interpolation of the geographic data on the user-defined grid. When performing nested runs, the *geogrid.exe* run produces a NetCDF file *geo_em.dxx.nc* containing the grid and geographic data for each domain, where xx stands for the code of the domain (01, 02, …).

- *ungrib.exe* is responsible for the decoding of the input GRIB files used as initial and boundary conditions. The GRIB files, which need to be linked to the work directory of WPS by means of the script *link_grib.csh*, are "ungribbed" and rewritten in an intermediate format suitable for further manipulations, excluding all the fields not needed for the following model run.

- *metgrid.exe* is responsible for the horizontal interpolation of the intermediate input files produced by ungrib.exe on the grid defined by geogrid.exe. Moreover, the geographic data contained in the *geo_em* files are ingested by metgrid and written on its output files. The output of metgrid.exe is in fact composed by the NetCDF files *met_em.dxx.YYYY-MM-DD_HH:00:00.nc*, each containing the interpolated boundary conditions and geographic data for the xx domain and for every timestep of the supplied GRIB files. In the case considered, as the CFSR dataset is composed of hourly data, the produced *met_em* files are hourly spaced too.

The whole WPS process is controlled by a single external configuration file: *namelist.wps*, which contains the user specified parameters defining the time length and the domain of the simulation as well as the time and space resolutions.

An additional manipulation is needed before launching the actual solver: the NetCDF data produced by metgrid.exe must be vertically interpolated onto the user- defined vertical levels of the WRF simulation. This task is performed by the *real.exe* executable, which, despite actually being a pre-processing routine, is not included in the WPS system. The real.exe run finally produces the NetCDF files needed by the bare solver: *wrfinput_dxx* and *wrfbdy_dxx*, containing respectively, for each of the nested domains under simulation, the initial condition inclusive of the domain geographic data and the boundary conditions forcing the domain over time.

The last step of a WRF-ARW model simulation is the *wrf.exe* solver run which performs the numerical integration and produces the final output files *wrfout_dxx_YYYY-MM-DD_HH:MN:SS,* one for each simulated domain and for every temporal frame in the total simulated period. Each wrfout file contains therefore the complete atmospheric variables set calculated by the ARW solver for every point of the user defined simulation 3-D grid at a single temporal frame.

Both real.exe and wrf.exe are controlled by *namelist.input*, an external configuration file gathering the user defined parameters regarding the vertical resolution of the simulation, the atmosphere microphysical parameters and, again, the time / length scales and resolutions of the simulation.

A script that makes all steps involved automatic in a WRF-ARW simulation procedure, from the set-up of the configuration files to the archiving of output files, was developed and tested extensively.

The above depicted working scheme is summarized in Figure A.3:

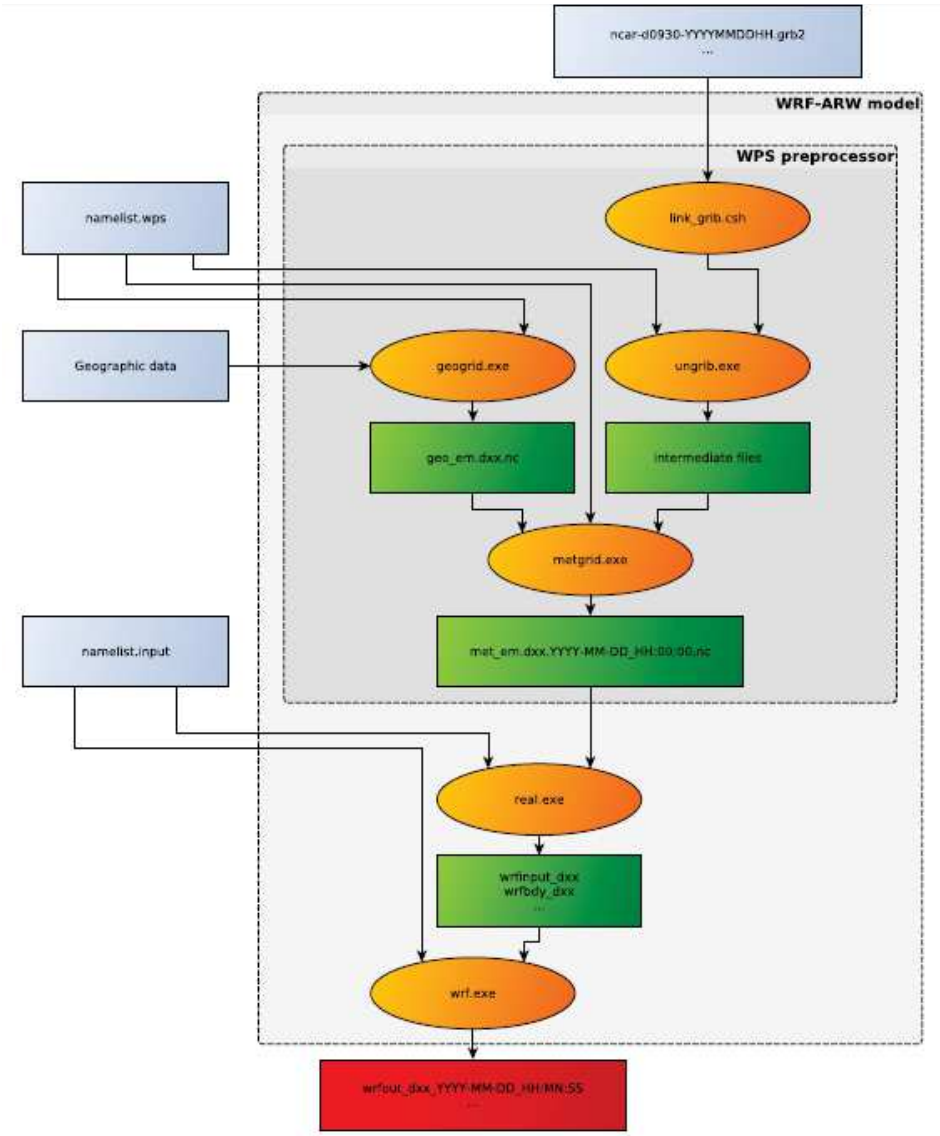

Figure A.3 Working scheme of the WRF-ARW model.

WRF-ARW domains, resolution, set-up in MWM

The preliminary set-up and tuning of the met-ocean models chain was performed simulating the month of November 1999, chosen for the remarkable number of very intense storms occurred over the Mediterranean Sea. The second step, before running the entire period 1979-2013, was done simulating one complete year, from November 1999 to October 2000, relying on 41 ground stations along the Mediterranean coast and 25 wave buoys for comparison. The results obtained in these steps are summarized in Contento et al. (2014), Contento et al. (2012-2014) and Donatini (2013).

The two-steps set-up started with the meteorological model *WRF-ARW*, adopting different configurations (domain size, resolution, run length, spin-up time) and comparing the wind speed and direction with observational data from ground stations. Since the *CFSR* (Saha et al, 2010) re-analysis dataset reproduces large scale events correctly, after several tests the final decision was to adopt three relatively small, overlapping domains, which cover respectively the Western, Eastern and Central Mediterranean Sea (Fig. A.4). Hereafter these domains will be referred as MEW, MEE and MEC respectively. The wind field obtained from the 3 domains was merged in a

single dataset by a bi-linear interpolation on a Lat-Lon grid and by a linear blending of the results inside the two overlapping zones (Fig. A.4).

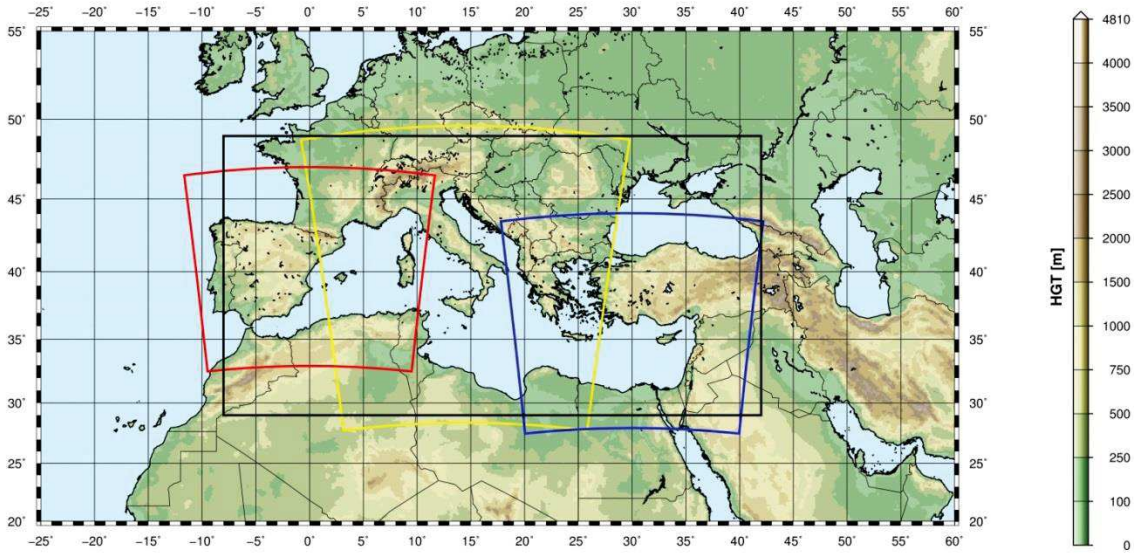

Figure A.4 WRF-ARW domains (red=domain MEW, yellow=domain MEC, blue=domain MEE) and interpolation/blending domain (black line).

The horizontal resolution of *WRF-ARW* was set to 10.53 km, with a grid ratio to the *CFSR* re-analysis data of 1:5 approximately. An additional domain (ITN) with a resolution of 3.51 km was run over Northern Italy as a nested domain of MEC.

The time length of the model run, in terms of hours simulated continuously between two consecutive model initializations with *CFSR* frames,proved to be among the most important parameters that influence the quality of the results. Keeping a small run length reduces the risk of model drift. On the other hand, shortening it excessively may lead to a too constrained behavior of the model, which prevents the correct development of the mesoscale weather structures. The problem of the model drift proved to be particularly tough over the Adriatic Sea where the orography is rather complex and the North-Eastern wind (Bora) can occasionally reach the speed of 150 km/h or more in very narrow zones.

A spin-up time window was used in order to let the model *WRF-ARW* ingest and process the coarser initial conditions from *CFSR*, thus letting it evolve and develop local weather structures. This spin-up window was overlapped with the tail of the previous run so that the data of the simulation during the spin-up window were discarded. The time length of this overlapping window is typically of few hours.

The Mediterranean Sea is a very complex basin from the meteorological point of view, with violent storms usually characterized by a short duration. The two examples given below show the importance of resolving the large space and time gradients of the variables.

Fig. A.5 shows a typical winter wind pattern (from the present simulations, 5 December 2009). The well-known 3 major narrow gates of the “Bora” wind over the Adriatic Sea are well captured by the model, i.e. Trieste (Italy), Rijeka and Sibenik (Croatia). The reference distance of these large variations is of 1° at most.

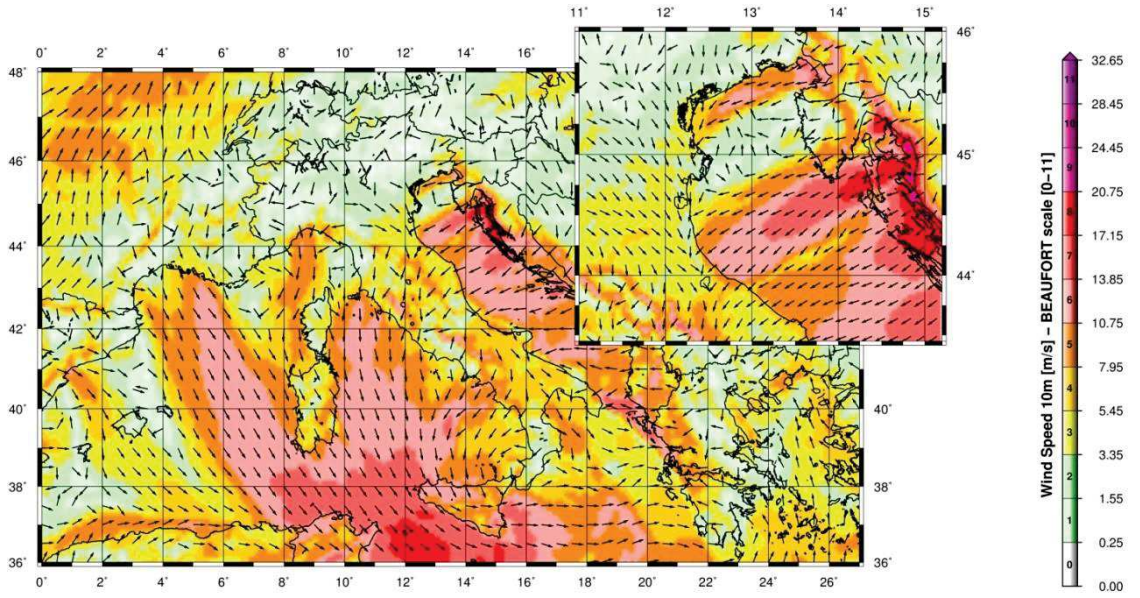

Figure A.5 A typical winter wind pattern over the Mediterranean Sea (from the present simulations, 5 December 2009). The well-known 3 major narrow gates of the "Bora" wind over the Adriatic Sea are well captured by the model, i.e. Trieste (Italy), Rijeka and Sibenik (Croatia). The upper-right figure shows a zoom over the Northern part of the Adriatic Sea (Istria peninsula).

Fig. A.6 (Contento et al., 2011) shows the time series of the wind speed during a squall event occurred on August 2008 in the Gulf of Trieste that caused the loss of two human lives and damages in the main harbor. The squall lasted about 10 min reaching more than 20 m/s from an almost calm situation. The red line corresponds to the results of the operational forecast meteorological model *WRF-ARW* run at that time by some of the authors of this work for ARPA FVG-OSMER, http://www.osmer.fvg.it/home.php. The black line corresponds to the measurement at the station PALOMA (45° 37' 06" N, 13° 33' 55" E) [*http://www.ts.ismar.cnr.it/node/84*]. The station is a fixed pole in the middle of the Gulf of Trieste. The measured wind speed is 5 min averaged with 5 min samples. The time step of the model is approximately 13 s. This situation is not uncommon in the Adriatic zone, mostly during the summer, with violent fronts from North and North-West then rotating to North-East.

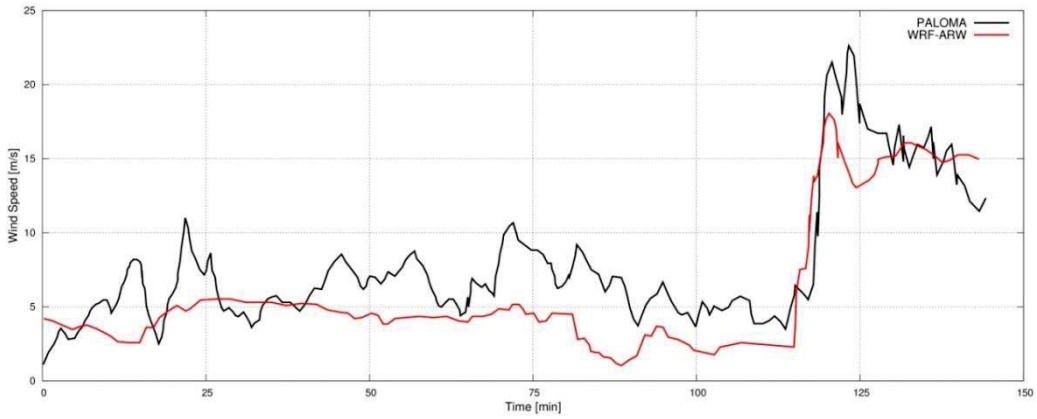

Figure A.6 Time series of the wind speed during a squall event occurred on August 2008 in the Gulf of Trieste. The squall lasts about 10 min reaching over 20 m/s from an almost calm situation. The red line corresponds to the results of the operational forecast meteorological model *WRF-ARW*. The black line corresponds to the measurement at the measurements station PALOMA (45° 37' 06" N, 13° 33' 55" E) [*http://www.ts.ismar.cnr.it/node/84*]. The measured wind speed is 5 min averaged with 5 min samples. The time step of the model is approximately 13 s.

MIKE 21 SW wave model

The wave modeling system includes the state of the art third generation spectral wind-wave model MIKE 21 SW, developed by DHI. MIKE 21 SW simulates the growth, decay and transformation of wind-generated waves and swell in offshore and coastal areas.

MIKE 21 SW includes two different formulations:

- Directional decoupled parametric formulation
- Fully spectral formulation

and includes the following physical phenomena:

- Wave growth by action of wind
- Non-linear wave-wave interaction
- Dissipation due to white-capping
- Dissipation due to bottom friction
- Dissipation due to depth-induced wave breaking
- Refraction and shoaling due to depth variations
- Wave-current interaction
- Effect of time-varying water depth

The discretization of the governing equation in geographical and spectral space is performed using cell-centered finite volume method. In the geographical domain, an unstructured mesh technique is used. The time integration is performed using a fractional step approach where a multisequence explicit method is applied for the propagation of wave action.

For the production of the MWM database, the fully spectral formulation has been adopted, based on the wave action conservation equation, as described in e.g. Komen et al. and Young where the directional-frequency wave action spectrum is the dependent variable.

The time integration of the governing equations is done by using a dynamically determined time step. The time step is determined in order to verify the stability criteria (CFL number).

The only driving force is represented by the two components of wind fields U10 and V10, (x and y component of wind at the elevation of 10m). The process by which the wind transfers energy into the water body for generating waves is controlled by a uncoupled air-sea interaction.

The spectral discretization adopted in the wave model has been deeply investigated and the final configuration is able to guarantee at the same time a high level of accuracy of the results and a reasonable computational effort.

The model domain covers the whole Mediterranean Sea but the spatial resolution is not the same everywhere: while in the offshore areas the spatial resolution is around 0.1°, when approaching the coast the spatial resolution increases up to around 0.03°.

The wave model is forced by the wind fields coming from the WRF Atmospheric models, illustrated above. The wave model generated results in terms of wave parameters (Significant Wave Height, Wave Periods, Wave Directions, etc.) over the whole domain and, in addition, spectral parameters in predefined output locations have been stored, too.

MIKE 21 SW domain, resolution, set-up in MWM

The model domain, covering the entire Mediterranean Sea, is illustrated in Figure A.7.

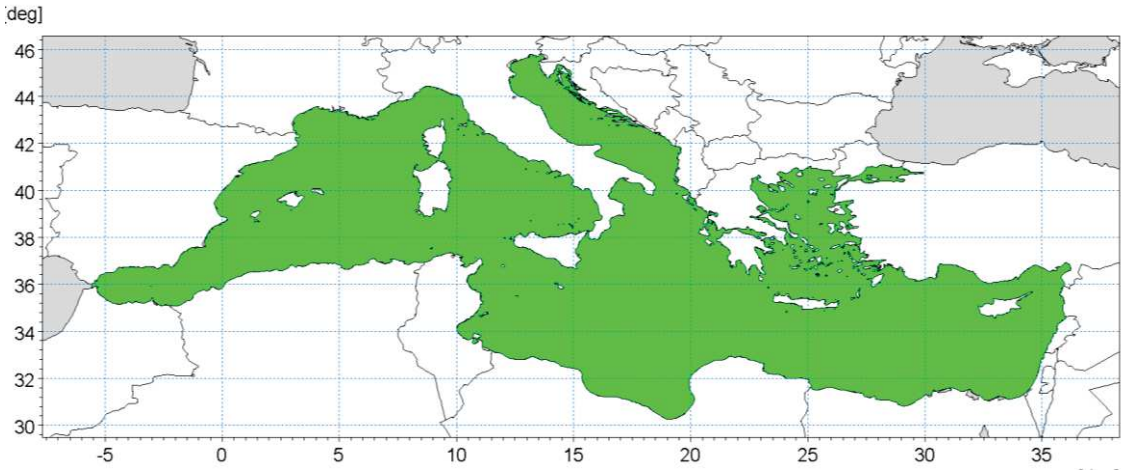

Figure A.7 Wave model domain filled in green

The unstructured mesh, generated over the entire domain by means of a specific tool included in MIKE 21 package, is characterized by different resolutions (in terms of mean length of triangle sides) over the domain. In particular the following criteria have been adopted:

- a coarser resolution of 0.1° (about 10 Km) is used for offshore areas;
- a finer resolution of 0.03° (about 3 Km) has been adopted in shallow water areas, where bathymetry is less than 100m depth or, in coastal areas characterized by very steep profiles, where the distance from the coastline is less than 5÷10 Km.

Figure A.8 illustrates the computational mesh of the Mediterranean wave model.

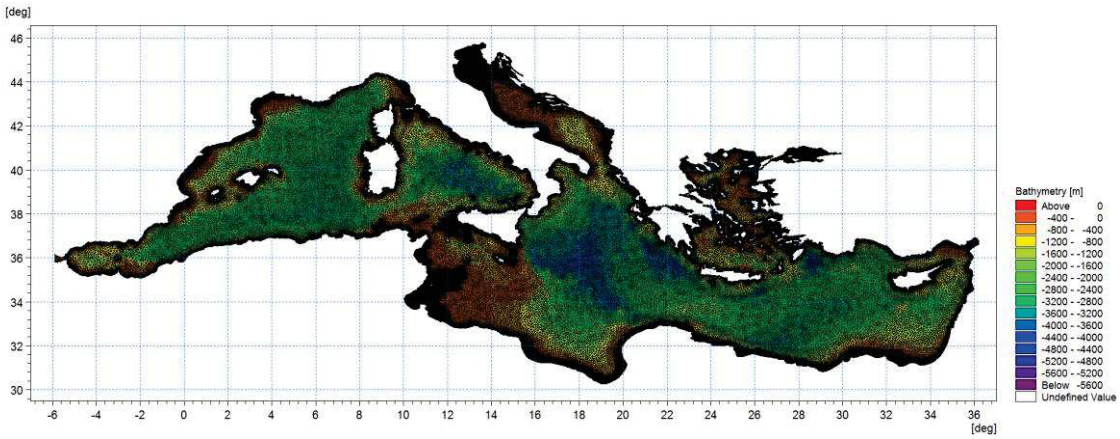

Figure A.8 - Mediterranean wave model computational mesh

Figure A.9 illustrates a detail of the above computational mesh, with special focus on the Adriatic Sea.

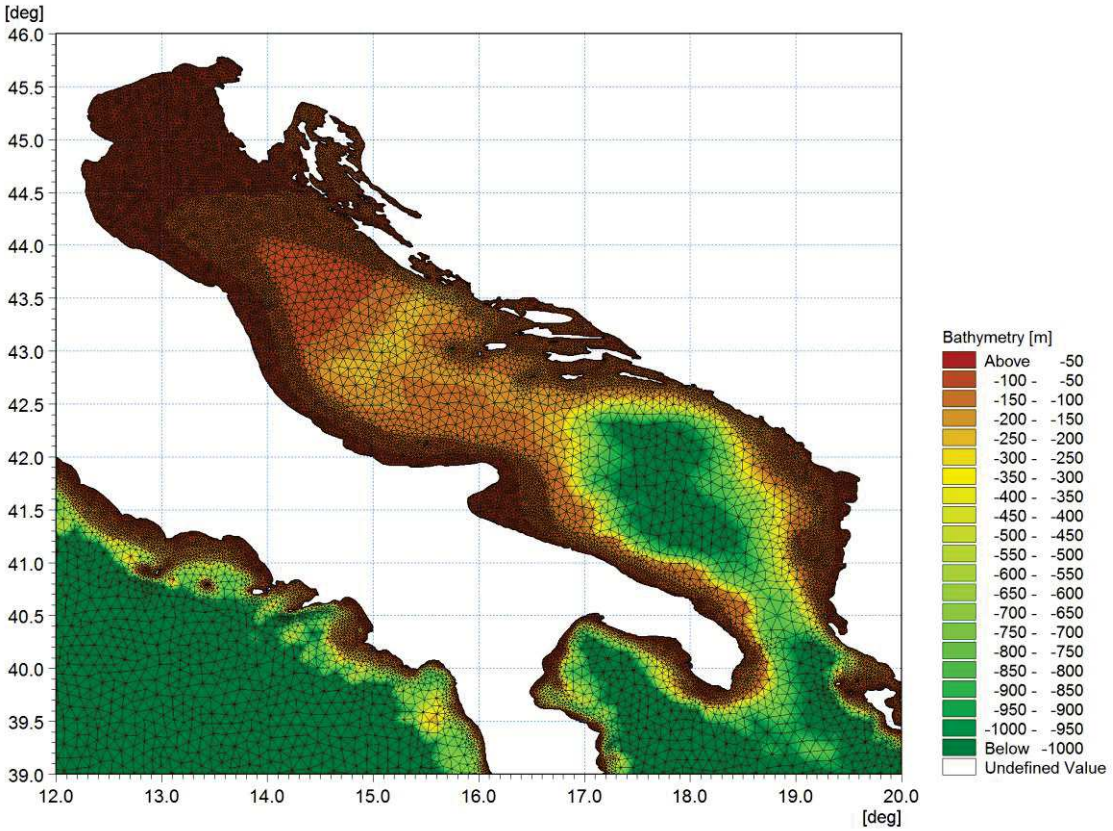

Figure A.9 - Detail of the mesh – Adriatic Sea

Scatter bathymetry data have been derived from GEBCO_08 database. The GEBCO_08 Grid is a 30 arc-second grid of global elevations and it is a continuous terrain model for ocean and land. The grid was generated by combining quality-controlled ship depth soundings with interpolation between sounding points guided by satellite-derived gravity data.

The gridded data are stored in a netCDF data file. Grids are stored as one dimensional arrays of 2-byte signed integer values. The complete data sets provide global coverage. Each data set consists of 21,600 rows x 43,200 columns, resulting in a total of 933,120,000 data points. The data start at the Northwest corner of the file, i.e. for the global file, position 89°59'45"N, 179°59'45"W, and are arranged in latitudinal bands of 360 degrees x 120 points/degree = 43,200 values. The data range eastward from 179°59'45"W to 179°59'45"E. Thus, the first band contains 43,200 values for 89°59'45"N, then followed by a band of 43,200 values at 89°59'15"N and so on at 30 arc-second latitude intervals down to 89°59'45"S. Data values are pixel centred registered, they refer to elevations at the centre of grid cells.

Figure A.10 illustrates GEBCO_08 scatter data for the entire area of the Mediterranean Sea.

GEBCO scatter data have not been used in the whole domain of the Mediterranean Sea. Following a detailed check of agreement and discrepancies between GEBCO database and nautical charts, it has been assumed to limit the use of GEBCO database for offshore areas (up to 500 m water depth) and to use nautical charts for shallower water areas (mainly coastal areas).

The nautical charts database which has been used is the CM93/3 database from CMAP.

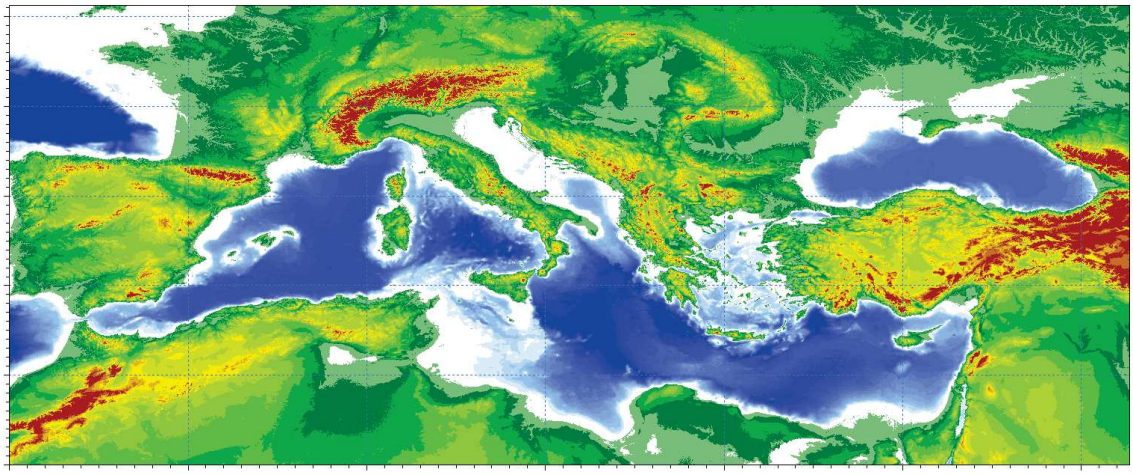

Figure A.10 - Scatter bathymetry data derived from GEBCO_08 database

The number of discrete frequencies and directions form the so called “spectral resolution”, which is a key parameter for wave models in general. The number of discrete frequencies and directions should in fact be high enough to properly represent the “real shape” of the wave spectrum and, on the other hand, it can’t be too high, since it would lead to unacceptable computational times and memory consumption.

In terms of frequency range, the minimum frequency f_{min} (which corresponds to the maximum wave period $T_{max,}$ according to the common relation $= \frac{1}{T}$) should be able to capture the longest wave periods that can occur in the Mediterranean Sea.

The analysis of ordinary and extreme waves in the Mediterranean Sea (from available data of wave buoys) has highlighted that almost all the wave energy associated to waves in the Mediterranean Sea are associated to wave periods between 1.5 seconds and 20 seconds.

In addition, a logarithmic distribution for the discrete frequencies acts better than a simple linear distribution, since most of the wave periods are concentrated below 8-10 seconds. A number of frequencies around 30 is widely considered as adequate for a proper discretization of wave energy spectra in the Mediterranean Sea. The following formulation has therefore been adopted:

$$f_{n=}0.04 \cdot \ 1.1^{n},$$

where n goes from 0 to 29 (30 frequencies in total). The discrete frequencies range from 0.04 Hz to 0.63 Hz (from 1.6s to 25.0s of Mean Wave Period T_m).

Also the choice of the number of discrete directions (directional discretization) is the result of detailed investigations and tests. In particular, a high number of wave model tests, each one characterized by a different spectral resolution (directional), i.e. by a different number of discrete directions have been setup and run.

Few examples of the results of the above model tests are illustrated from Figure A.11 to Figure A.13 in terms of short time series of wave heights extracted at 3 different locations where also measurements were available (La Spezia wave buoy, Ponza wave buoy, Cetraro wave buoy).

In all the below test cases, it appears that the two time series of wave height characterized by 24 and 36 discrete directions are almost coincident. Higher discrepancies can be found for a much limited number of discrete directions (12). After a high number of tests, the 24 directions solution has been assumed as a very good compromise between accuracy of results and computational time (the computational time of the wave model is linearly dependent on the number of discrete directions).

Provided that wave directions can vary within the 360° rose, the directional resolution of the wave model is 360°/24 = 15°

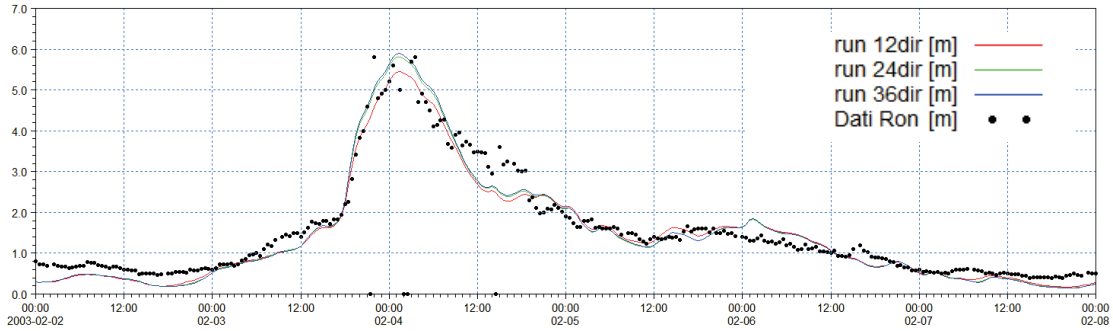

Figure A.11 - Time series of wave height at La Spezia buoy location for 3 different numbers of discrete directions

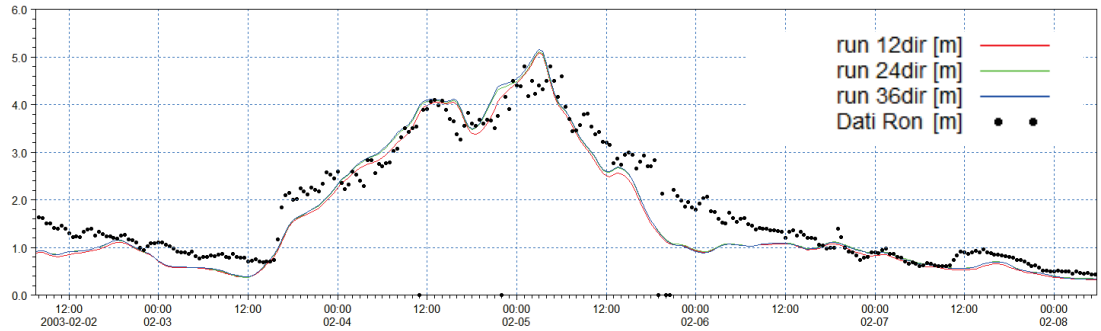

Figure A.12 - Time series of wave height at Ponza buoy location for 3 different numbers of discrete directions

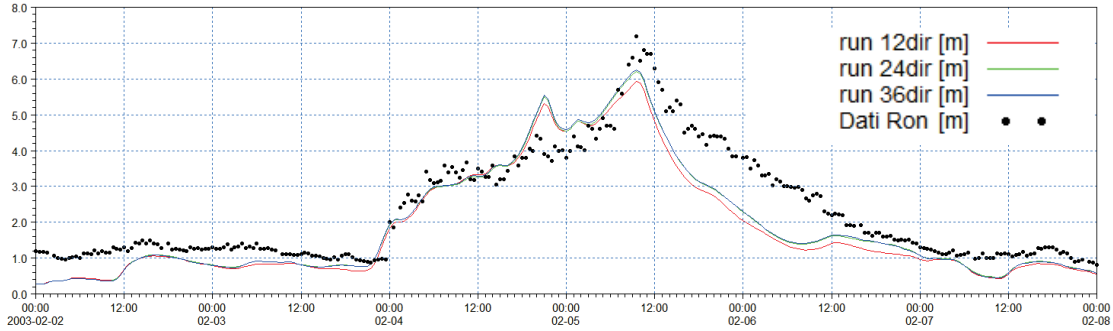

Figure A.13 - Time series of wave height at Cetraro buoy location for 3 different numbers of discrete directions

Available products of the MWM database

The results of the wind and wave model are stored, in the whole domain, in terms of wind parameters and wave parameters averaged over the wave period ("phase averaged results"). In particular, the following hourly time series are available:

- Wind speed, WS [m/s]
- Wind direction, WD [deg]
- Significant Wave height, Hs [m]
- Mean wave period, Tm [s]
- Peak wave period, Tp [s]
- Zero crossing period, Tz [s]
- Mean wave direction, MWD [deg]
- Peak wave direction, PWD [deg]
- Directional standard deviation, DSD [deg]

In addition, hourly spectral results (in terms of wave energy associated to the frequency-direction bins) are saved on a regular grid with an equidistant spatial resolution of 0.1°.

Figure A.14 and Figure A-15 illustrate respectively an example of phase averaged results over a portion of Mediterranean Sea (Hs) and an local example of spectral results.

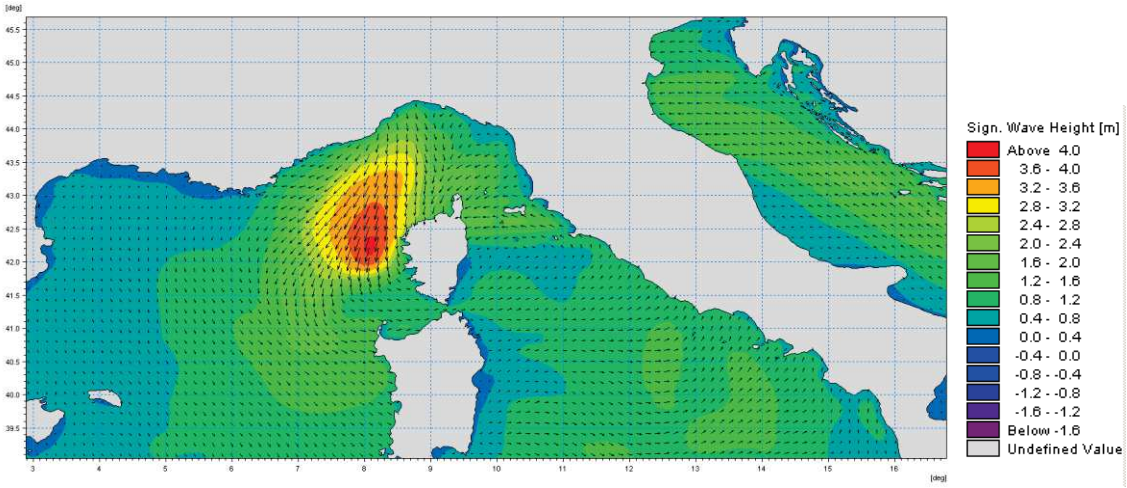

Figure A.14 Phase averaged results: Field of significant wave height and direction

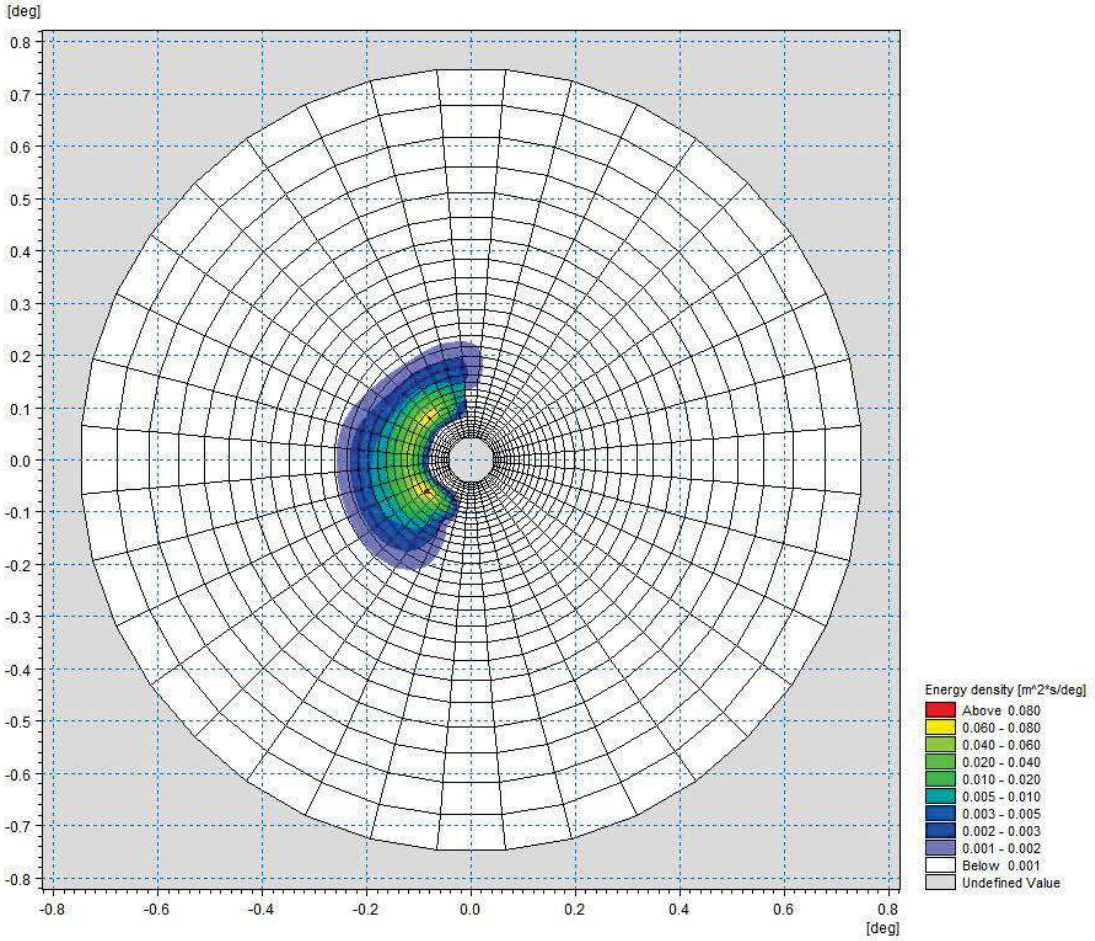

Figure A.15 Polar plot of spectral results. Wave energy density (coloured contours) as a function of directions (angular coordinate) and frequencies (radial coordinate)

References

Ardhuin, F., Bertotti, L., Bidlot, J.R., Cavaleri, L., Filipetto, V., Lefevre, J.M,, Wittmann, P., 2007, Comparison of wind and wave measurements and models in the Western Mediterranean Sea. *Ocean Engineering*, Vol. 34, pp. 526-541.

Athanassoulis, G., Stefanakos, Ch., Cavaleri, L., Ramieri, E., NoEL, C., Lefevre, J.M., Gaillard, P., 2004, RTP 10.10 / WW_MEDATLAS Scientific Report.

Battjes, J.A., Janssen, J.P.F.M., 1978, Energy loss and set-up due to breaking of random waves, Proceedings, 16th Int. Conf. Coastal Eng., ASCE, pp.569-587.

Bolaños-Sanchez, R., Sanchez-Arcilla, A., Cateura, J., 2007, Evaluation of two atmospheric models for wind-.wave modeling in the NW Mediterranean. *Journal of Marine Systems* 65:336-353.

Cavaleri, L., Bertotti, L., 2004, Accuracy of the modelled wind and wave fields in enclosed seas. Tellus, Vol. 56, pp. 167-175.

Cavaleri, L., 2005, The wind and wave atlas of the Mediterranean Sea – the calibration phase. *Advances in Geosciences*, Vol. 2, pp. 255-257.

Cavaleri, L., Sclavo., M., 2006, The calibration of wind and wave model data in the Mediterranean Sea. Coastal Engineering, Vol.53, pp. 613-627.

Chawla, A., Spindler, D.M., Tolman, H.L., 2013, Validation of a thirty year wave hindcast using the Climate Forecast System Reanalysis winds, Ocean Modelling, Vol. 70, pp. 189-206.

Contento, G., Lupieri, G., Venturi, M. Ciuffardi, T., 2011, A medium-resolution wave hindcast study over the Central and Western Mediterranean Sea, *Journal of Marine Science and Technology*, Vol. 16(2), pp. 181–201.

Contento, G., Lupieri, G., Donatini, L, Feudale, L, Pedroncini, A., Cusati, L.A., 2014, A state-of-the-art met-ocean model chain for wind&wave hindcast over the Mediterranean and Black Seas: implementation, tuning and validation against field data, accepted for presentation at the 21th Symposium Theory and Practice of Shipbuilding SORTA 2014, Oct. 2-4, 2014, Baška, Island of Krk, Croatia.

Contento, G., Lupieri, G., Donatini, L, 2012-2014, Project SEAPOL - Sistema modellistico ad Elevata risoluzione per l'Analisi storica e la Previsione del moto Ondoso nel mar Ligure, Department of Engineering and Architecture, University of Trieste, Technical Reports codes SEAPOL_UT_1.1.0 to SEAPOL_UT_5.1.0.

Donatini, L., 2013, Implementation of a state-of-art met-ocean model chain for hindcast wave simulations over the Mediterranean Sea and comparison of results with field data, Master Degree Thesis, Department of Engineering and Architecture, University of Trieste, Italy.

Donatini, L., Lupieri, G., Contento, G., 2014, A medium resolution wind&wave hindcast study for the Mediterranean Sea, Journal Paper, under review.

Hasselmann, K., Barnett, T.P., Bouws, E., Carlson, H., Cartwright, D.E., Enke, K., Ewing, J.A., Gienapp, H., Hasselmann, D.E., Krusemann, P., Meerburg, A., Mueller, P., Olbers, D.J., Richter, K., Sell, W., Walden, H., 1973, Measurements of wind-wave growth and swell decay during the Joint North Sea Wave Project (JONSWAP). Ergaenzungsheft zur Deutschen Hydrographischen Zeitschrift, Reihe, A(8), 12, 95 pp.

Hasselmann, S., Hasselmann, K., Allender, J.H., Barnett, T.P., 1985. Computations and parametrizations of the nonlinear energy transfer in a gravity-wave spectrum, Part II: Parametrizations of the nonlinear energy transfer for applications in wave models. J. Phys. Oceanogr. Vol. 15, pp. 1378–1391.

ISPRA (formerly APAT), 2004, Agenzia per la Protezione dell'Ambiente e per i servizi Tecnici, Dipartimento Tutela Acque Marine ed Interne, Servizio difesa delle coste, Analisi preliminare dei dati marini lungo le coste italiane – Atlante delle coste – Il moto ondoso al largo delle coste italiane, Technical Report (in Italian). http://www.apat.gov.it/site/_files/Atlante_coste/Introduzione.pdf.

Janssen, P.A.E.M., Abdalla, S., Hersbach, H., Bidlot, J.R., 2007: Error Estimation of Buoy, Satellite, and Model Wave Height Data. *J. Atmos. Oceanic Technol.*, Vol. **24**, pp. 1665–1677. doi: http://dx.doi.org/10.1175/JTECH2069.1

Michalakes, J., Chen, S., Dudhia, J., Hart, L., Klemp, J., Middlecoff, J., Skamarock, W., 2001, Development of a Next Generation Regional Weather Research and Forecast Model. *Developments in Teracomputing. In Proceedings of the 9th ECMWF Workshop on the Use of High Performance Computing in Meteorology.* Eds. Walter Zwieflhofer and Norbert Kreitz. World Scientific, 269-276.

Michalakes, J., Dudhia, J., Gill, D., Henderson, T., Klemp, J., Skamarock, W., Wang, W., 2005, The Weather Research and Forecast Model: Software Architecture and Performance. In *Proceedings of the 11th ECMWF Workshop on the Use of High Performance Computing in Meteorology.* Eds. Walter Zwieflhofer and George Mozdzynski. World Scientific, 56 - 168.

Ponce del León, S., Guedes Soares, C., 2008, Sensitivity of wave model predictions to wind fields in the Western Mediterranean Sea. *Coastal Engineering*, Vol. 55, pp. 920-929.

Puertos del Estado, Spain, 2009, – (http://www.puertos.es/oceanografia_y_meteorologia/), private communication.

Queffeulou, P., 2004, Long term validation of wave height measurements from altimeters. Marine Geodesy, Vol. 27, 495-510.

Queffeulou, P., Croizé-Fillon, D., 2010, Global altimeter SWH data set, version 7, Technical Report, Ifremer, ftp://ftp.ifremer.fr/cersat/products/swath/altimeters/waves/documentation/altimeter_wave_merge__7.0.pdf

Queffeulou, P., 2009, Altimeter Wave Height Measurements - Validation of Long Time Series.Poster: Ocean Surface Topography Science Team meeting, Seattle, Washington,USA.(http://www.aviso.oceanobs.com/en/courses/oststt/oststt-2009-seattle/posters/).

Saha, S., Moorthi, S., Pan, H., Wu, X., Wang, J., Nadiga, S., Tripp, P., Kistler, R., Wollen, J., Behringer, D., Liu, H., Stokes, D., Grumbine, R., Gayno, G., Wang, J., Hou, Y., Chuang, H., Juang, H., Sela, J., Iredell, M., Treadon, R., Kleist, D., VanDelst, P., Keyser, D., Derber, J., Ek, M., Meng, J., Wei, H., Yang, R., Lord, S., van den Dool, H., Kumar, A., Wang, W., Long, C., Chelliah, M., Xue, Y., Huang, B., Schemm, J., Ebisuzaki, W., Lin, R., Xie, P., Chen, M., Zhou, S., Higgins, W., Zou, C., Liu, Q., Chen,Y., Han, Y., Cucurull, L., Reynolds, R., Rutledge, G., Goldberg, M., 2010, The NCEP Climate Forecast System Reanalysis. *Bull. Amer. Meteor. Soc.*, Vol. 91, 1015–1057.

Skamarock WC, Klemp JB, 2007, A time-split nonhydrostatic atmospheric model for research and NWP applications. *J. Comp. Phys.* Special issue on environmental modeling.

Sorensen, O.R., Kofoed-Hansen, H., Rugbjerg, M. and Sorensen, L.S., 2004: A Third Generation Spectral Wave Model Using an Unstructured Finite Volume Technique. In Proceedings of the 29th International Conference of Coastal Engineering, 19-24 September 2004, Lisbon, Portugal.

Tolman, H.L., 2002a. Alleviating the garden sprinkler effect in wind wave models. Ocean Modelling, Vol. 4, pp. 269–289.

Tolman, H.L., 2002f, Validation of WAVEWATCH III, version 1.15 for a global domain. Tech. Note 213, NOAA/NWS/NCEP/OMB, 33p.

Tolman, H.L., 2008, http://cioss.coas.oregonstate.edu/CIOSS/workshops/Altimeter_workshop_08/Coastal_Alt_Presentations/18_Tolman_Sig_Wave_Ht.pdf

Sorensen, O.R., Kofoed-Hansen, H., Rugbjerg, M. and Sorensen, L.S., 2004: A Third Generation Spectral Wave Model Using an Unstructured Finite Volume Technique. In Proceedings of the 29th International Conference of Coastal Engineering, 19-24 September 2004, Lisbon, Portugal.

Komen,G.J., Cavaleri,L., Doneland,M., Hasselmann,K., Hasselmann,S. and Janssen,P.A.E.M., (1984). Dynamics and modelling of ocean waves. Cambridge University Press, UK, 560 pp.

Young,I.R., (1999). Wind generated ocean waves, in Elsevier Ocean Engineering Book Series, Volume 2, Eds. R. Bhattacharyya and M.E. McCormick, Elsevier.

WAMDI-group: S. Hasselmann, K. Hasselman, E. Bauer, P.A.E.M. Janssen, G.J. Komen, L. Bertotti, P. Lionello, A. Guillaume, V.C. Cardone, J.A. Greenwood, M. Reistad, L. Zambresky and J.A. Ewing, (1988) “The WAM model – a third generation ocean wave prediction model”, J. Phys. Oceanogr., 18, 1775-1810

General Bathymetric Chart of the Oceans (GEBCO) – www.gebco.net

CM-93 Edition 3.0, CM-93/3 - www.jeppesen.com/marine/commercial/professional/

Ole Baltazar Andersen (1995), Global ocean tides from ERS 1 and TOPEX/POSEIDON altimetry, J. of Geophys. Res., 100, C12, p. 25249-25260

Doodson, A. T., Warburg, H. D., 1941 “Admiralty manual of tides”

Web references

ARPA-FVG OSMER, [Online] http://www.osmer.fvg.it/home.php

ARW Online Tutorial.” [Online] Available at http://www.mmm.ucar.edu/wrf/OnLineTutorial/index.htm

CISL RDA: NCEP Climate Forecast System Re-analysis (CFSR) 6-hourly Products, January 1979 to December 2010.” [Online] Available at http://rda.ucar.edu/datasets/ds093.0/index.html#description

NOAA, Hourly/Sub-Hourly Observational Data.” [Online] Available at http://gis.ncdc.noaa.gov/map/viewer/#app=cdo&cfg=cdo&theme=hourly&layers=1&node=gis

The Weather Research&Forecasting Model Website.” [Online] Available at http://www.wrf-model.org/index.php